The Dynamics of Fluidised Beds

- with particular reference to the Stability of the Fluidised State

by

Thomas Bell Anderson, B.Sc.(Tech.)

Thesis presented for the Degree of Doctor of Philosophy of the University of Edinburgh in the Faculty of Science

March 1967

EDINBURGH UNIV. BIBL. EX

ACKNOWLEDGMENTS

I wish to express my gratitude to Mr. R. Jackson, Reader in Chemical Engineering at the University of Edinburgh, for his guidance throughout this work. I would also like to thank Mr. C. McLeod and the Workshop Staff of the Chemical Engineering Department of the University of Edinburgh for their help with the mechanical design and construction of the equipment.

I am indebted also to Imperial Chemical Industries Limited, specifically to the Management Services Section (Wilton Works), for calculation of power spectra and autocorrelation functions. Finally I wish to acknowledge the financial support provided by the Science Research Council through the award of a Research Studentship.

Contents

	Page Number
Symbols and Notation	IV
Chapter 1 Introduction and Literature Survey	1
Chapter 2 The Equation of Motion for Dispersed Two Phase Flow and Their Application to Fluidised Systems	13
Chapter 3 The Stability of the State of Uniform Fluidisation Some Possible Voidage Gradients in the Bed	30
Chapter 4 Effects of the Various Bed Parameters on the Propagation Properties of Small Disturbances	58
Chapter 5 Equipment and Experimental Method	76
Chapter 6 Some General Features of the Experimental Work	95
Chapter 7 Experimental Determination of Propagation Properties	105
Chapter 8 Comparison of Experimental Measurements with Theoretical Predictions of Disturbance Growth	135
Chapter 9 Discussion of the Present Work and Recommendations for Future Work	159
Appendices	
Appendix 1 - The Nature of Aggregative and Particulate Fluidisation	169
Appendix 2 - Discussion of the Voidage Functions appearing in the Equation of Motion	173
Appendix 3 - Expansion Data and Experimentally Determined Amplitudes and Frequencies	188
References	199

NOMENCLATURE

Notation

The following is only a partial list of symbols used in the text. In general, those symbols which are little used and which appear at only one point in the text are omitted. The quantities given below can be expressed in any consistent system of units.

(i) Roman Letters

A - surface bounding a volume V of the dispersion.

A - quantity dependent on system parameters and bed expansion determining the growth properties of a disturbance.

$A(f)$ - amplitude of a disturbance of frequency f.

$A(x)$ - amplitude of disturbance at height x above the distributor.

$A'(x)$ - amplitude of disturbance adjusted for frequency change.

A_f - total bounding surface of fluid in the volume V.

A_p - surface area of one particle.

A_s - total surface area of dispersed phase in V.

a - general real part of complex angular frequency s.

a_0, a_1, a_2 - constants in the voidage signal calibration.

B - quantity dependent on system parameters and bed expansion determining the growth properties of a disturbance.

$\underline{b}$, b_i - body force per unit mass.

b - quantity dependent on wave number and system parameters determining propagation properties of a disturbance.

$C(\tau)$ - autocorrelation function.

C_D - drag coefficient in Rowe's experimental drag law.

c - quantity dependent on wave number and system parameters determining propagation properties of a disturbance.

c' - constant determining wall effect.

c_m - Fourier coefficient in expansion of function $f(x)$.

D - quantity dependent on system parameters and bed expansion determining the growth properties of a disturbance.

D_d - diameter of disturbance imposed on uniformly fluidised bed.

D_{em} - maximum value of diameter of sphere with the same volume as a bubble.

d - general imaginary part of the complex angular frequency s.

d_p - particle diameter based on a sphere of equal volume.

d_t - diameter of tube containing the bed.

d_u - diameter of uniform core.

E - quantity dependent on system parameters and bed expansion determining the growth properties of a disturbance.

e_{pq} - rate of strain tensor { superscript f refers to fluid; superscript s refers to particles. }

e - quantity dependent on wave number and system parameters determining propagation properties of a disturbance.

F - quantity dependent on system parameters and bed expansion determining the growth properties of a disturbance.

$F(\bar{S})$ - functional relationship of $\bar{\varepsilon}$ to $\bar{S}$.

Fr - Froude number $(\bar{u}_o^2/gd_p)$.

$f(n)$ - general function of particle number density.

$f(S)$ - functional relationship of ε to S.

$f(x)$ - distribution of initial general disturbance in the x-direction.

$f(x)$ - experimental disturbance frequency at height x above the distributor.

$\underline{f}$ - fluid/particle interaction force per unit bed volume.

$\underline{f}_I$ } - interaction force exerted on one particle by the fluid.
f_{Ii} }

f - disturbance frequency.

Δf - frequency bandwidth.

f_m - folding frequency.

f_x - x-component of the interaction force.

$G(f)$ - power spectral density function for positive frequencies.

g - acceleration due to gravity.

h - deflection of signal from R.H.S. of chart.

$\underline{I}$ } - integral term appearing in the expression for the interaction force.
$\underline{I}_i$ }

I_o - intensity of collimated beam leaving source.

I_1 - reduced beam intensity due to all factors except particles.

$I_2(n,x,)$ - intensity of light beam entering photomultiplier.

$\underline{i}$ - unit vector in the upward vertical (x) direction.

J_o - Bessel function of order zero.

j - square root of -1.

K - constant quantity in the Carman-Kozeny equation.

$\underline{k}$ - wave number vector of the disturbance.

k_x, k_y, k_z - x, y, z components of $\underline{k}$.

k_x^m - wave number associated with distribution function f(x).

k_ρ - radial component of the wave number vector.

k - magnitude of $\underline{k}$.

δk_x - difference between k_x and k_x^m.

l - x-direction cosine of $\underline{k}$.

$\underline{M}_f$ - momentum of fluid in volume V.

$\underline{M}_s$ - momentum of dispersed phase in volume V.

$\underline{M}_T$ - total momentum of matter in volume V.

m - mass of one particle.

m - index of coefficients in Fourier expansion of f(x).

m - y-direction cosine of $\underline{k}$.

N - exponent in the Richardson and Zaki equation.

N_o - initial amplitude of a disturbance.

n - local particle concentration or number density.

n_o - number density of particles in undisturbed state of uniform fluidisation.

n_1 - perturbation added to n_o due to the disturbance.

n_T - total disturbance obtained by summation of all the disturbance components.

n_t - particle number density at the top of the bed.

$\underline{n}$ - outward directed surface normal.

n - z-direction cosine of $\underline{k}$.

$\bar{P}$ - total power over all positive frequencies.

$P(f, \Delta f)$ - average power associated with frequency bandwidth Δf.

$P(f)$ - cumulative power over frequencies from 0 to f.

p - interstitial mean fluid pressure.

p - quantity, defined by equation (3,8), determining disturbance growth.

p' - point value of the fluid pressure.

p'' - deviation of point value from the interstitial mean fluid pressure.

Δp - pressure drop across the bed.

q - quantity, defined by equation (3,9), determining disturbance growth.

$R(\underline{r})$ - general function of position for a disturbance.

$R(x)$ - datum level correction factor a light signal.

Re - Reynold's number.

$\underline{r}$ - position vector with components (x, y, z) or (x, ρ, θ).

S - chart signal.

$S(n, x)$ - chart signal for concentration n obtained at height x.

$\underline{S_f}$, S_{fij} - fluid viscous stress tensor defined for interstitial fluid velocity.

$\underline{S'_f}$, S'_{fij} - fluid viscous stress tensor defined for point fluid velocity.

$\underline{S''_f}$, S''_{fij} - fluid viscous stress tensor defined for deviations of point velocity from interstitial velocity.

S_o - chart signal reduced to voidage calibration datum level.

$S_f(t)$ fluctuating part of signal.

$s_{1,2}$ - complex angular frequencies for the disturbance.

T - time limit on any record.

$T(t)$ - general function of time for a disturbance.

$\underline{T_f}$, T_{fij} - fluid stress tensor defined for local interstitial mean flow quantities.

$\underline{T'_f}$, T'_{fij} - fluid stress tensor defined for point flow quantities.

$\underline{T''_f}$, T''_{fij} - fluid stress tensor defined for deviations of point from local interstitial mean flow quantities.

$\underline{T_s}$, T_{sij} - stress tensor for particulate phase continuum.

$\underline{t_s}$ - stress vector for dispersed phase.

t - time

Δt - sampling time interval for signal.

$\underline{u}$, u_i – local interstitial mean fluid velocity vector.

$\underline{u}'$, u_i' – point fluid velocity vector.

$\underline{u}''$, u_i'' – deviation of point fluid velocity from interstitial mean fluid velocity.

$\underline{u_o}$, u_{oi} – interstitial mean fluid velocity for uniform fluidisation.

$\underline{u_1}$, u_{1i} – perturbation added to $\underline{u_o}$ because of disturbance.

u_i – velocity quantity appearing in the Richardson and Zaki equation.

$\overline{u_o}$ – superficial fluid velocity.

$\overline{u_{omf}}$ – superficial fluid velocity at minimum fluidisation.

u_t – terminal falling velocity of a particle.

u_x – x-component of $\underline{u}$.

V – arbitrary volume of dispersion.

V_f – volume of fluid in V.

V_s – volume of dispersed phase in V.

V_m – mean speed of random movement of the particles.

$\overline{V^2}$ – mean square speed of random movement of the particles.

V_p – phase velocity of a disturbance

$\underline{v}$, v_i – local mean dispersed phase velocity vector.

$\underline{v}'$ – local particle velocity vector.

$\underline{v}''$ – deviation of local particle velocity vector from local mean particle velocity.

$v_I(t)$ variable rectilinear velocity of a single particle.

$\underline{v_I}$ – velocity vector of a single particle.

W – mass of solid material in the bed.

$W(k_x)$ complex angular frequency of a disturbance.

X – limit of distribution of initial disturbance in the x-direction.

x – Cartesian coordinate corresponding to the upwards vertical direction.

x_o – datum level for voidage calibration.

x_t – height of the top of the bed.

x_w – height quantity dependent on the mass of material in the bed.

Δx - growth distance for a rising disturbance.

y - Cartesian coordinate in the horizontal plane.

Z - zero signal for experimental records.

z - Cartesian coordinate in the horizontal plane.

(ii) Greek Letters

α - angle between position vector $\underline{r}$ and the x axis.

$\alpha(\varepsilon)$ - drag function appearing in Murray's equations of motion.

$\alpha(n)$ - quantity related to the particulate phase bulk "viscosity" and shear "viscosity" coefficients.

α_o - value of $\alpha(n)$ when $n = n_o$.

β - angle between position vector $\underline{r}$ and the y axis.

$\beta(\varepsilon)$, $\beta(n)$ - function determining dependence of drag force between fluid and particles on the concentration.

β_o - value of $\beta(n)$ when $n = n_o$.

β'_o - value of $d\beta/dn$ when $n = n_o$.

γ - angle between position vector $\underline{r}$ and the z axis.

Υ - coefficient of relative velocity of fluid and particles in a Stokesian drag force.

δ - thickness of the particle layer at the top of the bed.

δ - separation ratio of the particles in Rowe's drag equation.

δ_{ij} - Kronecker delta.

ε - local voidage.

$\bar{\varepsilon}$ - overall mean bed voidage.

ε_o - voidage for the undisturbed state of uniform fluidisation.

ε_f - voidage at the foot of the bed.

ε_t - voidage at the top of the bed.

$\varepsilon_f(t)$ fluctuating part of the local voidage.

ζ - bulk viscosity coefficient of the fluid.

η - angular frequency of a disturbance component.

$\theta(\varepsilon)$, $\theta(n)$ - virtual mass coefficient for an assembly of particles.

θ_o - virtual mass coefficient when $n = n_o$.

θ - angular component in horizontal plane of the position vector $\underline{r}$.

κ - permeability of the bed appearing in Pigford's equations.

$\kappa(n)$ - bulk "viscosity" coefficient of the particulate phase.

κ_o - value of $\kappa(n)$ when $n = n_o$.

λ - wave-length of a sinusoidal disturbance component.

μ - shear viscosity coefficient of the fluid.

ν - volume of a single particle.

ξ - amplification factor of a disturbance component.

ρ - radial component in the horizontal plane of the position vector $\underline{r}$.

ρ_f - density of the fluid phase.

ρ_s - density of the solid matter of which the particles are composed.

τ - lag time argument of the autocorrelation function.

$\phi(n)$, $\phi(n, |\underline{u} - \underline{v}|)$ - equivalent of the quantity in a Stokesian drag force for an assembly of particles.

ϕ - angle which projection of $\underline{k}$ on the yz plane makes with the y axis.

$\chi(n)$ shear "viscosity" coefficient of the particulate phase.

χ_o - value of $\chi(n)$ when $n = n_o$.

$\psi(\varepsilon)$ voidage function appearing in Rowe's drag equation.

ψ - difference between the angles Θ and ϕ.

$\Omega(\varepsilon)$, $\Omega(n)$ - particulate phase static normal stress.

Ω_o - value of $\Omega(n)$ when $n = n_o$.

Ω'_o - value of $d\Omega/dn$ when $n = n_o$.

The Dynamics of Fluidised Beds

CHAPTER 1

Introduction and Literature Survey

Introduction

The phenomenon of fluidisation has been known for some considerable time, but it is only in recent years that it has seen widespread industrial use. It occurs when a fluid is passed upward through a bed of solid particles at a sufficiently high flow rate for the drag on the particles to become equal to their buoyant weight, the particles separating to become suspended in the fluid stream.

Large scale use of this phenomenon for fluid - solid contacting in the chemical and allied industries dates from the Second World War, when the first fluid bed catalytic reactor was used for cracking petroleum vapour. Since then the use of this technique on an industrial scale has spread, with numerous applications in the process industries; typical uses are solids drying, catalytic reactors, and in the iron and steel industry for ore roasting and reduction of iron ore. The potential use of fluidised beds in the atomic energy industry is being explored. Some of these uses, and the advantages and disadvantages of the fluid bed reactor are discussed in the books by Zenz and Othmer (1) and Leva (2).

However, despite the extensive use of fluidised beds, the mechanism governing the behaviour of the bed was little understood and the problems of design of and "scale-up" for industrial beds were quite formidable, and most of the research work (see, for example, references (1) and (2)) was devoted to obtaining correlations on which to base the design of these beds. It is only in the last few years that a significant advance has been made in the understanding of the particle movement and fluid flow patterns which prevail in the bed. This advance has been due mainly to the experimental work of Rowe and his co-workers at A.E.R.E. Harwell and to the research programme of Harrison and Davidson at Cambridge. A useful summary of the results of much of this work

is given in the book by Davidson and Harrison (3).

The most striking feature of fluidisation is the appearance of two ostensibly different types of fluidisation. Some beds, most often fluidised by gases, have regions of very low particle concentration (called bubbles) which travel up through the bed and give it an appearance similar to a boiling liquid. This type of bed is said to exhibit aggregative fluidisation. The other type of fluidisation is called particulate fluidisation and is generally found with liquid fluidised beds. This type of bed is characterised by a smooth appearance and uniform expansion with increasing flow rate; no bubbles are present. Wilhelm and Kwauk (4) found that a useful criterion for predicting the type of behaviour to be expected from a bed was the Froude number $\bar{u}_{omf}^2/gd_p$ where $\bar{u}_{omf}$ is the minimum superficial fluidisation velocity, d_p is the particle diameter and g is the acceleration due to gravity. They found that if the Froude number was greater than unity, the system exhibited aggregative behaviour and if it was less than unity, particulate behaviour could be expected. However, the reason for the formation of bubbles in some fluidised systems and not in others was not understood.

In the past few years a number of attempts have been made to set up the basic differential equations of motion for a two phase system and this fundamental approach has proved fruitful in clearing up some of the puzzling features of fluidisation, (see, for example, references (5) and (6)). All the workers who have investigated the basic equations of motion for a fluidised system have found that the state of uniform fluidisation is unstable, so that when small internal disturbances are superposed on the uniform flow fields characterising this state, these disturbances grow in amplitude with time or distance from their first appearance. The differential equations of motion predict that these disturbances are propagated up the bed as waves of increasing amplitude. The propagation properties of these waves (amplification factor, wave-length and associated frequency, phase velocity and growth distance) can be calculated from the properties of the bed in the undisturbed state; the properties of interest being the superficial fluid velocity, the voidage and the physical properties of

the fluid and solid.

For one type of solid material, disturbances in gas - fluidised beds (where the density ratio of solid to fluid is large) are very rapidly amplified while for liquid beds (the density ratio being much lower than for the gas fluidised system), the disturbances are amplified much more slowly. Presumably this rapid amplification in gas - fluidised systems is related to the appearance of bubbles, the main feature of aggregative fluidisation. In a liquid fluidised bed which is not turbulent, this instability manifests itself as fairly regular bands of reduced particle concentration rising upwards through the bed.

The appearance of these regular rising disturbances in a deep liquid fluidised bed has been reported by Kramers, Westerman, de Groot and Dupont in 1962 (7) and by Jackson (5) in 1963. In most liquid fluidised beds, the tube diameter is quite large and the bed has a turbulent appearance with particles swirling around in large eddies. It is only in fairly narrow diameter tubes, when large scale turbulence seems to be suppressed, that these regular disturbances are clearly visible; this is probably the reason why their appearance has not been reported before.

Jackson (5), from the equations of motion he set up, calculated the growth distance (the distance in which the amplitude of a disturbance increases in the ratio e : 1) for the systems investigated by Wilhelm and Kwauk (4). Basing his calculations on a disturbance whose wave-length was a constant multiple of the particle diameter for each system, he compared the growth distance for the various systems with the Froude number criterion of Wilhelm and Kwauk, and found that the growth distance was small in normal aggregative systems and large in particulate systems. On this basis, he was able to classify the various systems. In fact, the Froude number is found to be one of the parameters determining the propagation properties of these disturbances. Harrison and Davidson (3) have also reported a method for determining the type of fluidisation to be expected, based on the rate of rise of a bubble in a fluidised bed and on an estimate of the maximum stable size obtained from this. A comparison of these two approaches by Jackson and the present author has been published (8) and is

reported in Appendix 1. These two approaches, the stability calculations and the maximum stable bubble size, although quite different physically, are found in fact to be complementary in their predictions.

The equations of motion, because of their complexity, can be solved only for a limited number of cases - one of the most important being for the flow patterns round a fully developed bubble in a fluidised bed. The purpose of the present work is to further investigate the equations of motion and, from a study of the rate of growth and the propagation properties of these disturbances, to ascertain, as far as possible, the validity of the equations and the dominant forces acting in the bed. It should be noted, however, that the predictions of the instability theory are strictly applicable only to very small disturbances and not to those which have grown to any appreciable size. However, this work may serve as some check on the equations, and thus support some of the other conclusions drawn from them.

Survey Of The Literature

The volume of literature dealing with all the various aspects of fluidisation is extremely large, but for the purpose of the present study, only those papers dealing with the equations of motion for a dispersion and their application to the fluidised state are really relevant and only these papers will be discussed here. Papers dealing with other aspects of fluidisation, for example, work done on the viscosity of fluidised beds, will be discussed when relevant to parts of this work at the appropriate place in the text.

The first paper, relevant to the present work, dealing with the equations of motion and mechanical energy balances for a two-phase flow system was published in 1960 by Van Deemter and Van der Laan (9). Their equations, based on continuum flow of both phases, are completely general for any kind of dispersed two-phase system. They make no attempt to elucidate the nature of the stress tensors and interaction forces involved in the application of their equations to any particular situation and consequently their equations are useful only as a starting point for

the investigation of fluidisation.

Soo (10) in 1962 published a paper dealing with the boundary layer motion of a gas - solid suspension. While he does not treat fluidisation, he does give a momentum balance equation for both phases together and an equation of motion for the particles, both derived on a continuum basis. His total momentum balance equation contains effects due to the stress tensors of both phases, but, for the particulate phase, normal stresses akin to the pressure of a fluid are neglected and the particulate phase stress tensor contains viscous terms alone. An expression is given for the viscosity of the particulate phase based on an analogy with the Kinetic Theory of Gases, and it is assumed that the bulk viscosity is zero. It is shown later in the present work that this is not necessarily a valid assumption. His solids momentum equation is

$$(\underline{v}.\text{grad})\underline{v} = F(\underline{u} - \underline{v})$$

where $\underline{v}$ is the solids velocity vector and $\underline{u}$ is the fluid velocity vector. F is a term depending on the particle concentration and is akin to the term $\beta(n)$ used in Jackson's equations (5) and in the present work. Body forces, the particulate phase stress tensor, virtual mass effects and the partial time derivative of $\underline{v}$ are omitted from the above equation and hence it can only give a very approximate indication of the behaviour of any system when taken in conjunction with his other equations.

A further set of equations for a dispersion were obtained by Hinze (11), again on a continuum basis, and these he applied to turbulent flow. He did not include the effect of stress in the dispersed phase itself, but introduced a composite stress tensor involving both fluid and dispersed phase velocities. The nature of the viscosity coefficient is not discussed. However, his equations are really invalidated by the form chosen for the particle - fluid interaction force terms (the force exerted by the fluid on the particles). He states, correctly, that this force should equal the weight force and the acceleration force on the particles, but includes with the acceleration force a virtual mass term. It is well known (from the work of Basset (12) and Lamb (13)) that the force due to the virtual mass effect

is not part of the inertial force but of the fluid - particle interaction force. Because of this, Hinze's total momentum balance equation for the two phases contains a virtual mass term and this, as Murray (14) points out, violates Newton's Third Law. Consequently the equations of Hinze are unimportant from the point of view of this work.

Of more direct importance are the equations describing the mechanics of a fluidised bed developed by Jackson (5), Wallis (15), Pigford and Baron (6) and Murray (14). The equations of Wallis and Jackson do not take account of viscous effects or virtual mass effects, while Pigford and Baron have attempted to show the effects of viscous stresses in the particulate phase. Murray's equations deal with all those effects and neglect only Basset forces (time dependent relative acceleration forces in the particle - fluid interaction force). Although Murray's equations are more complete than any of the other sets of equations, a further much more fundamental difference exists. This is readily seen by reducing all four sets of equations to their common basic form by omitting all viscous and virtual mass effects, when it is found that all the equations, apart from Murray's, become equivalent.

In the notation of the present work, the four sets of basic equations are as follows:

Jackson

$$\rho_s(1-\varepsilon)\left\{\frac{\partial \underline{v}}{\partial t} + (\underline{v}.\text{grad})\,\underline{v}\right\} - \rho_f(1-\varepsilon)\left\{\frac{\partial \underline{u}}{\partial t} + (\underline{u}.\text{grad})\,\underline{u}\right\} + \underline{i}\,(1-\varepsilon)(\rho_s-\rho_f)g - \beta(\varepsilon)(\underline{u}-\underline{v}) = 0 \qquad (1,1)$$

$$\rho_f\left\{\frac{\partial \underline{u}}{\partial t} + (\underline{u}.\text{grad})\,\underline{u}\right\} + \underline{i}\,\rho_f g + \text{grad}\,p + \beta(\varepsilon)(\underline{u}-\underline{v}) = 0 \qquad (1,2)$$

Wallis

$$\rho_s(1-\varepsilon)\left\{\frac{\partial \underline{v}}{\partial t} + (\underline{v}.\text{grad})\,\underline{v}\right\} + (1-\varepsilon)\,\text{grad}\,p + \underline{i}\,\rho_s(1-\varepsilon)g - \varepsilon(1-\varepsilon)K(\underline{u}-\underline{v})^m = 0. \qquad (1,3)$$

$$\rho_f\varepsilon\left\{\frac{\partial \underline{u}}{\partial t} + (\underline{u}.\text{grad})\,\underline{u}\right\} + \varepsilon\,\text{grad}\,p + \underline{i}\,\rho_f\varepsilon g + \varepsilon(1-\varepsilon)K(\underline{u}-\underline{v})^m = 0 \qquad (1,4)$$

Pigford and Baron

$$\rho_s(1-\varepsilon)\left\{\frac{\partial \underline{v}}{\partial t} + (\underline{v}.\text{grad})\,\underline{v}\right\} + (1-\varepsilon)\,\text{grad}\,p + \underline{i}\,\rho_s(1-\varepsilon)g - \frac{\mu}{K}(\underline{u}-\underline{v}) = 0 \qquad (1,5)$$

$$\rho_f \varepsilon\left\{\frac{\partial \underline{u}}{\partial t} + (\underline{u}.\text{grad})\,\underline{u}\right\} + \varepsilon\,\text{grad}\,p + \underline{i}\,\rho_f \varepsilon g + \frac{\mu}{K}(\underline{u}-\underline{v}) = 0 \qquad (1,6)$$

Murray

$$\rho_s(1-\varepsilon)\left\{\frac{\partial \underline{v}}{\partial t} + (\underline{v}.\text{grad})\,\underline{v}\right\} + \underline{i}\,(1-\varepsilon)(\rho_s-\rho_f)g - \alpha(\underline{u}-\underline{v}) = 0 \qquad (1,7)$$

$$\rho_f \varepsilon\left\{\frac{\partial \underline{u}}{\partial t} + (\underline{u}.\text{grad})\,\underline{u}\right\} + \underline{i}\,\rho_f g + \text{grad}\,p + \alpha(\underline{u}-\underline{v}) = 0 \qquad (1,8)$$

In the above equations, ρ_f and ρ_s are the densities of the fluid and solid, $\underline{u}$ and $\underline{v}$ are the continuum velocities of the fluid and solid, p is the fluid pressure and ε is the voidage. The quantities β, K, μ/K and α are all functions of voidage and the expression $(\underline{u}-\underline{v})^m$ is to be interpreted in the obvious way as a vector of magnitude $|\underline{u}-\underline{v}|^m$ in the direction of $(\underline{u}-\underline{v})$. $\underline{i}$ is the unit vector in the positive x direction i.e. pointing vertically upwards.

If $m = 1$ in equations (1,3) and (1,4), the equations of Wallis and Pigford and Baron are the same provided that μ/K can be identified with $\varepsilon(1-\varepsilon)K$. Jackson's equations, although at first sight they appear somewhat different, are also equivalent to those of Wallis and Pigford. Dividing through equation (1,6) by ε, one obtains equation (1,2) of Jackson if $\mu/K\varepsilon$ is identified with $\beta(\varepsilon)$. Equation (1,1) is readily obtained by eliminating grad p from (1,5) by use of equation (1,6). Murray's equations, (1,7) and (1,8) can in no way be obtained as a linear combination of any of the other pairs of equations and are quite different in structure.

To show where the difference lies, the way in which Murray's equations and the other three sets are obtained from the general equations of Van Deemter and Van der Laan (9) must be considered. Their equations are

$$(1-\varepsilon)\rho_s\left\{\frac{\partial \underline{v}}{\partial t} + (\underline{v}.\text{grad})\underline{v}\right\} + \underline{i}\,\rho_s(1-\varepsilon)g - \underline{f} = 0 \qquad (1,9)$$

$$\rho_f\varepsilon\left\{\frac{\partial \underline{u}}{\partial t} + (\underline{u}.\text{grad})\underline{u}\right\} + \underline{i}\,\rho_f\varepsilon g + \text{grad}\,p + \underline{f} = 0 \qquad (1,10)$$

where $\underline{f}$ is the interaction force between fluid and particles per unit bed volume, its form being unspecified. Pigford's equations can be obtained from the above pair by writing

$$\underline{f} = -(1-\varepsilon)\overset{\text{grad}\,p}{\lambda} + \frac{\mu}{K}(\underline{u}-\underline{v}) \qquad (1,11)$$

To obtain Murray's equations, the interaction force $\underline{f}$ must be given by

$$\underline{f} = \underline{i}\,\rho_f(1-\varepsilon)g + \alpha(\underline{u}-\underline{v}) \qquad (1,12)$$

in contrast to (11).

It would be expected that, as $\varepsilon \to 1$, the equation of motion for the solids would reduce to the basic form of the equation of motion for a single particle in a moving fluid. Corrsin and Lumley (16) give this equation as

$$\nu\rho_s\left\{\frac{\partial \underline{v}}{\partial t} + (\underline{v}.\text{grad})\underline{v}\right\} = \gamma(\underline{u}-\underline{v}) - \underline{i}\,(\rho_s-\rho_f)g\nu + \nu\rho_f\left\{\frac{\partial \underline{u}}{\partial t} + (\underline{u}.\text{grad})\underline{u}\right\} \qquad (1,13)$$

where ν is the volume of a single particle, γ is a constant in a Stokesian drag force and $\underline{v}$ is now the velocity of a single particle. All viscous forces, virtual mass forces and Basset forces have been neglected. Multiplying equation (1,1) by $\nu/(1-\varepsilon)$ and letting $\varepsilon \to 1$, it is seen that Jackson's equation degenerates into equation (1,13) if $\lim_{\varepsilon\to 1}\frac{\beta(\varepsilon)}{(1-\varepsilon)} = \gamma$ Note that $\beta(\varepsilon) \to 0$ as $\varepsilon \to 1$, but the ratio $\beta(\varepsilon)/(1-\varepsilon)$ remains finite. Murray's equation (1,7), however, reduces to

$$\nu\rho_s\left\{\frac{\partial \underline{v}}{\partial t} + (\underline{v}.\text{grad})\underline{v}\right\} = \gamma(\underline{u}-\underline{v}) - \underline{i}\,(\rho_s-\rho_f)g\nu$$

if $\lim_{\varepsilon\to 1}\frac{\alpha}{(1-\varepsilon)} = \gamma$. The fluid momentum term of equation (1,13) is missing from the right hand side of this equation.

This clearly points up the mistake in Murray's equations. From equations (1,11) and (1,12) it is seen that in calculating the reaction

of the fluid pressure gradient on the particles, Murray has considered only the change in hydrostatic head and neglected the effect of fluid acceleration, implicitly included in equation (1,11). The origin of the fluid acceleration term in equation (1,13) is clearly shown in the book by Hinze (17).

In addition, however, to this fundamental error, and perhaps stemming from it, there are other errors and inconsistencies in Murray's treatment. Many of these will be discussed at the corresponding part of the derivation of the present set of equations, but the more obvious ones will be demonstrated here. His complete momentum balance equations read

Solids

$$\rho_s(1-\varepsilon)\left\{\frac{\partial \underline{v}}{\partial t} + (\underline{v}.\text{grad})\,\underline{v}\right\} = -\underline{i}\,(\rho_s-\rho_f)(1-\varepsilon)g + \rho_s(1-\varepsilon)\,\underline{F_s} + (1-\varepsilon)\,\text{div}\,\underline{S_s}$$
$$+ \alpha(\varepsilon)(\underline{u}-\underline{v}) + \theta(\varepsilon)\rho_f(1-\varepsilon)\frac{d}{dt}(\underline{u}-\underline{v}) \qquad \text{——— (1,14)}$$

Fluid

$$\rho_f \varepsilon\left\{\frac{\partial \underline{u}}{\partial t} + (\underline{u}.\text{grad})\,\underline{u}\right\} = -\underline{i}\,\rho_f g + \rho_f \varepsilon\,\underline{F_f} - \text{grad}\,p + \varepsilon\,\text{div}\,\underline{S_f}$$
$$- \alpha(\varepsilon)(\underline{u}-\underline{v}) - \theta(\varepsilon)\rho_f(1-\varepsilon)\frac{d}{dt}(\underline{u}-\underline{v}) \qquad \text{——— (1,15)}$$

where $\underline{F_s}$, $\underline{F_f}$ are the external forces per unit mass on the solids and fluid respectively, $\underline{S_f}$ and $\underline{S_s}$ are the viscous stress tensors of the fluid and particulate phase respectively and $\theta(\varepsilon)$ is the virtual mass coefficient. The form of the term $\frac{d}{dt}(\underline{u} - \underline{v})$ is of no concern at the moment, but is discussed in more detail later.

It is seen that in equation (1,14), the quantities $\underline{F_s}$ and $\underline{ig}$ also have different coefficients. These are both body force terms, and since the matter in the bed cannot distinguish the origins of the different body forces acting on it and can only react to the total body force, the two body force terms in each equation should be the same apart from the difference in the vectors $\underline{F}$ and $\underline{ig}$. A similar error occurs with the coefficients of div $\underline{S_f}$ and grad p in equation (1,15). These two terms are both inseparable parts of the stress in the fluid - arising as two terms only because of the resolution of the stress tensor into a static and dynamic part. Thus they cannot logically appear with different

coefficients inside one equation.

Murray's particulate phase stress tensor initially contained a normal stress term representing collision forces between the particles rather like the pressure of a gas, but this term was subsequently dropped. It is shown later in the present work that even if this term is small compared to the fluid pressure, it may still exert considerable influence on the propagation properties of small disturbances and certainly should not be neglected. However, because he has neglected this term, Murray states that "to be consistent, we must replace ε by unity in the pressure term of the fluid stress tensor" and this accounts for the discrepancy mentioned above.

There are further errors in the above equations and in their derivation - some of these affecting the fundamental structure of the equations - but these are more properly discussed at the appropriate points in subsequent chapters.

Wallis (15), like Jackson (5), found that the state of uniform fluidisation was unstable, and on the basis of his equations managed to classify various systems, using the rate of amplification of small disturbas a criterion. His results are very similar to Jackson's.

Pigford and Baron (6) also found that the uniformly fluidised state was unstable and attempted to show the effect on the propagation properties of the bed's resistance to shear. To do this, they added a term - $-\eta\nabla^2[(1-\varepsilon)\underline{v}]$ to the left hand side of equation (5) - the equation of motion for the solid phase. The symbol η denotes some bed viscosity and the term $(1-\varepsilon)\underline{v}$ is seen to be the superficial solid phase velocity vector. The reason for this odd velocity term becomes clear if it is recalled that Pigford's equations were originally written in terms of superficial velocities, but this does not excuse its use in this context where, properly speaking, the term should be $\eta\nabla^2\underline{v}$. Even this, however, is wrong since it neglects a term in $\mathrm{div}\,\underline{v}$ in the rate of strain tensor, implying that the continuum flow of the solid phase is incompressible, which is obviously not the case by continuity. Thus Pigford's attempt to consider the effect of shearing stress in the bed (while it does show the effects on the propagation properties mentioned later) must be considered fairly crude.

At this point it may be as well to mention papers by Ruckenstein (19) and Zuber (20). Both try to investigate fluidisation in terms of the equation of motion for one particle in an assembly of other particles.

Zuber's analysis is based on the total momentum balance for the two phases and on the equation of motion of a single particle of the assembly moving with the representative continuum - based solids velocity. The particle equation is based on the equation of Corrsin and Lumley (16) for the motion of a single particle in a moving fluid stream. A modified fluid viscosity is included in his Stoke's drag term and from this Zuber showed that a particular case of the Richardson and Zaki relationship (21) could be obtained. By this means he attempts to take into account the interaction of neighbouring particles. However, no collisional or particle shearing effects are included and the stability of the bed is not investigated. In addition, his use of a representative particle of the assembly would seem to contradict his method of evaluating the virtual mass coefficient. This is based on Lamb's analysis (13) of the motion of a particle inside a fluid sphere - the boundaries of the fluid sphere in this case are assumed to be made up from the neighbouring particles. Since the physical situation concerned is the relative motion of a part of the assembly and the associated fluid and not the relative motion of two particles of the assembly and the fluid between, Zuber's analysis for the virtual mass coeffieient is not really relevant.

Ruckenstein's equation (19) for the motion of a single particle has the same fundamental error as Murray's equations, that is, the contribution of the rate of change of fluid momentum to the pressure gradient is neglected. Because of the way in which the virtual mass term arises from the particle - fluid interaction force, the coefficient he uses should in fact be divided by the voidage. Two criteria are given for the stability of the fluidised bed and Ruckenstein concludes that liquid fluidised beds are in general more stable than gas fluidised beds.

In fact, practically all the papers mentioned above have dealt with the stability of fluidised systems to small internal disturbances and all have found that the bed is unstable. However it is easily demonstrated, at least for the simpler equations, that the bed is always unstable provided at least one of the rate of change of momentum terms is included in the equations. The importance of the inertial terms in promoting instability is highlighted by the conclusions of Rowe (18) regarding this point. Using the force balance on a particle in a uniform assembly and stream, he concluded that a fluidised bed would be stable to small changes

in the particle concentration. However, the force balance for the uniform assembly is based on steady drag effects and buoyancy effects and cannot, by its very nature, include acceleration terms.

CHAPTER 2

The Equations of Motion for Dispersed Two Phase Flow and Their Application to Fluidised Systems

The following work is essentially a derivation and extension of the equations of Jackson (5). General equations, in which the actual form of the fluid - particle interaction force is not defined, are developed on a continuum basis and these are applicable to any type of dispersed two-phase flow for which the underlying physical assumptions are valid. The method used follows roughly that of Van Deemter and Van der Laan (9). These equations are then applied to a system of fluidised particles by a suitable choice of form for the interaction force.

The present set of equations, and all the equations discussed in the previous chapter, are based on continuum flow of both phases, and it is desirable at the outset to make clear the physical assumptions and inherent limitations of this method of description. The equations are derived for volume elements of the dispersion containing large numbers of particles (the dispersed phase) so that the characteristic length of volume element is very much larger than the particle size or spacing. Obviously there will be rapid local variations in the fluid velocity and pressure and the individual particle velocities due to the flow around the particles. These rapid fluctuations will be of a linear scale of the same order as the particle size. The physical assumption is made that the variation of the point values of the flow variables consist of these large rapid local variations superimposed an a relatively slow variation of a scale many times the particle size.

If p' and $\underline{u}'$ are the point values of the fluid pressure and velocity, then they can be written as

$$p' = p + p'' \quad \text{and} \quad \underline{u}' = \underline{u} + \underline{u}''$$

where p and $\underline{u}$ are interstitial mean values and p'' and $\underline{u}''$ represent the rapid local fluctuations. The local particle velocities are denoted by $\underline{v}'$ and can be written as above

$$\underline{v}' = \underline{v} + \underline{v}'' .$$

Note that p' and $\underline{u}'$ are defined only at points occupied by the fluid and

$\underline{y}'$ at points within the solids, while p, $\underline{u}$ and $\underline{y}$ are defined at all points in space, including points within the solids. This is because of the way in which these mean values are obtained - that is, by averaging over a volume element containing a large number of particles. Conveniently, the volume element could be a sphere centred at the point of interest.

The values obtained for the mean flow variables by this space averaging method will depend on the radius of the sphere used. However, if the scale of variation of p, $\underline{u}$ and $\underline{y}$ is widely different from the rapid variations p", $\underline{u}$" and $\underline{y}$" , then there will be a wide range of radii for which the rapid fluctuations are smoothed out without substantially effecting the variation of the interstial means, that is, although the rapid variation is smoothed out, the slow variation is virtually unaltered. A less primitive averaging method would be to use a suitably chosen weighting function which falls smoothly to zero instead of dropping abruptly to zero at the surface of the averaging sphere.

It cannot be over-emphasised that this assumption regarding the two widely differing scales of variation of the flow variables is basic to any continuum description of dispersion flow. It is assumed that the flow may be adequately described in terms of these continuous mean flow variables, although it is the rapid fluctuations which give rise to the form of the interaction force. As a consequence of this continuum treatment of the flow of both fluid and particles, any phenomenon arising from the equations must be of a size scale much larger than the particle spacing.

It is further assumed that no heat transfer diffusion or chemical reaction occure in the system and that the only body force acting is gravity. Generally, the flow will be referred to a Cartesian frame, whose origin at the moment need not be defined, but whose x-axis points vertically upwards in the direction of bulk flow of fluid in a fluidised bed.

Consider a volume element dV inside a volume V of the dispersion. A is the surface bounding V and dA the surface bounding dV. V_f is the volume of continuous phase inside V and A_f is the total bounding surface of V_f. The density of the particulate phase is ρ_s and the density of the continuous phase is ρ_f . Because of the continuum nature of this model, both phases can be regarded as homogenous interpenetrating phases occupying the same volume and with variable density determined by the particle concentration.

The space averaged quantities over the element dV are

$\underline{u} = \underline{u}(\underline{r}, t)$ - interstitial mean fluid velocity vector

$\underline{v} = \underline{v}(\underline{r}, t)$ - local mean dispersed phase velocity vector

$p = p(\underline{r}, t)$ - interstitial mean fluid pressure

$\varepsilon = \varepsilon(\underline{r}, t)$ - local void fraction

where $\underline{r}$ is the position vector of the element dV at time t. The continuity equation for the continuous (fluid) phase is

$$\frac{\partial}{\partial t}(\varepsilon \rho_f) + \operatorname{div}(\varepsilon \rho_f \underline{u}) = 0 \qquad (2,1)$$

and for the dispersed phase, it reads

$$\frac{\partial}{\partial t}[(1-\varepsilon)\rho_s] + \operatorname{div}[(1-\varepsilon)\rho_s \underline{v}] = 0 \qquad (2,2)$$

(a) Rates of Change of Momentum

Consider an arbitrary volume V(t) of the dispersion at time t. Associated with this volume are two momenta - one due to the fluid motion and the other due to the particle motion. The total momentum of this volume is the vector sum of the momenta of the two phases -

$$\underline{M}_t = \underline{M}_f + \underline{M}_s$$

In a time interval δt, the original volume V(t) will have changed to $V_f(t + \delta t)$ due to the motion of the fluid. This volume $V_f(t + \delta t)$ will contain all the fluid originally in the volume V(t). This volume V_f will have moved with the fluid and because of the continuum nature of the flow, no fluid will have crossed the boundary of this region. The fact that the fluid retains its identity does not, however, preclude the transfer of the other phase across the boundary - in accordance with the continuity equation for the fluid. Similarly, due to the continuum treatment of the particulate phase, V(t) will have changed to $V_s(t + \delta t)$, the material of this phase retaining its identity, although fluid may have crossed the boundary of this region.

The dispersion itself is not a continuum and the rates of change of the two momenta must be worked out separately. The above procedure is equivalent to taking the material co-ordinatio (the identification of the fluid material and solid material under discussion) of a volume element as $\underline{r}$ - the position vector at time t. The motion of the two phases is followed separately and thus Reynold's Transport Theorem (22) applies to both phases independently. For example, for the case of the

fluid this states

$$\frac{d}{dt}\int_{V(t)} \underline{P_f}\,(\underline{r},t)\,dV = \int_V \left[\frac{d}{dt}\underline{P_f} + \underline{P_f}\,(\nabla.\underline{u})\right] dV$$

and, since the fluid motion is being followed in this case

$$\frac{d}{dt} = \frac{\partial}{\partial t} + (\underline{u}.\text{grad})$$

$\underline{P_f}$ is any quantity, vector or scalar, moving with the fluid, and for the momentum case, $\underline{P_f} = \varepsilon\rho_f\,\underline{u}$. Combining this with the continuity equation, the rate of change of momentum of the fluid phase in the volume V(t) is

$$\frac{d}{dt}\underline{M_f} = \int_V \varepsilon\rho_f\left[\frac{\partial \underline{u}}{\partial t} + (\underline{u}.\text{grad})\underline{u}\right]dV \qquad \text{(2,3)}$$

Similarly, for the particulate phase

$$\frac{d}{dt}\underline{M_s} = \int_V \rho_s(1-\varepsilon)\left[\frac{\partial \underline{v}}{\partial t} + (\underline{v}.\text{grad})\underline{v}\right]dV \qquad \text{(2,4)}$$

In the following, when the operator $\frac{d}{dt}$ acts on either velocity, the convected term is always referred to the velocity on which it is acting unless otherwise stated.

(b) Forces Acting on the Volume V of Dispersion

Body forces act throughout the whole of this volume. In the present work, only gravity is considered. Surface forces act over the boundaries of the region and are made up of two parts - one due to stress in the fluid and the other due to particle - particle interactions. For the moment, this second force is introduced in a purely formal manner without reference to the physics of the situation.

The force exerted on one particle by the fluid is

$$\underline{f_I} = \int_{A_p} \underline{n}.\,\underline{T_f}'\,dA$$

where $\underline{f_I}$ is the force on one particle, $\underline{n}$ is the outward normal to the particle surface and $\underline{T_f}'$ is the fluid stress tensor defined in terms of the point values of the pressure and fluid velocity. A_p is the surface area of a particle of volume v. In suffix notation, the stress tensor can be written $T'_{fij} = -p'\delta_{ij} + S'_{fij}$ where S'_{fij} is the viscous stress tensor, which, if the fluid is Newtonian, takes the form

$$S'_{fij} = \zeta\frac{\partial u'_k}{\partial x_k}\delta_{ij} + \mu\left\{\frac{\partial u'_i}{\partial x_j} + \frac{\partial u'_j}{\partial x_i} - \frac{2}{3}\frac{\partial u'_k}{\partial x_k}\delta_{ij}\right\}$$

The shear viscosity is μ and the bulk viscosity coefficient is ζ. Because the stress tensor is linear in the pressure and velocity $\underline{T}_f' = \underline{T}_f + \underline{T}_f''$ where $\underline{T}_f$ is defined for the interstitial mean fluid pressure and velocity and $\underline{T}_f''$ for the deviations from these means. Obviously $\underline{T}_f$ and $\underline{T}_f''$ have the same form as $\underline{T}'$. Thus

$$f_{Ii} = \int_{A_p} T_{fij} n_j \, dA + \int_{A_p} T''_{fij} \, dA$$

Since p and $\underline{u}$ are defined at all points in space, Gauss's Theorem can be applied to the first integral, giving

$$f_{Ii} = \int_V \frac{\partial T_{fij}}{\partial x_j} \, dV + I_i$$

where I_j is the second integral in the above equation. Since $\underline{u}$ and p vary little over the particle size

$$f_{Ii} = v \frac{\partial T_{fij}}{\partial x_j} + I_i$$

Thus $\underline{f}_I = -v \, \mathrm{grad}\, p + v \, \mathrm{div}\, \underline{S}_f + \underline{I}$

The evaluation of the second integral is much more difficult and depends very much on the physical situation. Suffice it to say for the moment that it gives rise to the viscous drag and virtual mass effect. An attempt to evaluate it will be made when the general phenomenological equations are applied to the fluidised state.

If there are n particles per unit volume, the force per unit bed volume ($\underline{f}$) exerted by the fluid on the particles is given by

$$\underline{f} = n \underline{f}_I = -nv \, \mathrm{grad}\, p + nv \, \mathrm{div}\, \underline{S}_f + n\underline{I} \qquad \text{——————(2,5)}$$

The reaction force on the fluid is then $-\underline{f}$. Thus for a volume V of dispersion there is a force exerted by the particles on the fluid given by $-\int_V \underline{f} \, dV$.

The surface force exerted on the fluid in the volume V is given by

$$\int_{A_f} \underline{n} \cdot \underline{T}_f' \, dA_f$$

where $\underline{n}$ is the outward directed normal to dA_f. This area A_f consists of the surface area of the particles lying inside or partially inside the boundary of V together with that fraction of the surface A which is occupied by fluid. However if the effect of particles in the surface itself is neglected (this step will be justified below), the area dA_f can be written

$$dA_f = dA_s + dA$$

where dA_s is the total surface of the particles. Thus the above integral can be written in two parts

$$\int_A \underline{n}\cdot\underline{T}'_f \, dA + \int_{A_s} \underline{n}\cdot\underline{T}'_f \, dA_s$$

This second integral is the force exerted on the fluid by the particles and gives rise to the interaction force per unit volume - $\underline{f}$. In the preceding paragraphs where this interaction force was discussed, the normal $\underline{n}$ was directed inwards to the fluid and thus has the opposite sign to the $\underline{n}$ appearing in the above expression. In the second integral, the deviations from the mean flow variables are of paramount importance - determining the viscous drag and virtual mass effects. In the first integral, representing the force exerted on the fluid inside V by the fluid outside, the averaging procedure used to obtain the interstitial mean pressure and velocity smoothes out the rapid local fluctuations. Hence, in accordance with the description of the flow in terms of these space averaged quantities, $\underline{T}'_f$ in the first integral can be replaced by $\underline{T}_f$. Applying Gauss's Theorem, the surface force exerted on the fluid is given by

$$\int_{A_f} \underline{n}\cdot\underline{T}'_f \, dA_f = \int_V \left[- \operatorname{grad} p + \operatorname{div} \underline{S}_f \right] dV - \int_V \underline{f} \, dV \qquad \text{——— (2,6)}$$

Particle - particle interactions (collisions and interference of movement) gives rise to a force exerted on the particles alone. This can be taken into account by a stress tensor $\underline{T}_s$ - defined as the stress per unit total area (not just that area of the surface occupied by particles) arising from particle - particle interactions. It should be noted that this is defined for the particle continuum and is completely unrelated to the stress inside the particles. It is due solely to the motion of the dispersion. This stress tensor is continuous (defined for all points in space), but its form need not be discussed at present.

This stress tensor, acting across the whole surface area of the volume V gives the surface force exerted by the particles outside on the particles inside as $\int_V \frac{\partial T_{sij}}{\partial x_j} \, dV$

having applied Gauss's Theorem.

If $\underline{b}$ is the body force per unit mass acting, the body force on the

fluid is $\int_V \varepsilon \rho_f \underline{b}\, dV$ and on the particles, it is $\int_V (1-\varepsilon)\rho_s \underline{b}\, dV$.

It is now possible to obtain the momentum balance for the two phases in the volume V and to find the equations of motion for both phases separately.

Since the fluid - particle interaction force $\underline{f}$ is purely internal in its effect, acting as action and reaction on both phases, it does not appear in the total momentum balance. This reads as

$$\int_V \varepsilon \rho_f \left\{ \frac{\partial \underline{u}}{\partial t} + (\underline{u}.\text{grad})\underline{u} \right\} dV + \int_V (1-\varepsilon)\rho_s \left\{ \frac{\partial \underline{v}}{\partial t} + (\underline{v}.\text{grad})\underline{v} \right\} dV$$

$$= \int_V \varepsilon \rho_f \underline{b}\, dV + \int_V (1-\varepsilon)\rho_s \underline{b}\, dV + \int_V \text{div}\, \underline{T}_s\, dV + \int_V \left\{ -\text{grad}\, p + \text{div}\, \underline{S}_f \right\} dV$$

Since this volume is quite arbitrary,

$$\varepsilon \rho_f \left\{ \frac{\partial \underline{u}}{\partial t} + (\underline{u}.\text{grad})\underline{u} \right\} + \rho_s (1-\varepsilon) \left\{ \frac{\partial \underline{v}}{\partial t} + (\underline{v}.\text{grad})\underline{v} \right\}$$

$$= \left\{ \rho_f \varepsilon + \rho_s (1-\varepsilon) \right\} \underline{b} + \text{div}\, \underline{T}_s - \text{grad}\, p + \text{div}\, \underline{S}_f \qquad \text{——————} (2,7)$$

In this equation, the fluid stress tensor $\underline{T}_f$ is acting across the whole of the bounding surface and not just that part of it occupied by the fluid. Perhaps the easiest way to see why this should be so is to consider an assembly of stationary particles immersed in a stationary fluid with no body force acting. In general, a fraction $(1 - \varepsilon)$ of the bounding surface of the arbitrary volume V will be occupied by the particles. The force per unit area exerted across this surface by the matter on one side on the matter on the other will consist of the pressure p in the fluid and an identical pressure p in the solid, since, because the system is in equilibrium, the uniform stress p must exist inside this solid material. Another way of looking at this is to make the control volume much less arbitrary and ensure that its bounding surface never cuts any particles.

If, as Murray (14) considers, the force on the fluid were given by ε div $\underline{T}_f$ instead of div $\underline{T}_f$ alone, this force would have to be supplemented by a term $(1 - \varepsilon)$ div $\underline{T}_s$, where, for the moment only, $\underline{T}_s$ represents the stress <u>inside</u> the particles and not the stress due to the external effect

of particle - particle interaction. Formally this is in fact what Murray has written, but it is clear from his discussion of his solids stress tensor that it refers to the interaction effects in the solids continuum and not to the stress inside the material. This error is partly eliminated when he compensates for the assumed zero normal stress in the particulate phase (see Chapter 1).

However this point illustrates the difference between Murray's treatment and the present treatment. His total momentum balance is derived for the separate volumes of fluid and solid inside the control volume V, and it is this which leads to the voidage coefficients of the stress tensors which appear in his equations. In his derivation he has stated that the integrals of $\underline{T}_s$ and $\underline{T}_f$ over the actual particles themselves inside the control volume cancel as action and reaction - implying that the particulate phase stress tensor is in some way also responsible for the particle - fluid interaction term. It is here that Murray appears confused about the exact nature of his particulate - phase stress tensor and it only emerges later in his paper that in fact it represents the effect of particle - particle interactions. Integration of this stress tensor over the surface of the particles inside the control volume (the area A_s of the present work) is analogous, in the derivation of the equation of motion of a gas from the Kinetic Theory (see reference (23)), to integrating over the surface of the molecules themselves.

The forces acting on the dispersed phase are (i) the body force (ii) the fluid particle interaction force (iii) the particle - particle interaction force. The equation of motion for the solids is thus

$$\int_V (1-\varepsilon)\left\{\frac{\partial \underline{v}}{\partial t} + (\underline{v}.\mathrm{grad})\underline{v}\right\} dV = \int_V (1-\varepsilon)\rho_s \underline{b}\, dV + \int_V \mathrm{div}\,\underline{T}_s\, dV + \int_V \underline{f}\, dV$$

Writing $\underline{f}$ in terms of the fluid stress tensor and the integral $\underline{I}$ from equation (2,5) (remembering that $n\nu = 1-\varepsilon$), the above equation becomes

$$(1-\varepsilon)\left\{\frac{\partial \underline{v}}{\partial t} + (\underline{v}.\mathrm{grad})\underline{v}\right\} = (1-\varepsilon)\rho_s \underline{b} - (1-\varepsilon)\mathrm{grad}\, p + (1-\varepsilon)\mathrm{div}\,\underline{S}_f + n\underline{I} + \mathrm{div}\,\underline{T}_s \qquad (2,8)$$

The equation of motion for the fluid follows simply by subtracting equation (2, 8) from (2, 7). It could also be obtained by summing the body force and the surface force given by equation (2, 6). It reads

$$\rho_f \varepsilon \left\{ \frac{\partial \underline{u}}{\partial t} + (\underline{u}.\text{grad})\underline{u} \right\} = \rho_f \varepsilon \underline{b} - \varepsilon \,\text{grad}\, p + \varepsilon \,\text{div}\, \underline{S_f} - n\underline{I} \qquad \text{——————} \quad (2,9)$$

Although the discussion so far has been mainly in terms of particles, these equations as they stand are applicable to any type of dispersed two-phase flow which satisfies the assumptions under which these equations are derived. To apply them in any particular situation (for example, a bubble swarm rising in a liquid) the dependence of $\underline{T_s}$ and the integral $\underline{I}$ on the system parameters and flow variables must be known.

The Application of the Equations to the Fluidised State

In applying the above equations to a fluidised bed, it is further assumed that the solid particles are identical with equivalent spherical diameter d_p (generally they will be considered spheres) and that compressibility effects in the fluid can be ignored.

The mass of each particle of volume v is m, so that $\rho_s = m/v$; ρ_s and ρ_f are constant. It is convenient to have the equations in terms of the particle concentration n rather than the voidage ε, and since $\varepsilon = 1 - nv$, the continuity equations (2, 1) and 2, 2) become

$$\frac{\partial}{\partial t}(1 - n\,) + \text{div}\left[(1 - nv)\underline{u}\right] = 0 \qquad \text{——————} \quad (2,10)$$

$$\frac{\partial n}{\partial t} + \text{div}(n\underline{v}) = 0 \qquad \text{——————} \quad (2,11)$$

The momentum equation (2, 8) for the solid phase becomes

$$nm\left\{ \frac{\partial \underline{v}}{\partial t} + (\underline{v}.\text{grad})\underline{v} \right\} = nm\underline{b} - nv\,\text{grad}\, p + nv\,\text{div}\, \underline{S_f} + n\underline{I} + \text{div}\, \underline{T_s} \quad \text{——} \quad (2,12)$$

while (2, 9) for the fluid reads

$$\rho_f(1 - nv)\left\{ \frac{\partial \underline{u}}{\partial t} + (\underline{u}.\text{grad})\underline{u} \right\} = \rho_f(1 - nv)\underline{b} - (1 - nv)\,\text{grad}\, p + (1 - nv)\,\text{div}\, \underline{S_f} - n\underline{I} \qquad \text{——————} \quad (2,13)$$

(a) Particulate Phase Stress Tensor

This represents the force per unit total area exerted by the solid material outside the volume element on the solid inside. It was introduced in a purely formal manner to account for particle - particle interaction and it completes the similarity of the equations of motion for the two interpenetrating phases. It is now necessary to ascribe some form to the term.

$\underline{\underline{T}}_s$ is a second order tensor related to the stress vector on the surface of any volume element by $\underline{t}_s = \underline{n}.\underline{\underline{T}}_s$ where $\underline{t}_s$ is the stress vector and $\underline{n}$ the outwards normal. Because of the fluid-like behaviour of the bed, the most reasonable, and simple, approach is to assume that the particulate phase (treated here as a continuum) behaves as a quasi-Newtonian fluid and hence (written in suffix notation)

$$T_{s_{ij}} = \left(-\Omega + \alpha e^s_{pp}\right)\delta_{ij} + 2\chi e^s_{ij}$$

where e^s_{ij} is the rate of strain tensor for the solid phase and is defined in terms of the local mean particle velocity $\underline{v}$ thus

$$e^s_{ij} = \frac{1}{2}\left(\frac{\partial v_i}{\partial x_j} + \frac{\partial v_j}{\partial x_i}\right),$$

e^s_{pp} is the trace of the rate of strain tensor ie $\partial v_p/\partial x_p$ or div $\underline{v}$. The term Ω is similar to the hydrostatic pressure in a fluid and represents normal stresses in the solids continuum transmitted by particle collisions. The terms α and χ are constants - in fact, χ is the shear viscosity coefficient and α is related to the coefficient of bulk viscosity by $\alpha = \kappa - \frac{2}{3}\chi$ where κ is the bulk viscosity coefficient.

This type of relationship is the simplest which can be used and is probably a gross simplification of the actual state of affairs. It may be that under stress the bed behaves more like a solid mass obeying Hooke's law rather than that above or the behaviour may be more like a Bingham fluid. However the above simple relationship may serve to show the importance of the particle - particle interaction term.

Some necessary conditions for the above expression to be valid are -

(i) That the stress tensor is a continuous function of the rate of strain tensor;

(ii) that the particulate phase is homogenous, that is, the stress tensor is not an explicit function of time and position; this is reasonable in view of the continuum approach to the equations of motion;

(iii) that when $\underline{v}$ is everywhere zero and there is no bulk (that is, other than random collision movements) solid motion, the only stress acting is the normal stress Ω

(iv) that the particulate phase is isotropic; this assumption is doubtful in view of the fact that the bulk of the fluid motion is vertically upwards, so the components of random individual particle velocities (these become zero in the space averaging for $\underline{v}$) in the x - direction are likely to be greater than in the other two directions. However the effects of this are complex and will not be dealt with here.

The mechanism involved in the transmission of stress and the evaluation of the quantities Ω, α and χ is treated further in Appendix 2. These quantities will depend in some way on the physical properties of the system - particle size, density, bed expansion and flow rate. For any one physical system, they will depend on bed expansion and flow rate and so can be treated as functions of the local particle concentration only. Thus

$\Omega = \Omega(n)$: particulate phase collision "pressure"

$\chi = \chi(n)$: particulate phase shear "viscosity"

$\alpha = \alpha(n)$: particulate phase term related to the bulk "viscosity" by $\kappa(n) = \alpha(n) + \frac{2}{3}\chi(n)$

The quantity $\alpha(n)$ will be used in preference to the bulk viscosity. All three quantities are such that they tend to zero as n tends to zero.

Formally then

$$T_{sij} = \left(-\Omega(n) + \alpha(n)\frac{\partial v_k}{\partial x_k}\right)\delta_{ij} + \chi(n)\left(\frac{\partial v_i}{\partial x_j} + \frac{\partial v_j}{\partial x_i}\right)$$

and the divergence of this stress tensor appearing in the solids equation is

$$\frac{\partial T_{sij}}{\partial x_j} = -\frac{\partial \Omega(n)}{\partial x_i} + \frac{\partial}{\partial x_i}\left\{\alpha(n)\frac{\partial v_k}{\partial x_k}\right\} + \frac{\partial}{\partial x_j}\left\{\chi(n)\left(\frac{\partial v_i}{\partial x_j} + \frac{\partial v_j}{\partial x_i}\right)\right\} \qquad (2,14)$$

(b) The Fluid - Particle Interaction Force

Earlier in this chapter, it was shown that the interaction force per unit bed volume (acting on the particles) was given by equation (2,5) as

$$\underline{f} = -n\nabla \text{grad}\, p + n\nabla \text{div}\, \underline{S}_f + n\int_{A_p} \underline{n}\cdot\underline{T}_f'' \, dA$$

This interaction force takes into account both form drag and skin friction, together with the additional force due to bulk movement of the fluid. It is the integral in the above equation which gives rise to the viscous drag terms of the type used in the equations discussed in Chapter 1. In a packed bed with constant interstitial mean fluid velocity, the result of applying the above expression to the equation of motion for the fluid (2,9) gives an expression which can be identified with the Carman - Kozeny equation (see (25)) for the pressure drop. In fact, Pigford (6) used the Carman - Kozeny equation as a basis for the drag term in his equations.

Obviously the above integral cannot be obtained directly and its evaluation depends to a large extent on informed guesswork, based on an extension of the packed bed situation (briefly described above) and on an analogy with the case of an isolated particle in a uniform stream.

For a single small sphere of diameter d_p moving slowly with variable velocity $v_I(t)$ (suffix I refers to one individual particle) in a stationary fluid extending to infinity, Basset (12) gives the following expression for the force exerted by the fluid on the sphere

$$f_I = \frac{18\nu\mu}{d_p^2} v_I(t) + \frac{1}{2}\nu\rho_f \frac{dv_I(t)}{dt} - \frac{18\nu}{d_p}\sqrt{\frac{\rho_f\mu}{\pi}} \int_0^t \frac{dv_I(t-\tau)}{d\tau} \frac{1}{\sqrt{\tau}}\, d\tau .$$

where $v_I(0) = 0$. This equation is not vectorial, and is valid for rectilinear motion only. This expression was obtained by solving the linearised Navier - Stokes equation for an incompressible fluid using the appropriate boundary conditions imposed by the particle. Buoyancy and rotational effects are neglected. The first term is the normal viscous drag (in the case considered by Basset - the Stokesian drag); The second term is equivalent to the virtual mass term found in the mechanics of ideal fluids (see ref. (26)) and the third term is the so-called "Basset" force and is of a rather intractable nature. Houghton (24) gives reasons for neglecting this term - quoting results from Brownian motion studies and studies of particles in accelerating fluid fields. However, because so little is known about the term, they amount to little more than a rationalisation and the term could be quite significant. Following the usual procedure however, this term will be neglected in the following equations. There is some justification for this in the case of a fluidised system. The "Basset" term

depends on the complete past history of the particle motion, and in a fluidised bed this past history will be very rapidly erased by the random motions of the surrrunding particles.

Tchen (27) and Corrsin and Lumley (16) have extended Basset's equation to the case of a particle moving inaa moving fluid, and they both give the interaction force (in vector notation) as

$$\underline{f_I} = -\nu \, \text{grad}\, p + \gamma(\underline{u} - \underline{v_I}) + \frac{\nu}{2}\rho_f \frac{d}{dt}(\underline{u} - \underline{v_I})$$

where p is the fluid pressure and $\underline{u}$ is (for the moment) the fluid velocity in the neighbourhood of the particle, but far enough away to be unaffected by it. The factor $\frac{1}{2}$ in the last term is the virtual mass coefficient. The form $\frac{d}{dt}$ is, at present, unimportant. The second and third terms correspond to the first and second terms in Basset's equation and are due, as in the stationary fluid case, to the distortion of the fluid flow (together with the boundary conditions) round the particle. The parallel with the term $\underline{I}$ in equation (2,5), written in terms of the deviations from the interstitial mean, is clearly seen, even though the viscous part of the fluid stress tensor has been omitted by Tchen and Corrsin and Lumley.

It will be assumed that, in an assembly of particles moving in a moving fluid, the term $\underline{I}$ in equation (2,5) gives rise to two similar terms, namely, a viscous drag term and a virtual mass term. For one particle in the assembly, then, the integral $\underline{I}$ is given by

$$\underline{I} = \phi(\underline{u} - \underline{v}') + \nu\theta\rho_f \frac{d}{dt}(\underline{u} - \underline{v}')$$

where $\underline{u}$ is now the interstitial mean fluid velocity. The coefficient ϕ will depend now on the particle concentration and, if Stokes' law does not hold, on $|\underline{u} - \underline{v}'|$, as well as the particle diameter and fluid viscosity; the virtual mass coefficient for a particle in an assembly will probably depend on the concentration also and is denoted by θ. The interaction force per unit volume due to this term I is given by

$$n\underline{I} = n\phi(n, |\underline{u} - \underline{v}|)(\underline{u} - \underline{v}) + n\nu\theta\rho_f \frac{d}{dt}(\underline{u} - \underline{v}) \qquad \text{——— (2,15)}$$

where $\underline{v}'$ has been replaced by the space averaged particle velocity $\underline{v}$ in accordance with the description of the flow in terms of these mean quantities.

Thus the force per unit bed volume exerted by the fluid on the particles is given by

$$\underline{f} = -n\nabla \text{grad}\, p + n\nabla \text{div}\, \underline{S}_f + n\phi(n, |\underline{u} - \underline{v}|)(\underline{u} - \underline{v}) + n\nu\theta(n)\rho_f \frac{d}{dt}(\underline{u} - \underline{v}) \qquad (2,16)$$

The form of the term $\frac{d}{dt}(\underline{u} - \underline{v})$ is not at all obvious and depends very much on whether the virtual mass force arises from the difference in total acceleration between the fluid and particles or from the rate of change of relative velocity. For a single particle, Corrsin and Lumley (28) write the term in such a way that it depends on the rate of change of relative velocity so that, in the present case, the term would be given by

$$\frac{d}{dt}(\underline{u} - \underline{v}) = \frac{\partial(\underline{u} - \underline{v})}{\partial t} + (\underline{v}.\text{grad})(\underline{u} - \underline{v})$$

following the motion of the particles with $(\underline{u} - \underline{v})$ some quantity associated with this motion. If it depends on the relative acceleration then

$$\frac{d}{dt}(\underline{u} - \underline{v}) = \frac{\partial \underline{u}}{\partial t} + (\underline{u}.\text{grad})\underline{u} - \frac{\partial \underline{v}}{\partial t} - (\underline{v}.\text{grad})\underline{v}$$

and both fluid and particle motions are followed. While the first alternative seems slightly more reasonable, for the work that follows the second is much stronger, and so, if it is not correct, the effect of the virtual mass term will be overestimated. For this reason, the second form will generally be used in the following work.

Murray (14) proposed two completely different forms for this term -

$$\frac{d}{dt}(\underline{u} - \underline{v}) = \frac{\partial(\underline{u} - \underline{v})}{\partial t} + \left\{(\underline{u} - \underline{v}).\text{grad}\right\}(\underline{u} - \underline{v})$$

and, for the whole virtual mass term,

$$n\nu\theta\rho_f\left[\frac{\partial \underline{u}}{\partial t} + (\underline{u}.\text{grad})\underline{u} + \frac{1}{2}\left\{\frac{\partial(\underline{u} - \underline{v})}{\partial t} + (\underline{v}.\text{grad})(\underline{u} - \underline{v})\right\}\right]$$

The first suggestion has no obvious physical meaning since it follows neither fluid nor particle motion. The relatively complicated second term arises from a misunderstanding by Murray of the equation of Corrsin and Lumley (16). The first part of the term (fluid acceleration) arises from the overall pressure drop causing fluid motion and not from the

small scale motion round the particle which produces the virtual mass effect. This point was dealt with at some length in Chapter 1.

It is now possible to apply the general equations of motion for the dispersion to the particular case of a fluidised bed. Inserting equations (2,14) and (2,15) into equations (2,12) and (2,13) and writing these equations in suffix notation, referred to axes the resultant equations of motion for the solid and fluid phases are

$$nm\left\{\frac{\partial v_i}{\partial t} + v_j\frac{\partial v_i}{\partial x_j}\right\} = nmb_i - n\nu\frac{\partial p}{\partial x_i} + n\nu\frac{\partial S_{fij}}{\partial x_j} + n\phi(n,|\underline{u}-\underline{v}|)(u_i-v_i)$$
$$+ n\nu\theta(n)\rho_f\frac{d}{dt}(u_i-v_i) - \frac{\partial\Omega(n)}{\partial x_i} + \frac{\partial}{\partial x_i}\left\{\alpha(n)\frac{\partial v_k}{\partial x_k}\right\}$$
$$+ \frac{\partial}{\partial x_j}\left\{\chi(n)\left(\frac{\partial v_i}{\partial x_j} + \frac{\partial v_j}{\partial x_i}\right)\right\} \qquad \text{——————} (2,17)$$

and

$$\rho_f(1-n\nu)\left\{\frac{\partial u_i}{\partial t} + u_j\frac{\partial u_i}{\partial x_j}\right\} = \rho_f(1-n\nu)b_i - (1-n\nu)\frac{\partial p}{\partial x_i} + (1-n\nu)\frac{\partial S_{fij}}{\partial x_j}$$
$$-n\phi(n,|\underline{u}-\underline{v}|)(u_i-v_i) - n\nu\rho_f\theta(n)\frac{d}{dt}(u_i-v_i) \qquad \text{——————} (2,18)$$

It is worth noting that, apart from the virtual mass term and the difference in stress tensors, the equations of motion for the fluid phase and the solid phase are symmetric, that is, u_i can be replaced by v_i, $n\nu$ by $(1 - n\nu)$ and ρ_s by ρ_f and the same equations result. This is due to the continuum treatment of the flow and the way in which it is regarded as two interpenetrating phases. The differences in the equations enter only as a result of the detailed physics of the situation - when the actual nature of the forces involved is considered.

There are four equations (two continuity and two momentum equations) in the four fields p, n, $\underline{u}$ and $\underline{v}$ and theoretically it should be possible to solve them. However the non-linearity of the equations makes this virtually impossible and their solution can only be obtained in a few simple cases. Nevertheless one simplification can be made by eliminating the fluid pressure (and, incidentally, the viscous stress tensor) thus obtaining three equations in the three fields n, $\underline{u}$ and $\underline{v}$.

The resultant equation on multiplying (2,18) by $n\nu/(1 - n\nu)$ and subtracting this from (2,17) is

$$nm\left\{\frac{\partial v_i}{\partial t} + v_j\frac{\partial v_i}{\partial x_j}\right\} - n\nu\rho_f\left\{\frac{\partial u_i}{\partial t} + u_j\frac{\partial u_i}{\partial x_j}\right\} = n(m-\nu\rho_f)b_i +$$

$$+ \frac{n\phi(n,|\underline{u}-\underline{v}|)}{(1-n\nu)}(u_i-v_i) + \frac{n\nu}{1-n\nu}\theta(n)\rho_f\frac{d}{dt}(u_i-v_i) - \frac{\partial\Omega(n)}{\partial x_i}$$

$$+ \frac{\partial}{\partial x_i}\left\{\alpha(n)\frac{\partial v_k}{\partial x_k}\right\} + \frac{\partial}{\partial x_j}\left\{\chi(n)\left(\frac{\partial v_i}{\partial x_j} + \frac{\partial v_j}{\partial x_i}\right)\right\} \qquad (2,19)$$

This is equivalent to equation (3) of Jackson's paper (5) (equation (1,1) of the present work) with additional terms due to the virtual mass effect and particle - particle interaction.

The above equations are the basic equations of motion for a fluidised bed, under the present assumptions and can be solved in a limited number of cases, namely, uniform flow, a small disturbance from the state of uniform flow and, with a number of approximations, for the case of a fully developed bubble rising in a fluidised bed. Only the first two cases will be considered in the present work.

Uniform fluidisation occurs when the only body force acting is gravity and the particle concentration is constant throughout the bed. The fluid velocity is uniform and the particle velocity is zero throughout the bed. Under these conditions, in a reference frame Oxyz with the positive x-direction vertically upwards, $\underline{b} = \underline{i}g$, grad p $(= \underline{i}\,\partial p/\partial x)$ is uniform throughout the bed and can be written $\Delta p/\Delta x$ (Δx is the bed height) and $\underline{u} = \underline{i}u_0$; $\underline{i}$ is the unit vector in the x-direction. Equation (2,18) then becomes

$$-\rho_f g - \frac{\Delta p}{\Delta x} - u_0\frac{n\phi(n,|\underline{u}-\underline{v}|)}{1-n\nu} = 0.$$

Thus part of the pressure drop in the fluid is due to the change in head and part is due to the drag force on the particles. Neglecting the change in head the pressure drop due to drag is

$$\frac{\Delta p}{\Delta x} = -u_0\frac{n\phi(n,|\underline{u}-\underline{v}|)}{1-n\nu}$$

Thus, substituting the expression for $\Delta p/\Delta x$ into equation (2,16), the interaction force $\underline{f}$ for uniform fluidisation is given, neglecting gravity, by

$$\underline{f} = \underline{i}u_0\frac{n\nu}{1-n\nu}n\phi(n,|\underline{u}-\underline{v}|) + \underline{i}u_0 n\phi(n,|\underline{u}-\underline{v}|)$$

Thus $$\underline{f} = \underline{i}\, u_0 \frac{n\phi(n, |\underline{u}-\underline{v}|)}{1-nv}$$

$$= \underline{i}\, u_0 \beta(n)$$

where $\beta(n) = \frac{n\phi(n, |\underline{u}-\underline{v}|)}{1-nv}$ and this is the drag force as originally defined by Jackson (5) i.e. the force experienced by a uniform assembly of particles in a uniform stream in the absence of gravitational forces. From equation (2,19) it is seen that

$$n(m - v\rho_f)g = u_0\beta(n) \qquad \text{(2,20)}$$

that is, the drag force on the particles is equal to their buoyant weight.

Equation (2,19) can now be re-written as

$$nm\left\{\frac{\partial v_i}{\partial t} + v_j \frac{\partial v_i}{\partial x_j}\right\} - nv\rho_f\left\{\frac{\partial u_i}{\partial t} + u_j \frac{\partial u_i}{\partial x_j}\right\}$$

$$= n(m - v\rho_f) b_i + \beta(n)(u_i - v_i) + \frac{nv}{1-nv}\theta(n)\rho_f \frac{d}{dt}(u_i - v_i)$$

$$- \frac{\partial \Omega(n)}{\partial x_i} + \frac{\partial}{\partial x_i}\left\{\alpha(n)\frac{\partial v_k}{\partial x_k}\right\} + \frac{\partial}{\partial x_j}\left\{\gamma(n)\left(\frac{\partial v_i}{\partial x_j} + \frac{\partial v_j}{\partial x_i}\right)\right\}$$

(2,21)

and it is this equation, together with the two continuity equations, which is used in the investigation of the stability of the uniformly fluidised state, dealt with in the following chapter.

Before any quantitative results can be obtained, however, the dependence of the functions $\beta, \theta, \Omega, \alpha$ and γ on n must be known. These terms are discussed in Appendix 2 where it is shown that, for any one physical situation, it is reasonable to consider them as functions of the particle concentration alone.

CHAPTER 3

The Stability of the State of Uniform Fluidisation and Some Possible Voidage Gradients in the Bed

Section I: The Stability of the State of Uniform Fluidisation

As noted above in the section on the detailed equations for a fluidised bed, the state of uniform fluidisation is characterised by the equations, for a co-ordinate system Oxyz,

$$\frac{\partial p}{\partial x} = -\rho_f g - u_o \beta(n_o)$$

and
$$u_o \beta(n_o) = n_o (m - v\rho_f) g \qquad (2,20)$$

The particle concentration n_o is constant and all the flow fields are uniform with $\underline{u} = \underline{i}u_o$, $\partial p/\partial x = \Delta p/\Delta x$ (a constant) and $\underline{v}$ everywhere zero.

The stability of this state is investigated by a standard method, long used in the study of the stability of laminar boundary layers (see, for example, reference (28)). Small changes are superposed on the uniform flow fields and the growth or decay of these disturbances in time is studied. Thus the variables n, $\underline{u}$, $\underline{v}$ and p can be written as

$\underline{u} = \underline{u}_o + \underline{u}_1$, where $\underline{u}_o = \underline{i}u_o$ and $\underline{u}_1 \ll \underline{u}_o$

$\underline{v} = \underline{v}_1$ with $\underline{v}_1$ small

$n = n_o + n_1$ where $n_1 \ll n_o$

and $\text{grad}\, p = \underline{i}\frac{\Delta p}{\Delta x} + \text{grad}\, p_1$ with $\frac{\partial p_1}{\partial x}, \frac{\partial p_1}{\partial y}, \frac{\partial p_1}{\partial z} \ll \frac{\Delta p}{\Delta x}$

As noted above, the disturbances $\underline{u}_1$, $\underline{v}_1$, n_1 and $\text{grad}\, p_1$ are all small in magnitude. They are considered smooth and their gradients are also considered to be smooth and small, so that all quantities of second or higher order can be neglected. Because of this the equations of motion can be linearised and readily solved.

There are three equations in the three unknowns n, $\underline{u}$ and $\underline{v}$ (equation (2,21) and the two continuity equations). In equation (2,21) the factor $\frac{d}{dt}(u_i - v_i)$ appearing in the virtual mass term will be taken to have the

form $$\frac{d}{dt}\left(u_i - v_i\right) = \left\{\frac{\partial u_i}{\partial t} + u_j\frac{\partial u_i}{\partial x_j}\right\} - \left\{\frac{\partial v_i}{\partial t} + v_j\frac{\partial v_i}{\partial x_j}\right\} .$$

A comparison of the effects of using the above form and the form $\left\{\frac{\partial u_i}{\partial t} - \frac{\partial v_i}{\partial t}\right\} + v_j\frac{\partial}{\partial x_j}\left(u_i - v_i\right)$ will be made when discussing the final equations obtained. When the above expressions are substituted into equations (2,10) and (2,11) and second order quantities neglected, the continuity equation for the fluid becomes

$$-\nu\frac{\partial n_1}{\partial t} + \left(1 - n_0\nu\right)\frac{\partial u_{1i}}{\partial x_i} - \nu u_{0i}\frac{\partial n_1}{\partial x_i} = 0 \qquad \text{——————} \quad (3,1)$$

and that for the particulate phase becomes

$$\frac{\partial n_1}{\partial t} + n_0\frac{\partial v_{1i}}{\partial x_i} = 0 \qquad \text{——————} \quad (3,2)$$

These equations are in tensor notation and referred to reference frame Ox_i , i = 1, 2, 3.

Since $\beta(n)$, $\theta(n)$, $\Omega(n)$, $\chi(n)$ and $\alpha(n)$ are all considered functions of n alone (see Appendix 2), they can be expanded in a Taylor series about n_0 giving

$$f\left(n_0 + n_1\right) = f\left(n_0\right) + \left(\frac{df}{dn}\right)_{n=n_0} n_1 + O\left[n_1^2\right]$$

Indicating all first derivatives of these functions with respect to n and evaluated at n_0 as f_0' , e.g. $\left(\frac{d\Omega}{dn}\right)_{n=n_0}$ is Ω_0', and writing $\beta(n_0)$, $\chi(n_0)$, etc. as β_0, χ_0 etc., the linearised equation (2,21) becomes

$$\left\{n_0 m + \frac{n_0\nu}{1-n_0\nu}\rho_f\theta_0\right\}\frac{\partial v_{1i}}{\partial t} - \left\{n_0\nu\rho_f + \frac{n_0\nu}{1-n_0\nu}\rho_f\theta_0\right\}\left\{\frac{\partial u_{1i}}{\partial t} + u_{0j}\frac{\partial u_{1i}}{\partial x_j}\right\}$$

$$= n_0\left(m - \nu\rho_f\right)b_i + n_1\left(m - \nu\rho_f\right)b_i + u_{0i}\beta_0 + \beta_0\left(u_{1i} - v_{1i}\right) + u_{0i}n_1\beta_0'$$

$$- \Omega_0'\frac{\partial n_1}{\partial x_i} + \alpha_0\frac{\partial}{\partial x_i}\left(\frac{\partial v_k}{\partial x_k}\right) + \chi_0\frac{\partial}{\partial x_j}\left(\frac{\partial v_{1i}}{\partial x_j} + \frac{\partial v_{1j}}{\partial x_i}\right)$$

In dyadic notation, noting that $\underline{u}_0 = \underline{i}u_0$, $(\underline{u}_0 \cdot \text{grad}) = u_0\frac{\partial}{\partial x}$, $\underline{b} = -\underline{i}g$ and $u_0\beta(n_0) = n_0(m - \nu\rho_f)g$ the above equation reduces to

$$\left\{n_0 m + \frac{n_0 \nu}{(1-n_0\nu)}\rho_f\theta_0\right\}\frac{\partial \underline{v}_1}{\partial t} - \left\{n_0\nu\rho_f + \frac{n_0\nu}{1-n_0\nu}\rho_f\theta_0\right\}\left\{\frac{\partial \underline{u}_1}{\partial t} + u_0\frac{\partial \underline{u}_1}{\partial x}\right\}$$

$$= -\underline{i}\,n_1(m-\nu\rho_f)g + \beta_0(\underline{u}_1 - \underline{v}_1) + \underline{i}\,n_1\beta_0' u_0 - \Omega_0' \operatorname{grad} n_1 +$$

$$+ (\alpha_0 + \chi_0)\operatorname{grad}\operatorname{div}\underline{v}_1 + \chi_0\left(\frac{\partial^2}{\partial x^2} + \frac{\partial^2}{\partial y^2} + \frac{\partial^2}{\partial z^2}\right)\underline{v}_1$$

——————— (3,3)

The velocity vectors $\underline{u}_1$ and $\underline{v}_1$ can be eliminated from equations (3,1), (3,2) and (3,3) by taking the divergence of (3,3) and substituting for $\operatorname{div}\underline{u}_1$ and $\operatorname{div}\underline{v}_1$ from the continuity equations. The final equation obtained, after some manipulation, is

$$-\left\{\frac{m}{n_0\nu^2} + \frac{\rho_f}{1-n_0\nu} + \frac{\theta_0\rho_f}{n_0\nu(1-n_0\nu)^2}\right\}\frac{\partial^2 n_1}{\partial t^2} + \left[-\frac{2\rho_f u_0}{(1-n_0\nu)}\left(1+\frac{\theta_0}{1-n_0\nu}\right)\frac{\partial}{\partial x} -\right.$$

$$\left. - \frac{\beta_0}{n_0\nu(1-n_0\nu)} - \frac{\beta_0}{(n_0\nu)^2} + \frac{(\alpha_0+2\chi_0)}{(n_0\nu)^2}\nabla^2\right]\frac{\partial n_1}{\partial t} + \left\{\frac{u_0\beta_0}{(n_0\nu)^2}\frac{\partial}{\partial x} -\right.$$

$$\left. - \frac{u_0\beta_0'}{n_0\nu^2}\cdot\frac{\partial}{\partial x} - \frac{u_0\beta_0}{n_0\nu(1-n_0\nu)}\frac{\partial}{\partial x} + \frac{\Omega_0'}{n_0\nu^2}\nabla^2 - \frac{\rho_f u_0^2}{1-n_0\nu}\left(1+\frac{\theta_0}{1-n_0\nu}\right)\frac{\partial^2}{\partial x^2}\right\} n_1$$

$$= 0$$

Since $m/\nu = \rho_s$, the uniform voidage $\varepsilon_0 = 1 - n_0\nu$, $\beta_0 = (1-\varepsilon_0)(\rho_s - \rho_f)g/u_0$ and $\bar{u}_0 = \varepsilon_0 u_0$, where $\bar{u}_0$ is the superficial mean fluid velocity, the differential equation for n, is, after multiplying through by ε_0/ρ_f

$$\left[1 + \frac{\rho_s}{\rho_f}\cdot\frac{\varepsilon_0}{(1-\varepsilon_0)} + \frac{\theta_0}{\varepsilon_0(1-\varepsilon_0)}\right]\frac{\partial^2 n_1}{\partial t^2} + \left[2\left(\frac{\bar{u}_0}{\varepsilon_0}\right)\left(1+\frac{\theta_0}{\varepsilon_0}\right)\frac{\partial}{\partial x} + \frac{\rho_s-\rho_f}{\rho_f}\cdot\frac{\varepsilon_0}{(1-\varepsilon_0)}\cdot\frac{g}{\bar{u}_0} -\right.$$

$$\left. - \frac{(\alpha_0+2\chi_0)}{\rho_s(1-\varepsilon_0)}\cdot\frac{\rho_s}{\rho_f}\cdot\frac{\varepsilon_0}{(1-\varepsilon_0)}\nabla^2\right]\frac{\partial n_1}{\partial t} + \left[\frac{\rho_s-\rho_f}{\rho_f}\cdot\frac{\varepsilon_0}{1-\varepsilon_0}\cdot\frac{g}{\bar{u}_0}\left(1-2\varepsilon_0+\varepsilon_0\frac{n_0\beta_0'}{\beta_0}\right)\left(\frac{\bar{u}_0}{\varepsilon_0}\right)\frac{\partial}{\partial x} -\right.$$

$$\left. - \frac{n_0\Omega_0'}{\rho_s(1-\varepsilon_0)}\cdot\frac{\varepsilon_0}{1-\varepsilon_0}\cdot\frac{\rho_s}{\rho_f}\nabla^2 + \left(\frac{\bar{u}_0}{\varepsilon_0}\right)^2\left(1+\frac{\theta_0}{\varepsilon_0}\right)\frac{\partial^2}{\partial x^2}\right] n_1 = 0$$

——————— (3,4)

where $\nabla^2 \equiv \frac{\partial^2}{\partial x^2} + \frac{\partial^2}{\partial y^2} + \frac{\partial^2}{\partial z^2}$

If the other form of the virtual mass term is used i.e.

$$\frac{d}{dt}(\underline{u} - \underline{v}) = \frac{\partial}{\partial t}(\underline{u} - \underline{v}) + (\underline{v} \cdot \text{grad})(\underline{u} - \underline{v})$$

the left hand side of equation (3,3), after linearisation $\left(\frac{d}{dt}(\underline{u}-\underline{v}) = \frac{\partial \underline{u}_1}{\partial t} - \frac{\partial \underline{v}_1}{\partial t} \right)$, becomes

$$\left\{ n_0 m + \frac{n_0 \nu \rho_f \theta_0}{1 - n_0 \nu} \right\} \frac{\partial \underline{v}_1}{\partial t} - n_0 \nu \rho_f \left(1 + \frac{\theta_0}{1 - n_0 \nu} \right) \frac{\partial \underline{u}_1}{\partial t} - n_0 \nu \rho_f u_0 \frac{\partial \underline{u}_1}{\partial x}$$

After taking the divergence, the differential equation for n_1, equivalent to equation (3,4) is

$$\left[1 + \frac{\rho_s}{\rho_f} \cdot \frac{\varepsilon_0}{1-\varepsilon_0} + \frac{\theta_0}{\varepsilon_0(1-\varepsilon_0)} \right] \frac{\partial^2 n_1}{\partial t^2} + \left[\left(\frac{\bar{u}_0}{\varepsilon_0} \right) \left(2 + \frac{\theta_0}{\varepsilon_0} \right) \frac{\partial}{\partial x} + \frac{\rho_s - \rho_f}{\rho_f} \cdot \frac{\varepsilon_0}{1-\varepsilon_0} \cdot \frac{q}{d \bar{u}_0} - \right.$$

$$\left. - \frac{(\alpha_0 + 2\chi_0)}{\rho_s(1-\varepsilon_0)} \cdot \frac{\rho_s}{\rho_f} \cdot \frac{\varepsilon_0}{1-\varepsilon_0} \cdot \nabla^2 \right] \frac{\partial n_1}{\partial t} + \left[\frac{\rho_s - \rho_f}{\rho_f} \cdot \frac{\varepsilon_0}{1-\varepsilon_0} \cdot \frac{q}{d \bar{u}_0} \left(1 - 2\varepsilon_0 + \varepsilon_0 \frac{n_0 \beta_0'}{\beta_0} \right) \left(\frac{\bar{u}_0}{\varepsilon_0} \right) \frac{\partial}{\partial x} \right.$$

$$\left. - \frac{n_0 \Omega_0'}{\rho_s(1-\varepsilon_0)} \cdot \frac{\rho_s}{\rho_f} \cdot \frac{\varepsilon_0}{1-\varepsilon_0} \cdot \nabla^2 + \left(\frac{\bar{u}_0}{\varepsilon_0} \right)^2 \frac{\partial^2}{\partial x^2} \right] n_1 = 0 .$$

Obviously the effect of the virtual mass term in this form is not so great. In all the work which follows, it is the stronger form of the term which is used.

Defining

$$A = 1 + \frac{\rho_s}{\rho_f} \cdot \frac{\varepsilon_0}{1-\varepsilon_0} + \frac{\theta_0}{\varepsilon_0(1-\varepsilon_0)}$$

$$B = \frac{\rho_s - \rho_f}{\rho_f} \cdot \frac{\varepsilon_0}{1-\varepsilon_0} \cdot \frac{q}{d \bar{u}_0} \qquad [T^{-1}]$$

$$E = 1 - 2\varepsilon_0 + \varepsilon_0 \frac{n_0 \beta_0'}{\beta_0}$$

$$D = \frac{\rho_s}{\rho_f} \cdot \frac{\varepsilon_0}{1-\varepsilon_0}$$

$$F = 1 + \frac{\theta_0}{\varepsilon_0}$$

which quantities are constant for any one situation, equation (3,4) becomes

$$A\frac{\partial^2 n_1}{\partial t^2} + 2F\left(\frac{\bar{u}_0}{\varepsilon_0}\right)\frac{\partial^2 n_1}{\partial x\,\partial t} - \frac{D(\alpha_0 + 2\gamma_0)}{\rho_s(1-\varepsilon_0)}\frac{\partial}{\partial t}(\nabla^2 n_1) - \frac{D n_0 \Omega_0'}{\rho_s(1-\varepsilon_0)}\nabla^2 n_1$$

$$+ F\left(\frac{\bar{u}_0}{\varepsilon_0}\right)^2\frac{\partial^2 n_1}{\partial x^2} + B\frac{\partial n_1}{\partial t} + BE\left(\frac{\bar{u}_0}{\varepsilon_0}\right)\frac{\partial n_1}{\partial x} = 0 \qquad (3,5)$$

For this equation, a solution is required in which the variables are separable, that is, the disturbance n_1 has the form

$$n_1 = R(\underline{r})T(t)$$

and further, the function R is assumed to be sinusoidal. Because equation (3,5) is linear in n_1, an initial disturbance of the uniform state which is a solution of (3,5) can be synthesised from the superposition of monochromatic plane waves, which are also solutions of (3,5), by Fourier synthesis. A disturbance component sinusoidal in distance will have the form

$$n_1 = f(t)\exp[j\underline{k}\cdot\underline{r}]$$

where $\underline{k}$ is the wave number vector with Cartesian components k_x, k_y and k_z.

Substituting the above expression for n_1 into equation (3,5) the resultant equation is

$$A\frac{d^2 f}{dt^2} + \left[B + 2jF\left(\frac{\bar{u}_0 k_x}{\varepsilon_0}\right) + D\frac{(\alpha_0 + 2\gamma_0)}{\rho_s(1-\varepsilon_0)}(k_x^2 + k_y^2 + k_z^2)\right]\frac{df}{dt}$$

$$+ \left[jBE\left(\frac{\bar{u}_0 k_x}{\varepsilon_0}\right) + \frac{D n_0 \Omega_0'}{\rho_s(1-\varepsilon_0)}(k_x^2 + k_y^2 + k_z^2) - F\left(\frac{\bar{u}_0 k_x}{\varepsilon_0}\right)^2\right] f = 0.$$

Defining

$$b = \frac{\bar{u}_0 k_x}{\varepsilon_0} \qquad [T^{-1}],$$

$$c = \frac{(\alpha_0 + 2\gamma_0)}{\rho_s(1-\varepsilon_0)}(k_x^2 + k_y^2 + k_z^2) \qquad [T^{-1}],$$

$$e = \frac{n_0 \Omega_0'}{\rho_s(1-\varepsilon_0)}(k_x^2 + k_y^2 + k_z^2) \qquad [T^{-2}],$$

the second order ordinary differential equation with complex coefficients for f(t) is

$$A\frac{d^2f}{dt^2} + \left[B + cD + j2Fb\right]\frac{df}{dt} + \left[De - Fb^2 + jBEb\right]f = 0 \qquad (3,6)$$

This has a solution of the form $f(t) = \exp(st)$ and the roots of the auxiliary equation are

$$s_{1,2} = \frac{B}{2A}\left[-\left(1 + \frac{Dc}{B} + j\frac{2Fb}{B}\right) \pm \sqrt{\cdots}\right.$$

$$\left. \pm \sqrt{\left(1 + \frac{Dc}{B}\right)^2 + 4\left(\frac{b}{B}\right)^2\left\{F(A-F) - \frac{ADe}{b^2}\right\} - j4\left(\frac{b}{B}\right)\left\{AE - F - \frac{FDc}{B}\right\}}\right]$$

i.e. $$s_{1,2} = \frac{B}{2A}\left[-\left(1 + \frac{Dc}{B} + j\frac{2Fb}{B}\right) \pm \sqrt{(1 + p - jq)}\right] \qquad (3,7)$$

where $$p = 2\left(\frac{Dc}{B}\right) + \left(\frac{Dc}{B}\right)^2 + 4\left(\frac{b}{B}\right)\left\{F(A-F) - \frac{ADe}{b^2}\right\} \qquad (3,8)$$

and $$q = 4\left(\frac{b}{B}\right)\left\{AE - F - \frac{FDc}{B}\right\} \qquad (3,9)$$

From the work that has gone before and the discussion in Appendix 2, it is seen that each single term appearing in the above expression for the roots s_1 and s_2 is positive. Without calculations for various cases, little can be said, however, of their relative magnitudes and hence, of the signs of p and q — they could be either positive or negative quantities.

When all the possibilities of relative magnitude of all the terms and all the combinations of p either positive or negative with q either positive or negative are investigated in the complex plane, it is seen that expressions for s may take any of the forms –

(i) $s = a - jd$

(ii) $s = -a - jd$ (both roots are included)

(iii) $s = -a + jd$

where a and d are always positive. No combination of signs or magnitudes can ever give rise to an expression $s = a + jd$. Corresponding to these three cases, the disturbance component takes the form –

(i) $n_1 = N_0 \exp(at) \exp[j(\underline{k}.\underline{r} - dt)]$

(ii) $n_1 = N_0 \exp(-at) \exp[j(\underline{k}.\underline{r} - dt)]$

(iii) $n_1 = N_0 \exp(-at) \exp[j(\underline{k}.\underline{r} + dt)]$

where N_o is the amplitude of the original disturbance.

Case (i) represents a plane wave travelling in the direction of $\underline{k}$ with an amplitude increasing with time. Case (ii) represents a plane wave also travelling in the direction of $\underline{k}$ but with an amplitude which decreases with time, while case (iii) represents a plane wave propagating in the direction opposite to $\underline{k}$ but with an amplitude decreasing with time. The time origin is taken as the time of first appearance of a single disturbance.

Physically, a disturbance of type (i) is the most important since its amplitude increases during propagation, and if this type arises in a bed, the uniformly fluidised state as defined above would be unstable. A disturbance of either of the other two types has an amplitude which decays with time and if this type occurs, the uniformly fluidised state would be stable. The main interest is thus in disturbances of the form

$$n_1 = N_o \exp[\xi t] \exp[j(\underline{k}.\underline{r} - \eta t)] \qquad (3,10)$$

where $s = \xi - j\eta$ and ξ and η may be either positive or negative quantities, but generally appear, from most of the calculations of the present work, to be positive. This type of disturbance can only arise when the positive square root in equation (3,7) is taken; if the Argand diagram is drawn it is seen that the negative root cannot give rise to this type of expression for s . For any one physical situation, defined by constant ε_o and $\bar{u}_o$, ξ and η are functions of the components of $\underline{k}$.

$\xi = \xi(\underline{k})$ is the amplification factor and is given by

$$\xi(\underline{k}) = \frac{B}{2A}\left[-\left(1+\frac{Dc}{B}\right) + \sqrt{\frac{\left[(1+p)^2+q^2\right]^{1/2} + (1+p)}{2}}\right] \qquad (3,11)$$

and $\eta = \eta(\underline{k})$ is the angular frequency, given by

$$\eta(\underline{k}) = \frac{B}{2A}\left[\frac{2Fb}{B} + \sqrt{\frac{\left[(1+p)^2+q^2\right]^{1/2} - (1+p)}{2}}\right] \qquad (3,12)$$

The propagation properties of this wave are the wave-length λ , the phase velocity V_p , the rate of growth of the amplitude in time, the growth distance Δx (this last quantity being defined as the distance over which the amplitude increases in the ratio e : 1 i.e. 2.718 : 1) and the two quantities defined above. These propagation properties are, for any one fluidised state, functions of the components of the wave

number vector and are given by

$$\lambda = \frac{2\pi}{(k_x^2 + k_y^2 + k_z^2)^{1/2}} \qquad [L.]$$

$$V_p = \frac{\eta(\underline{k})}{(k_x^2 + k_y^2 + k_z^2)^{1/2}} \qquad [LT^{-1}]$$

$$\Delta x = \frac{\eta(\underline{k})}{\xi(\underline{k})\,(k_x^2 + k_y^2 + k_z^2)^{1/2}} = \frac{V_p}{\xi} \qquad [L]$$

and $$\frac{d}{dt}\left(N_0 \exp[\xi(\underline{k})t]\right) = N_0 \exp.[\xi(\underline{k})t].\ \xi(\underline{k}).$$

Note that Δx is a measure of the rate of growth of the disturbance with distance and that $\xi(\underline{k})$ determines its rate of growth in time.

Murray (14) has also attempted to investigate the stability of a uniformly fluidised bed. To obtain his dispersion relationship, he used a different method of solution of the four linearised simultaneous differential equations in p_1, n_1, $\underline{u}_1$ and $\underline{v}_1$. He anticipated a more complete form of the exponential or wave character of the disturbance, assuming they were given, in the notation of the present work, by expressions of the form

$$n_1 = N \exp\left[j\delta(y - ct) + \zeta(x - x_t)\right]$$
$$\underline{u}_1 = \underline{U} \exp\left[j\delta(y - ct) + \zeta(x - x_t)\right]$$
etc.

where N, $\underline{U}$ are constants, x_t is the height of the bed, δ is the wave number vector component in the horizontal y direction, ζ is the wave number component in the vertical x direction and c is the phase velocity. He considered only a two dimensional disturbance. If it is compared with the expression found in the present work - for a two dimensional disturbance this is

$$\exp\left[j(k_x x + k_y y)\right] \exp[st],$$

it is seen that there is one important difference. He uses a dimensionless parameter $z = \zeta/\delta$ to obtain his final dispersion relationship for c (equivalent to equation (3,7)). It is never explicitly stated whether c is complex or not. However Murray assumes that z is purely imaginary, and this can only occur for a travelling wave solution, if ζ is imaginary and δ real. Hence to obtain any solution capable of growth, the phase velocity c must be complex.

It now becomes obvious that Murray's disturbance cannot exist as a one dimensional wave travelling vertically upwards (for this δ is zero and only a stationary disturbance, independent of time, remains in the vertical direction). It is an oddly restricted form to choose.

Having chosen this form of disturbance, he substitutes the expressions for n_1, $\underline{u}_1$, $\underline{v}_1$ and p_1 into his four equations to give four equations in the constant vectors for $\underline{u}_1$ and $\underline{v}_1$ and the constants for n_1 and p_1. For a non-trivial solution, the eliminant of these four equations (six scalar equations) must be zero, and it is this determinant of the coefficients which gives the final dispersion relationship between the complex phase velocity and the wave number components. Murray has in no way simplified his equations and the method of solution thus involves evaluating, for a two dimensional solution, a 6 by 6 determinant of very complicated complex quantities.

One significant point does emerge from Murray's solution - his expression for the phase velocity "c" is a quartic equation with two quadratic factors, giving four possible disturbances, while the expression for the angular frequency "s" of the present work is a quadratic, giving only two possible disturbances. However these extra two solutions, while valid mathematically, are of little interest from the point of view of bubble origin and growth since they correspond to a solution for which there is no perturbation whatsoever of the uniform bed voidage.

If Murray's method of solution were to be used on the equations developed here, the basic equations to be solved would be (3,1), (3,2), (3,3) and the linearised version of (2,18). A solution assuming disturbances of the form

$m_1 = M \exp[j(k_x x + k_y y)] \exp[st]$ (where m_1 is any of the vector or scalar disturbances and M is constant) can be simplified by using eq.(3,4) and the equation in n_1 and p_1 obtained from the linearised version of (2,18) by taking the divergence and eliminating $\underline{u}_1$ and $\underline{v}_1$ using equations (3,1) and (3,2). The equations to be solved are thus reduced to two equations in n_1, $\underline{u}_1$ and $\underline{v}_1$ (the continuity equations), an equation in n_1 alone (eq.(3,4)) and an equation in n_1 and p_1.

Because one of these equations is solely in terms of n_1, the eliminant of the coefficients of the constant quantities M has as a factor the coefficient of n_1 obtained from equation (3,4) and this is exactly the quadratic in s obtained from equation (3,6). Another trivial factor turns out to be $(k_x^2 + k_y^2)$ and the third factor is the additional quadratic in s found by Murray. If the roots of this additional quadratic are used to find the two-dimensional disturbances, then

the first quadratic factor (the solution used here) cannot be zero unless the two factors are identical. Thus, from equation (3,6), n must be zero and there is no perturbation of the particle concentration. For this solution, since $n_1 = 0$, div $\underline{u}_1 = 0$ and div $\underline{v}_1 = 0$, that is, $\underline{k}.\underline{v}_1 = 0$ and $\underline{k}.\underline{u}_1 = 0$. This second solution therefore produces disturbances in the fluid velocity and solid velocity which are orthogonal to the wave number vector but which do not give any perturbation of the bed voidage.

(a) <u>One Dimensional Disturbance</u>

From the general relationships (3,7), (3,8) and (3,9) and a knowledge of the bed parameters and wave number components, it can be ascertained if any disturbance of the state of uniform fluidisation leads to a breakdown of the state. However before the propagation properties of any amplifying disturbance can be found, a knowledge of the boundary conditions in the yz plane is necessary. These boundary conditions determine the value of k_y and k_z and are treated in the next section.

There are no boundary conditions in the x direction because of the free surface and so k_x is some freely varying parameter within any one physical situation, although an upper bound of physical significance is set on k_x by the particle size. Because of the assumptions made in the derivation of the equations, a disturbance whose wave length is of the same order of smallness as the particle diameter has no meaning. For a one dimensional disturbance of any given uniform state, k_y and k_z are zero and the propagation properties are functions of k_x alone. This is the type of disturbance which would be produced by a piston source acting over the whole flow area if wall effects are neglected.

The results of the last section stand and the form of the disturbance leading to instability is

$$n_1 = N_0 \exp[\xi t] \exp[j(k_x x - \eta t)] .$$

where ξ and η are given by equations (3,11) and (3,12). It is worth considering the limits of the amplification factor and the phase velocity as the wave number tends to zero and to infinity (even though this latter case is physically meaningless). These limits give some insight into the importance of some of the bed parameters and afford a ready comparison with the case, discussed by Jackson (5) where particle - particle interaction effects are not considered.

For small values of k_x such that terms with powers of k_x higher than the second can be neglected, the equations for ξ, η and V_p reduce to

$$\lim_{k_x \to 0} \xi(k_x) = \frac{b^2}{B}\left[AE^2 + F(1-2E) - \frac{De}{b^2}\right]$$

$$\lim_{k_x \to 0} \eta(k_x) = bE \quad \text{giving}$$

$$\lim_{k_x \to 0} V_p = \frac{bE}{k_x} \qquad \text{(3,13)}$$

Thus, at low k_x, $\xi(k_x)$ is parabolic in k_x (since De/b^2 is independent of k_x) and the angular frequency $\eta(k_x)$ is given by

$$\eta(k_x) = \frac{\bar{u}_o k_x}{\varepsilon_o}\left(1 - 2\varepsilon_o + \varepsilon_o \frac{n_o \beta_o'}{\beta_o}\right)$$

and this tends to zero as k_x tends to zero. The phase velocity is independent of k_x and is given by

$$V_p = \frac{\bar{u}_o}{\varepsilon_o}\left(1 - 2\varepsilon_o + \varepsilon_o \frac{n_o \beta_o'}{\beta_o}\right)$$

The form of $\xi(k_x)$ is particularly interesting. It is seen that the particle "viscosity" term does not appear in the expression but the normal stress term may be of considerable importance. From the large number of calculations on a variety of systems carried out in the course of the present work, it was found that $[AE^2 + F(1 - 2E)]$ was positive (although this need not necessarily be so) so that the amplification factor is generally positive provided De/b^2 is small and positive. This term De/b^2 depends on the particle "pressure" term $n_o \Omega_o'$ (assumed positive) and if this is sufficiently large ξ will be negative. Thus the particle normal stress appears to have a stabilising effect on the bed and if sufficiently large, will damp out any disturbances present.

For large k_x (corresponding to disturbances of limited extent in the x direction) the limits of ξ, η and V_p are

$$\lim_{k_x \to \infty} \xi(k_x) = \frac{B}{2A}\left[1 + \frac{2b^2}{BDc}\left\{F(1 + A - F) - \frac{ADe}{b^2}\right\}\right]$$

$$\lim_{k_x \to \infty} \eta(k_x) = \frac{3bF}{A} \quad \text{giving}$$

$$\lim_{k_x \to \infty} V_p = \frac{3\bar{u}_o}{\varepsilon_o} \cdot \frac{F}{A} \qquad \text{(3,14)}$$

From the definitions of A and F, and provided AD_e/b^2 is sufficiently small, it is seen that the amplification factor is a positive constant (b^2/c is independent of k_x). This again demonstrates the stabilising effect of normal stresses in the dispersed phase. If the particulate phase "viscosity" term is neglected or is very small the amplification factor becomes infinite at very large k_x. This is the result obtained by Jackson (5). The limit of η is linear in k_x and so becomes large at large k_x while the phase velocity Vp remains constant.

The above limits at large and small k_x demonstrate the importance of the particulate phase stress tensor terms in stabilising the bed (though not necessarily producing complete stability). For disturbances of large wave-length, the shear stress terms are unimportant but for disturbances of short wave-length, they have the effect of reducing the amplification factor to a finite value. For both limits, the normal stress term may be extremely important.

It is difficult to generalise further about the effect of any of the bed parameters and computation for a number of specific cases is probably more useful for showing the dependence of the propagation properties on these bed parameters.

(b) Boundary Conditions and Bounded Flow

In the present work, it has been observed that disturbances appear just above the bed distributor and this is in keeping with Tamarin's explanation (29) of the origin of self-excited oscillations in a fluidised bed. If there is some residual velocity distribution through the distributor and if, as is fairly likely, especially for narrow tubes (with which most of the experimental work was concerned) this velocity distribution is axisymmetric, an axisymmetric form may well be imposed on the disturbance. This is likely to occur only in narrow tubes; in tubes of larger diameter, the distributor design will obviously be extremely important and the axisymmetric form is very unlikely.

The discussion here is concerned only with these axisymmetric disturbances. The origin of the co-ordinate system is now defined as being in the centre of the distributor with the x-axis vertically upwards as before. The position vector $\underline{r}$ has components x, y, z in the rectangular reference frame or x, ρ, θ in cylindrical co-ordinates

$$x \equiv x$$
$$y \equiv \rho \cos\theta$$
$$z \equiv \rho \sin\theta$$

Voidage profiles have been measured in both packed and fluidised beds (see, for example, ref.(2)) and it has been found that the voidage increases rapidly over a region a few particle diameters wide close to the wall. However this is a local packing effect and because of the smallness of the distance and the large variation in voidage across this distance, this phenomenon cannot be treated by the continuum equations used here. In the bulk of the flow area away from the walls, the variation in voidage due to packing effects is not very marked and hence, if no disturbances are present there is a region in the centre of the tube or vessel which could be described as a uniform core. It is in this region away from the walls that the equations of motion apply and may provide a satisfactory description of voidage changes inherent in the fluidised state.

However the walls will have some effect other than this packing effect. In narrow fluidised beds, there appears to be a layer of particles close to the wall whose movement is not so marked as the movement in the core. The fluid at the walls has zero velocity parallel to them and this will induce some drag on the particles close to the wall. In addition there will be some frictional resistance between the moving particles and the walls even though considerable slip is exhibited.

Consider a disturbance of the uniformly fluidised bed away from the walls. There will be some drag on the particle movement (the velocity $\underline{y}$) at the edge of this uniform core due to wall effects, and the most extreme case possible is where the particle velocity $\underline{y}$ due to the disturbance becomes zero. This implies that at the edge of the uniform core the perturbation of the particle concentration n_1 is zero.

If d_u is the diameter of the uniform core then, if the extent of the wall effect is $c'd_p/2$ in from the wall,

$$d_u = d_t\,(1 - c'd_p/d_t) \qquad \text{(3,15)}$$

where d_t is the tube diameter and d_p is the particle diameter. c' is some constant.

If $d_p/d_t \ll 1$, $d_u \sim d_t$.

Thus, for an axisymmetric disturbance, the most extreme boundary condition possible is $n_1 = 0$ at $\rho = d_u/2$. The constant c' would be expected to be less than 10. It must be emphasized that this is an extreme case and what actually occurs will probably be something of a compromise between the extremes of n_1 becoming zero at the wall and the disturbance being in no way limited by the wall.

It is now possible to obtain some idea of how the walls of the bed effect the propagation of a disturbance wave; in particular, the boundary condition given above enables a value to be given to the horizontal components of the wave number vector. The disturbance wave propagating in a narrow column is considered axisymmetric and can be treated by the standard methods for wave propagation in a waveguide (see (30)).

The initial value of the axisymmetric disturbance is N_0 and for all x and t, $n_1 = 0$ at $\rho = d_u/2$. The general solution of equation (3,5) leading to instability gives as a component of the general disturbance, a monochromatic plane wave, travelling in the direction of $\underline{k}$, of the form

$$n_1 = N_0 \exp[\xi t] \exp[j(k_x x + k_y y + k_z z - \eta t)]$$

where ξ and η are functions of k_x and $(k_y^2 + k_z^2)$.

In cylindrical co-ordinates, for axial symmetry, the general differential equation for n is

$$A\frac{\partial^2 \mathcal{M}_1}{\partial t^2} + \left[B + 2F\left(\frac{\bar{u}_0}{\varepsilon_0}\right)\frac{\partial}{\partial x} - \frac{D(\alpha_0 + 2\gamma_0)}{\rho_s(1-\varepsilon_0)}\left(\frac{\partial^2}{\partial x^2} + \frac{1}{\rho}\frac{\partial}{\partial \rho} + \frac{\partial^2}{\partial \rho^2}\right)\right]\frac{\partial \mathcal{M}_1}{\partial t}$$

$$+ \left[BE\left(\frac{\bar{u}_0}{\varepsilon_0}\right)\frac{\partial}{\partial x} + F\left(\frac{\bar{u}_0}{\varepsilon_0}\right)^2\frac{\partial^2}{\partial x^2} - \frac{D\mathcal{M}_0\Omega_0'}{\rho_s(1-\varepsilon_0)}\left(\frac{\partial^2}{\partial x^2} + \frac{1}{\rho}\frac{\partial}{\partial \rho} + \frac{\partial^2}{\partial \rho^2}\right)\right]\mathcal{M}_1 = 0$$

——————————— (3,16)

This equation could be solved in the normal manner by separating the variables. However it is more convenient to construct the axisymmetric disturbance i.e. a cylindrical wave, from the general disturbance. Figure 3,1 shows the wave number vector $\underline{k}$ and the position vector $\underline{r}$; $\underline{k}$ has direction cosines l, m, n and ϕ is the angle which the projection

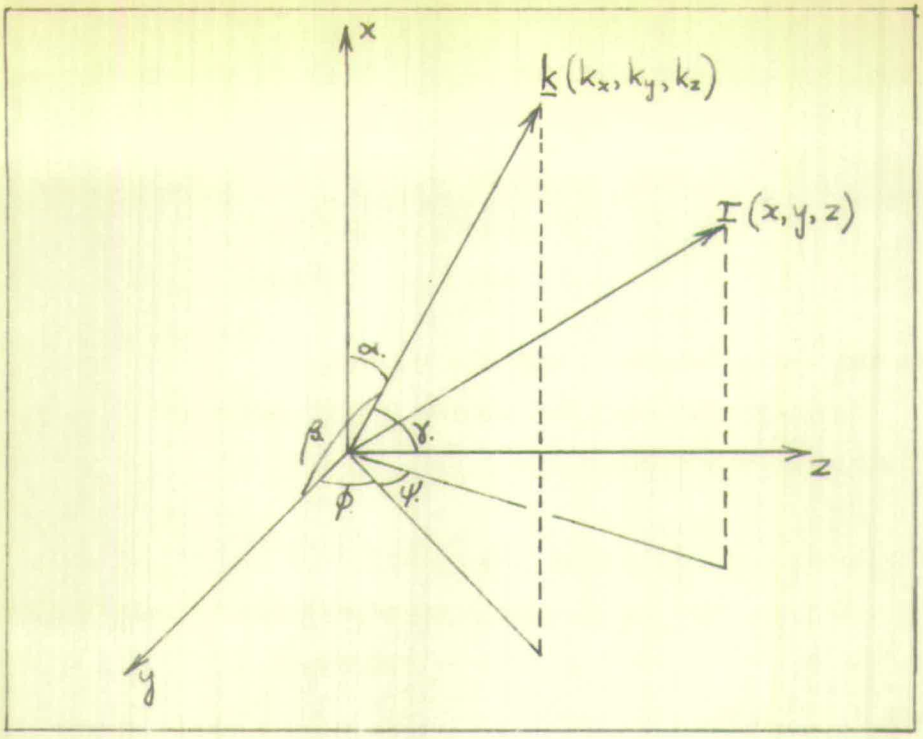


FIGURE 3.1 RELATIONSHIP BETWEEN WAVE NUMBER VECTOR AND POSITION VECTOR.

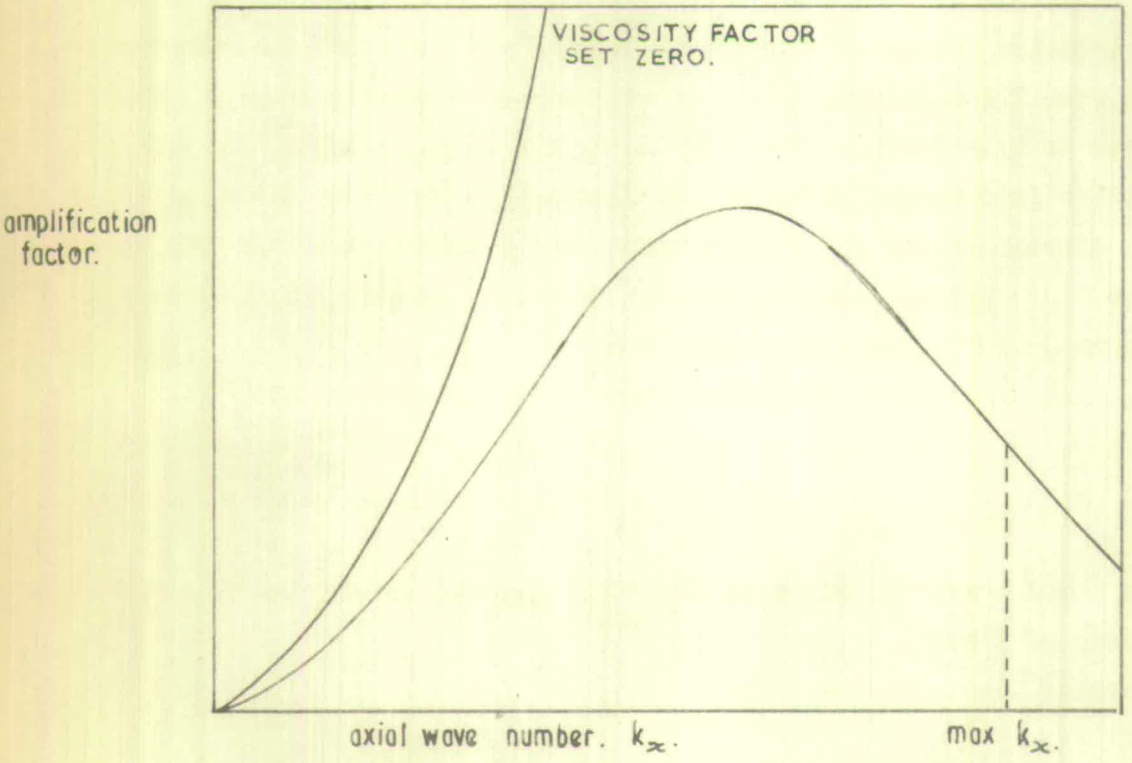


FIGURE 3.2 EFFECT OF PARTICULATE PHASE VISCOSITY ON AMPLIFICATION FACTOR.

of the wave number vector on the yz plane makes with the y-axis.

$$l = \cos\alpha$$
$$m = \cos\beta = \cos\phi\sin\alpha$$
$$n = \cos\gamma = \sin\phi\sin\alpha$$

α is the angle between $\underline{k}$ and the x-axis.

Consider the position vector $\underline{r}$ with components (x, y, z) or, in cylindrical co-ordinates, (x, ρ, θ)

$$\begin{aligned} k_x x + k_y y + k_z z &= k(lx + my + nz) \\ &= k(x\cos\alpha + \rho\cos\theta\cos\phi\sin\alpha + \rho\sin\theta\sin\phi\sin\alpha) \\ &= k(x\cos\alpha + \cos\psi\sin\alpha) \end{aligned}$$

where $\psi = \theta - \phi$.
Thus the general plane wave disturbance is

$$n_1 = N_0 \exp[\xi t] \exp[jk(x\cos\alpha + \rho\cos\psi\sin\alpha) - j\eta t]$$

To construct the required cylindrical wave, the sum is taken of an infinite number of plane waves making the same angle α with the x-axis and with the magnitude k of the wave number vector constant. Individual waves in this total differ only in k_y and k_z <u>i.e.</u> in ϕ. To find the total effect at any point on the circle (x, ρ) of all the plane waves, the expression for n_1 is integrated over ϕ from 0 to 2π or over ψ from 0 to 2π. The cylindrical wave so obtained, because of the linearity of equation (3,16), is also a solution.

At any time t, the cylindrical wave disturbance is given by

$$n_{1\,TOTAL} = \int_0^{2\pi} N_0 \exp[\xi t] \exp[j\{k(x\cos\alpha + \rho\cos\psi\sin\alpha) - \eta t\}]\, d\psi .$$

Now ξ and η are functions of $(k_y^2 + k_z^2)$ <u>i.e.</u> of $k^2\sin^2\alpha$ and so are independent of ϕ or ψ.
Dropping the subscript TOTAL

$$n_1 = N_0 \exp[\xi t] \exp[j(k_x x - \eta t)] \int_0^{2\pi} \exp[jk\rho\sin\alpha\cos\psi]\, d\psi$$

This integral is Sommerfeld's integral for the Bessel function of zero

order so that

$$n_1 = 2\pi N_0 J_0(k \sin\alpha . \rho) \exp[\xi t] \exp[j(k_x x - \eta t)]$$

Defining $k_\rho = k \sin\alpha$, since the disturbance is axisymmetric

$$n_1 = 2\pi N_0 J_0(k_\rho \rho) \exp[\xi t] \exp[j(k_x x - \eta t)] \qquad (3,17)$$

It is obvious from the above working that $k_\rho^2 = k_y^2 + k_z^2$.

For all x and t, $n_1 = 0$ at $\rho = d_u/2$ so that $J_0(k_\rho d_u/2) = 0$

From the present work, it appears that, for narrow tubes at least, only a single mode occurs across the whole tube so that only the argument for the first zero of the Bessel function is needed.

For

$$J_0\left(k_\rho \frac{d_u}{2}\right) = 0 \quad , \quad k_\rho \frac{d_u}{2} = 2.405$$

$$\text{so that} \quad k_\rho = \frac{4.810}{d_u}$$

Thus for an axisymmetric disturbance in a narrow tube where only one mode appears, the cylindrical wave components of the disturbance are of the form

$$n_1 = N_0 2\pi J_0\left(\frac{4.810}{d_u}\rho\right) \exp[\xi(k_x, k_\rho)t] \exp[j(k_x x - \eta(k_x, k_\rho)t)] \qquad (3,18)$$

The amplification factor $\xi(k_x, k_\rho)$ and the angular frequency $\eta(k_x, k_\rho)$ are exactly the same as for a general disturbance (equations (3,11) and (3,12)) but with $(k_y^2 + k_z^2)$ replaced by k_ρ^2 i.e. by $\left(\frac{4.810}{d_u}\right)^2$

The phase velocity and the wave length are given by

$$V_p = \eta(k_x, k_\rho)/k_x \quad \text{and} \quad \lambda = 2\pi/k_x$$

The same equation (3,18) is obtained if equation (3,16) is solved for a disturbance separable in x, ρ and t and in which X(x) is sinusoidal.

It is also possible to solve the equation (3,5) for a two dimensional disturbance propagating in a wave guide. This can be done either by considering the total effect of incident and reflected rays at the boundary or by separation of the variables. However this does not represent any possible physical situation. A two dimensional fluidised bed is the closest, but here no single disturbance would exist across the whole extent of the distributor.

For the sake of completeness however, the results for one single component of a disturbance propagating in the xy plane (all quantities independent of z) will be given. The boundary conditions are $n_1 = 0$ for $y = d_u/2$ (related to the half-width of the bed) at all x and t. The cosine solution is chosen since the disturbance is symmetric about $y = 0$. For a single mode appearing in the flow area, $k_y = \pi/d_u$ so that

$$n_1 = N_o \cos\left(\frac{\pi}{d_u} y\right) \exp.[\xi t] \exp[j(k_x x - \eta t)]$$

(c) Synthesis of a General Disturbance

This section shows that recognisable wave-packets can be synthesised from dispersive and amplifying components, and that these wave packets can propagate, initially at least, approximately unchanged apart from the amplification. A necessary condition for this is that there is some wave-length of maximum amplification. The wave making up this wave-packet must lie in a narrow range of wave numbers centred on this wave number of maximum amplification.

It is necessary at this stage to anticipate one of the main features of the results of the computational work discussed in Chapter 4; this is the effect of shear stresses in the dispersed phase on the amplification factor.

For any one physical situation with constant k_ρ the amplification factor of an axisymmetric disturbance is a function of k_x alone. Theoretically at least, all other parameters are determined by $\bar{u}_o$ and $\bar{\varepsilon}_o$ and the physical constants for the system. However values of the solids "viscosity" term $(\alpha_o + 2\gamma_o)$ are practically unknown. When the effect of solids shear is neglected it is found that $\xi(k_x)$ is a monotonic increasing function but when this "viscosity" term is included in the equation for ξ, using reasonable values estimated from previous work on the viscosity of fluidised beds (see Appendix 2), the amplification factor is found to exhibit a maximum value for one specific wave length in the range of physical interest. This is found to occur for both typically aggregative and typically particulate systems and is illustrated in Figure 3,2.

In a fluidised bed, the disturbances all appear to have more or less the same wave-length and this presumably corresponds to the wave-

length at which maximum amplification occurs. Thus the dominant wave in any disturbance is likely to be this one.

A typical monochromatic disturbance component, with axial symmetry, was found to have the form

$$n_1 = N_0 J_0(k_\rho \rho) \exp[j(k_x x - Wt)]$$

where W is the complex angular frequency $W(k_x) = \eta(k_x) + j\xi(k_x)$
The total disturbance at time t = 0, when the disturbance is first imposed on the uniform flow field, will occupy some finite region in space. The radial distribution is described by the Bessel function and the axial distribution by some function f(x) extending, if the disturbance appears just above the distributor, over some distance x = 0 to x = X. At t = 0, x > X, f(x) = 0. Associated with f(x), there will be some mean wave number k_x^M say, and some angular frequency $W(k_x^M)$. The extent of f(x) i.e. X, while small, is considerably greater than the wave-length $2\pi/k_x^M$.

At t = 0, the total disturbance, obtained by a summation of all the components, will thus have the form

$$n_T = N_0 J_0(k_\rho \rho) f(x) \exp[jk_x^M x]$$

If f(x) is expanded in a Fourier series

$$f(x) = \sum_{m=-\infty}^{\infty} c_m \exp\left[j \frac{2\pi m}{X} x\right]$$

where $$c_m = \frac{1}{X} \int_0^X f(x) \exp\left[-j \frac{2\pi m}{X} x\right] dx$$

Thus for any one component $k_x = k_x^M + \delta k_x$ where $\delta k_x = 2\pi m/X$. Now if f(x) is such that n_T does not contain components with wave numbers greatly different from k_x^M (equivalent to saying that c_m is significant only for small ranges of m on either side of 0) and if $X \gg 2\pi/k_x^M$, then $\delta k_x^m \ll k_x^M$

Thus at t = 0, each component has the form

$$n_1 = N_0 J_0(k_\rho \rho)\, c_m \exp[j(k_x^M + \delta k_x)x]$$

and at time t,

$$n_1 = N_0 J_0(k_\rho \rho)\, c_m \exp\left[j\left\{(k_x^M + \delta k_x)x - W(k_x^M + \delta k_x)t\right\}\right] .$$

Since $\delta k_x \ll k_x^M$, W can be expanded as a Taylor series retaining only first derivative terms so that

$$n_1 = c_m N_o J_o(k_p \rho) \exp\left[t\left\{\xi(k_x^M) + \left(\frac{d\xi}{dk_x}\right)_{k_x^M} \delta k_x\right\}\right] \times$$

$$\times \exp\left[j(k_x^M x - \eta(k_x^M)t)\right] \exp\left[j\,\delta k_x\left\{x - \left(\frac{d\eta}{dk_x}\right)_{k_x^M} t\right\}\right]$$

Identifying k_x^M with the wave number of maximum amplification, then $\left(\frac{d\xi}{dk_x}\right)_{k_x^M} = 0$ and the total disturbance at time t is, after summing over the components

$$n_T = N_o J_o(k_p \rho) \exp\left[\xi(k_x^M)t\right] f\left(x - \left(\frac{d\eta}{dk_x}\right)_{k_x^M} t\right) \exp\left[j(k_x^M x - \eta(k_x^M)t)\right]$$

where $$\sum_m c_m \exp\left[j\frac{2\pi m}{X}\left(x - \frac{d\eta}{dk_x}.t\right)\right] = f\left(x - \frac{d\eta}{dk_x}t\right) .$$

Thus after a time t, the amplitude of the total disturbance has increased by a factor $\exp[\xi(k_x^M)t]$ and the distribution of the disturbance in space has moved through a distance $t\left(\frac{d\eta}{dk_x}\right)_{k_x^M}$

The velocity of the distribution (the group velocity) is thus $\left(\frac{d\eta}{dk_x}\right)_{k_x^M}$

This is the usual expression for the group velocity of non-amplifying waves but it is interesting to notice in this case that it depends on there being a wave length of maximum amplification.

It is now possible to calculate the propagation properties of a disturbance for any one uniformly fluidised state (defined by $\bar{u}_o$, ε_o, ρ_s ρ_g, ρ_s, d_p, d_t, and μ) and to show the significance of wall effects and the effects of the various parameters. The discussion of these effects, both within one system and for different systems is covered in Chapter 4, where the detailed results of computational work are reported.

Section II – Some Possible Voidage Gradients in a Fluidised Bed

Apart from the state of uniform fluidisation, there is another possible steady state solution of the equations of motion. This solution describes a situation, called regular fluidisation, for which, as with the case of uniform fluidisation, no internal disturbances are present and the space averaged particle velocity vector is everywhere zero. The difference is that with regular fluidisation, the voidage, which is assumed uniform over any cross section of the flow area, varies continuously in the direction of bulk fluid flow. For this time invariant, one dimensional situation $\underline{v} = 0$, $\underline{u} = \underline{i}u_x$, $\underline{b} = -\underline{i}g$ and $u_x = \bar{u}_o/\varepsilon$, where ε is the voidage at any height x above the distributor and $\bar{u}_o$ is constant.

Under these conditions, equation (2,21) becomes

$$-\left[\bar{u}_o^2 \rho_f \frac{(1-\varepsilon)}{\varepsilon}\left(1+\frac{\theta(\varepsilon)}{\varepsilon}\right) + \frac{d\Omega}{d\varepsilon}\right]\frac{d\varepsilon}{dx} + \left[\bar{u}_o \frac{\beta(\varepsilon)}{\varepsilon} - g(\rho_s-\rho_f)(1-\varepsilon_o)\right] = 0 \qquad (3,19)$$

It has been assumed that $\frac{d}{dt}(\underline{u}-\underline{v}) = \frac{\partial \underline{u}}{\partial t} + (\underline{u}.\text{grad})\underline{u} - \frac{\partial \underline{v}}{\partial t} - (\underline{v}.\text{grad})\underline{v}$

If the other form of the virtual mass term were used

ie. $\frac{d}{dt}(\underline{u}-\underline{v}) = \frac{\partial}{\partial t}(\underline{u}-\underline{v}) + (\underline{v}.\text{grad})(\underline{u}-\underline{v})$

then the virtual mass coefficient $\theta(\varepsilon)$ would not appear at all in (3,19). Because of lack of information about some of the terms of (3,19), the following discussion is rather qualitative in nature and so, for simplicity, the virtual mass term is dropped.

Equation (3,19) is satisfied by $\varepsilon = \varepsilon_o$, independent of x, if

$$\bar{u}_o \beta(\varepsilon_o)/\varepsilon_o = g(\rho_s-\rho_f)(1-\varepsilon_o)$$

This is the equation for uniform fluidisation (equation (2,20) written in terms of voidage rather than particle concentration). However this condition for uniform fluidisation is not satisfied for the particles at the top of the bed. On this top layer of particles there is an additional force due to particle collisions below, which is not compensated for above the bed (note that the particle velocity vector being zero does not preclude random particle movement). At the extreme top of the bed there

is a very rapid increase in the voidage to a value of unity. This is a very localized phenomenon extending over a distance of about one particle diameter and the continuum equations do not apply to this situation. The concern here is rather with an element at the top of the bed several particle diameters thick, where it is assumed that the continuum equations do hold. For this element of the bed, there is a representative voidage ε_t (corresponding to a particle concentration n_t) which is the true boundary condition for the equations of motion i.e. at $x = x_t$, $\varepsilon = \varepsilon_t \neq 1$, where x_t is the height of the bed.

The forces acting on the particles in the top element of the bed are (i) gravity (ii) collision forces from underneath and (iii) the fluid-particle interaction force - including the fluid pressure, the drag force and the virtual mass force. The force balance on the particles in the top element of the bed is thus

$$\Omega(\varepsilon_t) + f_x \delta = (1-\varepsilon_t)\rho_s g \delta$$

where δ is the thickness of this element and the interaction force f_x now acts vertically upward. The force f_x can be obtained from equation (2,16) if $-\text{grad}\, p$ at the top of the bed is replaced by $(p_1 - p_2)/\delta$, with p_1 the fluid pressure below the element and p_2 the fluid pressure immediately above the top of the bed. Neglecting the virtual mass term and the fluid viscosity term (this term is eliminated when the pressure term is eliminated), the interaction force per unit bed volume (f_x) is given by

$$f_x = (1-\varepsilon_t)(p_1 - p_2)/\delta + n_t \phi(\varepsilon_t) u_x$$

Contributing to this pressure change in the fluid are the changes in momentum flux and hydrostatic head over the element and the drag force on the particles.

An extended form of Bernoulli's equation for the fluid is

$$p_1 + \rho_f u_x^2 + \rho_f g(x_t - \delta) = p_2 + \rho_f \bar{u}_o^2 + \rho_f g x_t + \frac{n_t \phi(\varepsilon_t)}{1 - n_t v} u_x \delta$$

where $\frac{n_t \phi(\varepsilon_t) u_x \delta}{1 - n_t v}$ takes account of the loss due to the drag exerted on the top layer of particles. The above equation can be obtained from equation (2,17). Thus

$$(p_1 - p_2) = -\rho_f \bar{u}_o^2 \left(\frac{1}{\varepsilon_t^2} - 1\right) + \rho_f g \delta + \frac{n_t \phi(\varepsilon_t)}{1 - n_t v} u_x \delta$$

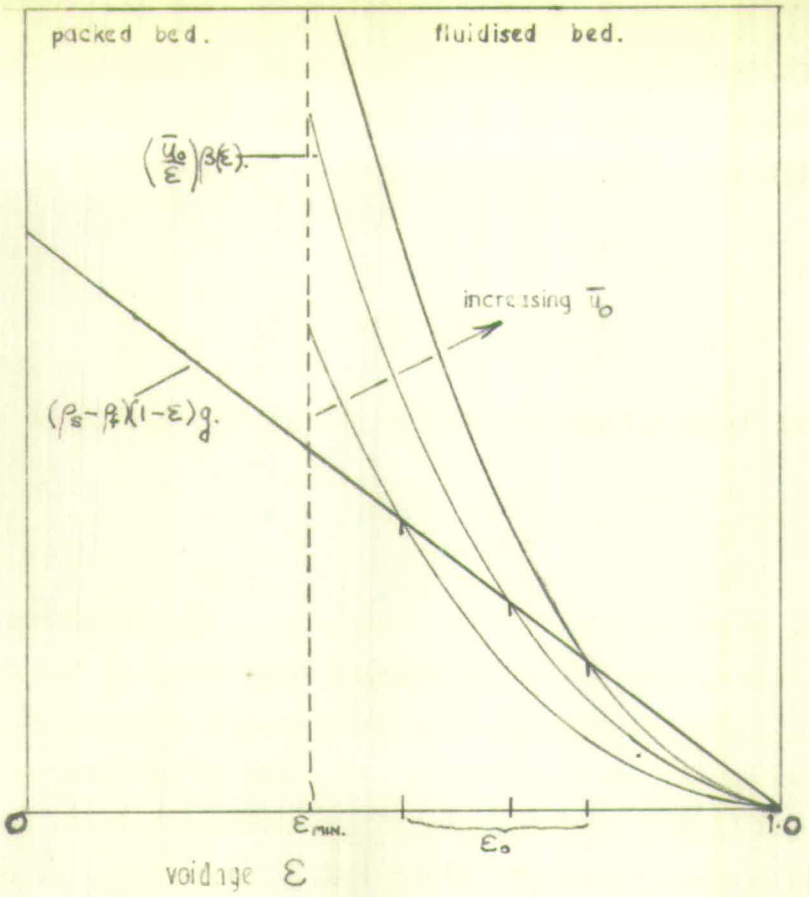


FIGURE 3.3 DRAG FUNCTION $\beta(\varepsilon)$ AND GRAVITY FUNCTION $(\rho_s-\rho_f)(1-\varepsilon)g$.

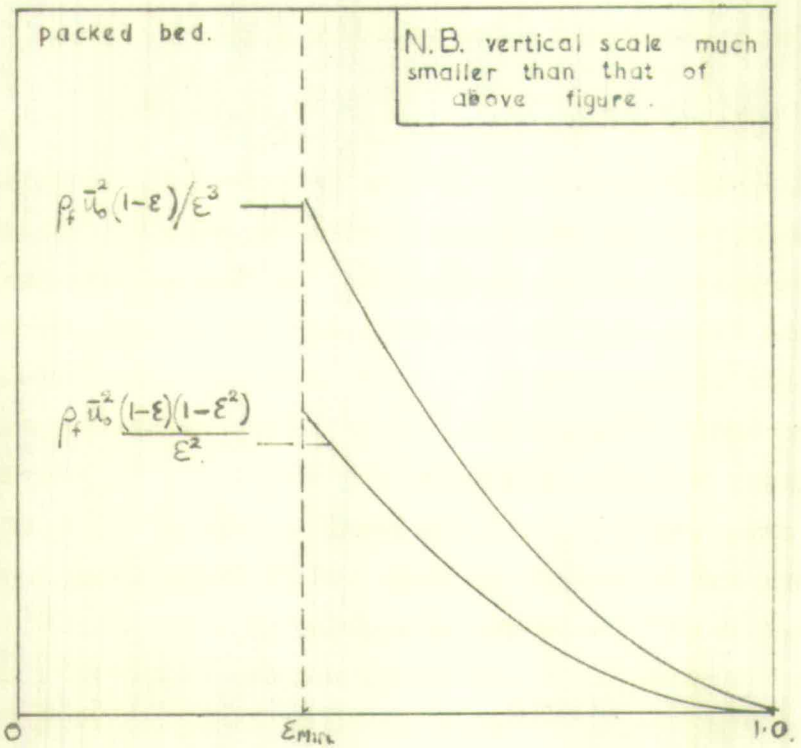


FIGURE 3.4 FLUID MOENTUM CHANGE FUNCTIONS.

The first term on the R.H.S. is the change in momentum flux, the second is the change in head and the third is the loss due to drag exerted on the particles. The interaction force f is therefore given by

$$f = -\frac{(1-\varepsilon_t)}{\delta}\rho_f \bar{u}_o^2\left(\frac{1}{\varepsilon_t^2}-1\right) + (1-\varepsilon_t)\rho_f g + \beta(\varepsilon_t)\frac{\bar{u}_o}{\varepsilon_t}$$

where $\beta(\varepsilon_t) = \frac{\mathcal{M}_t \phi(\varepsilon_t)}{1-\mathcal{M}_t v}$ and $u_x = \frac{\bar{u}_o}{\varepsilon_t}$

The force balance at the top of the bed thus reads

$$\left[\Omega(\varepsilon_t) - \rho_f \bar{u}_o^2\left(\frac{1-\varepsilon_t^2}{\varepsilon_t^2}\right)(1-\varepsilon_t)\right]\frac{1}{\delta} = (\rho_s-\rho_f)g(1-\varepsilon_t) - \beta(\varepsilon_t)\frac{\bar{u}_o}{\varepsilon_t} \qquad (3,20)$$

To solve equation $(3,19)_\lambda$ (see p.49) numerically, the functions $\beta(\varepsilon)$ and $\Omega(\varepsilon)$ must be known, together with boundary conditions at the foot or top of the bed. The two functions are unknown and so there is little hope of achieving any exact solution. However by considering equations (3,19) and (3,20), certain qualitative conclusions can be drawn about possible voidage gradients in the bed, if the forms, at least, of $\beta(\varepsilon)$ and $\Omega(\varepsilon)$ can be deduced. These functions are discussed in some detail in Appendix 2.

It is a simple matter to evaluate $\beta(\varepsilon)$ for any system if the bed is uniformly fluidised - for this situation

$$\beta(\varepsilon) = \varepsilon_o(1-\varepsilon_o)(\rho_s-\rho_f)g/\bar{u}_o \qquad \left(\begin{matrix}\text{this equation}\\ \text{defines } \varepsilon_o\end{matrix}\right)$$

and, using this relation, $\beta(\varepsilon)$ has been plotted, in Appendix 2, from measurements of bed height and fluidising velocity for one of the experimental situations dealt with. If the uniform condition does not hold, the above equation obviously does not apply; however it seems reasonable to assume that $\beta(\varepsilon)$ will be of the same form and probably of the same order of magnitude. This latter assumption can be justified by considering probable magnitudes for $\bar{u}_o^2\rho_f(1-\varepsilon)/\varepsilon^3$, $d\varepsilon/dx$ (say a maximum value of 0.1 cms^{-1}) and $d\Omega/d\varepsilon$. The possible size of $d\Omega/d\varepsilon$ is discussed in the following and subsequent chapters and it seems likely from the numerical work that it will be of the same order as $\bar{u}_o^2\rho_f(1-\varepsilon)/\varepsilon^3$. For the present situation $\bar{u}_o$ is a constant and so $\bar{u}_o\beta(\varepsilon)/\varepsilon$ has the form shown in Figure 3.3. Figure 3.4 shows plots of $\frac{\rho_f\bar{u}_o^2(1-\varepsilon)}{\varepsilon^3}$ and $\frac{\rho_f\bar{u}_o^2(1-\varepsilon^2)(1-\varepsilon)}{\varepsilon^2}$ from equations $(3,19)_\lambda$ and (3,20). Note that the latter quantity tends asymptotically to zero as the voidage tends to unity. In Appendix 2, the form of the

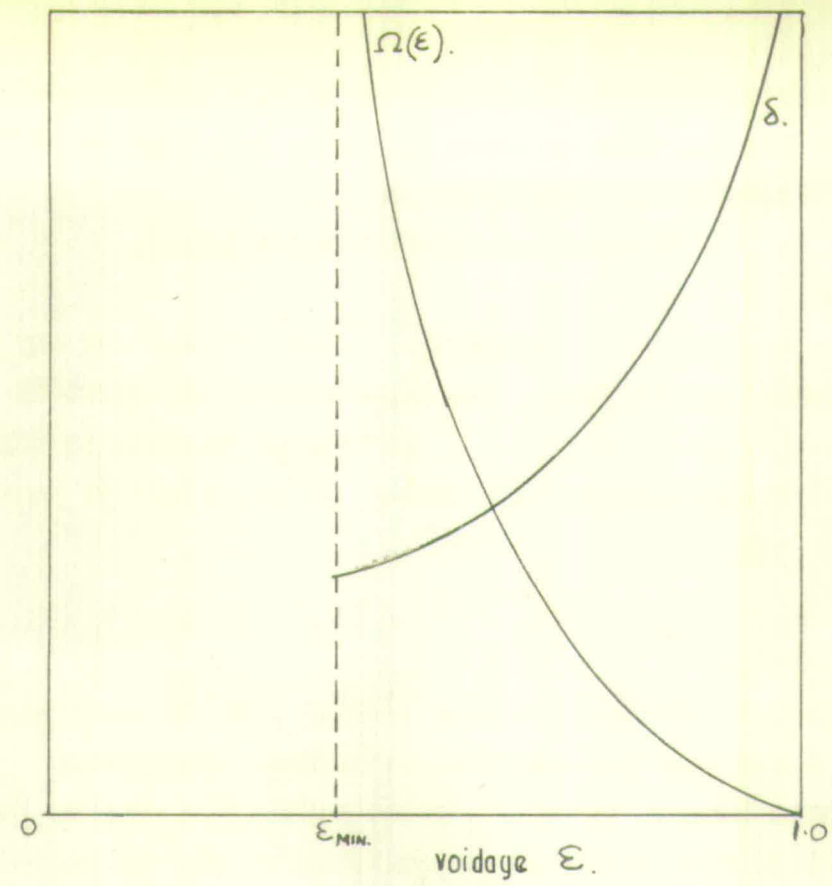


FIGURE 3.5 DEPENDENCE OF $\Omega(\varepsilon)$ AND δ ON VOIDAGE.

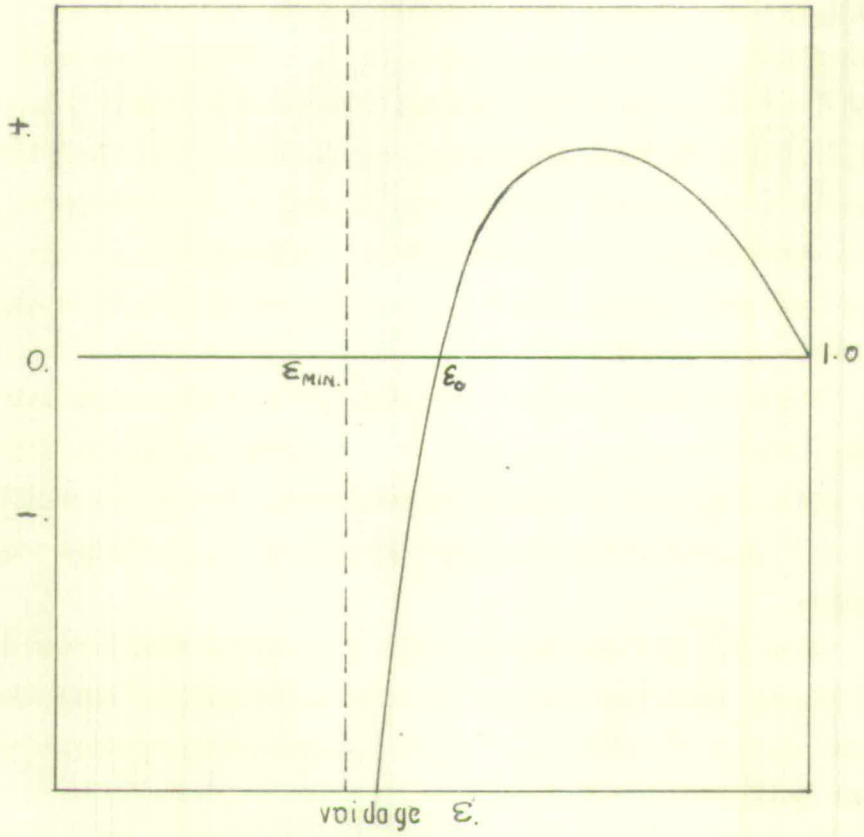


FIGURE 3.6 R.H.S. OF EQUATIONS (3,19) AND (3,20).

particulate phase static normal stress $\Omega(\varepsilon)$ is discussed and the most likely form for this is shown in Figure 3.5, together with the top layer thickness δ. Note that as

$\varepsilon \rightarrow \varepsilon_m$ (the minimum fluidisation voidage), $\delta \rightarrow$ a finite limit, and as

$\varepsilon \rightarrow 1.0$, $\delta \rightarrow \infty$ since $x_t \rightarrow \infty$ as $\varepsilon \rightarrow 1.0$ for any given quantity of material in the bed. The dependence of the quantity $\left[g(\rho_s-\rho_f)(1-\varepsilon) - \bar{u}_o \beta(\varepsilon)/\varepsilon\right]$ on voidage is shown in Figure 3.6.

For the following discussion, it is as well to recall equation (3,19), viz

$$\left[\left|\frac{d\Omega}{d\varepsilon}\right| - \bar{u}_o^2 \rho_f \frac{(1-\varepsilon)}{\varepsilon^3}\right]\frac{d\varepsilon}{dx} = g(\rho_s-\rho_f)(1-\varepsilon) - \bar{u}_o \frac{\beta(\varepsilon)}{\varepsilon} \qquad (3,19)$$

The virtual mass term has been omitted from the above equation.

Apart from the condition of uniform fluidisation ($d\varepsilon/dx = 0$), the force balance for which is not valid at the top of the bed, the right hand side of the above equation can only be zero if

$$\bar{u}_o^2 \rho_f \frac{(1-\varepsilon)}{\varepsilon^3} = \left|\frac{d\Omega}{d\varepsilon}\right|$$

If there occurred voidage gradients in the bed such that $d\varepsilon/dx$ changed sign i.e. the shape of the voidage profile is $\smile$ or $\frown$ then at the point where $d\varepsilon/dx = 0$, the R.H.S. = 0. However, at this changeover point ($\varepsilon = \varepsilon_o$), the R.H.S. cannot change sign since ε is either $\geq \varepsilon_o$ or $\leq \varepsilon_o$. Thus if $d\varepsilon/dx$ is to change sign, so also must its coefficient. It would be a very great coincidence indeed if the two pairs of these four terms, physically quite independent, became equal at the same voidage. It is much more likely that $d\varepsilon/dx$ will retain the same sign throughout the whole length of the bed.

The situation where $d\varepsilon/dx$ retains the same sign but at some point in the bed there is a voidage $\varepsilon = \varepsilon_o$ corresponding to the R.H.S. being zero again implies a similar coincidence, for if the R.H.S. changes sign at $\varepsilon = \varepsilon_o$ so also must the coefficient of $d\varepsilon/dx$ change sign at this voidage.

Thus for any one system with a constant fluid flow rate, it seems most likely that the voidage is either greater or less than ε_o for all values of x, and that $d\varepsilon/dx$ is either positive or negative, but not both in the same bed.

The following discussion applies to a bed with constant fluidising

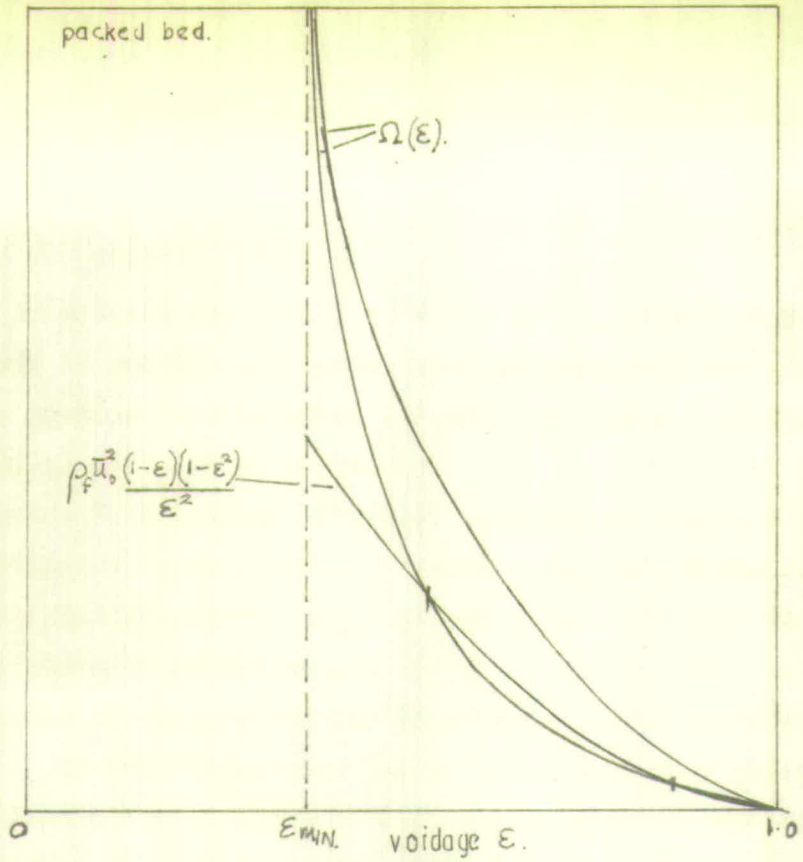


FIGURE 3.7 RELATIVE MAGNITUDES OF L.H.S. TERMS APPEARING IN EQUATION (3,20)

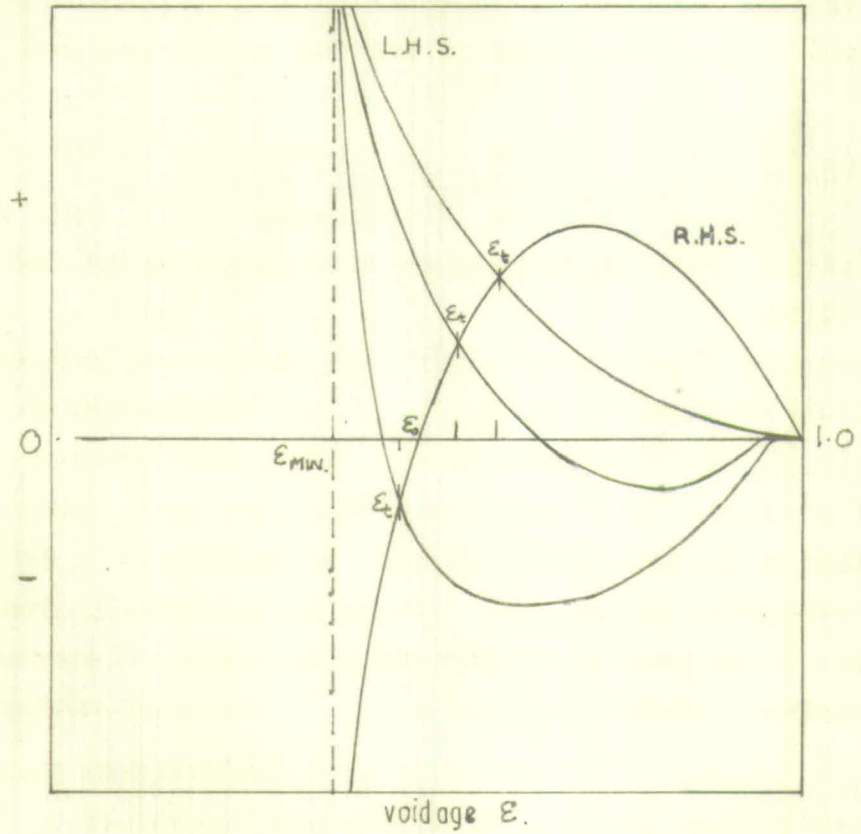


FIGURE 3.8 POSSIBLE TOP VOIDAGES FROM EQ. (3,20)

velocity and constant overall mean voidage given by

$$\bar{\varepsilon} = \frac{1}{x_t}\int_0^{x_t} \varepsilon(x)\, dx .$$

If the R.H.S. and L.H.S. of equation (3,20) are plotted as functions of voidage, the intersection point gives the voidage at the top of the bed. Figures 3.4 and 3.5 show the dependence on voidage of the terms $\Omega(\varepsilon)$ and $\rho_f \bar{u}_o^2(1-\varepsilon)(1-\varepsilon^2)/\varepsilon^2$ appearing in equation (3,20) and Figure 3.7 shows the various possible relative magnitudes of these two terms. The normal stress term may either lie always above the latter term or it may be less than this term over some part of the voidage range though not near ε_{MIN} or $\varepsilon = 1.0$. If the two curves do intersect, they must always intersect twice, because of the way the normal stress term increases rapidly near close packing and because of the way $\rho_f \bar{u}_o^2(1-\varepsilon)(1-\varepsilon^2)/\varepsilon^2$ approaches zero tangentially to the horizontal as the voidage tends to unity. The various possibilities for the L.H.S. of equation (3,20) and the way in which these possibilities determine the voidage at the top of the bed are shown in Figure 3.8. It is obvious that the greater the normal stress, the greater is this top voidage and that if

$\Omega(\varepsilon) > \rho_f \bar{u}_o^2(1-\varepsilon)(1-\varepsilon^2)/\varepsilon^2$ for $\varepsilon \le \varepsilon_t$, then $\varepsilon_t > \varepsilon_o$ and $\varepsilon(x) > \varepsilon_o$

and $\Omega(\varepsilon) < \rho_f \bar{u}_o^2(1-\varepsilon)(1-\varepsilon^2)/\varepsilon^2$ for $\varepsilon \le \varepsilon_t$, then $\varepsilon_t < \varepsilon_o$ and $\varepsilon(x) < \varepsilon_o$.

The solution $\varepsilon_t = \varepsilon_o$ is possible and corresponds to the state of uniform fluidisation.

Consider first the situation where the voidage is greater than the uniform fluidisation voidage. If, as seems reasonable, a large value of $\Omega(\varepsilon)$ implies a large $|d\Omega/d\varepsilon|$, then, from equation (3,19) the voidage gradient will be positive. Note also that a large value of $\Omega(\varepsilon)$ makes it unlikely that $d\varepsilon/dx$ will be negative as ε_t is then the lowest voidage in the bed, and ε_t could be considerably greater than ε_o and close to the possible voidage where the L.H.S. of equation (3,20) becomes zero. However $\Omega(\varepsilon) > \rho_f \bar{u}_o^2(1-\varepsilon)(1-\varepsilon^2)/\varepsilon^2$ does not necessarily mean that $\left|\frac{d\Omega}{d\varepsilon}\right| > \rho_f \bar{u}_o^2(1-\varepsilon)/\varepsilon^3$, and it is quite possible that the bed will have a negative voidage gradient, especially with low values of $\Omega(\varepsilon)$.

Similarly for the case where the bed voidage is less than the uniform fluidisation voidage, the voidage gradient may be either

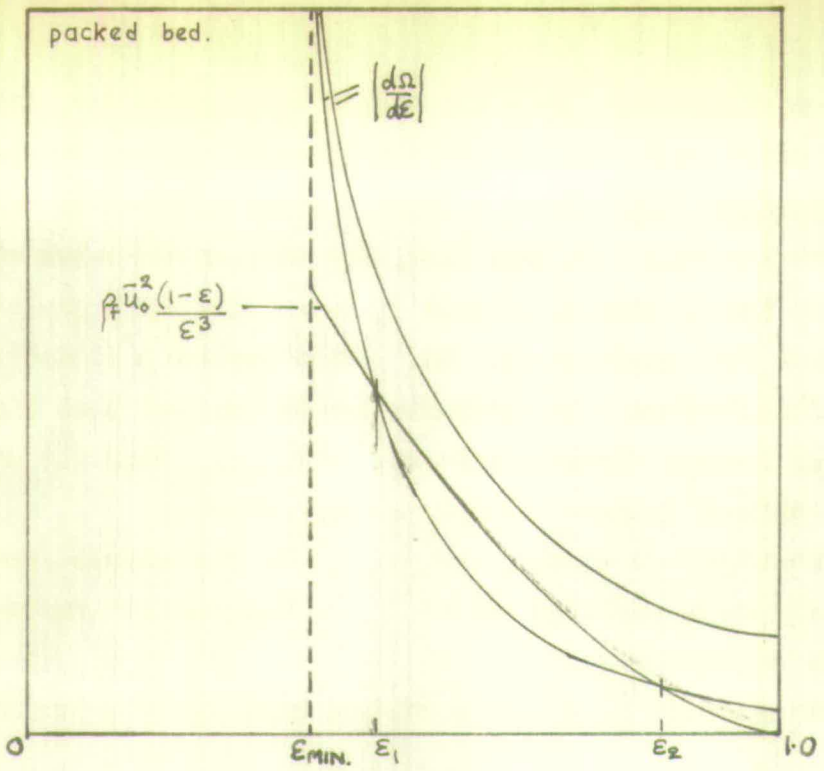


FIGURE 3.9. RELATIVE MAGNITUDES OF TERMS ON L.H.S. OF EQUATION (3,19).

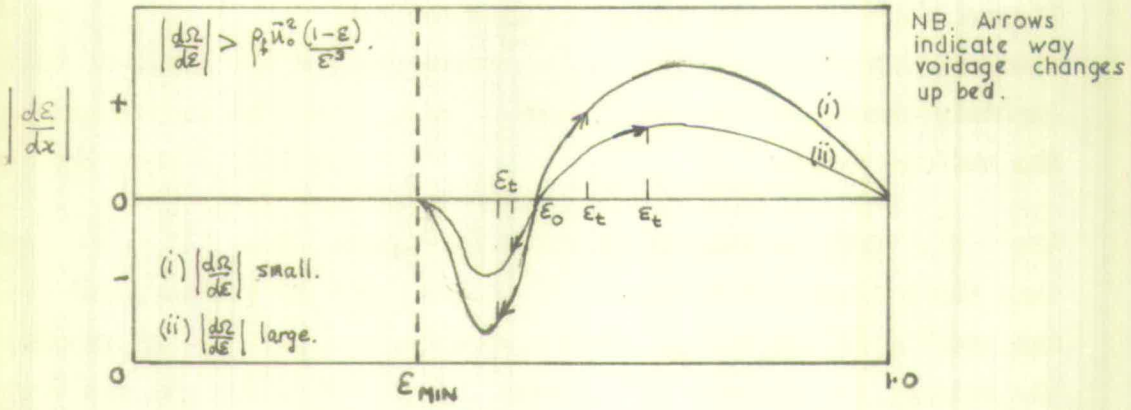
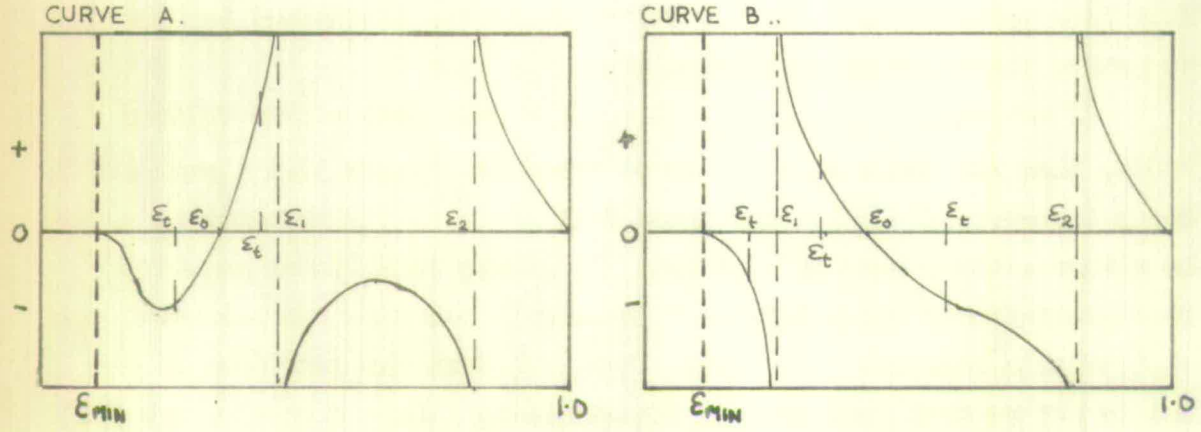


FIGURE 3.10. VOIDAGE GRADIENT AS A FUNCTION OF VOIDAGE COEFFICIENT OF $d\varepsilon/dx$ IN EQ.(3,19) POSITIVE.



FIGURES 3.11 A&B. $d\varepsilon/dx$ AS A FUNCTION OF VOIDAGE. COEF.^{T} NEGATIVE OVER PART OF ε RANGE.

positive or negative. Here also there is a limitation, especially at low flow rates where the uniform fluidisation voidage is close to the minimum voidage, thus giving a smaller range of possible voidages throughout the bed. In this case, the smaller the value of $\Omega(\varepsilon)$, the greater is the difference between ε_t and ε_o and for a positive $d\varepsilon/dx$, the smaller this gradient will be. This implies a situation close to uniform fluidisation - in contradiction to the fact that there is a relatively large difference between ε_t and ε_o. Thus the positive voidage gradient appears unlikely in this case.

Tentatively it appears that if $\varepsilon_t > \varepsilon_o$, the voidage gradient is more likely to be positive and if $\varepsilon_t < \varepsilon_o$, the voidage gradient is more likely to be negative.

From equation (3.19), the voidage gradient is given by

$$\frac{d\varepsilon}{dx} = \frac{g(\rho_s - \rho_f)(1-\varepsilon) - \bar{u}_o \beta(\varepsilon)/\varepsilon}{\left|\frac{d\Omega}{d\varepsilon}\right| - \bar{u}_o^2 \rho_f (1-\varepsilon)/\varepsilon^3}.$$

If $\Omega(\varepsilon)$ has the expected form, then the shape of $|d\Omega/d\varepsilon|$ is as shown in Figure 3.9. This can either be greater than $\rho_f \bar{u}_o^2 (1-\varepsilon)/\varepsilon^3$ over the whole voidage range or the $|d\Omega/d\varepsilon|$ curve may cut the graph of this latter quantity twice, at voidages ε_1 and ε_2 say, somewhere in the middle of the voidage range. If $\left|\frac{d\Omega}{d\varepsilon}\right| > \rho_f \bar{u}_o^2 \frac{(1-\varepsilon)}{\varepsilon^3}$ for all ε, then the shape of the $d\varepsilon/dx$ curve is roughly as shown in Figure 3.10. If $\varepsilon_t > \varepsilon_o$ but less than the voidage for maximum $d\varepsilon/dx$, then $d\varepsilon/dx$ is positive and the voidage profile in the bed is concave upwards. If $\varepsilon_t < \varepsilon_o$ but greater than the voidage for minimum $d\varepsilon/dx$, then $d\varepsilon/dx$ is negative and the voidage profile is concave downwards. If the two extrema occur between ε_o and ε_t, points of inflexion would be introduced into the voidage profile. This does not seem very likely, but is of little importance in trying to assess the relative magnitudes of $|d\Omega/d\varepsilon|$ and $\rho_f \bar{u}_o^2 (1-\varepsilon)/\varepsilon^3$

If however, $|d\Omega/d\varepsilon| < \rho_f \bar{u}_o^2 (1-\varepsilon)/\varepsilon^3$ over part of the voidage range, then the shape of $d\varepsilon/dx$ is as shown in Figures 3.11 A and 3.11 B. Curve A occurs if $\varepsilon_1 > \varepsilon_o$ and curve B if $\varepsilon_1 < \varepsilon_o$. With curve A, ε_t can be either greater than or less than ε_o, giving positive or negative voidage gradients respectively. However ε_t can also lie between ε_1 and ε_2, giving a negative $d\varepsilon/dx$ with $\varepsilon_t > \varepsilon_o$. Thus the condition of the bed is far removed from uniform fluidisation. This situation was dealt

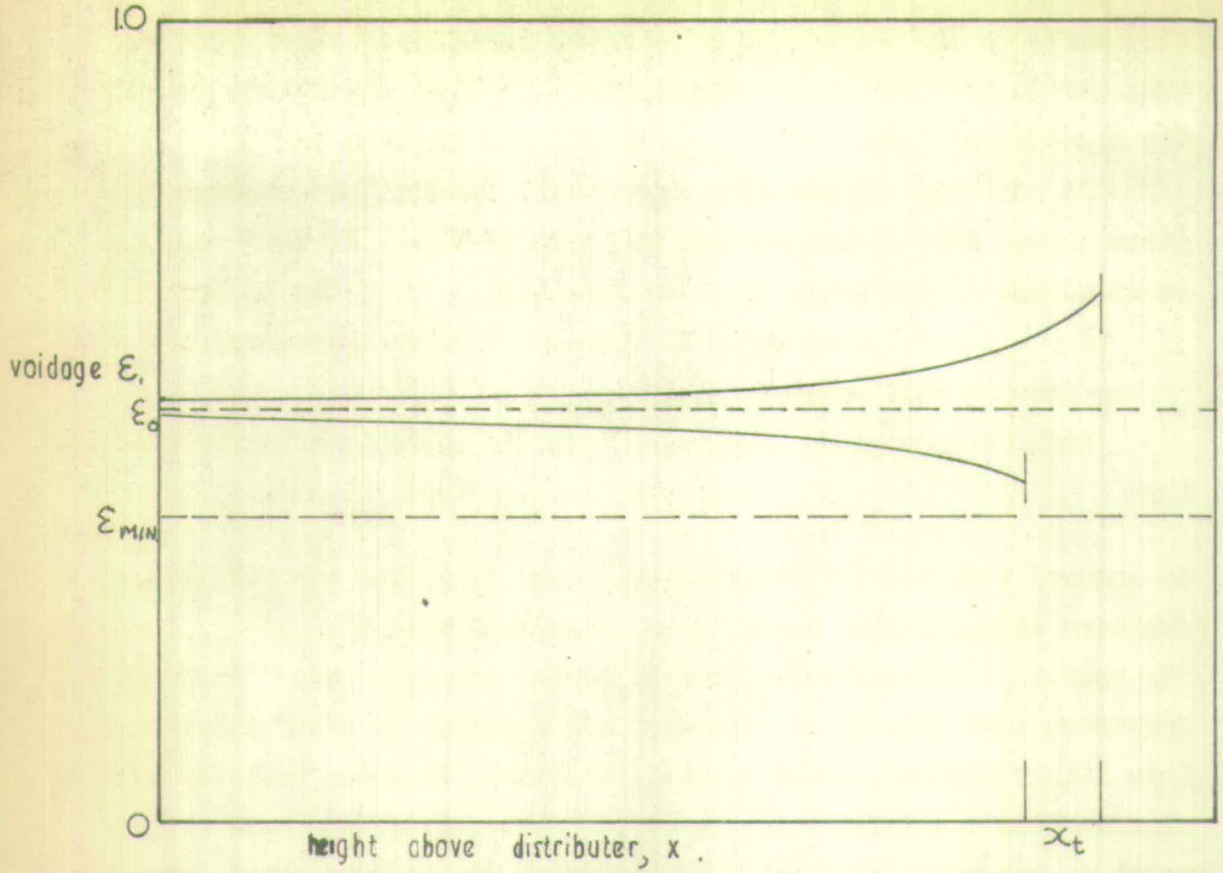


FIGURE 3.12. VOIDAGE PROFILES FOR A STABLE SOLUTION.

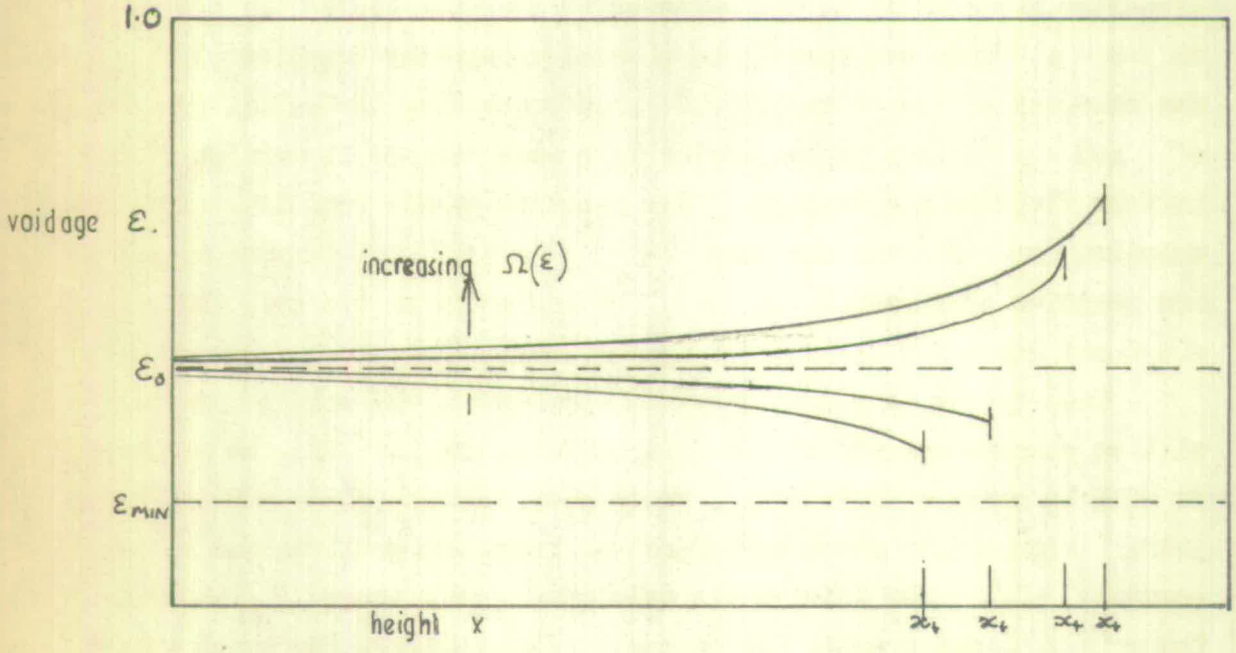


FIGURE 3.13 EFFECT OF SIZE OF PARTICLE NORMAL STRESS ON VOIDAGE PROFILE.

with above in the discussion of possible voidages at the top of the bed, and is not felt to be very probable. Curve B presents exactly the opposite picture. If $\varepsilon_t > \varepsilon_o$, $d\varepsilon/dx$ is negative and if $\varepsilon_t < \varepsilon_o$, $d\varepsilon/dx$ is positive and possibly negative. For the same reasons as given above, this situation does not seem likely. If this case can be dismissed as unlikely, then the fact that $|d\Omega/d\varepsilon|$ may be less than $\rho_f \bar{u}_o^2(1-\varepsilon)/\varepsilon^3$ for some range of voidage is of no importance if ε_t and ε_o lie outside this range.

From the foregoing discussion then, it seems more likely than not that $\left|\frac{d\Omega}{d\varepsilon}\right| > \rho_f \bar{u}_o^2 \frac{(1-\varepsilon)}{\varepsilon^3}$. This conclusion follows automatically if it is assumed that the differential equation (3,19) for the voidage as a function of height has a stable solution such that the voidage approaches the uniform fluidisation voidage on moving down the bed. There is no guarantee that this is so, however, and a number of other possibilities, less likely perhaps, could occur. It should be noted that the uniform fluidisation condition ($d\varepsilon/dx = 0$) can never actually obtain at any point in the bed if $d\varepsilon/dx$ has a non-zero value at some other point in the bed. If $d\varepsilon/dx$ is zero, it must remain so throughout the bed - this situation corresponds to the solution of equation (3,19) if $d\varepsilon/dx = 0$ at $\varepsilon = \varepsilon_t$. This can readily be checked by writing equation (3,19) with the constant $g(\rho_s - \rho_f)$ on the R.H.S. and expanding the L.H.S. (a function of ε and $d\varepsilon/dx$) as a Taylor series in a small change in voidage from the uniform fluidisation voidage. The solution of the resulting differential equation for $d\varepsilon/dx$ has the form $\varepsilon = \varepsilon_o \pm a\exp[-bx]$, where a and b are positive constants. If $\varepsilon = \varepsilon_o$ at any point in the bed, then $a = 0$ and hence $\varepsilon = \varepsilon_o$ is the only solution.

Thus if the stable solution is applicable, the voidage profile will be concave upwards if $d\varepsilon/dx$ is positive and, if $d\varepsilon/dx$ is negative, it will be concave downwards. These possibilities are shown in Figure 3.12. Figure 3.10 shows the effect of large and small values of the quantity $|d\Omega/d\varepsilon|$ for this stable solution. If a large $\Omega(\varepsilon)$ implies a large $|d\Omega/d\varepsilon|$ and a small $\Omega(\varepsilon)$ a small $|d\Omega/d\varepsilon|$, then, for equal values of the voidage the large $\Omega(\varepsilon)$ gives a small $d\varepsilon/dx$ and vice versa. However the value of ε_t is greater the greater the value of $\Omega(\varepsilon)$. This is shown in Figure 3.13 for a positive voidage gradient. As $\Omega(\varepsilon)$ is increased, the expected voidage gradient (initially negative) approaches

closer and closer to zero (the uniform fluidisation situation) and on further increase the gradient becomes positive. The larger the normal stress becomes the further does the situation depart from the uniform fluidisation situation. The difference in the profiles highlights the importance of the particulate phase normal stress term. Note that the height of the bed, and hence the mean bed voidage also depends on the size of this term - this is a necessary consequence of a stable solution to equation (3,19).

It must be emphasised that these conclusions are very tentative indeed and serve mainly to illustrate the importance of the particulate normal stress. No conclusions of a quantitative nature are possible without much more detailed knowledge of the terms involved. However reasonable assumptions about the nature of these terms lead to reasonable voidage profiles in the bed.

Voidage gradients in fluidised beds have been reported (see Lava (2)), but these have always been found in beds of particles of mixed sizes or particles with a wide size range. These gradients are in the main attributable to segregation, the larger particles dropping to the feet of the bed and the smaller particles rising to the top. Voidage gradients attributable to collisions have not been reported and it would be rash indeed to state that they do exist. However a positive voidage gradient in the bed is not inconsistent with the observed phenomenon of beds fluidising from the top downwards or with the observation in the present work of portions of the bed close to the distributer remaining unfluidised at flow rates just above that necessary for minimum fluidisation.

However only experimental work can hope to decide the form of the voidage profile and give some information concerning the terms involved. It may be possible to get some information about $\Omega(\varepsilon)$ from pressure drop measurements.

The total momentum balance for both phases, equation (2,7), reduces in the present situation to

$$-\rho_f \frac{\bar{u}_o^2}{\varepsilon^2} \frac{d\varepsilon}{dx} = -g(1-\varepsilon)\rho_s - g\rho_f \varepsilon - \frac{dp}{dx} - \frac{d\Omega}{d\varepsilon} \cdot \frac{d\varepsilon}{dx}$$

where fluid viscous effects have been neglected. Integrating this over the whole length of the bed from $x = 0$ to $x = x_t$, with $\varepsilon = \varepsilon_f$ at $x = 0$ and $\varepsilon = \varepsilon_t$ at $x = x_t$ gives

$$-\rho_f \bar{u}_o^2 \int_{\varepsilon_f}^{\varepsilon_t} \frac{1}{\varepsilon^2}\, d\varepsilon = -g\rho_s(1-\bar{\varepsilon})x_t - g\rho_f \bar{\varepsilon} x_t - p(x_t) + p(0) - \Omega(\varepsilon_t) + \Omega(\varepsilon_f)$$

so that $$\Delta p + \Delta\Omega + \rho_f \bar{u}_o^2 \left[\frac{1}{\varepsilon_f} - \frac{1}{\varepsilon_t}\right] = g(\rho_s - \rho_f)(1-\bar{\varepsilon})x_t + g\rho_f x_t \qquad (3,21)$$

where $\Delta p = p(0) - p(x_t)$ and $\Delta\Omega = \Omega(\varepsilon_f) - \Omega(\varepsilon_t)$

A knowledge of Δp, $\bar{\varepsilon}$, ε_f and ε_t may thus give some indication of the value of $\Delta\Omega$, if the particle size range is very narrow.

If the solution of equation (3,19) is stable, then the voidage at the foot of the bed will not be too different from the uniform fluidisation voidage, and thus the presence of voidage gradients should make little difference to the growth of disturbance originating close to the distributor. The uniform fluidisation situation is a possible solution of equation (3,19) and any stable solution of (3,19) implies that

$$\left|\frac{d\Omega}{d\varepsilon}\right| > \rho_f \bar{u}_o^2 \frac{(1-\varepsilon)}{\varepsilon^3}.$$

The virtual mass term was dropped from the discussion leading to this inequality, and if the virtual mass effect is such that

$$\frac{d}{dt}(\underline{u} - \underline{v}) = \frac{\partial \underline{u}}{\partial t} + (\underline{u}.\mathrm{grad})\underline{u} - \frac{\partial \underline{v}}{\partial t} - (\underline{v}.\mathrm{grad})\underline{v}$$

then this inequality should be amended to

$$\left|\frac{d\Omega}{d\varepsilon}\right| > \rho_f \bar{u}_o^2 \frac{(1-\varepsilon)}{\varepsilon^3}\left(1 + \frac{\Theta(\varepsilon)}{\varepsilon}\right)$$

CHAPTER 4

Effects of the Various Bed Parameters on the Propagation Properties of Small Disturbances

This chapter deals mainly with the dependence of the propagation properties (wave-length, frequency, phase velocity, amplification factor and growth distance) on the variables appearing in equations (3,8), (3,9), (3,11) and (3,12). These variables depend largely on the constants defining the physical situation - the solid and fluid densities, the fluid viscosity, the particle diameter and the bed diameter - and on the state of the bed, determined by the superficial fluid velocity.

For a disturbance leading to possible instability of the state of uniform fluidisation, the initial concentration perturbation n_1 was found to be of the form

$$n_1 = N_0 \exp\left[\xi(\underline{k})t\right] \exp\left[j(\underline{k}.\underline{r} - \eta(\underline{k})t)\right]$$

where the amplification factor ξ and the angular frequency η are given by

$$\xi(\underline{k}) = \frac{B}{2A}\left[-\left(1+\frac{Dc}{B}\right) + \sqrt{\frac{\left[(1+p)^2+q^2\right]^{1/2} + (1+p)}{2}}\right] \qquad (3,11)$$

and

$$\eta(\underline{k}) = \frac{B}{2A}\left[\frac{2Fb}{B} + \sqrt{\frac{\left[(1+p)^2+q^2\right]^{1/2} - (1+p)}{2}}\right] \qquad (3,12)$$

The quantities p and q are given by

$$p = 2\left(\frac{Dc}{B}\right) + \left(\frac{Dc}{B}\right)^2 + 4\left(\frac{b}{B}\right)^2\left[F(A-F) - \frac{ADc}{b^2}\right] \qquad (3,8)$$

and

$$q = 4\left(\frac{b}{B}\right)\left[AE - F - \frac{FDc}{B}\right] \qquad (3,9)$$

so that $\xi(\underline{k})$ and $\eta(\underline{k})$ are rather complicated functions of the physical constants and the bed state, as well as, for any one bed state, the

components of the wave number vector. In addition, parameters appear in the above relationships which are, one supposes, uniquely determined by the overall bed parameters but whose dependence on these bed parameters if for the most part unknown; these parameters being the drag coefficient $n_0\beta_0'/\beta_0$, the virtual mass coefficient $\theta(\varepsilon)$, and the terms associated with the particulate phase stress tensor. For any one physical situation, values of these terms may be guessed and the nature of these terms (and the associated inspired guesswork) is discussed in detail in Appendix 2.

Three main points of interest regarding the propagation properties arise:-

(i) their dependence, for any one situation on the components of the wave number vector - especially on the vertical component and radial component for an axisymmetric disturbance; the way in which the various bed parameters affect this dependence is of the utmost importance;

(ii) for any one system, their dependence on the flow conditions;

(iii) the way in which they change from system to system.

The usual way of tackling a problem like this is to attempt to form dimensionless groups thus reducing the number of variables. In the present instance, there are too many variables, all dependent in some way or other on the basic quantities outlined above, to make this approach worthwhile. In addition the expressions are too complex to be able to predict by inspection how the propagation properties will vary so that probably the most convenient way is to carry out a series of detailed calculations for some widely differing physical situations. Calculations covering a wide variety of systems, based on the simpler set of equations which result when virtual mass and particle - particle interaction terms are neglected (see ref.(5)) are reported in Appendix 1. These calculations, however, deal only with the amplification of disturbances and not with phase velocities or frequencies.

Some indication of the way in which the phase velocity changes with flow rate, within one system, may be obtained by a closer study of the limits for one dimensional disturbances of large and small wave-length. These limits are (equations (3,13) and (3,14))

$$\lim_{k_x \to 0} V_p = \frac{\bar{u}_0}{\varepsilon_0}\left(1 - 2\varepsilon_0 + \varepsilon_0 \frac{n_0\beta_0'}{\beta_0}\right) \quad \text{and} \quad \lim_{k_x \to \infty} V_p = \frac{3\bar{u}_0 F}{\varepsilon_0 A}$$

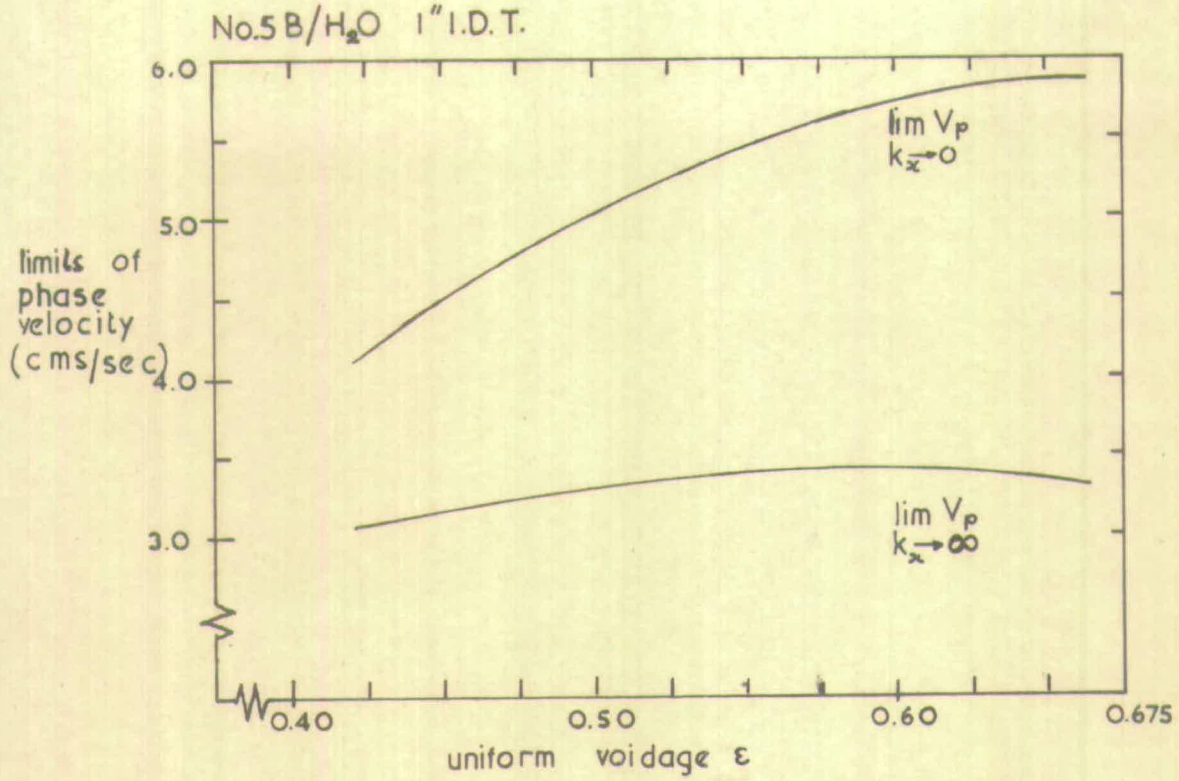


FIGURE 4.1 LIMITS OF V_p AS FNS. OF VOIDAGE.

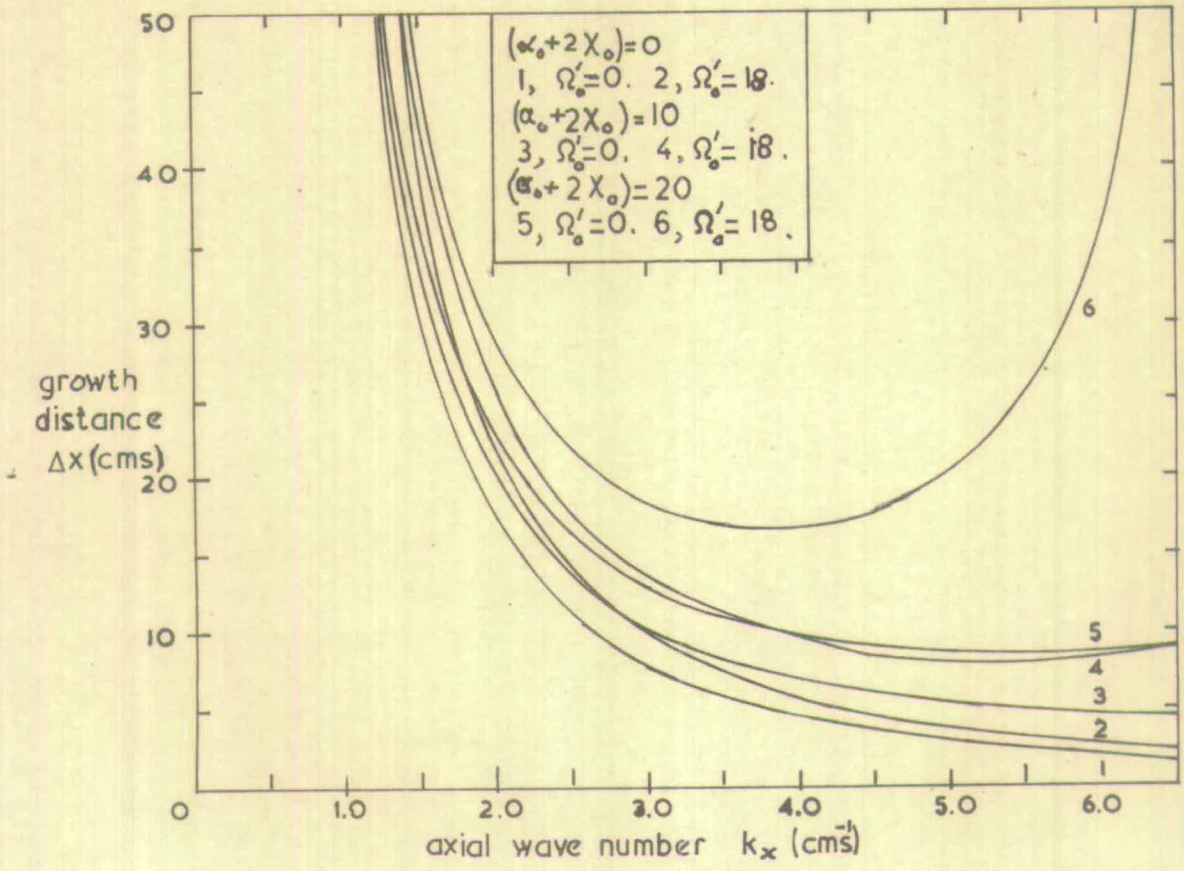


FIGURE 4.2 EFFECT OF SOLID STRESS ON GROWTH DISTANCE.

In Figure 4.1, these two limits of the phase velocity are plotted as a function of voidage for the system No.5 Ballotini/water. The fluidisation data used were taken from experimental results obtained in a one inch diameter tube. The values of the drag parameter $n_o\beta_o'/\beta_o$ were taken from results quoted in Appendix 2 and the virtual mass coefficient was assumed constant at 0.5. The plots show that both limits increase as the flow rate increases, although at higher voidages they both increase towards a maximum and then decrease. This maximum however is not really important in any physical sense as any regular disturbances appearing in the bed are broken up by turbulence setting in at the higher flow rates. This question of turbulence is further discussed in Chapter 5. For voidages not too far beyond incipient fluidisation, it would seem likely that the phase velocity will increase with flow rate. Intuitively one might expect to find that both phase velocity and frequency increase with flow rate.

The limits of the frequency at high and low wave lengths are

$$\lim_{k_x \to 0} \eta(k_x) = bE$$

and

$$\lim_{k_x \to \infty} \eta(k_x) = \frac{3bF}{A}$$

where $E = \left(1 - 2\varepsilon_o + \varepsilon_o \frac{n_o\beta_o'}{\beta_o}\right)$, $b = \frac{\bar{u}_o k_x}{\varepsilon_o}$ and $A = 1 + \frac{\rho_s}{\rho_f} \cdot \frac{\varepsilon_o}{1-\varepsilon_o} + \frac{\theta_o}{\varepsilon_o(1-\varepsilon_o)}$

and $F = 1 + \frac{\theta_o}{\varepsilon_o}$

For a liquid fluidised bed, $\bar{u}_o$ is given by the Richardson and Zaki (21) relationship as $\bar{u}_o = u_t \varepsilon_o^N$ where N is at least 2.5. Using this relationship and the form of $n_o\beta_o'/\beta_o$ obtained in Appendix 2 from the Carmen - Kozeny* equation viz. $\frac{n_o\beta_o'}{\beta_o} = \frac{2}{\varepsilon_o}$, it is a simple matter to show that the

*It is not perhaps very logical to use the Richardson and Zaki relationship to find $\bar{u}_o$ and the Carmen - Kozeny equation to estimate $n_o\beta_o'/\beta_o$. However at low voidages, the values of $n_o\beta_o'/\beta_o$ found from the Richardson and Zaki equation and the Carmen - Kozeny equation are not very different. The simplicity of the equation for $n_o\beta_o'/\beta_o$ from the Carmen - Kozeny equation facilitates the investigation of the limits.

limit of the angular frequency at low wave numbers increases with flow rate. Like the phase velocity, the limit of the frequency at high wave numbers exhibits a maximum near $\varepsilon_o = 1$ after which it rapidly tends to zero. This, as with the phase velocity, occurs because of the limit of the quantity A as $\varepsilon_o \rightarrow 1.0$

The limits of the amplification factor were discussed early in Chapter 3 and the significance of the various terms, especially the particle normal stress term ($|d\Omega/d\varepsilon|$) and the particulate phase "viscosity" term dealt with. These are of crucial importance in determining the behaviour of the bed. It is not easy, however, to predict by inspection how the amplification factor will vary with flow rate. This will be discussed in the following section, which deals with the detailed calculations for specific systems.

Results of the Detailed Calculations

It was decided to carry out detailed calculations for a typically particulate system and a typically aggregative system. For convenience, since the density and diameter of the solid were already known and because, for the liquid system, detailed expansion data were available from the experimental work, the systems chosen were No.5 ballotini fluidised by air and water. Other calculations on a variety of systems were carried out, but these merely reinforced the conclusions obtained from calculations for the above mentioned systems. The results for the chosen systems show very clearly the effects the various parameters have on the propagation properties. The effects of different particle size, density ratio etc. are shown up well in Appendix 1, where the growth distances for a number of different systems are compared. Virtual mass and particle "viscous" effects are not included, and the calculations are for a disturbance whose wave length is a constant multiple of the particle diameter, but it is not expected that this would significantly change the conclusions.

It is convenient at this stage to point out the main difference between typical liquid fluidised systems and typical gas fluidised systems. For a liquid fluidised bed, where there generally occurs a smooth bed expansion, the superficial fluid velocity is related to the mean bed voidage $\bar{\varepsilon}$ by the Richardson and Zaki (21) relationship - $\bar{u}_o = u_t \bar{\varepsilon}^N$, $\frac{d_p}{d_t} \ll 1$

where u_t is the terminal falling velocity of the particle in the liquid and N is a constant for the system. Thus the voidage is determined by $\bar{u}_o$. For aggregative systems, however, no such relationship obtains and the bulk of the fluid flow over that required for incipient fluidisation appears to pass through the bed as bubbles, the voidage of the dense phase remaining at a more or less constant value close to that of minimum fluidisation. (This point is dealt with in some detail by Davidson and Harrison (3)). To calculate the propagation properties of small disturbances appearing in the dense phase of such a system at different flow rates, the voidage appearing in the equations should remain constant. Any disturbance originating close to the distributor sees only the dense phase voidage. However it is not at all clear what happens just above the distributor in an aggregative bed.

Equations (3,11) and (3,12) were programmed for a Ferrenti - Sirius computer to calculate phase velocity, frequency, amplification factor and growth distance as a function of the axial wave number k_x for any given set of bed conditions. These quantities were calculated for different values of the various bed parameters - generally unknown but constant for any flow rate - to illustrate the effect they have on the propagation properties. The effect of boundary conditions on an axisymmetric disturbance was investigated. Calculations, at least in the case of the water fluidised system, were carried out for a range of flow rates.

The values of the parameters from the particulate phase stress tensor ($|d\Omega/d\varepsilon|$ and $(\alpha_o + 2\gamma_o)$) were obtained as outlined in Appendix 2. Values for the drag coefficient $n_o\beta_o'/\beta_o$ were taken from the values predicted by the Richardson and Zaki equation for the No. 5 B/H_2O system. These are reported in Appendix 2. The same values of this term were used for the system No. 5 B/Air and while, as explained above, this is not likely to be very accurate, it does give values to use in the equations. Except where the virtual mass coefficient was varied, it was taken to have a value of 0.5. The radial wave number was calculated from

$$k_\rho = 4.81/d_u$$

where $d_u = d_t(1 - c'd_p/d_t)$. When the effect of the radial wave number was being investigated, the constant c' was varied between -30 and +5; the

negative values, while not physically meaningful, serve to impose a less severe boundary condition than $n_1 = 0$ at $\rho = d_u/2$. At all other times the constant c' was taken as zero. For all systems investigated the limit of physical meaningfulness of the smallest wave length was taken about five particle diameters.

For No. 5 glass ballotini, the solid density is 2.86 gms/cc and the particle diameter is 0.086 cms. The density and viscosity of air were taken as 1.3×10^{-3} gms/cc. and 1.8×10^{-4} poise, while for water the density was taken as 1.0 gms/cc. Values of the superficial fluid velocity for the liquid system were taken from experimental values obtained in a 1 inch diameter tube. The velocity of the air was calculated by the methods described on p.14 of ref.(3). It was assumed that the bed was at incipient fluidisation (corresponding to an assumed voidage of 0.420) and the propagation properties of the air fluidised bed were calculated only for this state. For the No. 5 B/H_2O system, all calculations were carried out for a voidage of 0.460 except when changes in the flow conditions were being investigated.

Parameter values used for the liquid fluidised system are tabulated below.

ε_o	$\bar{u}_o$ (cms/sec.)	$n_o \beta_o' / \beta_o$	χ_o (poise)	$d\Omega/d\varepsilon$
0.420	1.00	3.91	8	-16
0.460	1.27	3.48	5	-18
0.500	1.61	3.11	3	-20

All quantities are in c.g.s. units. The normal stress term appearing in the expressions for the propagation properties is

$$e = \frac{n_o \Omega_o'}{\rho_s (1-\varepsilon_o)} \left(k_x^2 + k_\rho^2\right)$$

Since $n_o v = 1 - \varepsilon_o$, $n_o \Omega_o' = (1-\varepsilon_o)\left|\frac{d\Omega}{d\varepsilon}\right|$ so that $e = \left|\frac{d\Omega}{d\varepsilon}\right| \frac{(k_x^2 + k_\rho^2)}{\rho_s}$.

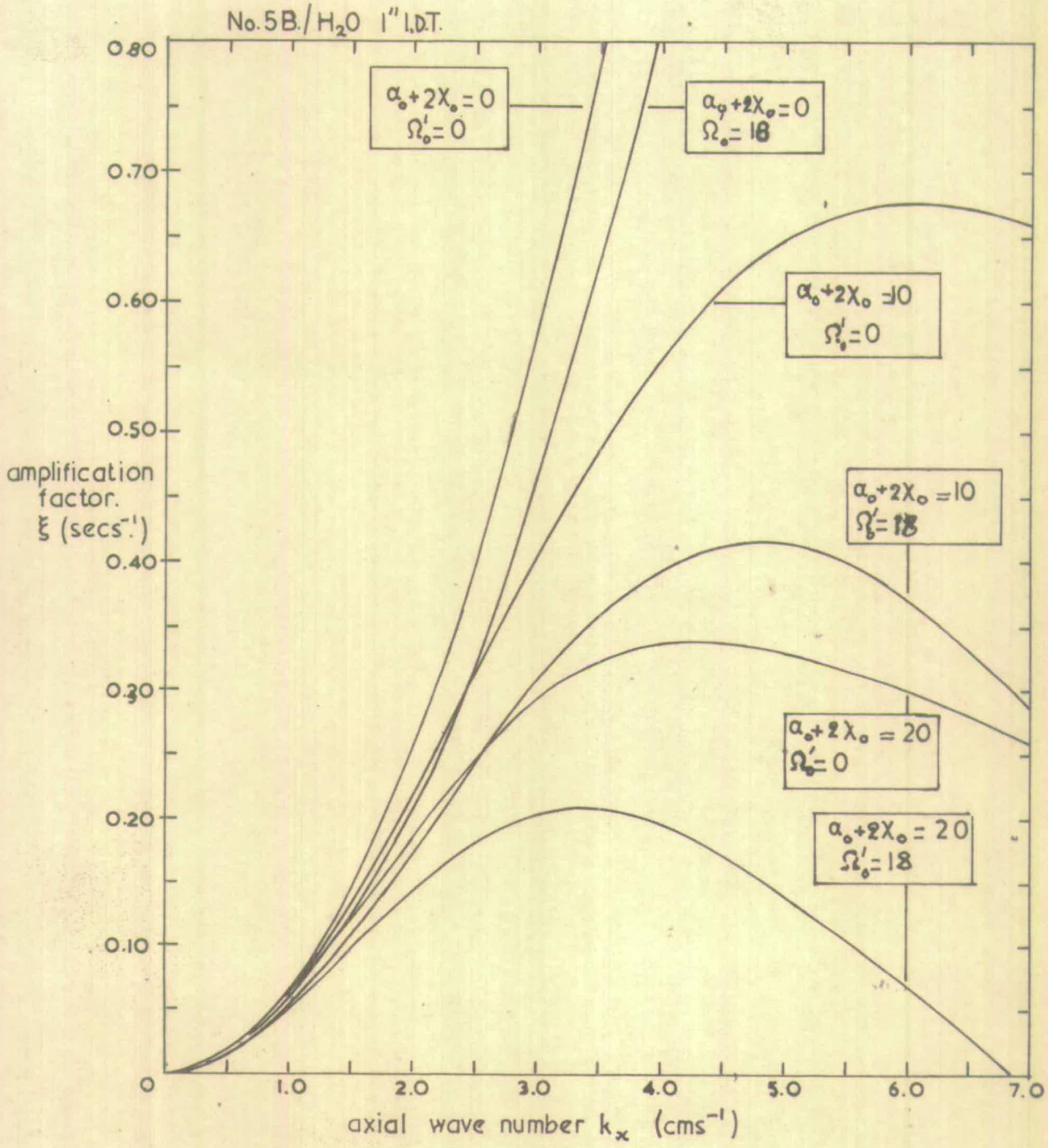


FIGURE 4.3 EFFECT OF SOLIDS STRESS ON AMPLIFICATION FACTOR.

(for Ω_0', read N.S.)

The units of $d\Omega/d\varepsilon$ are dynes/cm.^{2} unit voidage change. The values of the particulate phase shear "viscosity" were based on the experimental results of Anderson and Bryden (31) (discussed in Appendix 2) and the value of the term $(\alpha_o + 2\chi_o)$ varied between χ_o and $4\chi_o$.

The parameters whose effects on the growth properties were investigated were

i) the particulate phase "viscosity" term $(\alpha_o + 2\chi_o)$
ii) the particulate phase normal stress term Ω'_o
iii) the virtual mass coefficient $\theta(\varepsilon_o)$
iv) the radial wave number k_ρ
v) the viscous drag term $n_o\beta'_o/\beta_o$

These were varied in turn inside one flow situation for selected values of the other parameters.

The conclusions reached about the importance of the various parameters are illustrated first by reference to the calculations done on the water system. The results of calculations for the air fluidised system are then reported and serve mainly to reinforce these conclusions, as well as to highlight the effect of density ratio.

In the figures of the following pages, the term P.V. stands for $(\alpha_o + 2\chi_o)$ and N.S. for $\left|\frac{d\Omega}{d\varepsilon}\right|$

(a) Effect of the Particulate Phase Stress Tensor Terms

These calculations for the No. 5 B/H_2O system are reported for a uni-dimensional disturbance only. The value of the "viscosity" term $(\alpha_o + 2\chi_o)$ was varied between zero and five times the shear "viscosity" i.e. between P.V. = 0 and 25 poise for $\varepsilon_o = 0.460$. For each value of P.V., $|d\Omega/d\varepsilon|$ was varied between 0 and 24 dynes/cm.^{2}/unit voidage change. The results are quoted for N.S. = 0 and 18 and for P.V. = 0, 10 and 20 poise. The voidage is 0.460 and the radial wave number is zero.

Figure 4,3 shows the effect these terms have on the amplification factor (written A.F. in all that follows). The effect of the particulate phase "viscous" term is quite spectacular. For zero particulate phase "viscosity", the A.F. increases monotonically with wave number; this is the result expected from the simpler equations (5) with no particulate phase stress tensor included. Its inclusion in the calculations markedly reduces the A.F. and introduces a maximum into the A.F. - k_x curve within

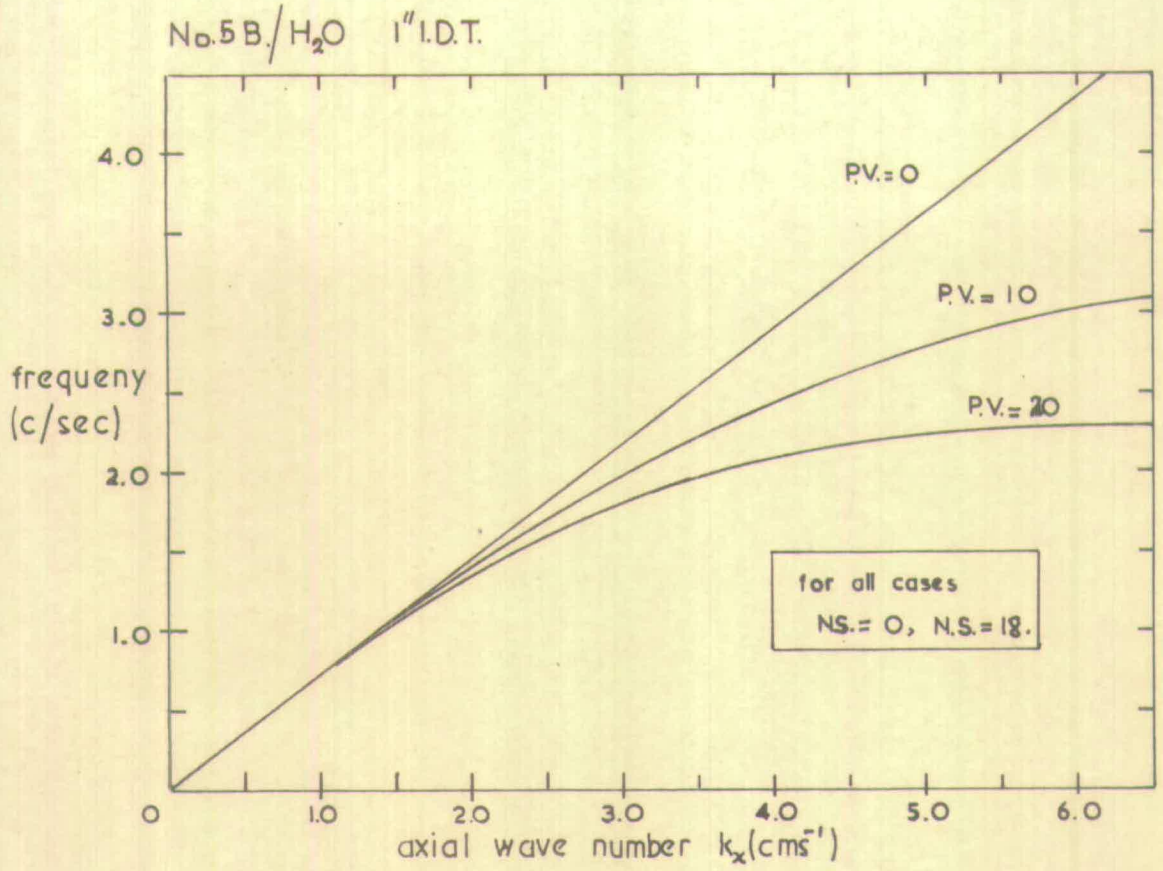


FIGURE 4.4 EFFECT OF SOLIDS STRESS ON FREQUENCY.

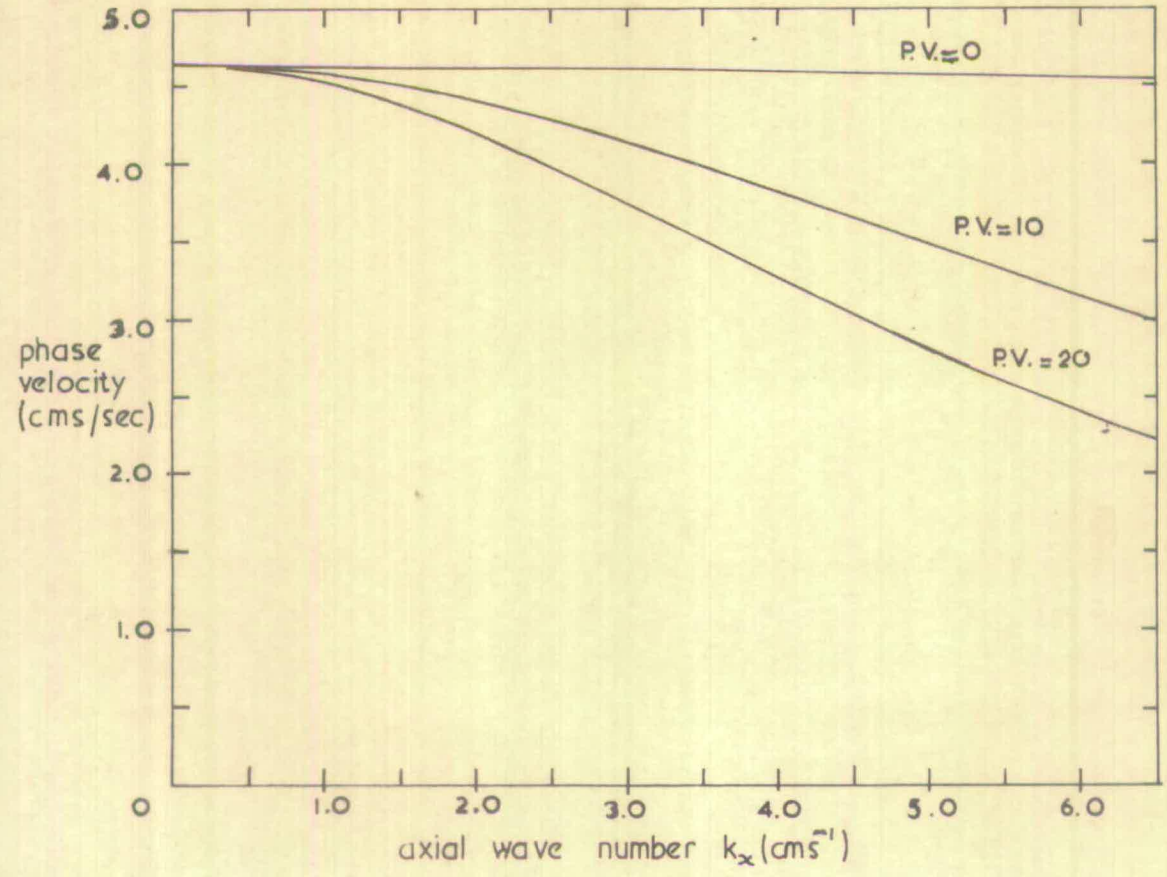


FIGURE 4.5 EFFECT OF SOLIDS STRESS ON VELOCITY.

the range of meaningful wave number, and, as shown in Chapter 3, gives the A.F. a finite limit as the wave number tends to infinity. Increasing the value of the "viscous" term reduces the maximum and shifts its position to a smaller wave number.

This property of the shear and bulk "viscosity" term is extremely important, implying that, out of the whole spectrum of disturbances of different wave lengths which might be present in any situation, there is one disturbance of a certain wave-length which will amplify faster in time than the others. Pigford (6) found the same effect when he included a solids "viscosity" term in his equations (see Chapter 1). However after the maximum, the A.F. became zero at large values of the wave number - an effect not encountered in the present work. The reason for this is not clear.

The normal stress term appears, from the calculations, to have a significant effect only on the A.F. It reduces the value of the A.F. although its inclusion in the equations, without the "viscosity" term, does not produce a maximum. However, once the maximum has been attained because of the inclusion of the "viscosity", the effect of the normal stress term can be profound. It reduces the value of the maximumm and the value of the wave number at which this maximum appears and causes the A.F. curve to decrease much more rapidly after the maximum. At higher wave numbers, after the initial maximum, the normal stress term may cause the A.F. to go negative. High enough values of the normal stress term will lead to the A.F. being negative over the whole range of k_x, thus producing stability (this point is discussed later).

In Figures 4.4 and 4.5, the frequency and phase velocity are plotted as functions of the wave number. Inside this range of wave numbers the effect of the normal stress term appears to be negligible. This conclusion is reinforced by the results quoted in Chapter 8. Only for the cases where the "viscosity" term was zero did the normal stress term exhibit some very slight effect on the phase velocity or frequency. The fact that this term is of so little importance to the frequency implies that the significant contribution to the square root part of equation (3,12) comes from "q", since the normal stress appears only in the term "p".

The effect of the "viscosity" term is again profound. For

this term zero, the frequency is almost linear in k_x and hence the phase velocity is practically constant. Inclusion of the "viscosity" term, however, reduces the frequency below the values given by this linear relation and eventually, as the "viscosity" term is increased, introduces a maximum into this curve. The phase velocity is correspondingly reduced and becomes strongly dependent on k_x; the system now exhibiting dispersion (dependence of the phase velocity on the wave number). Intuitively, the reduction of phase velocity and frequency is the type of effect one might expect to find by inclusion of this term, although the maximum in the lower curve of Fig. 4.4. is unexpected.

The growth distance is plotted in Figure 4.2 for various values of the "viscosity" and normal stress term. The maximum produced in the A.F. by the "viscosity" produces a minimum in the growth distance, although this is not very pronounced for low "viscosity" values and no normal stress. However, inclusion of the normal stress introduces a very pronounced minimum into the growth distance curve. The position of this minimum (the value of k_x at which it occurs) does not correspond to the position of the maximum in the corresponding A.F. curves. This is due to the dependence of phase velocity on wave number and means that the disturbance component which grows fastest in time is not the component which amplifies fastest in distance - this component having a larger wave number and hence shorter wave length.

The calculations described above give some indication of the profound effect the particulate phase stress terms can have on the probable behaviour of the bed - particularly the possible emergence of a dominant wave length from a general disturbance with a whole spectrum of wave lengths.

(b) Effect of Boundary Conditions

Again these calculations were carried out for the system No. 5 B/H_2O at a voidage of 0.460.

It is only really practicable to apply boundary conditions to the axisymmetric disturbance case, since, for any other situation, the evaluation of k_y and k_z is not altogether easy. For the axisymmetric case $k_y^2 + k_z^2 = k_\rho^2$ with $k_\rho = 4{\cdot}810/d_u$, $d_u = d_t\left(1 - c' d_p/d_t\right)$.

No. 5 B./H_2O: 1" I.D.T.

for all figures, P.V. = 20
curve (1) N.S. = 0, $k_p = 0$, . curve (2.) N.S. = 0, $k_p = 1.89$, .
curve (3) N.S. = 18, $k_p = 0$, . curve (4.) N.S. = 18, $k_p = 1.89$, .

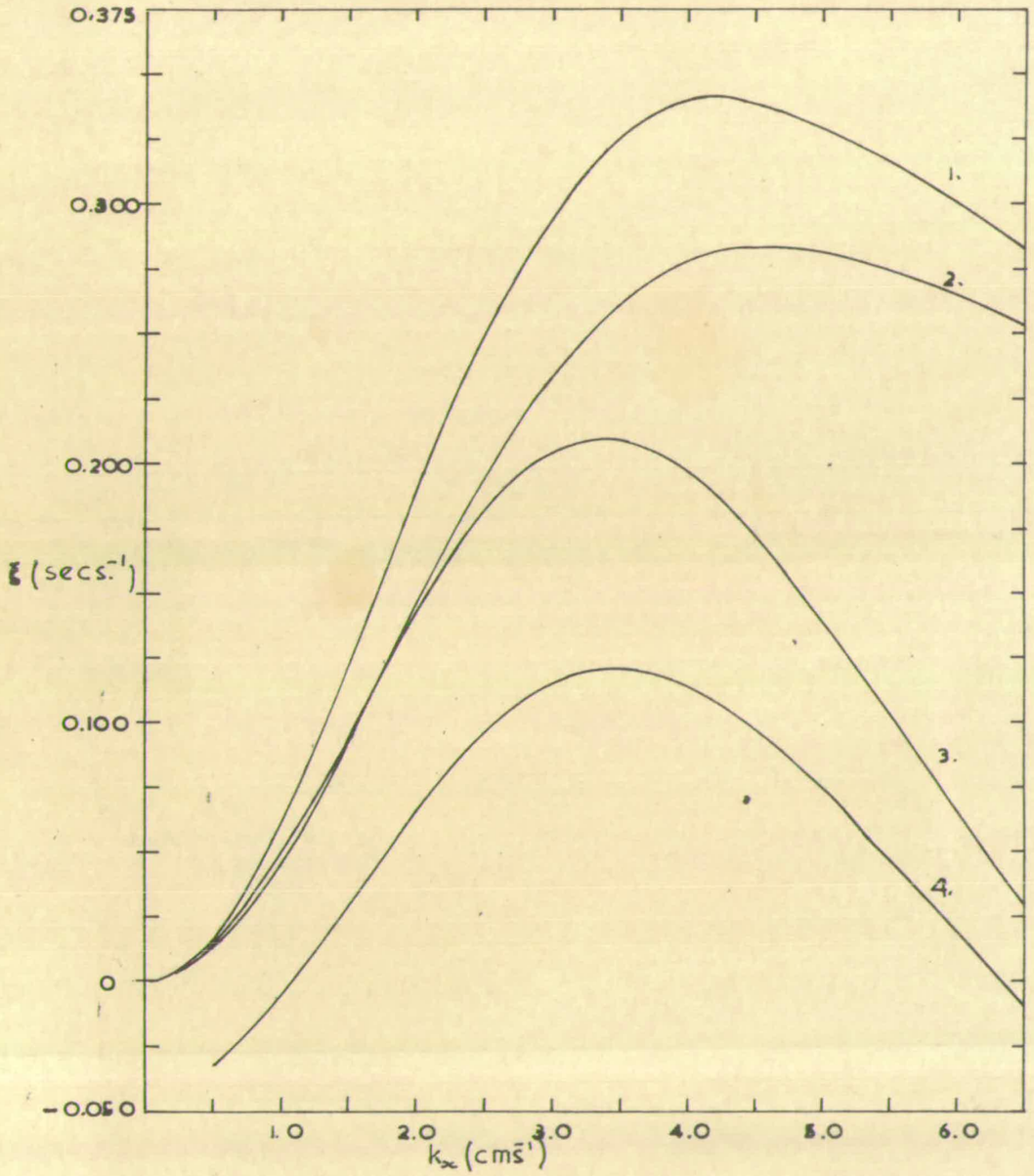


FIGURE 4.6 EFFECT OF RADIAL WAVE NUMBER ON AMPLIFICATION FACTOR.

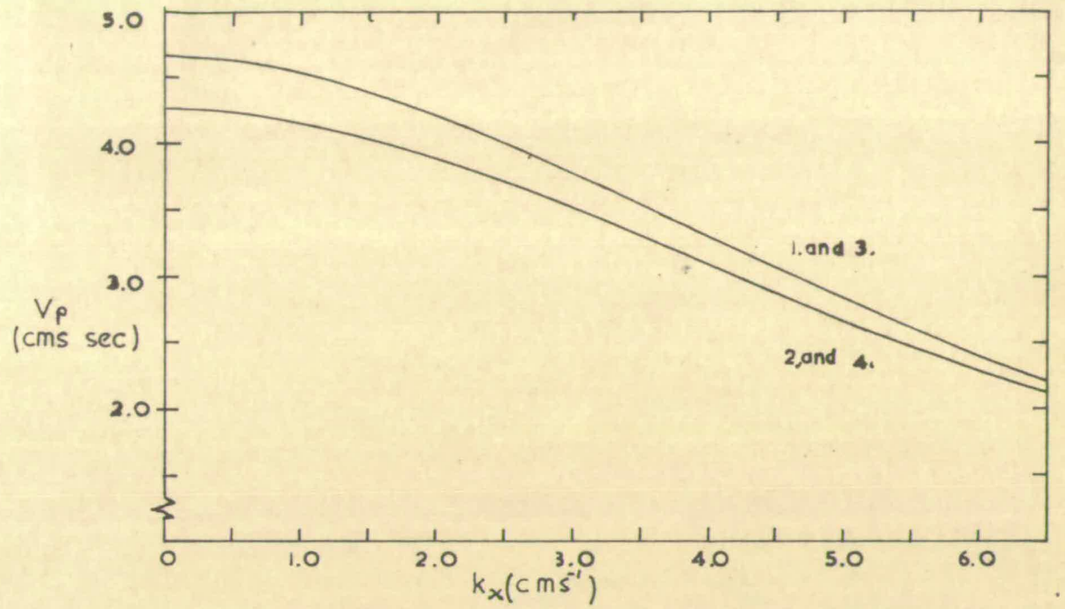


FIGURE 4.7 EFFECT OF RADIAL WAVE NUMBER ON PHASE VELOCITY.

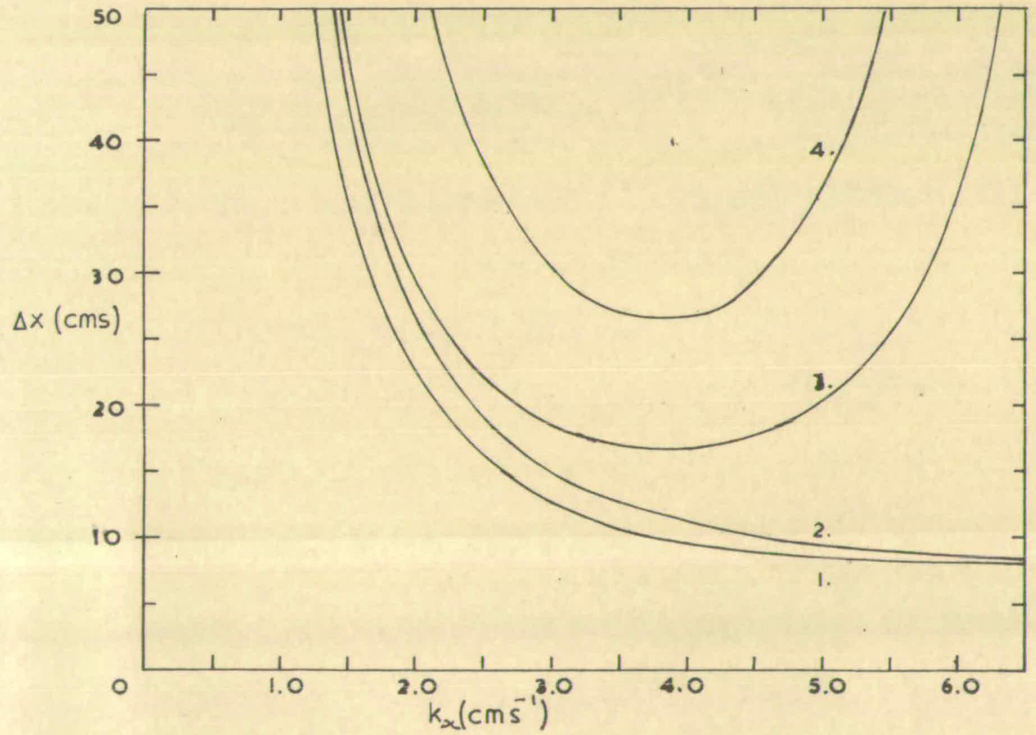


FIGURE 4.8 EFFECT OF RADIAL WAVE NUMBER ON GROWTH DISTANCE.

For the figures shown, $c' = 0$ so that the diameter of the uniform core $d_u = d_t$ — that is, at $\rho = d_u/2$, $n_1 = 0$. While this is perhaps rather an extreme case because of particle slip at the walls, it does serve to show the effects boundary conditions have. The bed diameter used was 1 inch.

The boundary conditions impose a finite size on the radial wave length and hence increase the wave number from zero to some value k_ρ. The effect of imposing boundary conditions is to reduce the A.F., the frequency and the phase velocity. Intuitively this is so, and the conclusion is borne out by inspection of the expressions for these quantities. The term k_ρ always appears in expressions containing the terms from the particulate phase stress tensor, viz.

$$c = \frac{(\alpha_o + 2\gamma_o)}{\rho_s(1-\varepsilon_o)}(k_x^2 + k_\rho^2) \quad \text{and} \quad e = \frac{|d\Omega/d\varepsilon|}{\rho_s}(k_x^2 + k_\rho^2)$$

Thus when $k_\rho \sim k_x$, it effectively increases the value of the terms c and e and its inclusion should merely reinforce the effects of these terms described in the previous section. When k_ρ is very much less than k_x, it should have little effect on the propagation properties.

Figure 4.6 illustrates the effect it has on the A.F.. The curves are plotted for a value of the "viscosity" term equal to 20 poise. The effect of k_ρ when the normal stress term is zero is relatively small. When this term is not zero, however, the effect is quite important — reducing the value of the maximum and increasing the value of k_x at which it occurs. Together with the normal stress term, it also profoundly effects the values of the A.F. at low k_x — making the A.F. become negative. This is due to the term $-De/b^2$ which contains the expression $(1 + k_\rho^2/k_x^2)$ This causes negative values of the growth distance after the discontinuity at A.F. equal to zero, but these negative values are physically meaningless and have not been included in the figures.

A finite value for the radial wave number slightly reduces the phase velocity, as expected, but this effect does not appear to be too important. However, because of the large effect of the normal stress in conjunction with the radial wave number, the growth distance becomes much larger and its minimum much more pronounced. The value of k_x at which this minimum occurs is also brought much nearer the value of k_x at which the maximum in the A.F. occurs. This is shown in Figure 4.8.

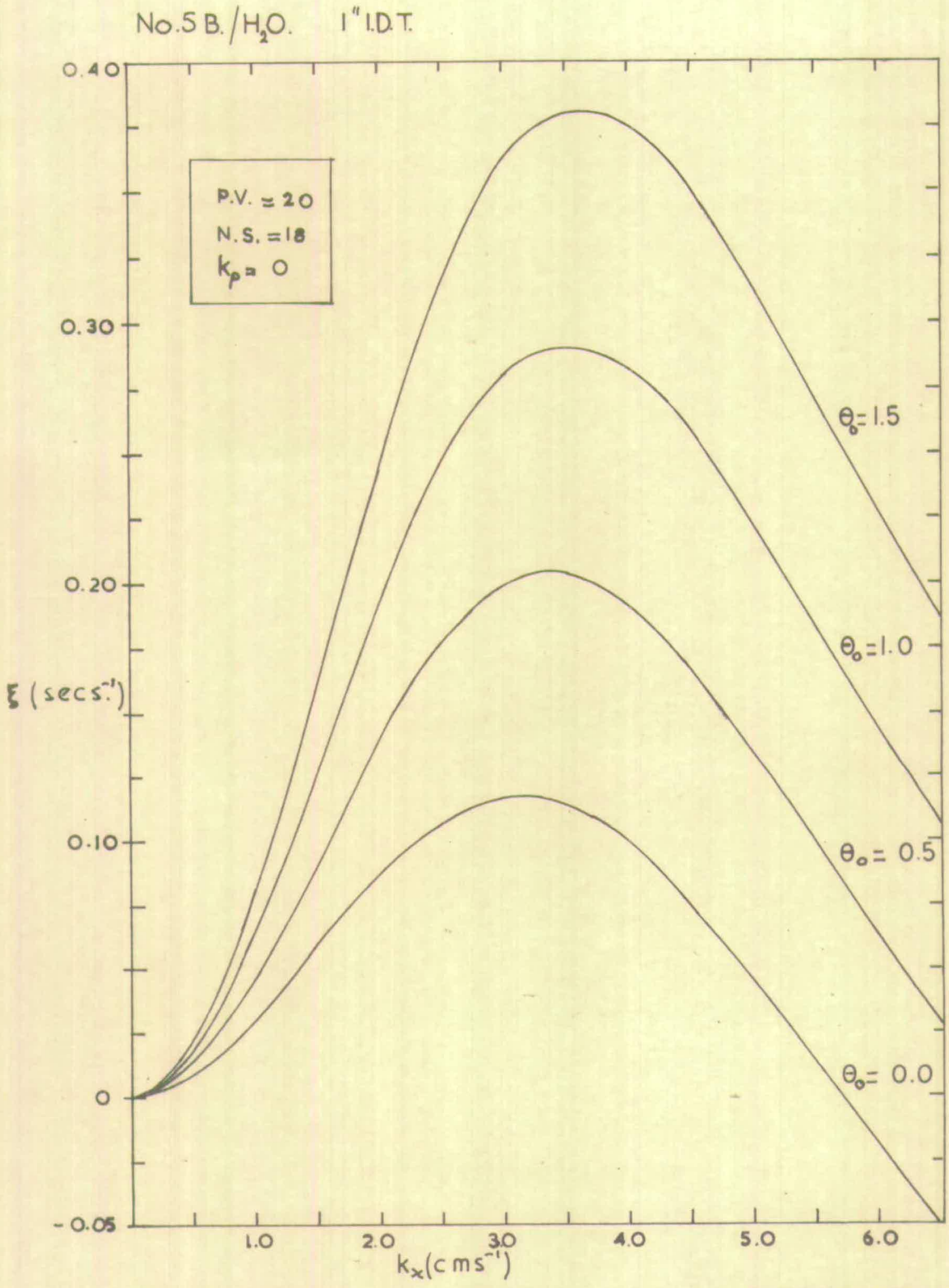


FIGURE 4.9 EFFECT OF VIRTUAL MASS COEFFICIENT ON AMPLIFICATION FACTOR

(c) Effect of the Virtual Mass Coefficient

It is almost impossible to predict, at least by inspection, how variations of this term would cause the propagation properties to change because of the number of terms it effects in the dispersion relationship For calculationpurposes, the propagation properties of a disturbance appearing in the No. 5B/H_2O_λ system at a voidage of 0.460 were calculated for values of the virtual mass coefficient equal to 0, 0.5, 1.0 and 1.5.

The function $\Theta(n)$ is completely unknown, but, apart from this, there is a further uncertainty about the form of the differential operator d/dt appearing in the virtual mass term. The form used in these calculations is

$$\frac{d}{dt}(\underline{u} - \underline{v}) = \left\{\frac{\partial \underline{u}}{\partial t} + (\underline{u}.\text{grad})\underline{u}\right\} - \left\{\frac{\partial \underline{v}}{\partial t} + (\underline{v}.\text{grad})\underline{v}\right\}$$

This is a fairly strong form for the term, as is readily seen on comparing equations (3,4) and its equivalent when $\frac{d}{dt}(\underline{u} - \underline{y})$ is taken as

$\frac{\partial}{\partial t}(\underline{u} - \underline{y}) + (\underline{v}.\text{grad})(\underline{u} - \underline{y})$.

Thus the calculations described below indicate only some of the possible effects.

Varying the virtual mass coefficient (V.M.C.) over the range described above did not change significantly the frequency or phase velocity. Its effect on the A.F. and growth distance was however very marked and this is shown in Figure 4.9. As the V.M.C. is increased so also is the A.F. and hence the growth distance is reduced. The value of the wave number at which the maximum occurs slightly increases with increasing V.M.C.

This quantity could therefore be very important in determining the growth of any disturbance, at least in a liquid fluidised bed. However, to properly assess its importance, the form of the virtual mass term and the dependence of the coefficient on voidage must be known.

(d) Effect of the Drag Coefficient

The effect of changing the drag term $n_0\beta_0'/\beta_0$ is shown in Figures 4.10 and 4.11 in which the A.F. and the phase velocity are plotted. The values of $(\alpha_0 + 2\chi_0)$ and $|d\Omega/d\Sigma|$ were taken, as before, as 20 P and

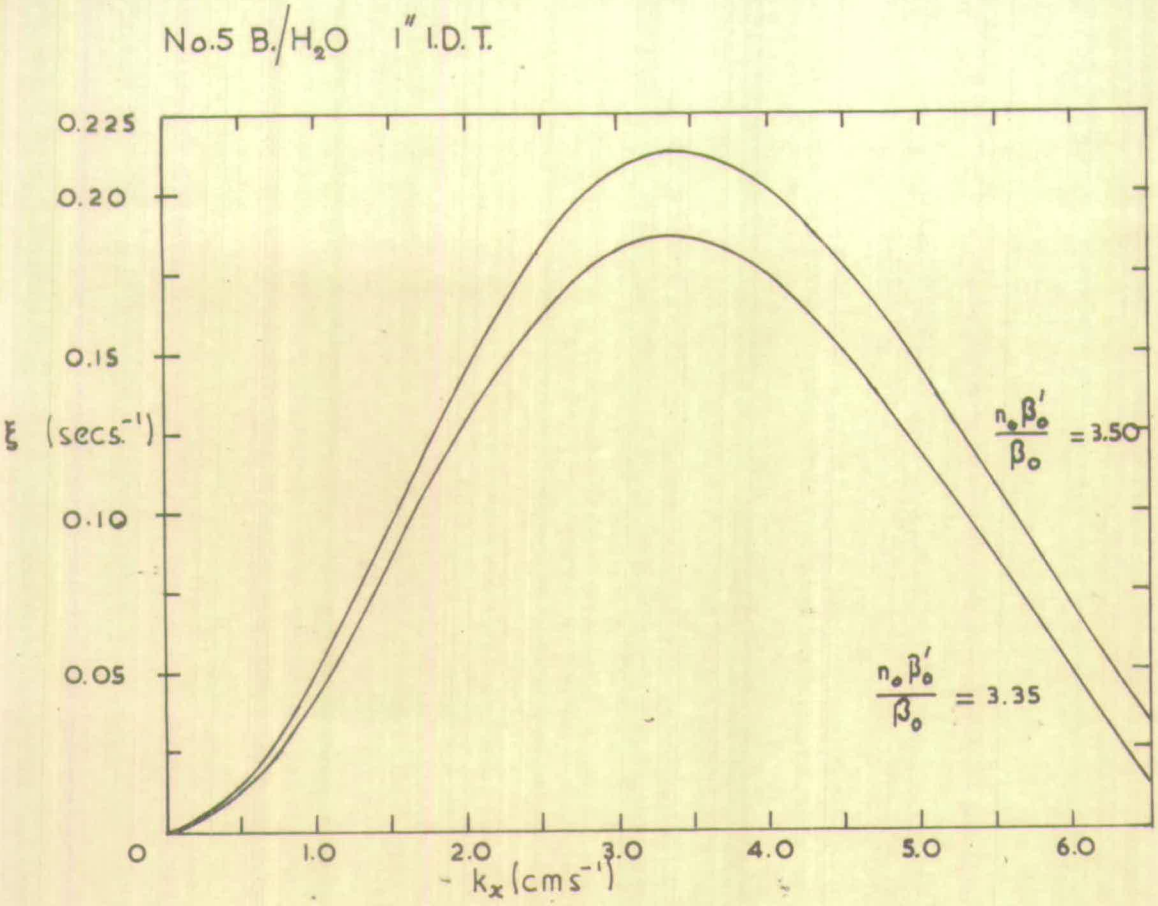


FIGURE 4.10 EFFECT OF DRAG PARAMETER ON AMPLIFICATION FACTOR.

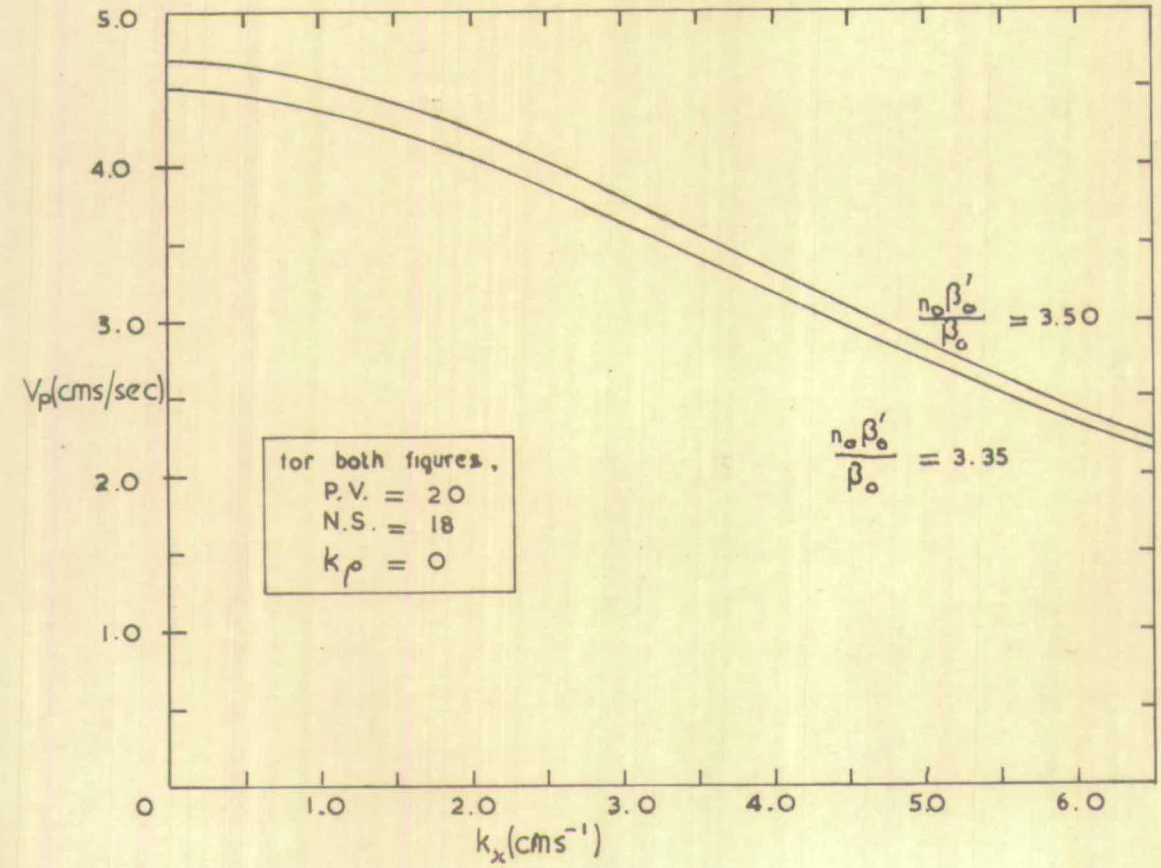


FIGURE 4.11 EFFECT OF DRAG PARAMETER ON PHASE VELOCITY.

18 dynes/cm^2/unit voidage change for the system No.5 B/H_2O. Only a one dimensional disturbance was considered. Reducing the drag coefficient is seen to lower the A.F. and phase velocity, and hence the frequency, although the position of maximum A.F. is not affected. Although not shown, the growth distance is increased.

(e) <u>The Air Fluidised System No.5 B/AIR</u>

The propagation properties for this system were calculated at $\varepsilon_o = 0.420$ - a value probably close to the voidage at incipient fluidisation. The superficial fluid velocity was calculated as being around 92 cms/sec.. The particulate phase "viscosity" term was taken to be the same as in the liquid fluidised bed - the values are in accordance with experimental values found for air fluidised beds (see Appendix 2). Values of $|d\Omega/d\varepsilon|$ equal to 20 dynes/cm^2/unit voidage change (similar to the liquid fluidised bed) and 200 dynes/cm^2/unit voidage change were used. For the figures shown, the radial wave number was taken as 1.13 cms^{-1}, corresponding to a value of -20 for c' and a 1" diameter bed; The virtual mass coefficient was, as before, taken as 0.50; the value of $n_o\beta_o'/\beta_o$ was taken as 3.91 - the value obtained for the system No.5 B/H_2O.

The effects of boundary conditions and variations in the drag coefficient are much the same as for the liquid fluidised bed. The boundary condition imposed increases the growth distance and decreases the other quantities, and decreasing the drag coefficient decreases the A.F. and phase velocity. Changing the virtual mass coefficient, however, changes the growth properties only very slightly - in contrast to the liquid fluidised bed, but as expected because of the small mass of displaced fluid. However slight, the changes do occur in the same way. The fact that virtual mass has very little effect in this system is presumably due to the large density ratio, which far outweighs the effect of virtual mass in the term "A" appearing in the propagation property expressions. Surprisingly, although the effect is very slight, affecting two out of four significant figures, the virtual mass coefficient does alter the frequency and phase velocity for the air bed rather more than for the liquid bed.

Figures 4.12, 4.13, 4.14 and 4.15 illustrate the effect of changing the "viscosity" term for the conditions outlined above. The most obvious differences between this system and the water fluidised bed are th

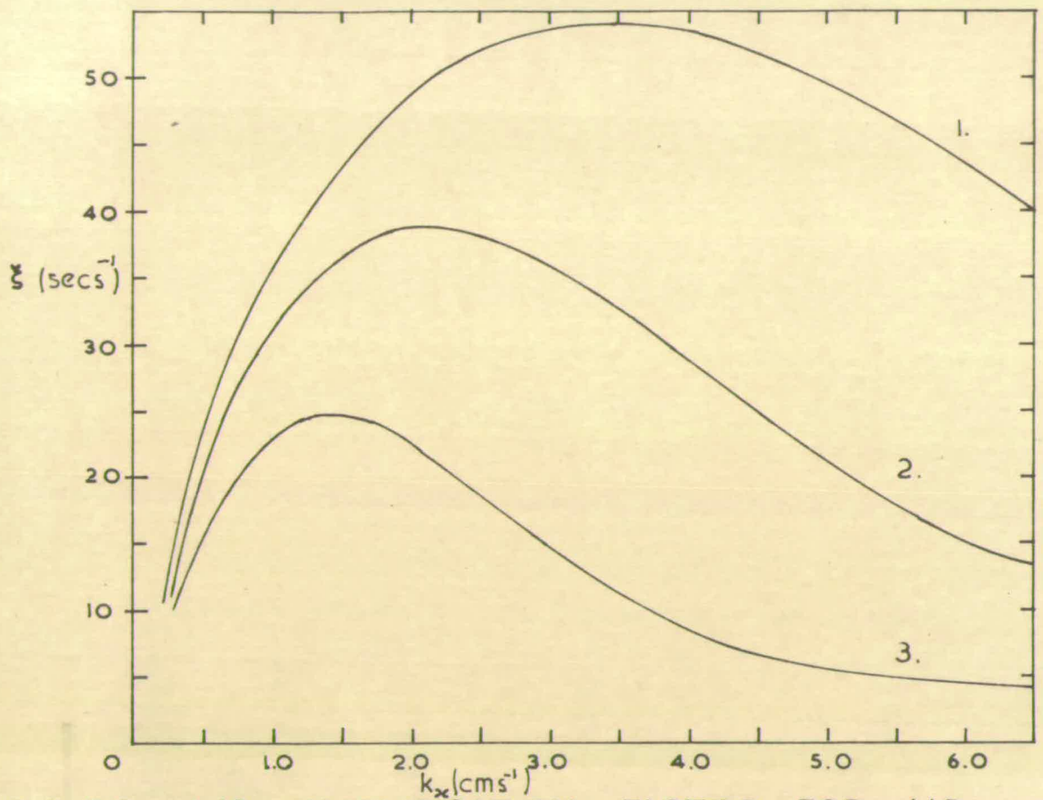


FIGURE 4.12 AMPLIFICATION FACTOR FOR AIR FLUIDISED BED.

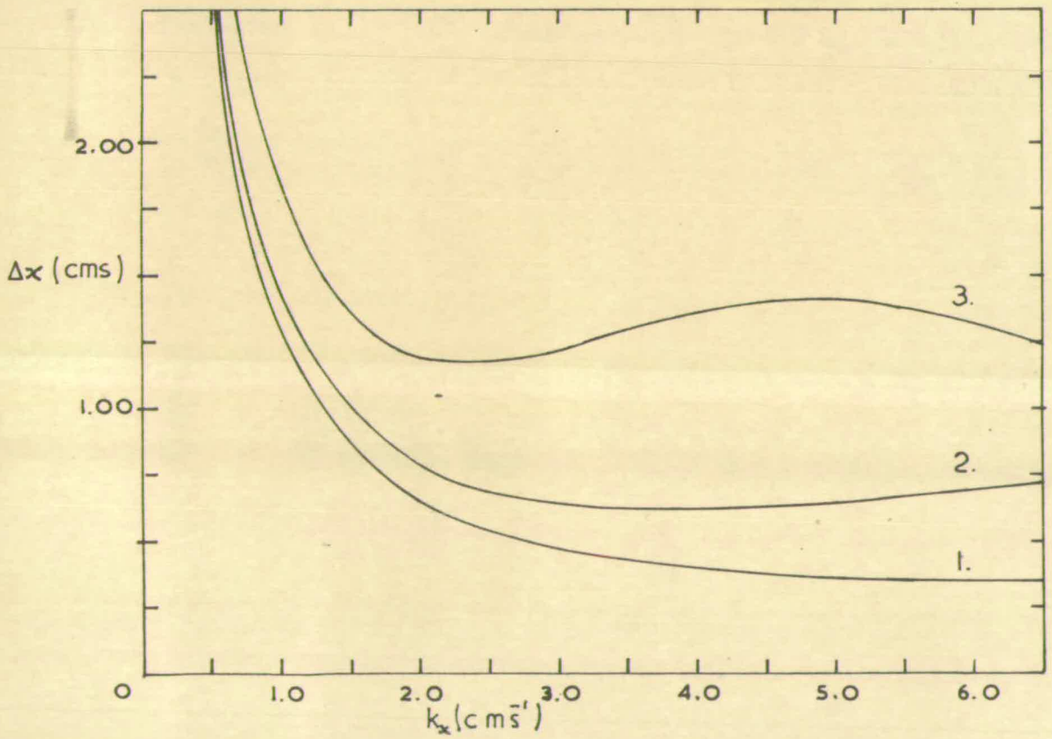


FIGURE 4.15 GROWTH DISTANCE FOR AIR BED.

for all figures, N.S.=20., k_p=1.13.,
curve (1) P.V. = 8, curve (2) P.V. = 16,
curve (3) P.V. = 32,

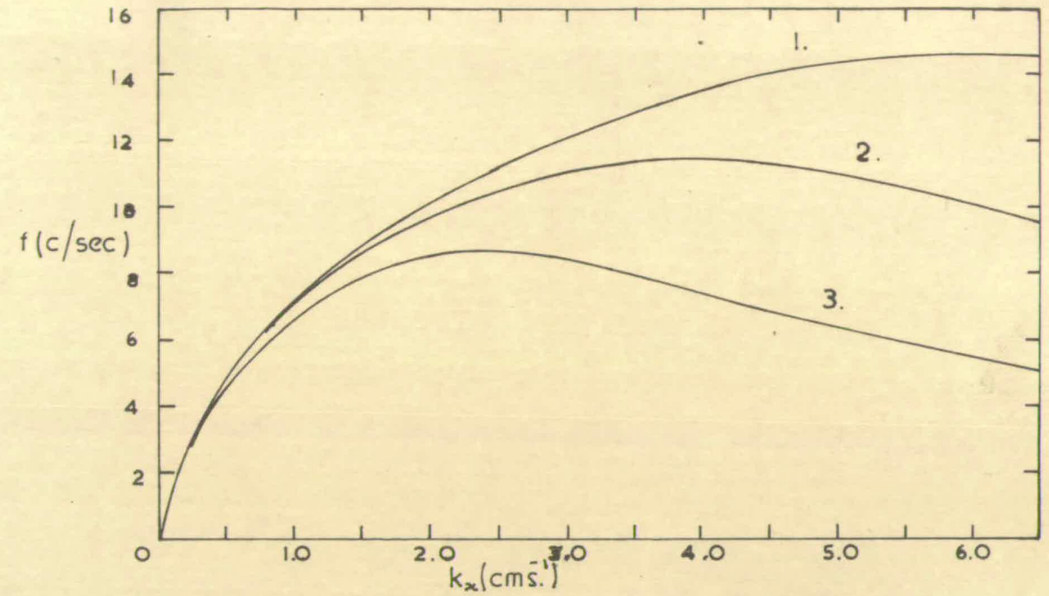


FIGURE 4.13 FREQUENCY FOR AIR BED.

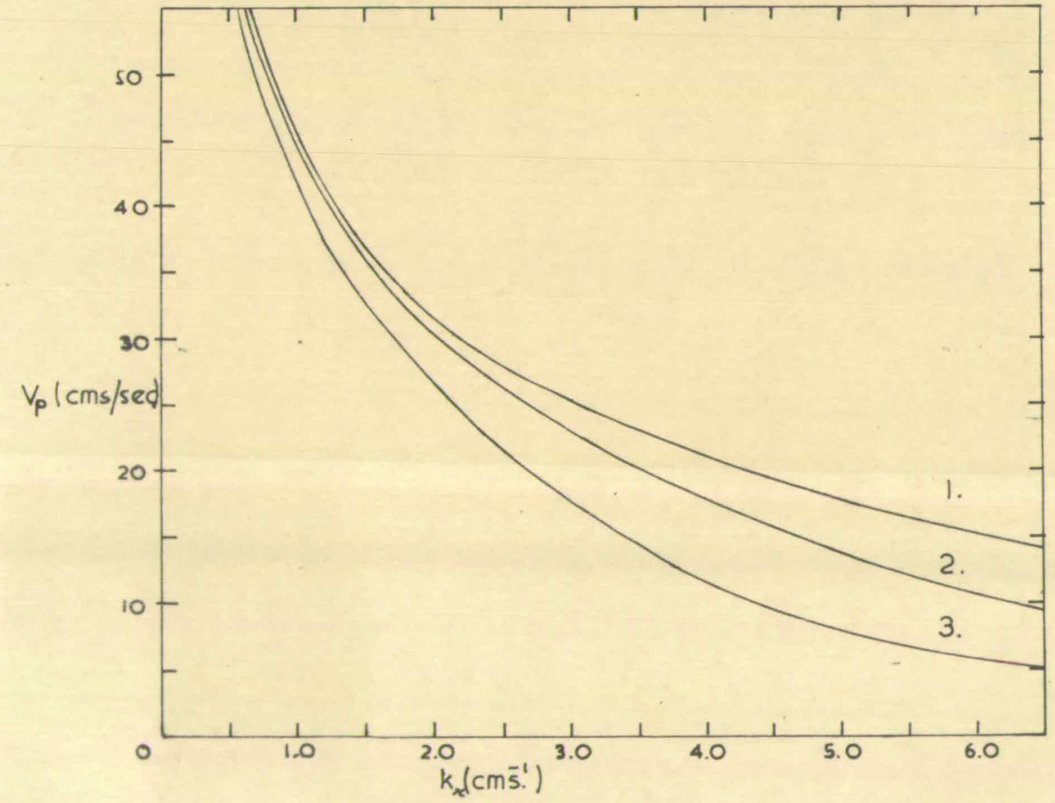


FIGURE 4.14 PHASE VELOCITY FOR AIR BED.

very large increases in A.F., phase velocity and frequency, and the corresponding decrease in growth distance. Again, as happens with the liquid fluidised bed, increasing the particulate phase "viscosity" attenuates the A.F., the frequency and the phase velocity and introduces a maximum into the A.F. curve. From a qualitative point of view, this is probably the most important single effect. The minima in the growth distance curves are not very pronounced and the curve for the high "viscosity" term has both a minimum and a maximum. This slight maximum is due to the rapid decrease of the A.F. from the maximum to a fairly constant value and the steady decrease in the phase velocity. This maximum is not found with higher values of the normal stress term, which, as before, introduces a very strong minimum into the growth distance curve and makes the A.F. go negative at very low and very high values of k_x. The value of $|d\Omega/d\varepsilon| = 20$, which applies for the figures shown, little effects the propagation properties. This figure was chosen to give a comparison with the liquid fluidised case, and when a value of 200 dynes/cm.^{2}/unit voidage change was used, the effect on the A.F. and growth distance was very much larger. This value of 200 is the value necessary to ensure a stable solution to the voidage gradient equation (3,19) for the air bed. Unlike the effect (or non-effect) it has on the liquid fluidised bed, this term $|d\Omega/d\varepsilon|$ does slightly increase the frequency and phase velocity of the disturbances as it itself is increased.

Thus for both systems, the normal stress term has little effect on the growth quantities until it becomes of the same order as the quantity $\rho_f \bar{u}_o^2 (1-\varepsilon)/\varepsilon^2$. This point is dealt with in more detail later in this chapter.

In Figure 4.12, the shape of the A.F. curves near $k_x = 0$ is not shown. The values of the normal stress and radial wave number perhaps cause the A.F. to go negative - thus making the bed stable over a very small range of wave numbers close to zero. However this does not affect the qualitative picture for the intermediate range of wave numbers, and it is still apparent that the air fluidised bed is very much more unstable than the liquid fluidised bed, although the same gross features are to be observed in both systems.

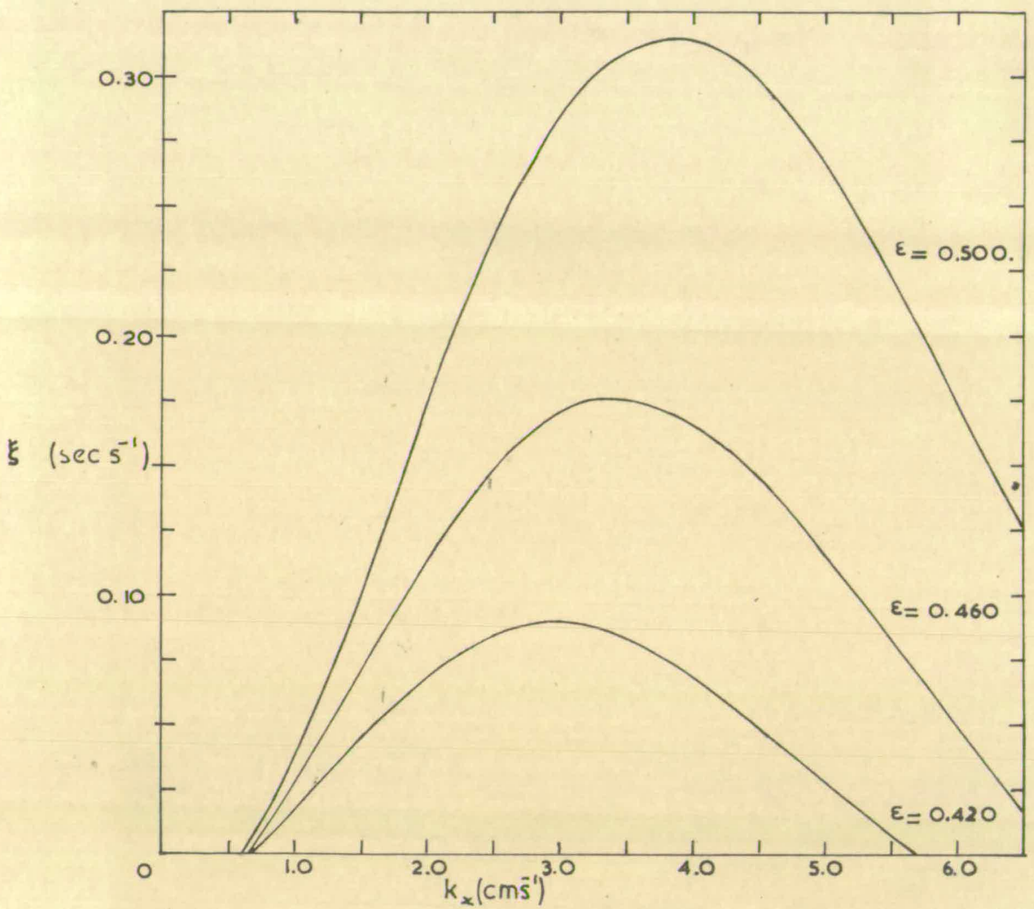


FIGURE 4.16 CHANGE OF A.F WITH FLOW RATE.

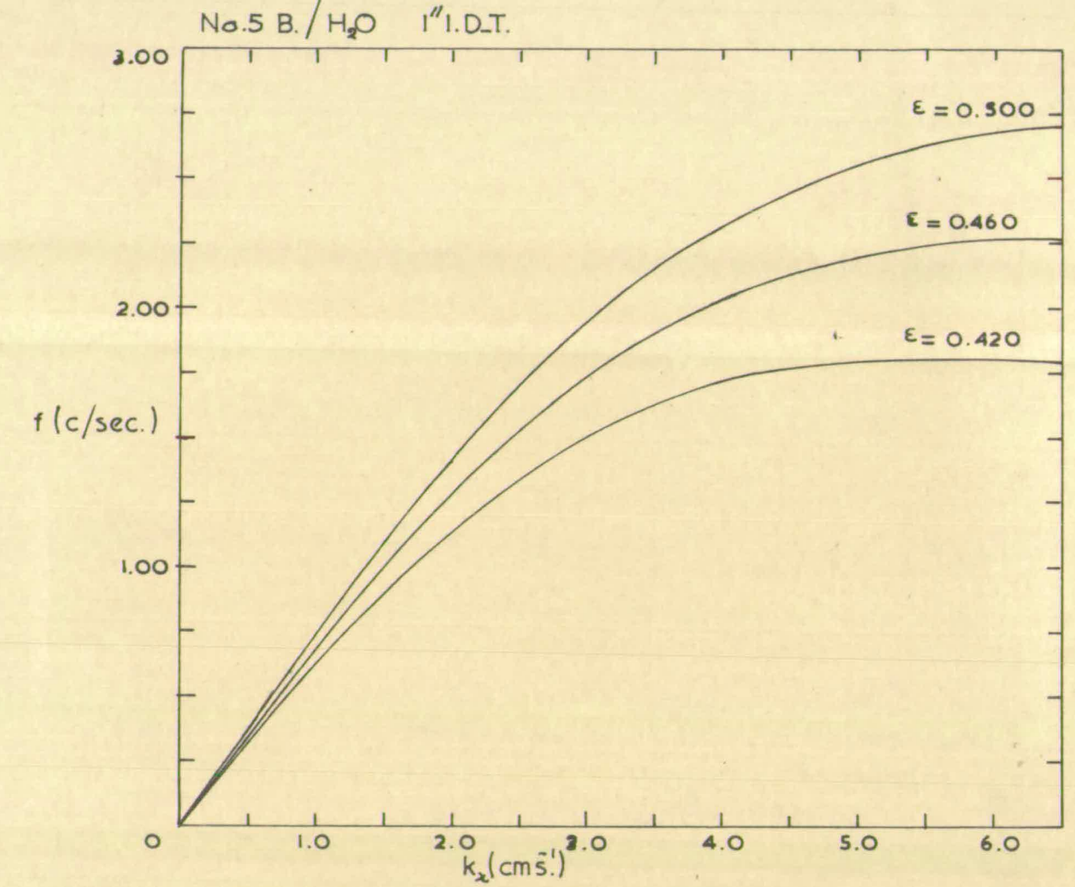


FIGURE 4.17 CHANGE OF FREQUENCY WITH FLOW RATE.

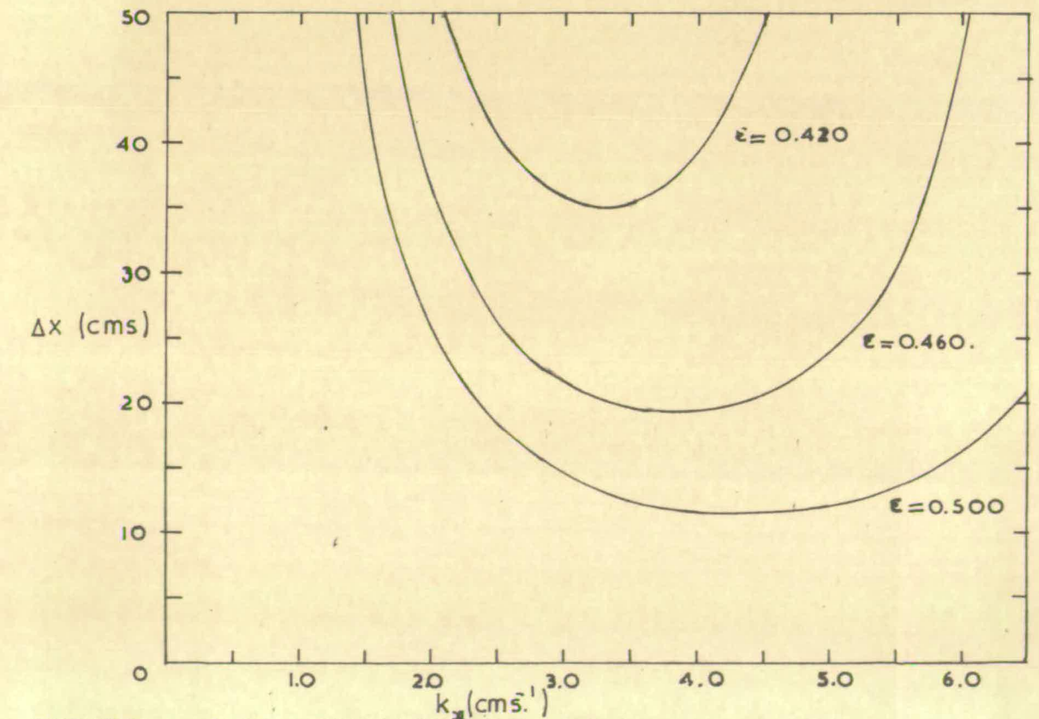


FIGURE 4.19 CHANGE OF GROWTH DISTANCE WITH

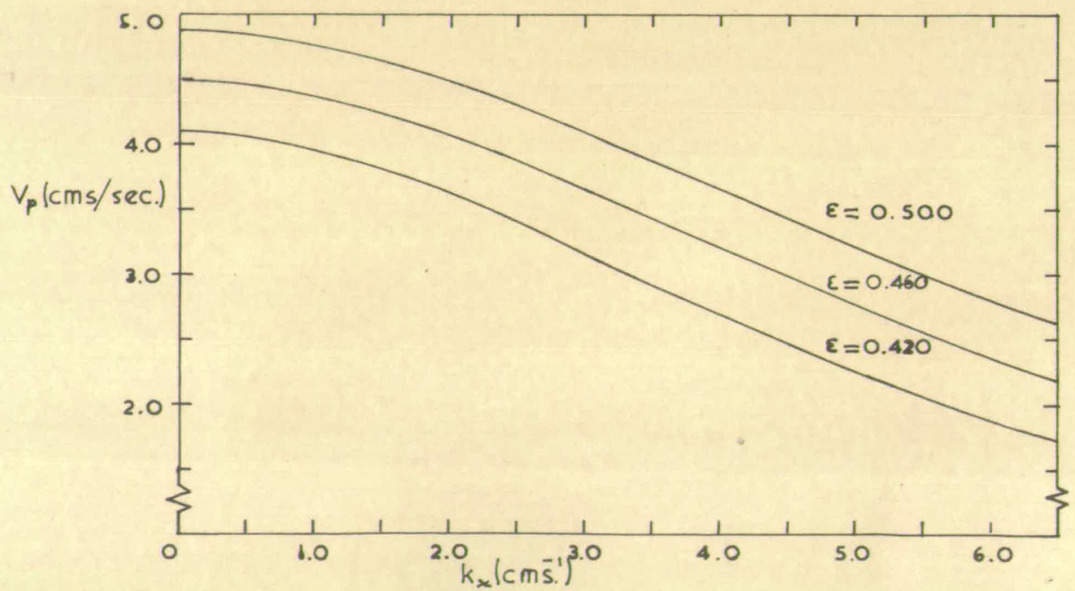


FIGURE 4.18 CHANGE OF PHASE VELOCITY WITH FLOW RATE.

(f) Change of Flow Rate for No.5 B/H_2O

The way in which the propagation properties of a disturbance change with flow rate is illustrated in Figures 4.16, 4.17, 4.18 and 4.19. These curves were calculated for No.5 B/H_2O at three different flow rates corresponding to voidages of 0.420, 0.460 and 0.500 and the virtual mass coefficient was assumed constant at 0.50 and the radial wave number was 1.13 $cms.^{-1}$. The other data used appear in the table preceding this discussion. The particulate phase "viscosity" term was taken as four times the value of the shear "viscosity".

Again the results are much as expected. Increasing the flow rate increases the frequency, phase velocity and amplification factor and reduces the growth distance. It also appears that as the flow rate increases, the wave number of minimum growth distance (the preferred wave number) increases and thus the wave length decreases. However these results only give a rough indication of the bed behaviour, simply because of the number of assumptions and unknown quantities in the equation If, for example, the virtual mass coefficient is a decreasing function of voidage, then, since in the liquid fluidised case the A.F. is strongly dependent on this term, the value of the A.F. would be correspondingly increased at the lower voidages, thus bringing the maxima in Figure 4.16 closer together.

It should also be noted the way in which the minimum of the growth distance changes. As the voidage is increased, the curve becomes much flatter near the minimum - indicating a spread of wave lengths over which disturbance components amplify at much the same rate with distance, even though there is very narrow band of wave numbers which amplify fastest in time.

The calculations and figures described above indicate the importance of the various parameters. Basically the density difference between fluid and solid, the fluid viscosity (because of the marked dependence of the fluidising velocity on it) and the particle size determine the behaviour of the bed, and the results, given in Appendix 1, for the less complex equations where particulate phase stress and virtual mass effects are neglected indicate reasonably well how the propagation properties change from system to system. Generally speaking, the

greater the density difference between solid and fluid, the more unstable is the system.

For systems with the same densities and fluid viscosity, but a different particle size it is not so obvious which of the two systems would be more unstable (for most systems do in fact appear to be unstable) - taking growth distance as a criterion. Certainly the fluidising velocity is greater for the larger particle size but this also means an increased particulate phase "viscosity" and the effects of these may cancel each other out. No definite statement can be made. However calculations carried out for sand fluidised by air (roughly the same density but one tenth of the size of No.5 ballotini) indicated that the sand/air system is more stable than the No.5 B/AIR system. The effect of particle size is considered further in the discussion of the experimental work.

Apart from these general observations, perhaps the most important single feature of the calculations is the prominent part played by the particulate phase stress tensor terms in determining the degree of instability of the bed. The "viscosity" term from this attenuates the A.F. and produces the maximum in this quantity. It also effectively fixes the wave number at which this occurs. Because the fluidised bed is a dispersive system however, this maximum of the A.F. does not necessarily imply a minimum in the growth distance and it is the normal stress term which causes this - due to the way this term causes the A.F. to fall off rapidly after the maximum. These two extrema do not generally occur at the same wave number (the A.F. maximum occurs at the lower value of k_x). Thus the wave which amplifies fastest in time is not the wave which amplifies fastest with distance.

Experimental results for the ballotini/water system suggest that the dominant wave length for this system is around 2 cms., giving a wave number around 3 cms^{-1}. To produce a maximum in the A.F. curve about this value, the "viscosity" term required was about four times greater than the shear "viscosity" found from experimental work, i.e.

$$(\alpha_o + 2\gamma_o) \sim 4\gamma_o$$

giving $\alpha_o \sim 2\gamma_o$.

Since the bulk "viscosity" $K_o = \alpha_o - \frac{2}{3}\gamma_o$ (under the present assumption that the bed behaves as a quasi-Newtonian fluid), $K_o \sim 3\gamma_o$.

This is of the same order as Murray (14) found, even though there is some confusion about the meaning of his stress tensor terms.

The effect of the normal stress term in producing a pronounced minimum depends very much on the size and sign of the quantity

$$F(A - F) - ADe/b^2 \qquad \text{(see equation (3,8))}$$

Neglecting virtual mass and considering only a one dimensional disturbance, this quantity becomes

$$D(1 - De/b^2) \qquad \text{if } \frac{\rho_s}{\rho_f} \gg 1.$$

i.e. $$D\left(1 - \frac{\rho_s}{\rho_f}\cdot\frac{\varepsilon_o}{1-\varepsilon_o}\cdot\left|\frac{d\Omega}{d\varepsilon}\right|\cdot\frac{\varepsilon_o^2}{\rho_s \bar{u}_o^2}\right).$$

Recalling that in Appendix 2 it was assumed, in order to obtain some idea of the possible size of $|d\Omega/d\varepsilon|$, that this quantity was of the same order as the change of fluid momentum term in equation (3,19), that is

$$\left|\frac{d\Omega}{d\varepsilon}\right| \sim \rho_f \bar{u}_o^2 \frac{(1-\varepsilon_o)}{\varepsilon_o^3} \qquad \text{- neglecting virtual mass}$$

then it is easy to see why this term has such a marked effect on the A.F. when values obtained in this way are used in the calculations; the above expression becomes zero. The virtual mass coefficient will alter the situation slightly, but the terms will still be of the same order.

It was found that when $|d\Omega/d\varepsilon|$ was increased to about twice the value of the term $\rho_f \bar{u}_o^2 \frac{(1-\varepsilon_o)}{\varepsilon_o}\left(1 + \frac{\Theta_o}{\varepsilon_o}\right)$

the A.F. became negative over the whole range of axial wave number considered i.e. the bed was stable to any small disturbance. As most systems appear to be unstable, this sets an upper bound on the value of the normal stress term. Certainly it would seem that the particulate phase normal stress term has a very important part to play in determining the stability of the state of uniform fluidisation and should not be omitted from the equations of motion as suggested by Murray (14).

Inclusion of the radial wave number in the calculations shows how the presence of the walls tends to damp down the disturbances. This wave number effectively increases the terms containing the particulate phase "viscosity" and normal stress, and may cause the A.F. to go negative

over the whole or part of the meaningful wave number range. The most important effect of this term however, is to make more pronounced the minimum in the growth distance curve.

For any one flow situation, the parameters which have been varied in the above calculations are in fact uniquely determined by the values of ρ_s, ρ_f, d_p, d_t and μ, and by $\bar{u}_o$ and ε_o. If the bed is unstable and if there is a minimum in the growth distance, then there is one wave-length with associated frequency and phase velocity, corresponding to this minimum, which will amplify faster in distance, and which will eventually dominate disturbance components of any other wave length. The wave length at which this minimum occurs will vary from flow situation to flow situation but will be constant within any one situation. From the evidence of the literature and the experimental evidence of the present work, it would seem that most systems are unstable and that there is no great variation in values of the dominant wave length (about two to three centimetres generally). If this is so, this dominant wave length may be related to the particle diameter by $\lambda_D = \gamma d_p$ where γ is some function of the system parameters. Thus the dominant wave number is $k_{xD} = \frac{2\pi}{\gamma} \cdot \frac{1}{d_p}$

From equations (3,8) and (3,9), it is seen that one of the quantities determining the growth properties of a disturbance is the ratio (b/B), where

$$b = \frac{\bar{u}_o k_x}{\varepsilon_o} \quad \text{and} \quad B = \frac{\rho_s - \rho_f}{\rho_f} \cdot \frac{\varepsilon_o}{1-\varepsilon_o} \cdot \frac{g}{k_o}$$

For the minimum growth distance, if the above relation applies, the quantity (b/B) thus contains the term $\bar{u}_o^2/gd_p$. This is seen to be the Froude number used by Wilhelm and Kwauk (4) as a criterion for the type of fluidisation exhibited by a system. It has been shown by Jackson (5) that the stability calculations are a much more fundamental way of classifying the type of fluidised system and it is seen that the Froude number arises quite naturally from the stability calculations.

Typically aggregative beds have very short growth distances and typically particulate systems have much larger growth distances. Examples of this have been seen with the two systems studied in detail above. With an aggregative system, the very rapid growth of small disturbances leads one to suppose that initial disturbances close to the distributor are related in some way to the appearance of bubbles in this

type of system. Even if a disturbance does develop into a complete bubble, this change cannot be followed analytically because of the complexity of the equations and their non-linear nature. The general appearance of particulate beds is of smooth uniform fluidisation. However this is usually caused by general turbulence (unlike aggregative beds, which have been shown to have streamline gas flow (31)) and not by the slow growth of disturbances. This point is dealt with in more detail later when the experimental work is discussed.

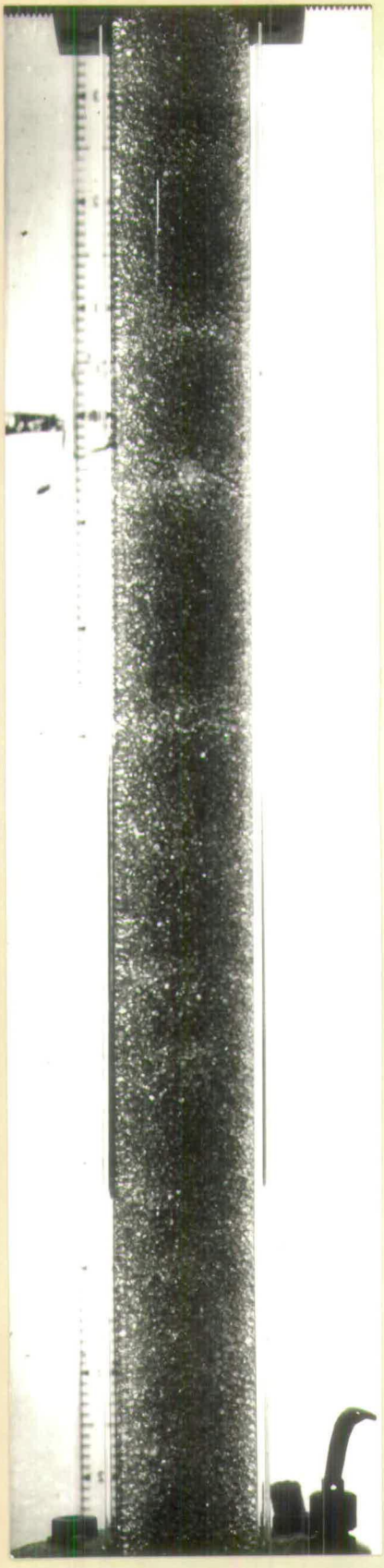
In the light of the probable development of disturbances into bubbles, it is of interest to consider the results of some frequency calculations for small sand fluidised by air. The diameter of the sand was about 0.01 cms., the fluidising velocity 1 cm/sec., and the density around 2.65 gms/cc. For a single disturbance, the calculated frequency seemed to be approximately 1.0 c/sec. for a wave length of 1.5 cms. Lancaster (34) measured bubble frequencies for this system in a six inch diameter bed and found that close to the distributor, the bubble frequency was of the order 8 or 9 per second. If the horizontal diameter of the disturbance extends, say about 4 cms., (a reasonable figure, both from observation and X-ray studies (33)), then the disturbance frequency over the whole area is around 10 or 12 per second. Bearing in mind just how approximate both these figures are, the closeness of the two values is rather striking, and could, perhaps, repay further investigation.

There appears to be little or no relationship between bubble velocity and disturbance phase velocity. The rise velocity of a single bubble in a fluidised bed was found by Davidson and Harrison (3) to be

$$U_B = 0.71\sqrt{gV_B}$$

where U_B is the velocity and V_B is the volume of the bubble. This shows no dependence on bed parameters and the only point of similarity between the bubble velocity and phase velocity is their dependence on the size of the bubble and disturbance respectively. Pigford (6) has considered how an originally sinusoidal particle concentration disturbance could develop a shock wave profile because of the dependence of phase velocity on voidage but this, while giving some indication of the possible development, does not really relate these two extreme cases.

1.



2.

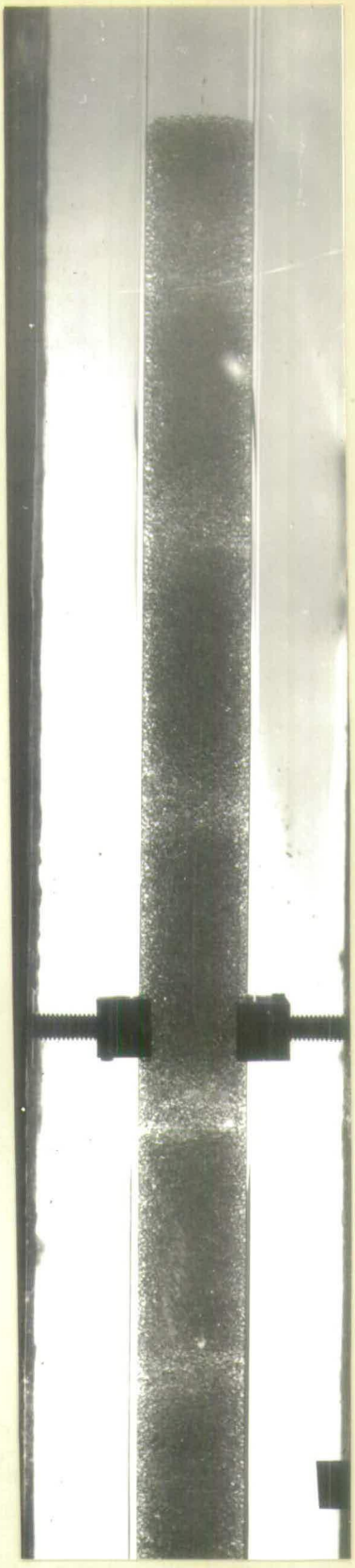


PLATE 5.1 DISTURBANCE GROWTH IN A TYPICAL NON-TURBULENT LIQUID FLUIDISED BED.

CHAPTER 5

Equipment and Experimental Method

Because of the rapid growth of disturbances in most gas - fluidised systems, it was decided to study the growth and propagation properties of disturbances appearing in liquid - fluidised systems. The most convenient system is glass ballotini fluidised by water. Glass ballotini are convenient because of their uniformity in size and shape and because a wide range of particle diameters is available. Rough preliminary experiments by Jackson (5) indicate that the propagation properties predicted from the linearised equations of motion (strictly applicable only to small disturbances) give fair agreement with experiment, and so experimentally determined values of the velocity of propagation, frequency, wave-length and growth distance should provide a substantial check on the equations of motion.

Preliminary experiments on the ballotini water system showed that when the bed diameter was large (greater than about 2½ inches for particle diameters of about two millimetres) large scale turbulence set in and the disturbances were broken up. By large scale turbulence is meant the swirling movement of large groups of particles in a random manner across the flow area. This set an upper limit on the tube diameter which could be used. In tubes of this diameter and less only one mode of the disturbance wave appeared across the tube and the velocity of propagation could readily be measured by timing the rise of the disturbances over a length of the bed. Frequency could also be measured visually, but only when the frequency is small and even then this method would seem to be rather crude. Plate 5.1 shows photographs of disturbances travelling up through the bed. These were obtained with 2.m.m. ballotini fluidised by water in a 1½ inch diameter tube. The rising bands of reduced particle concentration are clearly visible and their appearance is typical of the systems studied in the present work.

To obtain the amplitude of the disturbances and the mean voidage as a function of vertical distance above the distributor, the experimental method adopted was to measure local voidage changes by the scattering of a beam of light. Other methods were considered, in particular, γ-ray transmission or the use of a capacitance probe or ring. However to obtain an instantaneous record of the disturbances using γ-ray transmission, a large number of counts in a very short time interval is required and the size of source necessary for

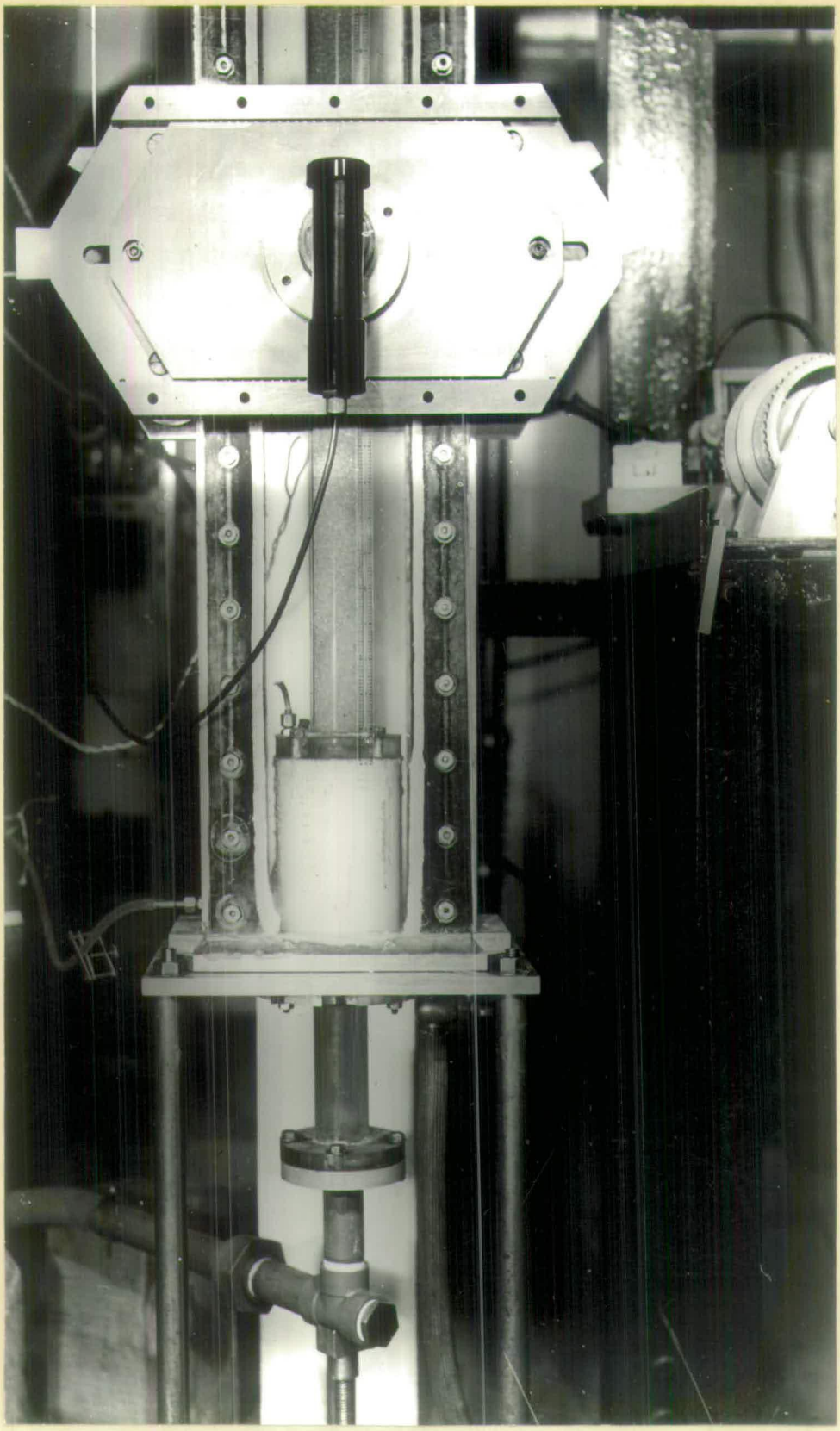


PLATE 5.2 BASE OF EXPERIMENTAL COLUMN.

this is quite prohibitive (calculations show it to be of the order of several curies). Nevertheless, it is an eminently practical method of measuring the mean voidage at any point since this does not require following the disturbance in time; thus only a small source is necessary. The disadvantages of a capacitance probe are its inflexibility (it is stationary at one point in the bed) and, because the probe is situated inside the bed, disturbance of the flow. These disadvantages are eliminated by using a capacitance ring (two strips of metal sliding on the outside of the tube) and this has been used to good effect by Lancaster (34) in measuring bubble frequencies in a fluidised bed. However, because the axial spread of the field does not give the vertical resolution required to follow disturbances of short wave length, it is only really capable of measuring gross effects.

The light transmission method is not without its limitations. It is limited to transparent particles. Because the bed is fairly dense, most of the light is scattered and a very sensitive photoelectric device is needed to pick up the tiny fraction which is transmitted through the bed. If a powerful lamp is used, the added complication of forced cooling may become necessary. A collimated light beam is also necessary and, because the fluidising medium has a different refractive index from air and because the bed is contained in a cylindrical tube, an optical box enclosing the bed is required to ensure that the light beam retains its collimation after passing through the bed.

The diameter of the light beam is also limited. In order to get, as nearly as possible, a record of changes in the local voidage, the diameter of the light beam has to be small compared with the disturbance wave-length. However, if the diameter is nearly the same size as the particles, the whole beam may be obscured by one particle near the tube wall, thus introducing a great deal of noise into the signal. The beam must also be large enough to allow sufficient light through the bed, and so some sort of compromise must be reached. In practice, this was achieved by starting with the smallest possible beam diameter and increasing it in stages until a reasonable signal was obtained.

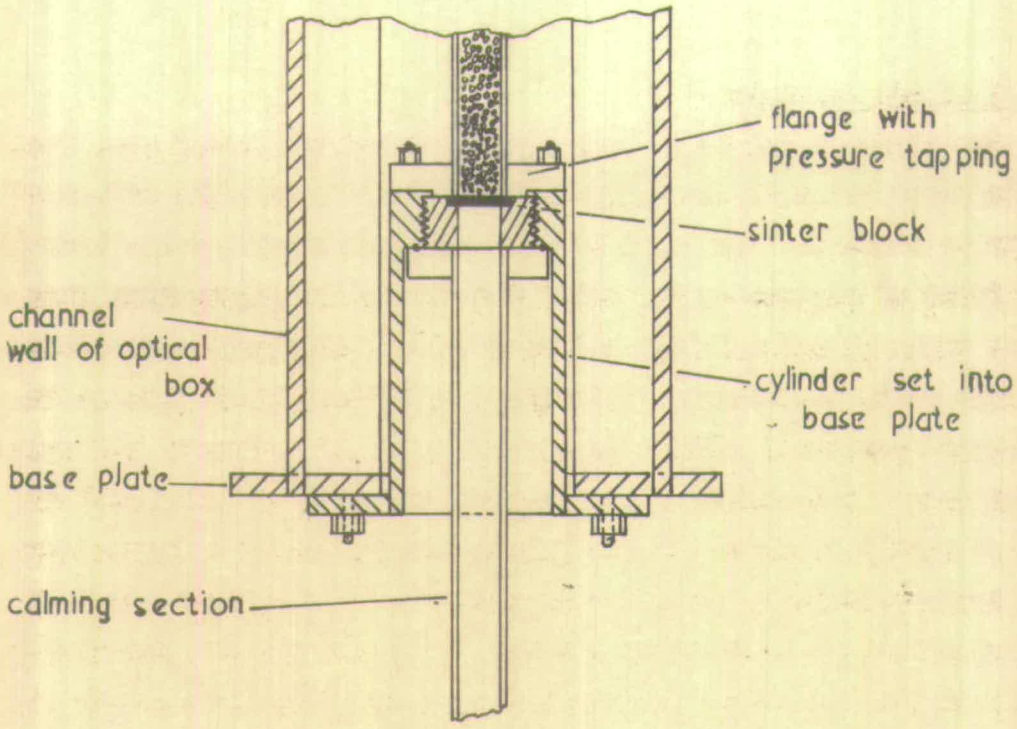


FIGURE 5.1 DIAGRAMATIC SECTION OF COLUMN BASE.

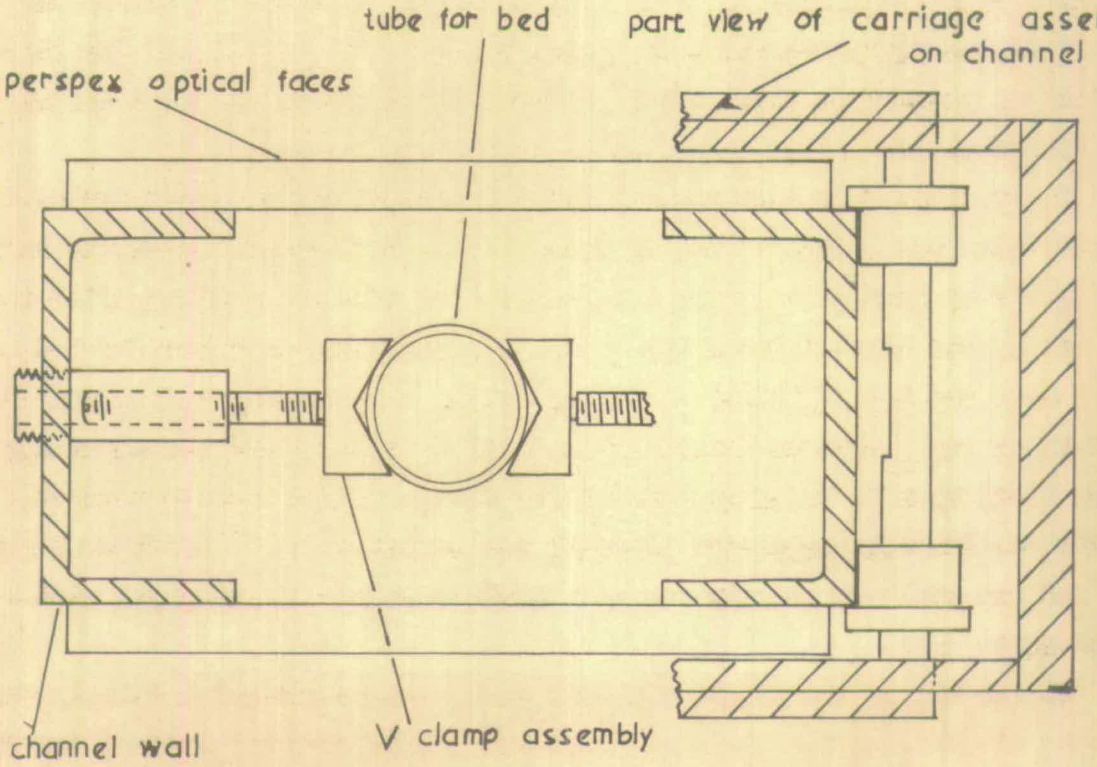


FIGURE 5.2 PLAN VIEW OF OPTICAL BOX.

Description of the Apparatus.

For the experimental work, four sizes of glass ballotini were fluidised by water in three tubes of varying diameter, thus allowing the effect of tube diameter to be studied. For some of the work, polystyrene beads were used to show the effect of changes in the solid density on the propagation properties. Narrow bore tubes ($\frac{1}{2}$ inch, 1 inch and $1\frac{1}{2}$ inches in diameter) were chosen to prevent large scale turbulence and to allow sufficient light through the bed for measurement purposes. These tubes were extruded "Perspex" and approximately eleven feet long - this height allowing complete study of the growth of disturbances from just above the distributor to the top of a fairly high bed.

The tubes containing the bed were enclosed in an optical box filled with the fluidising medium, in this case, water. Figures 5.1 and 5.2 show the arrangement at the base of the column and a section through the optical box. The box as approximately twelve feet high and was constructed from aluminium channel, with clear "Perspex" sheet for the optical faces. The tubes were held centrally in the box by a series of five adjustable "V" clamps set in the centre line of the channel. These clamps could be screw adjusted across the box to give good vertical alignment of the tubes inside the box; it being ensured every time the equipment was set up that the box was vertical. The light system was held on a carriage which moved on the aluminium channel, thus allowing readings to be taken at any height in the bed.

The distributors used were sintered bronze discs, slightly larger in diameter than the inside of the column. There were set in aluminium blocks which could be screwed into the top end of an aluminium cylinder about six inches long set in the base of the optical box. The flanged tube for the bed was then bolted onto the top of the aluminium cylinder. A calming section containing glass tubes was pushed up inside the aluminium cylinder and sealed against the sinter block by a "O" ring set in the top flange of the calming section. The calming section and associated pipework was seated on a "V" block on a screw jack and the seal was made by pressure exerted on the "O" ring and sinter block by the screw jack.

At the top of the column a series of removable flanges and seals reduced the tube diameter to the pipework diameter. Provision was made at the top of the column for adding ballotini, and this ballotini could be removed from the

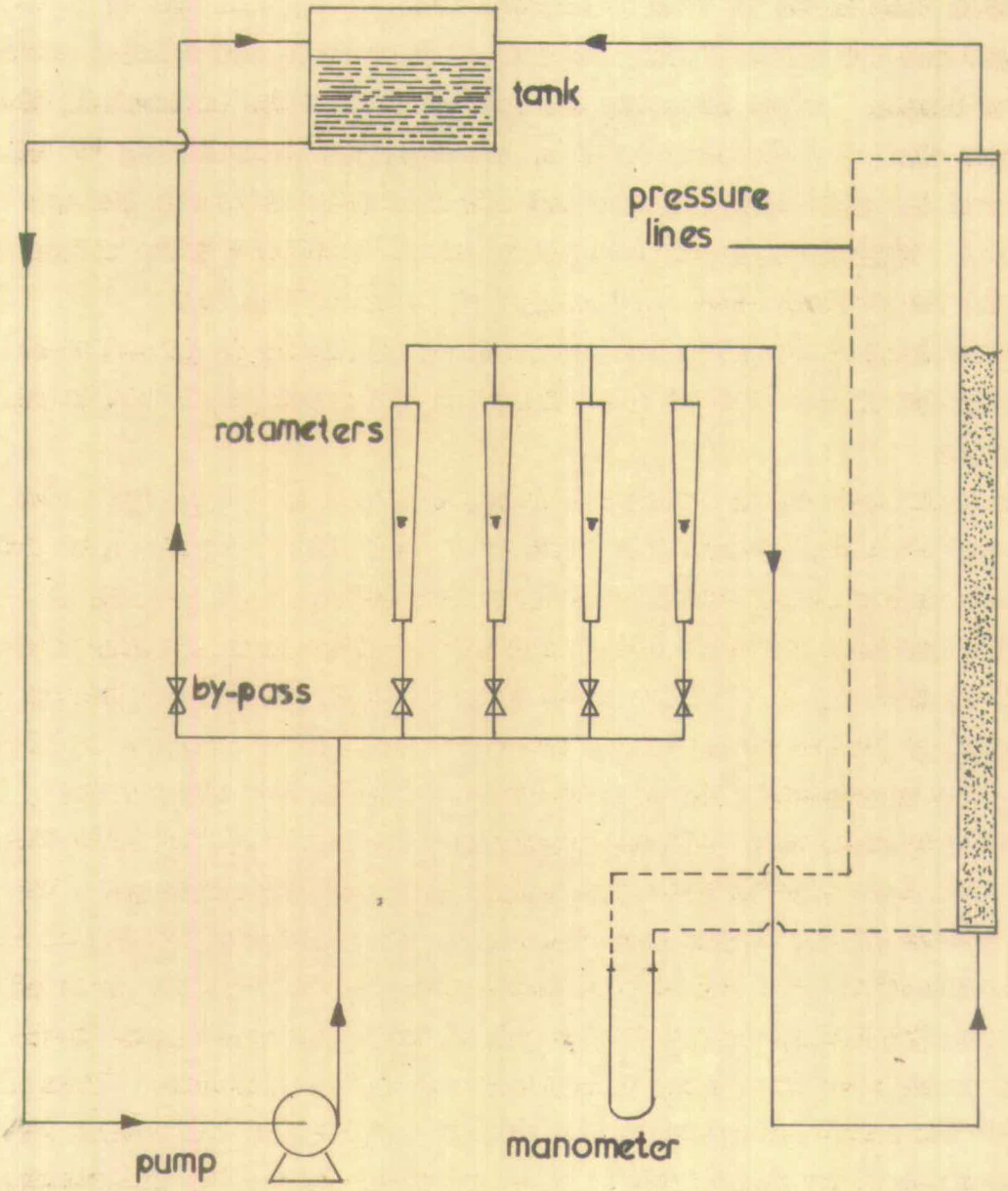


FIGURE 5.3 FLOW DIAGRAM OF EQUIPMENT.

column by unscrewing the sinter block at the foot of the column with a specially made key. Pressure tappings, protected by fine gauze to prevent ballotini getting into the piezometer ring, were set in the top and bottom flanges of the tube. Each tube could be readily removed from the optical box by removing the top flanges and the corresponding section of pipe work, the calming section and the sinter block. After lowering the optical box to the horizontal, the nuts holding the aluminium cylinder could be removed, the centralising "V" clamps loosened and the aluminium cylinder and attached tube withdrawn through the base of the box. This arrangement facilitated changing of the tubes without breaking the seal of the optical faces on the channel sides of the box.

A flow diagram of the equipment is shown in Figure 5. 3. and Plate 5. 2 is a photograph of the base of the column and the carriage for the light source and receiver.

The light system, as mentioned above, was held on a carriage which could be moved up and down the column, the edges of the aluminium channel used for the optical box acting as runners for the carriage pulleys (see Fig. 5. 2) That part of the carriage to which the source and receiver were attached could be moved laterally so that the light beam could be centred on the tube. During construction of the carriage it was ensured that the source, situated on one side of the carriage, was accurately aligned with the receiver on the other side. The source and receiver systems were held on the carriage by screwing them onto thick plates, which in turn were screwed into the movable sides of the carriage. The distance from the bottom of the carriage to the centre of the light beam was $4\frac{1}{2}$ inches, so if the fluidisation tube had been attached directly to the base plate of the optical box, the lowest height in the bed at which any measurement could have been made would have been about 5 inches above the distributor. Thus the purpose of the aluminium cylinder inserted in the base of the column was to enable readings to be taken down to about $1\frac{1}{2}$ inches above the distributor.

The light system consisted of a lamp held on one side of the tube and a photomultiplier situated exactly opposite. The lamp provided a collimated beam of light (by means of a series of lenses and stops) which passed through the optical box and into the bed. That part of the original beam which passed through the bed was picked up on the photomultiplier. The optical box filled with water ensured that the light beam retained its collimation after passing through the water filled tube.

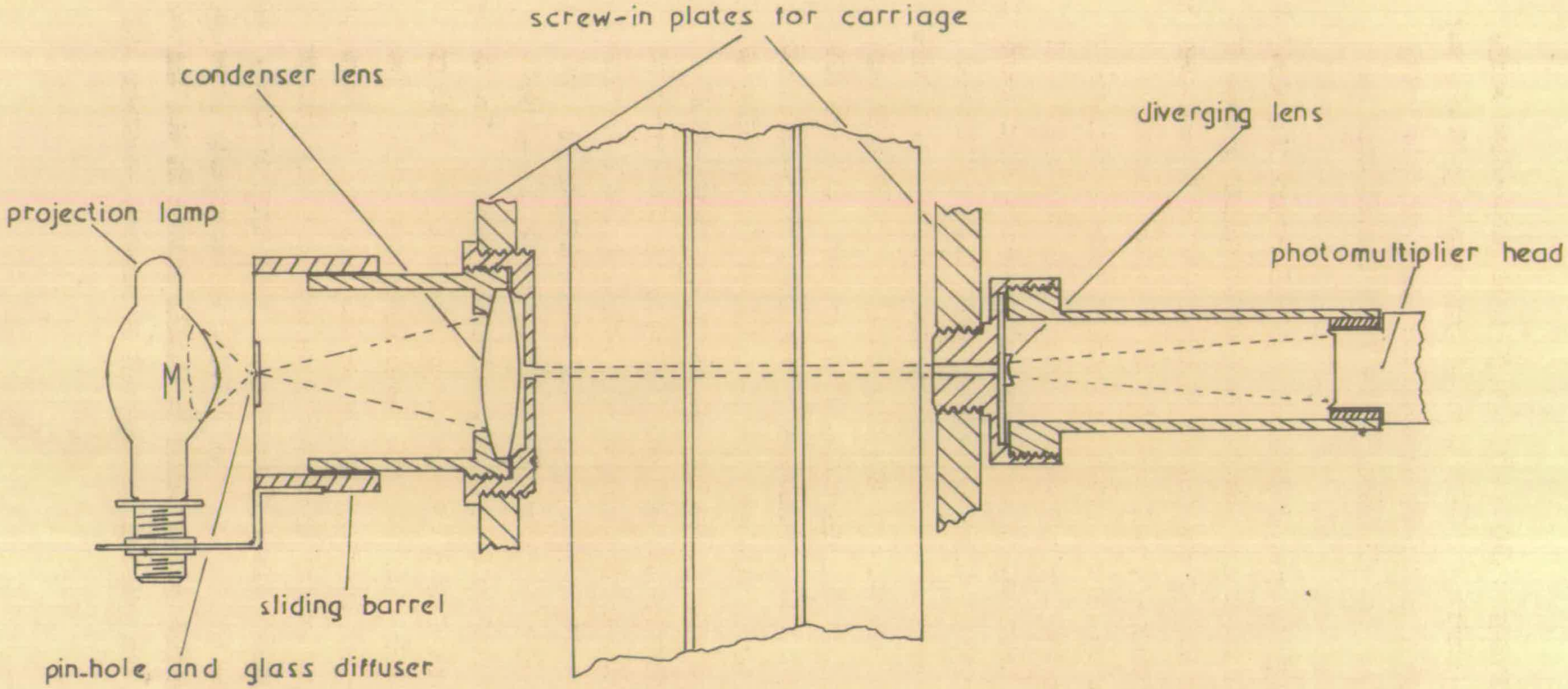


FIGURE 5.4 SECTION VIEW OF OPTICAL SET-UP.

The lamp used as a light source was a Philips 50 watt projection lamp, which did not require forced cooling. This type of lamp has a prefocus cap with a silvered back acting as a condenser mirror, the focus of this being about 5 centimetres in front of the filament. The light system used is shown in Figure 5.4. A screen with a pin-hole was situated at the focus of the lamp and a piece of lightly-ground glass was placed behind the pin-hole to break up the lamp filament image and provide even illumination across the beam. In turn this pin-hole source was placed at the focus of a condenser lens, the resultant parallel beam being stopped down to the required diameter.

The condenser lens and stop were mounted in a brass barrel, threaded on the outside to hold it in the thick plate which screwed into the side of the carriage. The pin-hole was situated in the centre of a screen which covered the end of a second brass barrel.. This was made a good sliding fit over the barrel carrying the lens. Attached to this second brass barrel was a bracket which carried the lamp. The position of the lamp could be moved both vertically and horizontally, with respect to the pin-hole, which in turn could be moved relative to the lens, so that a fine adjustment of the beam was possible.When a parallel beam of light had been achieved, the position of the sliding barrel was fixed by tightening down a wing screw bearing on to the fixed barrel.

The light which passed through the bed was picked up by the receiver. This consisted of a tunnel the same diameter as the original beam, blackened on the inside to prevent stray light getting to the photomultiplier. At the end of this tunnel was situated a small diverging lens, which spread the parallel beam of light over the face of the photomultiplier head. The tunnel section was fixed to the carriage by a flat plate and the lens was held in place by a screw-in barrel which also held the photomultiplier head. The length of this barrel was determined by the focal length of the lens and the diameter of the beam employed. The photomultiplier head used was that employed on the Evans Electroselenium "E.E.L." Micro-Photometer. This type of head, which holds the photomultiplier tube (an R.C.A. Type 931-A), is accurately machined to fit inside a microscope barrel and so could be easily fitted in the barrel used here. Plate 5.3 shows the general arrangement of source, receiver and carriage.

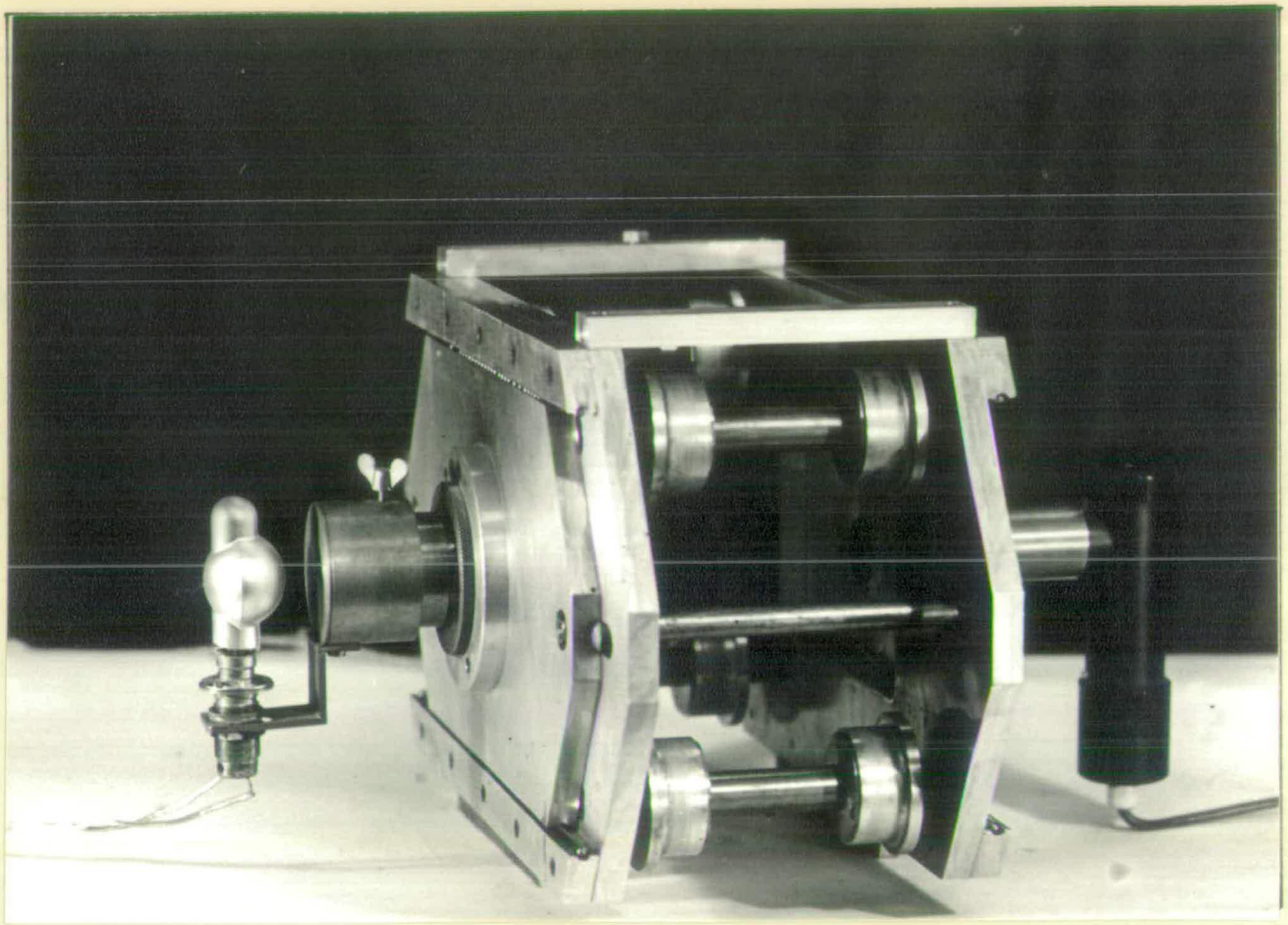


PLATE 5.3 LIGHT SOURCE, RECEIVER AND CARRIAGE.

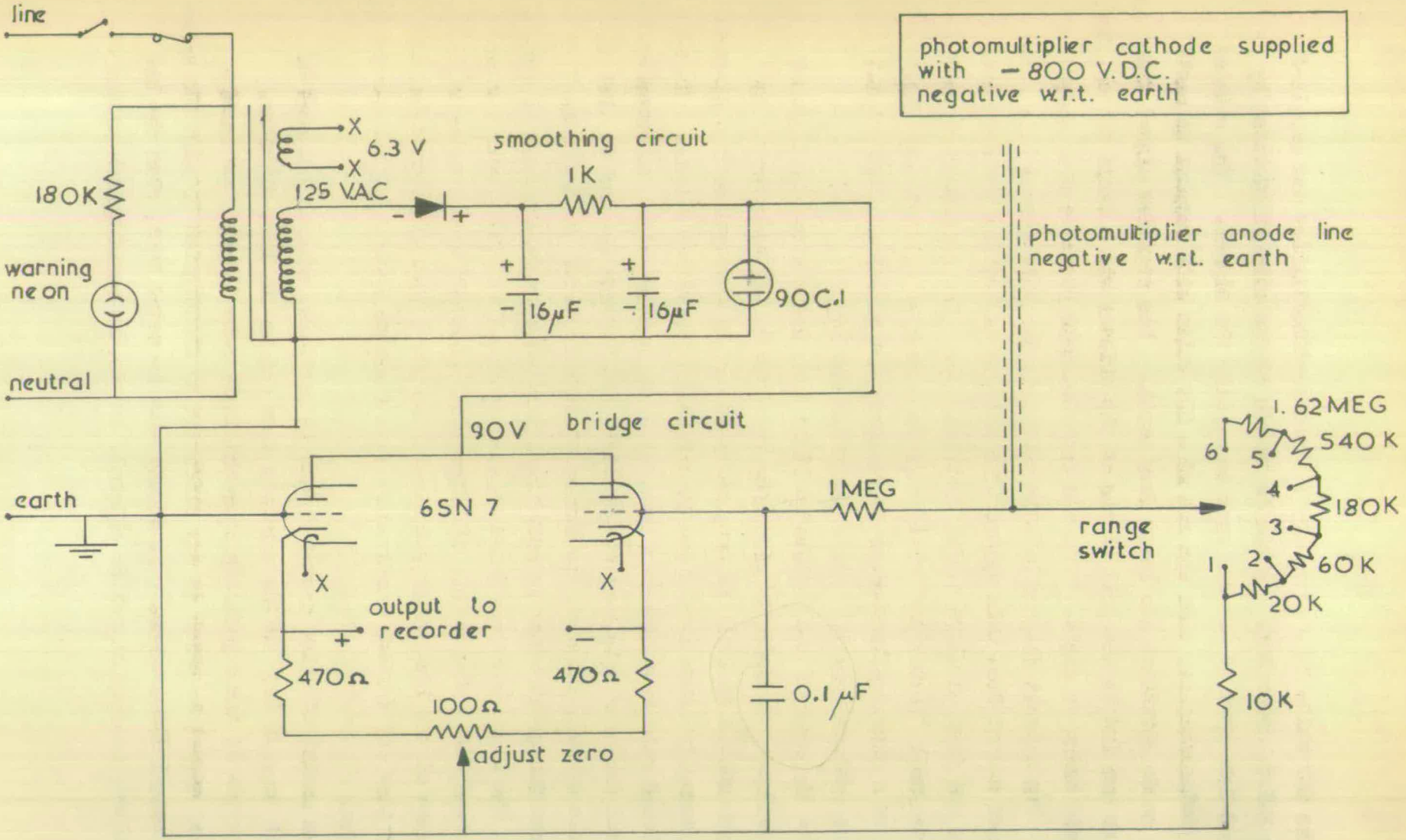


FIGURE 5.5 CIRCUIT DIAGRAM OF DOUBLE TRIODE BRIDGE.

The 800 volts D.C. necessary for the photomultiplier was supplied from an E.H.T. generator. A double triode bridge circuit (devised by Barer and Underwood (35).) was used to amplify the signal. The cathode of the photomultiplier tube was run at - 800 volts with respect to earth and the anode potential was lower than earth. The negative signal from the anode was fed to the grid of one of the triodes via a range switch, the other grid being at earth. The two cathodes were positive with respect to earth. The circuit diagram of this bridge is shown in Figure 5.5. The unbalanced output from this bridge (the voltage across the two cathodes) was then fed into an ultra violet oscillograph. The oscillograph used was a Honeywell "Visicorder" which employs a beam of ultra-violet light falling on a mirror galvanometer to register the signal on ultra-violet sensitive emulsion paper. The chart width was 12 cms..

The diameter of the collimated light beam was eventually fixed at 4 millimetres. In order to give good resolution, the diameter of the light beam should be small in comparison to the wave-length of the disturbances (generally about 1 cm.) and it was initially set at 2 mms.. However it was found with this diameter that, with the smaller sized ballotini in the 1 inch diameter tube, not enough light got through the bed to give a measurable signal, and with the larger sized ballotini, the noise in the signal was too great - due to individual particles obscuring much of the light. The 4 mm. beam was found to give reasonable signals over a wide range of systems. While this diameter still produced a very noisy signal in the case of the largest size ballotini in the 1 inch diameter tube, it was felt that any further increase in beam diameter would give unsatisfactory resolution.

The amount of noise caused by single particles cutting out most of the light depends both on the particle size and on the tube diameter. A combination of large particle size and small tube diameter produced a very noisy signal in which it was difficult to distinguish between the noise and the actual disturbance. It should also be noted that, when the bed is turbulent, a noisy signal is obtained due to the rapid random motion of

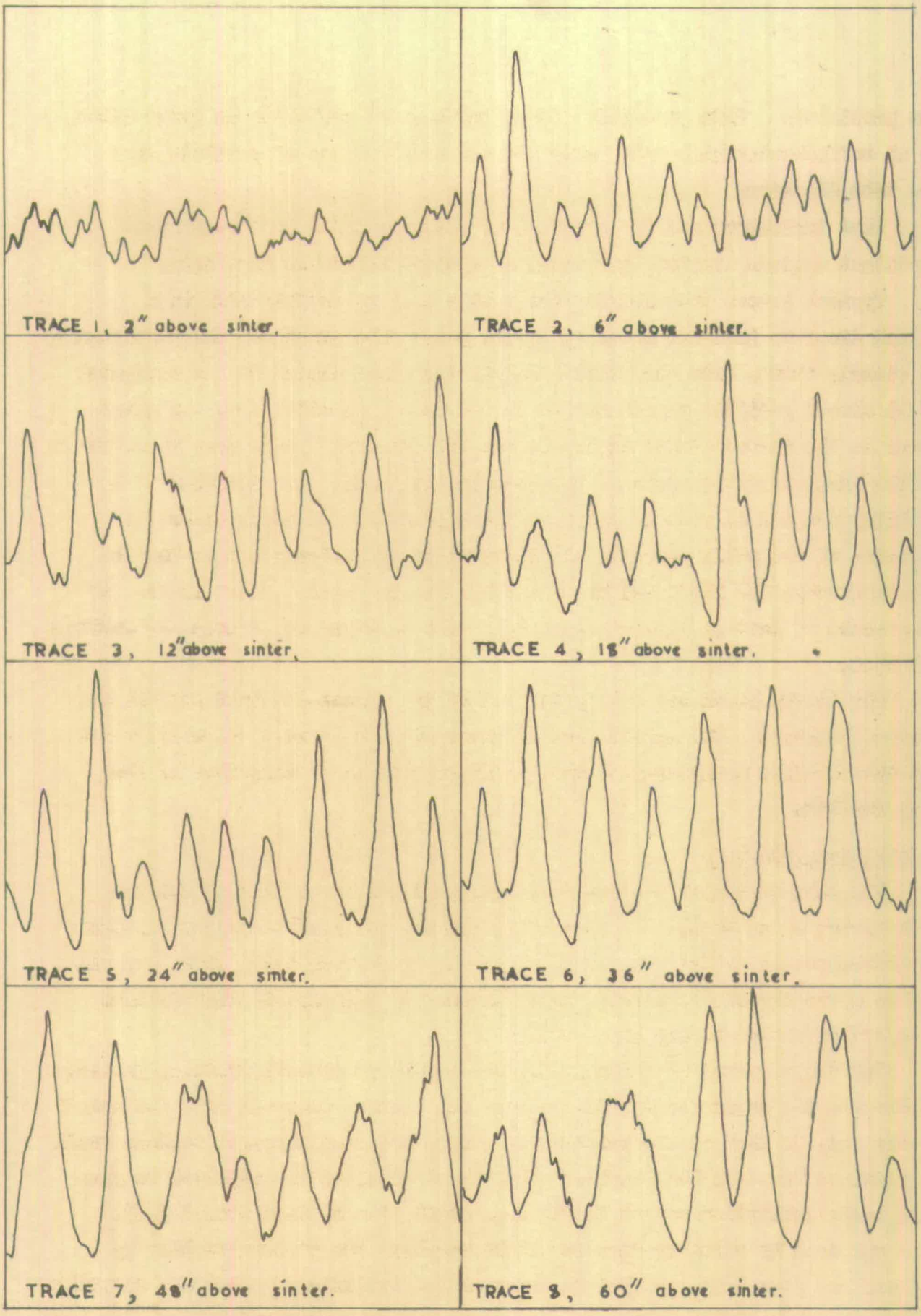


FIGURE 5.6 TYPICAL TRACES OBTAINED AT VARIOUS HEIGHTS ABOVE THE SINTER.

the particles. This generally occured with small particles in large tubes or at sufficiently high flow rates for all combinations of particle size and tube diameter.

Thus turbulence and the presence of excessive noise in certain non-turbulent systems limited the number of systems available for study.

Typical traces obtained for the system No.3 Ballotini/Water in a 1 inch diameter tube are shown in Figure 5.6. The growth of the disturbances is clearly shown, from the initial fairly irregular signal to the emergence of an almost periodic signal higher up the bed. Qualitatively, the noise level in the records taken higher up the bed does not appear very significant, so the irregular appearance of the records taken near the distributor is probably due not so much to noise of the type discussed above as to the presence of the whole spectrum of disturbances of difference wave-length and frequency, and hence different initial growth rates. The disturbance components of fastest growth emerge from this spectrum and eventually dominate the rest.

The traces shown are fairly typical of the traces obtained for all the systems studied. The calibration of these signals in terms of voidage and the quantitative estimation of the growth properties is described in the next section.

Calibration Procedure

The calibration of voidage against signal had to be carried out for each system under study. This calibration was carried out on beds of about 3½ inches packed height, the position of the light beam being about 2 or 2½ inches above the distributor. In small beds of this height disturbances have not developed to any great extent.

For the purposes of calibration, the effect of possible voidage gradients in the bed was neglected and the voidage was assumed constant over the height of the bed, so that at the calibration point, the time averaged voidage could be obtained from the bed height. The signal obtained was adjusted to give full scale deflection across the 12 cms. chart at a voidage around 0.65. This was done by stopping down the light reaching the photomultiplier by filters and using the appropriate range on the amplifier. The high sensitivity ranges of the amplifier were used to ensure that the photomultiplier tube was operating, as nearly as possible, in its linear response range.

The mean voidage range was usually from about 0.35 to 0.65 and this was calibrated against the mean deflection of the signal from the zero

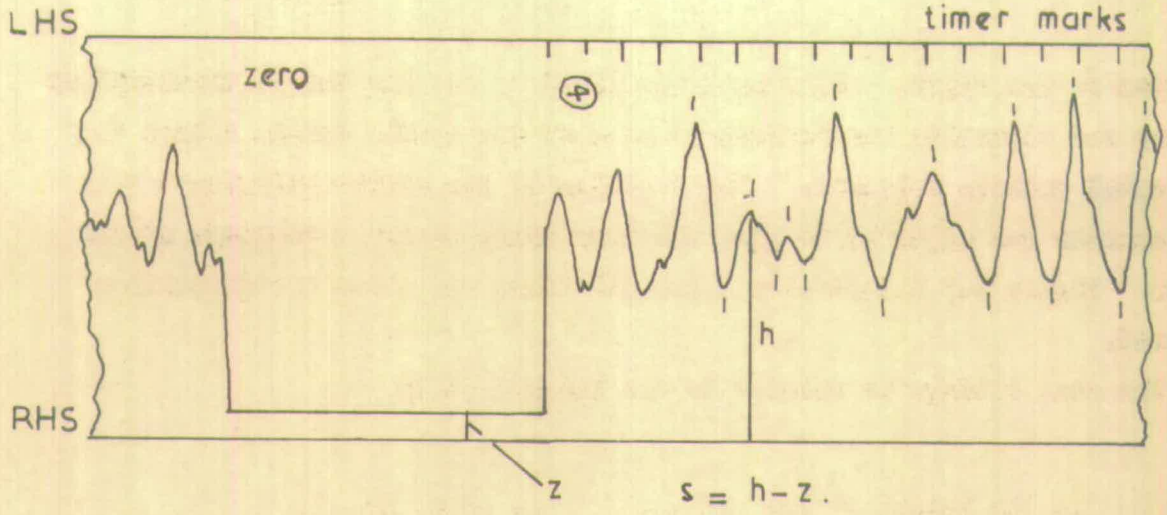


FIGURE 5.7 QUANTITIES MEASURED FROM TRACE.

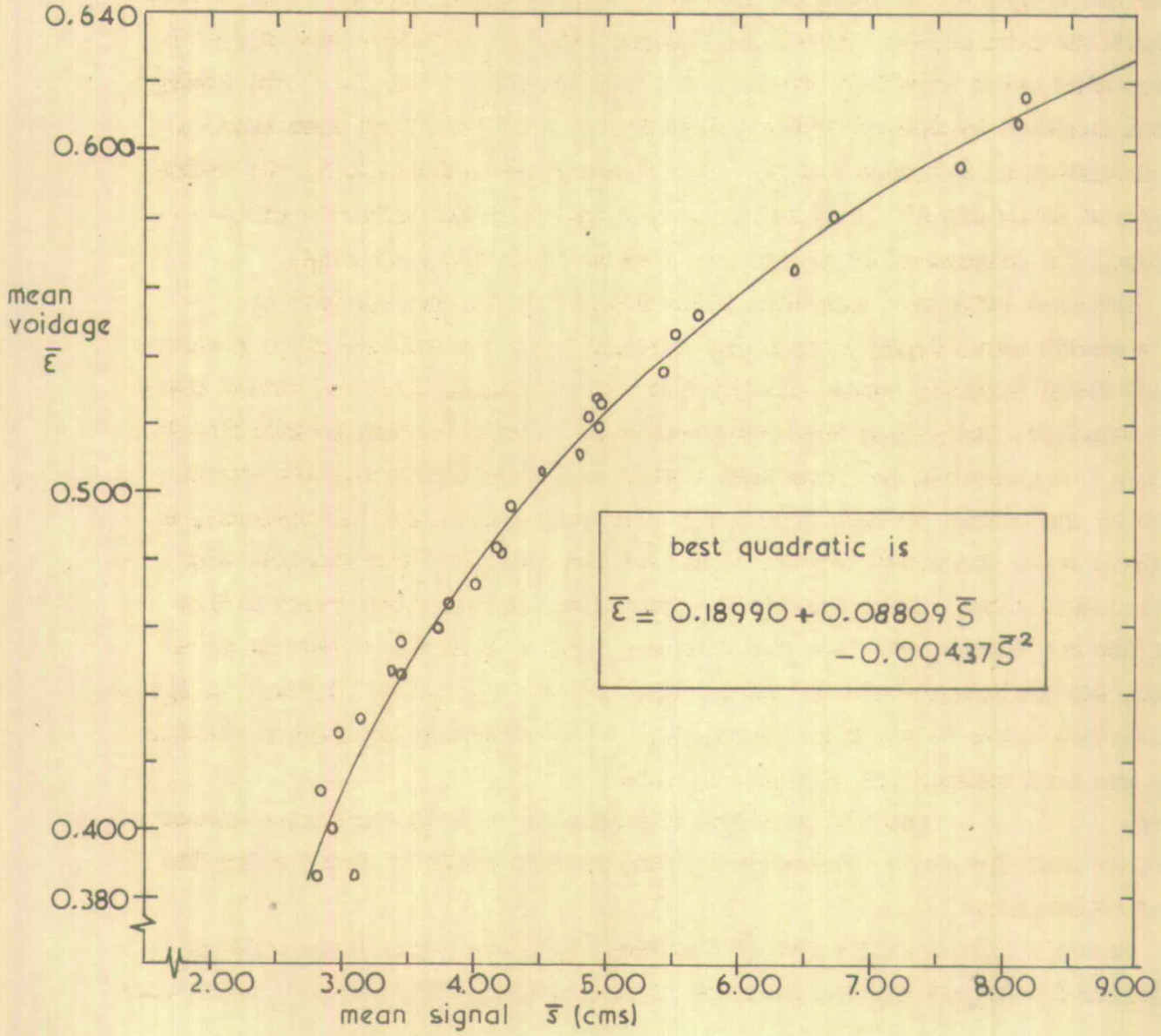


FIGURE 5.8 TYPICAL VOIDAGE CALIBRATION CURVE

position on the chart. This zero was fixed by closing the photomultiplier shutter and adjusting the resistance arms of the double triode bridge to give equal cathode voltages. The position of the mirror galvanometer in the recorder was adjusted to give the zero trace close to the edge of the paper. Figure 5.7 illustrates a typical trace and shows the quantities measured.

The mean voidage is related to the bed height by

$$\bar{\varepsilon} = \frac{x_t - x_w}{x_w}$$

where x_t is the height of the bed and x_w is given by

$$x_w = \frac{4W}{\pi d_t^2 \rho_s}.$$

W. is the weight of material in the bed. For each flow rate, $\bar{\varepsilon}$ was calibrated against the mean signal $\bar{S}$ obtained from the trace. The flow rate for each $\bar{\varepsilon}$ was also noted to obtain the relationship between $\bar{u}_o$ and $\bar{\varepsilon}$. The average signal wasfound by measuring the deflection S at 60 points on each record. The variation in estimate decreased continuously with increase in the number of points taken and it was found that it became constant after 40 points. However, the average of 60 points was used to be on the safe side.

The mean voidage $\bar{\varepsilon}$ was then plotted against the mean deflection $\bar{S}$ and a smooth curve drawn through the points. For the voidage range covered, it was found that the second differences of $\bar{\varepsilon}$ obtained from the smooth curve were constant, indicating that a quadratic in $\bar{S}$ was a reasonable relationship to use. A quadratic in $\bar{S}$ was then fitted to points taken from the smooth curve by the method of least squares. For each calibration carried out, a smoothed curve was drawn to make sure that the quadratic relationship was in fact reasonable. The expression was fitted to the smooth curve rather than the raw data. When the raw data was used to find the quadratic as a check, the difference between the two expressions was insignificant. A typical calibration curve is shown in Figure 5.8. The quadratic expression obtained from the mean voidage and signal $\bar{S}$, i.e. $\bar{\varepsilon} = a_0 + a_1\bar{S} - a_2\bar{S}^2$ _____(5,1) where a_0, a_1, a_2 are all positive, was assumed to hold for instantaneous values of S, so that for any S, the corresponding voidage could be found using the above expression.

Possible errors in the use of equation (5,1) may result from voidage gradients in the bed and the presence of large fluctuations in the signal used

to find $\bar{S}$. If there is assumed to be no voidage gradients in the bed so that the mean point voidage is the same as the overall mean voidage, then

$$\varepsilon = \bar{\varepsilon} + \varepsilon_f \qquad \text{and} \qquad S = \bar{S} + S_f$$

where the subscript f refers to fluctuations about the mean. Now $\varepsilon = f(S)$ and this can be expanded in a Taylor series about $\bar{S}$, giving

$$\varepsilon = f(S) = f(\bar{S}) + S_f f'_{\bar{S}} + \frac{1}{2!} S_f^2 f''_{\bar{S}} + \text{---}$$

Taking mean values of the above expression

$$\bar{\varepsilon} = f(\bar{S}) + \frac{1}{2!} \overline{S_f^2} f''_{\bar{S}}$$

since $\bar{\varepsilon}_f = 0$ and $\bar{S}_f = 0$.

If the fluctuating components are small, second and higher order terms can be neglected so that $\bar{\varepsilon} = \bar{f}(S) = f(\bar{S})$.

and the use of the above calibration procedure is justified. Near the distributor, disturbances have not grown to any great extent, so that $\overline{S_f^2}$ can be considered small.

However at high voidages, the calibration bed generally became turbulent, introducing large fluctuations into a signal, and so $f(\bar{S})$ is not necessarily equal to $\bar{f}(S)$.. Denoting the mean voidage signal calibration by $F(\bar{S})$, then

$$F(\bar{S}) = f(\bar{S}) + \frac{1}{2!} \overline{S_f^2} f''_{\bar{S}} + \text{-----}$$

where $f(S)$ is the true voidage signal calibration. Because of the general shape of the voidage signal calibration curve, it is immediately obvious that $f''(S)$ is negative, so that, if the fluctuations are large, $F(S)$ would give smaller values of the voidage than the true calibration $f(S)$. An estimate of the magnitude of this effect can easily be obtained. The mean square signal fluctuation is readily obtained from the records and F'' is a reasonable approximation to f'' i.e. $f'' \sim -2a_2$. Calculations were carried out for cases where the calibration records had visually large fluctuations and in no case was the difference found to be more than 1%.

The above calibration procedure is based on the assumption that there is no voidage gradient in the short calibrating bed. In general this is not true because of non-uniformity in particle size. Particles tend to segregate, the larger particles moving to the foot of the bed and the smaller particles rising to the top, leading to an increase in voidage towards the top of the bed. However if the size range is narrow, this effect is not too important since the

segregation process takes place very slowly. This was tested using clear ballotini of average diameter 0.086 cms. and blue ballotini of average diameter 0.067 cms. After about two hours, there was visible segregation at the top and bottom of the bed, but in the large section of the middle of the bed the particles appeared to be very well mixed.

More important are the possible voidage gradients discussed in Chapter 3. However, it is impossible, without prior knowledge of this voidage gradient, if it exists, to gauge the effect it has on the calibration procedure. Under these circumstances, the procedure adopted in the present work is the best that can be achieved. It is to be hoped that, as the position of signal measurement was near enough the middle of the calibration bed, the deviation of the local mean voidage from the overall mean voidage obtained from the bed height is not at all large.

Other sources of error appear in the actual measurement of the signal and bed height. Measurement of the signals for all the records produced in the present work would have been too laborious with the limited facilities available to the writer, so all traces were digitised by Benson-Lehner Ltd. on an "Oscar" chart reader. They gave readings as accurately as possible to 0.01 cms. but no knowledge of the actual errors involved is available. The measurement of bed height introduced errors because of parallax and as a result of difficulty in reading the true mean height because of the rapid movements of the top of the bed. The height of a packed bed could be determined to within less than 0.05 inches giving a possible error of about 2%.

The above discussion of calibration refers entirely to calibration of voidage with signal at one particular height in the bed. A second stage of calibration is involved in the establishment of a basis for comparing signals at different bed heights, as is necessary in measuring propagation characteristics. This was found necessary because the light transmission properties of the optical box and tube varied from place to place, due probably to changes in thickness in the Perspex faces and extruded tube and the presence of dirt in the box and on the faces .

The factors affecting the final intensity of the light beam reaching the photomultiplier can be separated into two parts - the effect of the bed alone and the effect of the rest of the equipment - tube, faces and dirt. If I_o is the intensity of the light in the parallel beam from the source, I_1 is the intensity of the beam reduced by all the factors except the particles themselves, and I_2 is the intensity of the light beam entering the photomultiplier, then

$$I_1 = \alpha I_o$$

where α is the stopping power of everything apart from the particles. I_o is constant (provided the lamp voltage is constant) but α is some function $\alpha(x)$ of the height of the light beam above the distributor.

The intensity of light reaching the receiver is

$$I_2 = \beta I_1$$

where β is the stopping power of the bed itself, and is some function $\beta(n)$ of the particle concentration only.

Thus $I_2(n,x) = \beta(n)\,\alpha(x)\,I_o$

If there are no particles in the tube, but instead a filter of stopping power γ then

$$I_2(0,x) = \gamma\,\alpha(x)\,I_o$$

If the position of calibration of the voidage close to the distributor is chosen as the datum level x_o, then $I_2(0,x_o) = \gamma\,\alpha(x_o)I_o$

so that $\alpha(x) = \alpha(x_o)I_2(0,x)/I_2(0,x_o)$

With the bed present, but no filter

$$I_2(n,x) = \alpha(x)\,\beta(n)\,I_o$$

so that $$I_2(n,x) = \alpha(x_o)\,\frac{I_2(0,x)}{I_2(0,x_o)}\,I_2(n,x_o)$$

Thus $$I_2(n,x) = \frac{I_2(0,x)}{I_2(0,x_o)}\,I_2(n,x_o)$$

To apply the voidage calibration obtained at one point near the foot of the bed, disturbance records obtained anywhere else in the bed must be reduced to the signal which would be obtained for the same voidage at the calibration point. Thus

$$I_2(n,x_o) = \frac{I_2(0,x_o)}{I_2(0,x)}\,I_2(n,x)$$

is in fact the intensity required for the voidage calibration, but it has to

be transformed into terms of the chart signal S.

The response of the photomultiplier tube was not linear over all its range, but only at low levels of illumination. The amplifier system used has a linear response to the anode signal provided the characteristics of the triode valve are linear. The recorder response is virtually linear, so that, as long as the photomultiplier tube was operated in its linear range the chart deflection was proportional to the intensity of light reaching the photomultiplier.

To obtain any signal taken at any height in terms of the datum signal for the same voidage, it was necessary to know the ratio $I_2(0,x_0)/I_2(0,x)$. This was obtained by using filters to stop down the light reaching the photomultiplier to the lowest possible level of illumination, and measuring the signals obtained at various heights up the bed with only water present in the tube. Because the measuring equipment was being operated in the linear range,

$$\frac{I_2(0,x_0)}{I_2(0,x)} = \frac{S(0,x_0)}{S(0,x)} = R(x)$$

so that

$$I_2(n,x_0) = R(x)\, I_2(n,x)$$

When the bed was in the tube, however, it was not always so easy to ensure operation in the linear range. Some compromise had to be made between the need to stop down the light and the need to obtain reasonable sized signals for measurement. In all the runs carried out, however, the light was stopped down so that the amplifier was operating on the two most sensitive ranges and calculations based on the photomultiplier characteristics showed that this was never very far outside the linear range.

Thus it had to be assumed that

$$\frac{S(n,x_0)}{S(n,x)} = \frac{I_2(n,x_0)}{I_2(n,x)}$$

although at times this was not absolutely correct.

The relationship

$$S(n,x_0) = R(x)\, S(n,x) \qquad \text{(5,2)}$$

enabled the signal obtained at any height to be reduced to the equivalent datum level signal for the same voidage. The voidage calibration found at the datum level could then be used.

Experimental Method

Before each experimental run, the light system was checked to ensure that the beam was in fact collimated. The light transmission properties of the equipment changed, albeit shlowly, from day to day so this calibration was carried out immediately before each set of runs for one particular particle size. The optical faces of the column were cleaned with chamois leather just before the calibrations were made. This appeard not to leave electrostatic charge on the perspex faces - thus dust was not attracted and would not change their light transmission properties during the run.

Light filters were placed in front of the diverging lens in the receiver to cut the signal down to about three centimetres deflection on the most sensitive range of the amplifier. The light system carriage was traversed up and down the column, thus giving two records of the signal at various predetermined heights above the distributor. The mean of these two results was used to find R(x). A small known weight of ballotini was then placed in the tube for the voidage calibration. This weight was calculated to give a packed height of about 3½ inches. The light was again filtered down to give deflection across the whole width of the chart for the voidage range used in the calibration. The most sensitive ranges on the amplifier were used if possible. Records were then taken of the signal at the chosen datum level for about 30 different flow rates.

A large known weight of ballotini was then added - this weight always being sufficient to give bed heights of about 60 inches or more so that the growth of the disturbances could be followed right through. For each flow rate studied, records were taken at all the calibrated positions up the bed. For each system studied, records of the disturbances were taken for generally about three flow rates - the number being limited by the onset of turbulance at the higher flow rates.

From these records the variation in voidage with time at each point in the bed could be obtained, thus giving the frequency and growth distance. The actual analysis of the records is discussed in the next section. The propagation velocity of the disturbances was measured by timing their rise over a known

distance as close to the foot of the bed as possible. The wave length of the disturbances was measured from flash photographs of the disturbances near the foot of the bed. The bed height for each flow rate and the pressure drop across the bed were also noted.

Measurements of the propagation velocity and wave length were also made for situations where it was impossible to get records because of the high noise level in the system. This was generally the case when the ratio of particle diameter to tube diameter was large. Frequencies in this case were measured by counting the number of disturbances passing a point in a certain time.

This method of measuring frequencies is not at all accurate. Considerable coalescence of disturbances was observed in every system studied; the frequency had to be measured well above the distributor where the disturbances were readily visible. Coalescence will have decreased the original frequency so that these visually measured frequencies will be too low. The velocity of propagation also had to be measured well above the distributor and may also have changed due to coalescence. However measurements of the velocity made at various heights up the bed indicated that the velocity decreased only very slowly on moving up the bed, so that this method gave fairly reliable estimates of the initial velocity of propagation of the disturbances.

Methods of Analysis

The propagation characteristics obtained in the theoretical section refer to one single sinusoidal component of any disturbance present whereas the records obtained were not sinusoidal but in fact indicated the presence of other components of different wave lengths and frequencies, together with noise due to individual particle motion and possible noise generated in the electronics. In this situation, the best method of analysis is to find the power spectral density function. This is a measure of the power or the amplitudes associated with the various frequencies present in the signal. Obtaining the power spectra at various heights up thebed would thus give the changes in amplitude at various frequencies as the disturbances propagated through the bed.

At any position in the bed, the record of the fluctuating voidage is a function of time. The voidage may be expressed as the sum of the mean voidage and a disturbance $\varepsilon_f(t)$ with zero mean value. Because the flow conditions are steady and because these disturbances are always present it can be assumed that this function $\varepsilon_f(t)$ is stationary i.e. the statistical properties of a population composed of instantaneous values of this function do not change with time. The numerical procedure involved in obtaining the power spectrum depends on this property.

If $A(f)$ is the amplitude of a sinusoidal component of the disturbance with a frequency f, the power associated with this component is $A^2(f)/2$. $P(f)$ is the cumulative power over all the frequencies from 0 to f and $P(f, \Delta f)$ is the average power associated with a frequency bandwidth Δf centred on f. The power spectral density function (power spectrum) can be defined (see, for example, references (36), (37) and (38)) as

$$G(f) = \lim_{\Delta f \to 0} \frac{P(f + \Delta f/2) - P(f - \Delta f/2)}{\Delta f} = \lim_{\Delta f \to 0} \frac{P(f, \Delta f)}{\Delta f}$$

for the positive frequency range $0 \leq f \leq \infty$.

The total power over all positive frequencies is given by

$$\bar{P} = \int_0^\infty G(f)\, df \qquad \text{(5,3)}$$

since there is zero power at $f = 0$. (Mean values are subtracted out of the signal for a power spectrum analysis.) The total (time average) power for a single record is given by

$$\bar{P} = \lim_{T \to \infty} \frac{1}{2T} \int_{-T}^{T} \varepsilon_f^2(t)\, dt \qquad \text{(5,4)}$$

and if the ergodic hypothesis holds, this is the variance of the fluctuating signal over an ensemble of different records.

It is obvious from the above that $G(f)$ represents the average power per unit frequency contained in a narrow bandwidth Δf centred on f or, more precisely, $G(f)$ represents the contribution to the variance from frequencies between $(f + \Delta f/2)$ and $(f - \Delta f/2)$ for positive frequencies. (Blackman and Tukey (39)).

The autocorrelation function of $\varepsilon_f(t)$ is defined as

$$C(\tau) = \text{Ave}\left[\varepsilon_f(t)\, \varepsilon_f(t+\tau)\right]$$

$$= \lim_{T \to \infty} \frac{1}{2T} \int_{-T}^{T} \varepsilon_f(t)\, \varepsilon_f(t+\tau)\, dt \qquad \text{(5,5)}$$

Because $\varepsilon_f(t)$ is stationary, $C(\tau)$ is dependent only on the lag time τ and it is independent of t. The properties of autocorrelation functions and their interpretation are discussed in references (36) and (37). If the ergodic hypothesis holds, they are equivalent to the autocovariance used in statistical work.

It is shown in the references quoted above that, for stationary processes, the power spectrum is given by the Fourier transform of the autocorrelation function

$$G'(f) = \int_{-\infty}^{\infty} C(\tau) \exp\left[-j\,2\pi f \tau\right] d\tau$$

and conversely,

$$C(\tau) = \int_{-\infty}^{\infty} G'(f) \exp\left[j\,2\pi f \tau\right] df$$

For these transforms, the power spectrum $G'(f)$ is given as an even function, the power being assumed distributed over the whole of the frequency range $-\infty \leq f \leq \infty$.

The functions $C(\tau)$ and $G'(f)$, being even functions of their respective arguments, can be written as one sided cosine transforms, viz

$$C(\tau) = \int_{0}^{\infty} 2\,G'(f) \cos(2\pi f \tau)\, df \qquad \text{——————} \quad (5,6)$$

and

$$G'(f) = \int_{0}^{\infty} 2\,C(\tau) \cos(2\pi f \tau)\, d\tau \qquad \text{——————} \quad (5,7)$$

If τ is put equal to zero in (5,5), $C(\tau)$ becomes the variance or power of $\varepsilon_f(t)$ — see equation (5,4) — and equation (5,6) becomes

$$\overline{P} = \int_{0}^{\infty} 2\,G'(f)\, df$$

Hence, for $0 \leq f \leq \infty$, $2G'(f) = G(f)$.

Over a narrow bandwidth Δf, the average power is given by

$$P(f,\Delta f) = \int_{f-\Delta f/2}^{f+\Delta f/2} G(f)\, df \doteq G(f)\,\Delta f$$

If this average power $P(f,\Delta f)$ is a reasonable estimate of the power associated with a sinusoidal component of that frequency, then

$$\tfrac{1}{2} A^2(f) = P(f,\Delta f) = G(f)\Delta f$$

and the amplitude of a disturbance component of frequency f can be estimated from this relationship.

The Fourier transforms quoted above form the basis of most practical methods for obtaining power spectra from single records and details of the calculation

The autocorrelation function of a pure sine wave is itself sinusoidal, so the presence of any dominant sinusoidal component in the signal is indicated by the appearance of a periodicity in the autocorrelation function. The power spectrum of a purely sinusoidal signal is the unit impulse function and the presence of a large sinusoidal component in any signal is indicated by a large peak in the power spectrum appearing at the frequency of that component. Both the dominant frequency and the amplitude of this dominant component can thus be obtained from the power spectrum.

In the present work, the disturbances appear to have frequencies around one or two cycles per second, both from the calculations and rough visual measurement. The power spectrum must be calculated at least over a range of 0 to 5 c/sec. and preferably over the range 0 to 10 c/sec. It is expected that the signal will not contain frequencies higher than this. Thus the minimum folding frequency in the present work was taken as 5 c/sec. The folding frequency is that frequency above which "aliasing" takes place. This occurs because in sampling the signal at equal intervals of time, some of the high frequency content is confused with the low frequency content, and if there are present in the signal components whose frequency is greater than the folding frequency, their energies will be attributed to the "alias" frequencies, below the folding frequency. This question of aliasing is dealt with by Bendat (36) and Blackman and Tukey (39). They recommend that at least two samples per cycle of the highest frequency should be obtained. Thus the sampling time interval must be less than or equal to $\frac{1}{2fm}$, where fm is the folding frequency.

For fm = 5 c/sec,

The period of the dominant frequency is of the order of one second, so that for any information to be obtained from the autocorrelation function about this period, the A.C.F. (autocorrelation function) should be known over about 5 seconds. Blackman and Tukey state that the length of record necessary to give a reasonable estimate of the A.C.F. over the range required should be ten times the maximum value of lag time required. For a maximum value of 5 seconds, the record length should therefore be at least 50 seconds.

procedure and limitations of the methods are given in the book by Blackman and Tukey (39) and the paper by Swinnerton-Dyer (40). In most cases the numerical work involved is quite formidable.

The autocorrelation function of a pure sine wave is itself sinusoidal, so the presence of any dominant sinusoidal component in the signal is indicated by the appearance of a periodicity in the autocorrelation function. The power spectrum of a purely sinusoidal signal is the unit impulse function and the presence of a large sinusoidal component in any signal is indicated by a large peak in the power spectrum appearing at the frequency of that component. Both the dominant frequency and the amplitude of this dominant component can thus be obtained from the power spectrum.

In the present work, the disturbances appear to have frequencies around one or two cycles per second, both from the calculations and rough visual measurement. The power spectrum must be calculated at least over a range of 0 to 5 c/sec. and preferably over the range 0 to 10 c/sec. It is expected that the signal will not contain frequencies higher than this. Thus the minimum folding frequency in the present work was taken as 5 c/sec. The folding frequency is that frequency above which "aliasing" takes place. This occurs because in sampling the signal at equal intervals of time, some of the high frequency content is confused with the low frequency content, and if there are present in the signal components whose frequency is greater than the folding frequency, their energies will be attributed to the "alias" frequencies, below the folding frequency. This question of aliasing is dealt with by Bendat (36) and Blackman and Tukey (39). They recommend that at least two samples per cycle of the highest frequency should be obtained. Thus the sampling time interval Δt must be less then or equal to $1/2f_m$, where f_m is the folding frequency. For $f_m = 5$ c/sec, $\Delta t \leq 0.1$ secs..

The period of the dominant frequency is of the order of one second, so that for any information to be obtained from the autocorrelation function about this period, the A.C.F. (autocorrelation function) should be known over about 5 seconds. Blackman and Tukey state that the length of record necessary to give reasonable estimates of the A.C.F. over the range required should be ten times the maximum value of lag time required. For a maximum value of 5 seconds, the record length should therefore be at least 50 seconds.

Thus to obtain one power spectrum (P.S.) it is seen that the number of points to be digitised from one record has to be at least 500 and is probably nearer 1000. To fully study the growth of the disturbances, at least 8 records would be required for any one flow situation and for all the situations studied in the present work, about 150 power spectra would have to be computed. Data logging or chart reading facilities which could cope with this volume of work were not available and the cost of getting the records digitised by contractors would have been too great. However, thanks are due to the Management Services Section of Imperial Chemical Industries Limited, who digitised some of the records and computed power spectra for two flow situations. To deal with the bulk of the records, the following much more crude method of analysis had to be adopted.

This method was measurement of the "peak to peak" frequency and amplitude directly from the records. The chart heights (marked as "h" on Fig. 5.7) of successive maxima and minima were measured and these readings then transformed to voidage measurements. The differences between the successive maxima and minima were averaged to give the mean amplitude of the disturbances. The mean value of all the readings also gave a measure of the mean voidage at that point. The time duration spanned by these readings (from the first maximum to the first maximum after the last minimum) was measured from timer marks at the side of the chart and gave a measure of the mean frequency. The mean values of amplitude and frequency were then identified with the values of the dominant frequency and amplitude for the purposes of comparison with the theoretically predicted values. These mean values were obtained by averaging over 30 cycles or 60 points and in all cases tested it was found that the averages had settled to stable values before the sample size was reached.

This rather unsophisticated method of analysis was all that was practicable, lacking any facilities for rapid on-line digitisation. It would be expected to give not unreasonable accuracy at higher points in the bed where the disturbances have developed far enough to give a fairly regular, almost periodic signal. Even here, however, confusion sometimes arose between peaks due to genuine disturbances and two peaks very close together due to coalescence or noise. Because of this, the frequencies obtained from these records might be too high .

Further down the bed, where the signal became much more irregular it was sometimes difficult to distinguish genuine maxima and minima caused by the passage of the disturbances. Again the contribution of higher frequencies in the signal might be expected to increase the mean frequency.

A typical chart is shown in Figure 5.7 with the significant peaks marked. The signal S is given by

$$S = h - Z$$

where h is the distance from the right hand side of the paper and Z is the height of the zero signal, measured from the same edge of the paper.
The signal is reduced to the signal at the datum level (the level at which the voidage was calibrated) by the appropriate value of $R(x)$ at that point,

i.e. $S_o = RS$.

and is then transformed to a voidage value by the calibration

$$\varepsilon = a_o + a_1 S_o - a_2 S_o^2$$

The above process was carried out both for the bulk of the results and the few records analysed in detail by power spectrum computations.

The voidage calculation procedure and the averaging process for the "peak to peak" analysis described above were programmed for a Ferranti-Sirius Computer. All records obtained (except for power spectrum analysis records) were digitised by Benson-Lehner Ltd., who prepared the digital records both on punched tape ready for use as input to Sirius, and as a typewritten table of numbers. All records were digitised as centimetres deflection from the right hand side of the chart, the zero signal for each record appearing before and the time appearing after the block of 60 points taken from the record.

From the few power spectra available and from the "peak to peak" method of analysis the frequency and amplitude of the disturbances as a function of height above the distributor were obtained. The results of this experimental work for a variety of situations and a comparison of these results with the theoretical predictions is presented in the next chapters.

CHAPTER 6

General Features of the Experimental Work

This chapter gives a general outline of some of the phenomena encountered in the experimental work which, in the main, are not directly concerned with the disturbance growth. The phenomena dealt with include turbulence, slugging, coalescence and bed expansion and, in general, they are not susceptible to any great degree of quantitative analysis.

(a) The Measurement of Propagation Properties

In Chapter 5, the equipment, and the calibration procedures for this equipment, necessary to obtain a record of the local time - varying voidage at any point in the bed were described. It was shown how both methods of analysis - the power spectrum (P.S.) method and the "peak to peak" method - gave an estimate of the amplitude and frequency of the regular rising disturbances appearing in the bed. These quantities could thus be obtained as functions of the height above the distributor.

From the linearised equations of motion, the real part of any single disturbance component was shown to have the form

$$n_1 = N_0 J_0(k_\rho \rho) \exp[\xi t] \cos(k_x x - \nu t) \quad . \quad \text{(see page 45.)}$$

if the disturbance is assumed to have axial symmetry. This expression applies to one component of one disturbance originating at time t = 0, whereas in the practical situation a train of disturbances is propagating through the bed. The amplitude of the above disturbance component at the centre of the tube is $N_0 \exp[\xi(k_x, k_\rho)t]$. If this disturbance is assumed to originate at the distributor then at time t it will have travelled a distance $x = V_p t$. The amplitude is thus

$$A'(x) = N_0 \exp\left[\frac{\xi}{V_p} x\right]$$

i.e.

$$A'(x) = N_0 \exp[x/\Delta x]$$

In the "peak to peak" analysis, the amplitude of each "cycle" of the signal (see Figures 5.6 and 5.7) is calculated. To calculate the propagation properties, each cycle is considered to be a separate disturbance having its own time origin and is assumed to be quite independent of any previous cycles in the train of disturbances. The average amplitude of a number of these cycles is calculated - giving an estimate of the mean amplitude (at least, twice the mean amplitude for maximum to minimum values) of the disturbance at height x above the distributor. Likewise the average of the periods of each cycle (the time duration of the record divided by the number of cycles) gives an estimate of the frequency of the disturbances.

Figures 5.6 and 7.1 illustrate clearly the growth of disturbances with height above the distributor. Between 6 inches and one foot above the distributor a strongly periodic signal has emerged. This presumably corresponds to the wave length of maximum growth (in this case, minimum growth distance, since it is the amplification of the disturbances with distance which is being measured) which has emerged from the spectrum of disturbances present at the foot of the bed. (Experimental observations and the records obtained indicate that disturbances do in fact originate very close to the distributor.) The average values of amplitude and frequency obtained from the "peak to peak" analysis are identified with the amplitude and frequency of the dominant wave number.

The P.S. method gives the dominant frequency and a measure of its amplitude directly and hence is a much more reliable analytical tool than the "peak to peak" method. However the P.S. shown in Chapter 7 (Figures 7.3 and 7.14) show that this dominant frequency decreases with bed height and for every experimental situation considerable coalescence of individual disturbances was observed. This coalescence alters the frequency and increases the amplitude of disturbances, thus giving a false picture of their natural amplification.

Phase velocities of the disturbances were measured by timing the rise of regions of reduced particle concentration between two fixed points in the bed and taking an average. This phase velocity appeared to be reasonably constant over the length of the bed, dropping only very slightly in value over a three foot difference in measuring points. If the phase velocity remains constant throughout the bed, the decrease in frequency due to coalescence must cause a corresponding increase in the wave-length ($\lambda = V_p / f$); this can be observed visually.

Since the disturbances originate at the distributor, a plot of dominant frequency versus height in the bed extrapolated back to zero gives the dominant frequency without coalescence. The maximum effect that coalescence can have on the disturbance amplitude can be corrected for by multiplying the measured amplitude $A(x)$ by the ratio $f(x)/f(0)$ where $f(x)$ is the frequency at height x and $f(0)$ is the frequency at the distributor. If now this adjusted value of the amplitude $A'(x)$ is plotted against x on semilogarithmic paper a straight line graph will be obtained if the growth is exponential. The value of $A(0)$ gives the initial value of the disturbance. If $A(0) = N_0$, a plot of $A'(x)/A(0)$ vs. x should allow the growth distance to be evaluated.

The dominant wave-length is evaluated from the relationship $\lambda = V_p / f(0)$.

The "peak to peak" analysis is very crude, both in its assumptinn that the mean frequency is equivalent to the dominant frequency and in its reliance on a subjective assessment of significant peaks in the traces, especially those obtained lower down the bed. Figure 7.1 shows a set of traces obtained for the system No.5B/H_2O in the 1" internal diameter tube (I.D.T). Comparing this with the traces shown in Figure 5.6. it is immediately obvious that the fluctuations are not so great and thus it becomes much more difficult to pick out significant peaks (the peaks chosen for digitising are marked). This difficulty in deciding upon significant peaks in situations where the peaks are not well defined is one of the major shortcomings of this method of analysis. Obviously it does not arise with the P.S. method. Benson-Lehner Ltd. digitised all the records obtained in the present work (except the P.S records) and instruction was given in doubtful cases which peaks were to be read. The amplitudes and frequencies obtained from this method of analysis are given in Appendix 3:

From the P.S. shown in the next chapter (Figures 7.3. and 7.14), near the distributor the power seems to be fairly evenly distributed overall the frequencies present. The traces shown (Figure 5.6 and 7.1), which are typical of all the traces obtained, do not show very much apparent noise at higher levels in the bed so that the irregular signal near the foot of the bed would seem to be caused mainly by the presence of a whole spectrum of disturbances, rather than noise from individual particle movement. If the power is evenly distributed over the range of frequencies (and hence, wave numbers) lower down the bed then the average amplitude may not be too bad an estimate of the dominant wave length amplitude. The frequency estimate from the "peak to peak" analysis is likely to be high because of these irregular disturbances.

One other possible source of error (which may occur with both types of analysis) should be mentioned. The photomultiplier picks up a light signal which has passed through the whole width of the bed and is thus an average signal over the tube diameter. The measured amplitude due to growth at height x_1 is $A(x_1) f(x_1) / f(0)$ and at height x_2 it is $A(x_2) f(x_2) / f(0)$. The disturbance amplitudes at the centre of the tube are $m_1(x_1) = N_0 \exp[x_1/\Delta x]$ and $m_1(x_2) = N_0 \exp[x_2/\Delta x]$ .There is no guarantee that the average signal across the tube is such that

$$\frac{A(x_1) f(x_1)}{A(x_2) f(x_2)} \equiv \frac{m_1(x_1)}{m_1(x_2)} = \exp\left[\frac{x_1 - x_2}{\Delta x}\right]$$

This arises because of scattering of light by the particles close to the walls of the tube.

(b) Turbulence and Slugging in Liquid Fluidised Beds

As indicated in the previous chapter, it was found that for the ballotini/water systems studied in this work, regular bands of reduced particle concentration rising through the bed were only observed when the system was obviously not turbulent. These bands of reduced particle concentration are obviously manifestations of the instability of the uniformly fluidised state.

In this situation, the particles moved, apart from individual particle movement over short path lengths caused by collisions, in a fairly gentle oscillatory fashion occasioned by the passage of disturbances and there was little obvious rapid transport of particles from one part of the bed to another. This was in complete contrast to obviously turbulent beds, where large groups of particles were seen to move about in a random fashion, presumably following the large turbulent eddies in the fluid. It is turbulence in liquid fluidised beds which gives the smooth appearance of the so-called particulately fluidised systems.

Murray (14) implies that all liquid fluidised beds (at least, beds with a small density ratio) are turbulent and concludes from his stability investigation that unstable disturbances lead to bubbles for aggregative systems and to turbulence in particulate systems. Certainly small unstable disturbances are the direct cause of turbulence in boundary layer flow of a fluid but the presence of some velocity gradient produced by a wall is necessary. Also these disturbances causing breakdown of laminar flow are external disturbances and not characteristic of the system (for a more detailed discussion of this point see Schlichting (28)). For a fluidised bed, the dominant wave length is an inherent property determined by the system parameters, and instability does not depend on velocity gradients. From the visual evidence available, and the fact that bubbling beds have streamline gas flow (Rowe and Partridge 41), instability of the uniformly fluid state would not seem to be the cause of turbulence in the bed.

It is a well known fact that extremely high concentrations of particles have the effect of "freezing out" turbulence (Bagnold (42)), i.e. the presence of particles in what would otherwise be a turbulent stream tends to damp out turbulence. This effect is particularly well illustrated in the photographs of fluid flowing across banks of heat exchanger tubes obtained by Wallis(43).

The turbulent wake is confined to a progressively smaller region behind each tube as the distance between the tubes is decreased. With a fluidised bed, as the flow rate increases and the particles move apart, the wake behind the particles can extend over a larger area; turbulent eddies will increase in size and energy and eventually be sufficient to overcome the inertia of the particles. The particles will move with these large eddies and overall bed turbulence will set in. Ordered instability disturbances could perhaps complement this process, for, as the flow rate increases, their frequency and phase velocity increase and they may merge into the general turbulent spectrum but in themselves they are not the cause of it.

However for many systems studied (eg. No. 5 B/H_2O, 1½" I.D.T.) there is no gradual transition with increase of flow rate as the bed assumes a turbulent appearance as soon as it is fluidised. The system No. 5 B/H_2O, 1" I.D.T. exhibited streamline flow with clearly defined distrubances just above incipient fluidisation but there was a gradual transition to turbulent flow as the flow rate was increased. This effect was observed with a number of systems eg. with No. 7B/H_2O, ½" I.D.T. there was a gradual transition but in a 1" I.D.T. the bed was always turbulent, and a similar effect was observed with the systems No. 3 B/H_2O, 1" I.D.T. and No. 3 B/H_2O, 1½" I.D.T. Clearly the diameter of the bed plays an important part in determining the nature of the flow. The onset of turbulence in some beds was one of the major factors limiting the number of systems available for study in the present work.

Insufficient data is available at present, however, to arrive at any transition criterion. It is probably a combination of some Reynolds number, the voidage and the ratio of particle to tube diameter, but it is not at all clear how any Reynolds number should be defined in this situation. What part do the solids density and voidage play?; is the Reynolds number written in terms of the superficial or interstitial fluid velocity?; does it depend on the particle diameter, the tube diameter or some volumetric equivalent diameter? Much experimental work is needed before these questions can be resolved and any transition criterion based on the flow parameters arrived at.

A further limitation, apart from turbulence, was the development of slugging in some systems. This was very similar in appearance to the slugging observed with aggregatively fluidised beds in narrow tubes, where the bubble occupies the whole cross-sectional area of the tube. The amount of light transmitted through these slugs was very great in comparison to the light transmitted through the normal fairly dense bed and hence the slugs produced a signal from the amplifier with a series of sharp peaks much greater than the maximum design signal of the recorder galvanometer.

The slugging observed in the present work was found to occur in two systems with a relatively large ratio of particle diameter to tube diameter (a value of 1 : 10 for the system No. 3B/H_2O, $\frac{1}{2}$" I.D.T. and 1 : 8 for the system 2 mm. B/H_2O 1" I.D.T.). Normal disturbances were observable over a distance of about six inches to a foot above the distributor when there was an abrupt transition of the normal disturbances to slugs. The transition point became lower as the flow rate was increased. There appeared to be no significant change in disturbance velocity after the transition.

There is no immediately obvious reason for the appearance of these slugs. The amplification rate for the systems No. 3 B/H_2O and 2 mm. B/H_2O is small compared to typically aggregative systems, and the high value of dp/dt implies a large wall effect inhibiting the growth of disturbances. It is possible that their appearance is related to growth distance and the horizontal extent of the disturbance, but the abrupt transition would not seem to correspond to the steady growth of disturbances into bubbles or slugs. Obviously the effect of the walls (~~a low value of dp/dt~~) is very important as slugs do not appear with these systems in larger tubes, and it is likely that some non-linear mechanism causes this sudden growth of the apparently already well developed disturbances.

The question of turbulence and slugging is returned to in the final chapter. These phenomena, together with the type of signal produced by some systems and the amount of light it was possible to get through the bed, limited the systems studied to the following:

2 mm. B/H_2O, $1\frac{1}{2}$" I.D.T.
No. 3 B/H_2O, 1" I.D.T.
No. 5 B/H_2O, 1" I.D.T.
No. 5 B/H_2O, $\frac{1}{2}$" I.D.T.
No. 7 B/H_2O, $\frac{1}{2}$" I.D.T.

In addition, for the systems where slugging occurred, it was still possible to obtain values of the phase velocity Vp and visual estimates of the frequency and wave-length below the transition point. The systems studied in this way were

2 mm. B/H_2O, 1" I.D.T. and
No. 3 B/H_2O, $\frac{1}{2}$" I.D.T.

To give some indication of the effect of particle density, polystyrene beads were also used. These have a density only marginally greater than water. The relevant physical properties of the above systems are detailed in Appendix 2

and Chapter 7.

The results at various flow rates for the above systems are given in full in Appendix 3 (these are the results of the "peak to peak" analysis processed by Benson-Lehner Ltd.) and their growth characteristics discussed in the next chapter.

(c) Bed Expansion

In the voidage signal calibration procedure, flow rates corresponding to each mean bed voidage used were also measured. The superficial fluid velocity is tabulated against the voidage in the tables in Appendix 3.

These measurements allowed the evaluation of a Richardson and Zaki (21) type expansion equation for each system. The general form for this equation is

$$\bar{u}_o = u_i \, \bar{\varepsilon}^N$$

where $\log_{10} u_i = \log_{10} u_t - dp/d_t$.
If these equations are generally valid, the terminal falling velocity of the particles can be evaluated from expansion data.

No. 5 B/H$_2$O For the 1" I.D. tube the expansion data in Table 2 of Appendix 3 is correlated by the correlation

$$\bar{u}_o = 11.91 \, \bar{\varepsilon}^{2.88}$$

The particle diameter is 0.086 cms. so that u_t = 12.88 cms./sec.
The calculated value of the terminal falling velocity was 17 cms./sec.
With u_t = 12.9 cms./sec., $Re = \frac{u_t \, dp \, \rho f}{\mu} = 111$

Richardson and Zaki give the expression for N in this Reynolds number range as

$$N = (4.45 + 18 \, dp/d_t) \, Re^{-0.1}$$

so that the calculated value for N is 3.16. This is 9% greater than the experimental value.

For the ½" I.D. Tube, the data in Table 9/5 gives the expansion equation as

$$\bar{u}_o = 11.72 \, \bar{\varepsilon}^{3.11}$$

with dp/d_t = 0.0670, u_t = 13.70 cms./sec. Thus Re = 118 and the calculated value of N is 3.52. Again there is some discrepancy between the experimental and the calculated values of the exponent N.

No. 3 B/H$_2$O 1" I.D.T. The data in Tables 4/3 and 6/3 give the equation as

$$\bar{u}_o = 16.30 \, \bar{\varepsilon}^{2.45}$$

with d_p/d_t = 0.050, u_t = 18.32 cms./sec. compared to a calculated value of 22 cms./sec. for u_t. With the experimental value of u_t and d_p = 0.127 cms. Re = 233. For this value of the Reynolds number, Richardson and Zaki give the equation for the exponent as

$$N = 4.45\, Re^{-0.1}$$

This predicts a value of 2.58 for N and is again higher than the experimental value.

2 mm. B/H_2O, 1½" I.D.T. The expansion data in Table 11/2 are correlated by the equation

$$\bar{u}_o = 20.42\, \bar{\varepsilon}^{1.96}$$

With d_p/d_t = 0.0543, u_t = 23.1 cms./sec. compared to a calculated value of 31 cms./sec. Again the equation for the exponent is

$$N = 4.45\, Re^{-0.1}$$

which, with an actual Reynolds number of 479 gives a value for N of 2.40. The lower limit given by Richardson and Zaki for the exponent N is 2.39 for Reynolds numbers greater than 500. The exponent found with this system is much lower than this limit.

With all the systems used in the present investigation, the terminal falling velocity predicted by Heywood's method (see reference (25)) was always greater than that found from the expansion equations. The exponent N found experimentally was in every case smaller than that predicted from the relationships of Richardson and Zaki. However the general form of their expansion equation is well confirmed by the results.

Because of the low values of the exponent N found experimentally it is of interest to see how they affect the drag parameter $n_o\beta_o'/\beta_o$ appearing in the dispersion relationship. In Appendix 2 it is shown that using a Richardson and Zaki type equation, $n_o\beta_o'/\beta_o$ is given by

$$\frac{n_o\beta_o'}{\beta_o'} = \frac{1}{\varepsilon_o}\left[(N-1)(1-\varepsilon_o) + \varepsilon_o\right]$$

Note that, for this equation, $n_o\beta_o'/\beta_o = N$ for all systems at $\varepsilon_o = 0.500$. For the system No. 5 B/H_2O, the experimental value of N is 2.88 so that at $\varepsilon_o = 0.500$, $n_o\beta_o'/\beta_o = 2.88$. From Figure A.3 the computed value at this voidage is 3.10. Figure 4.10 and 4.11 show that a 6% increase in can decrease the growth distance by 7%.

For all the computational work the values given in Figure A.3 were used for the parameter $n_o\beta_o'/\beta_o$, and these were based on the equations for N given by Richardson and Zaki. The above equation is based on the assumption of uniform fluidisation. There is no guarantee that this assumption is valid and, if it is not, there is considerable uncertainty about the actual voidage close to the distributor (see the tables in Appendix 3). Thus there is little to be gained by using the experimental values in preference to the predicted values.

(d) Some General Observations

Equation (3.21) gives the pressure drop across a fluidised bed as

$$\Delta p = g(\rho_s - \rho_f)(1-\bar{\varepsilon})x_t + g\rho_f x_t - \Delta\Omega - \rho_f \bar{u}_o^2\left[\frac{1}{\varepsilon_f} - \frac{1}{\varepsilon_t}\right]$$

Pressure drop measurements were made on all the systems investigated to obtain, if possible, some information on the particulate phase, normal stress term. However, for every system, the pressure drop was found to equal the buoyant weight of the bed. This means that either ε_f has much the same value as ε_t (uniform fluidisation) or that $\Delta\Omega$ is of the same order of magnitude as $\rho_f \bar{u}_o^2\left(1/\varepsilon_f - 1/\varepsilon_t\right)$ and that these terms are probably much smaller than the pressure drop and buoyant weight terms - reinforcing the conclusions reached in Chapters 3 and 4 concerning these terms.

Minimum fluidisation voidages were noted for the small beds used in the voidage-signal calibration runs. These were, for the following systems and tube diameters -

2 mm. B/H_2O, 1½" I.D.T., $\varepsilon_{mf} = 0.410$, $dp/d_t = 0.0543$.
No. 3 B/H_2O, 1" I.D.T., $\varepsilon_{mf} = 0.420$, $dp/d_t = 0.0500$.
No. 5 B/H_2O, 1" I.D.T., $\varepsilon_{mf} = 0.450$, $dp/d_t = 0.0339$
No. 5 B/H_2O, ½" I.D.T., $\varepsilon_{mf} = 0.500$, $dp/d_t = 0.0678$.
No. 7 B/H_2O, ½" I.D.T., $\varepsilon_{mf} = 0.470$, $dp/d_t = 0.0503$.

It appears that as the particle size increases, the minimum fluidisation voidages (and, incidentally the close packed voidages) decrease - the ratio of particle diameter to tube diameter remaining reasonably constant. The high value of the minimum fluidisation voidage for No. 5 B/H_2O, ½" I.D.T. is probably due to a greater packing effect. For the above systems, in the same order, the random close packed voidages were 0.342, 0.386, 0.387, 0.410 and 0.414. The trend of the minimum fluidisation voidages and the packed voidages is somewhat surprising but may be due to a narrower size range and better shape obtaining with the larger sized particles which are manufactured by a different method from the

smaller particles.

Throughout the experimental programme, it was observed both with long beds and the short calibration beds, that there was considerable bed expansion, particle movement and channeling before the bed could be said to be properly fluidised. With some of the long beds used to measure propagation properties it was noticed that at flow rates just greater than that necessary for incipient fluidisation in the short calibration beds, part of the bed just above the distributor was not properly fluidised and that particle movement occurred through channeling. This was probably due to insufficient pressure drop across the distributor - the fluid thus flowing towards the region of least flow resistance with ensuing maldistribution of fluid at the foot of the bed. In some cases, records were taken at these flow rates because of the small range of flow rates over which streamline flow prevailed in the bed. For these records, the height at which the bed was truely fluidised was carefully noted.

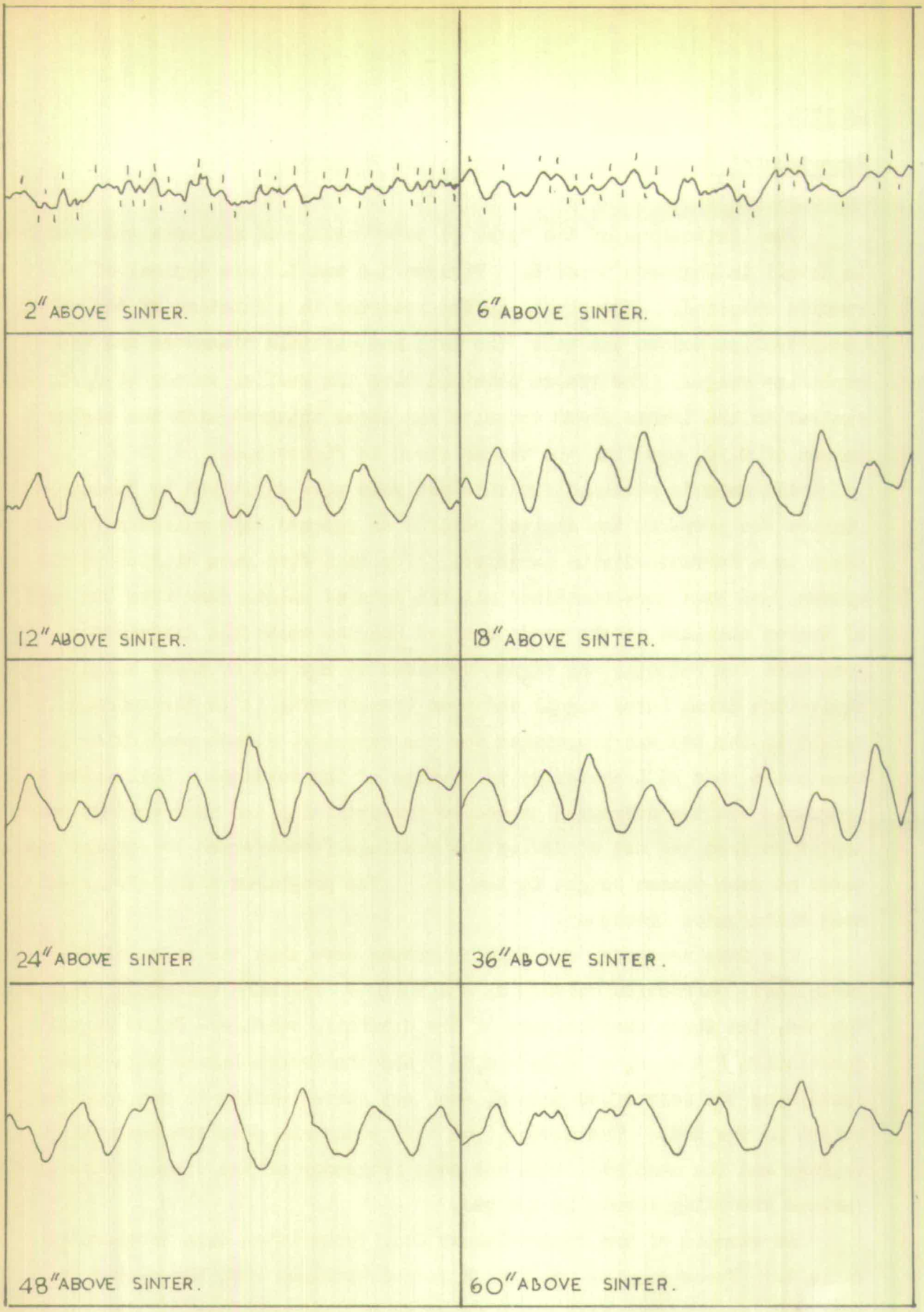


FIGURE 7.1 TYPICAL TRACES OBTAINED FROM A SYSTEM WITH A SMALL VALUE OF THE RATIO d_p/d_t.

CHAPTER 7

Experimental Determination of Propagation Properties

The limitations of the "peak to peak" method of analysis are discussed in detail in Chapters 5 and 6. Figures 5.6 and 7.1 are typical of all the records obtained. The signal to the recorder is a function of the particle concentration across the tube, the tube and particle diameters and the amplifier range. The traces obtained with the smaller values of d_p/d_t are similar to the traces shown opposite and those obtained with the higher values of d_p/d_t are like the traces shown in Figure 5.6.

All records obtained for this analysis were digitised by Benson-Lehner Limited who prepared the digital records on punched tape suitable for use as input to a Ferranti-Sirius computer. For each flow rate studied within one system, one data tape contained all the sets of points read from the series of traces obtained at the predetermined heights above the distributor. The procedure for reducing any signal obtained at any one of these heights to the equivalent datum level signal and then transforming it to the voidage at that height in the bed was programmed for the computer. Each reading on the data tape could thus be transformed to a value of the voidage. Built into the programme was the averaging procedure for obtaining the mean voidage and mean amplitude from the set of deflection readings (transformed to voidage readings) taken at each chosen height in the bed. The programme also calculated the mean disturbance frequency.

The data necessary for this programme were thus the value of $R(x)$ - the datum level correction factor $(S_o = R(x)S)$ - for each recording height in the bed, the three coefficients of the quadratic voidage - datum signal correlation ($\varepsilon = a_o + a_1 S_o - a_2 S_o^2$) and the Benson-Lehner data tape containing the sets of 60 points, each set corresponding to one specific height in the bed. The output from this programme gave the mean point voidage and the mean amplitude and mean frequency of the disturbances at the various recording levels in the bed.

An example of the Benson-Lehner Ltd. typewritten data is shown in Table 1. These results are from a record obtained with the system No. 5 B/H_2O, 1" I.D.T. at a superficial fluid velocity of 1.47 cms./sec.. The figures in front of each block of 60 points are the zero signals and the 60 points are the heights of successive maxima and minima taken from the record. All

Table 1:- Digital output from Benson - Lehner Limited

Record No.2 12/1/65

No.5 B/H 0, 1" I.D. Tube, R.R. = 12.0

Trace 1

0.50

5.31	4.92	5.18	5.06	5.43	5.06	5.26	4.84
5.09	5.00	5.22	4.84	5.06	4.92	5.12	5.03
5.37	5.28	5.48	4.83	5.35	4.99	5.22	5.02
5.27	5.15	5.41	5.05	5.52	5.02	5.26	4.88
5.25	4.92	5.04	4.76	5.04	4.96	5.28	4.86
5.35	5.11	5.29	4.98	5.05	4.82	5.17	4.98
5.15	4.84	5.25	4.84	4.93	4.73	5.17	4.88
5.09	4.85	5.08	4.72				

28.2

Trace 2

0.50

5.45	4.90	5.30	5.16	5.36	4.98	5.48	5.10
5.33	5.10	5.33	5.17	5.53	4.93	5.41	5.02
5.45	5.13	5.30	5.12	5.36	4.90	5.41	4.90
5.39	5.22	5.62	4.97	5.28	5.10	5.38	4.93
5.22	5.06	5.50	5.13	5.48	5.00	5.48	4.88
5.28	5.06	5.33	5.12	5.60	5.10	5.56	4.98
5.46	5.30	5.60	5.44	5.61	5.33	5.68	5.19
5.38	5.18	5.51	5.13				

26.4

Trace 3

0.50

5.61	4.72	5.52	5.12	5.64	5.08	5.48	4.88
5.41	5.17	5.46	5.05	5.43	5.08	5.58	5.34
5.69	5.13	5.51	5.12	5.52	5.16	5.40	5.22
5.50	5.00	5.32	5.08	5.82	5.21	5.43	5.20
5.33	5.12	5.42	4.96	5.78	5.33	5.90	5.12
5.52	5.29	5.67	5.19	5.73	5.06	5.73	4.86
5.43	5.08	5.75	5.39	5.69	5.06	5.58	5.22
5.75	5.05	5.90	5.02				

23.5

Trace 4

0.50

6.00	4.96	5.96	5.19	5.98	5.28	5.95	5.38
5.75	5.46	6.34	5.08	5.95	5.33	5.84	5.20
6.02	5.17	5.57	5.08	6.07	5.26	5.83	5.25

28.2

Trace 5

0.50

6.01	5.08	5.79	4.73	5.62	5.13	5.63	5.12
5.64	5.20	5.72	5.03	5.81	5.19	5.90	5.01
5.89	5.03	6.06	5.20	5.78	5.06	5.78	5.02
5.69	5.23	5.98	4.79	6.05	4.92	6.11	5.29
5.67	4.95	5.84	4.87	5.82	5.26	5.93	4.95
6.15	4.98	5.90	5.37	5.86	5.27	6.03	4.98
5.83	4.93	5.99	5.05	5.67	5.12	5.53	4.76
6.38	4.98	6.03	5.12				

26.1

Trace 6

0.50

5.90	4.81	5.74	5.28	5.66	5.35	6.23	5.30
5.74	5.21	5.62	5.14	5.60	5.02	5.88	5.33
5.95	4.93	6.18	5.19	5.98	5.05	6.02	4.96
6.22	5.36	5.69	4.94	5.76	5.04	5.82	5.12
5.87	4.92	6.04	4.89	5.75	5.08	5.96	4.90
6.20	5.20	5.80	5.22	6.08	5.54	5.88	5.30
5.84	5.34	5.69	5.09	5.91	5.03	5.70	5.12
6.18	5.22	5.53	5.14				

28.4

Trace 7

0.50

5.89	5.10	5.62	5.16	6.03	4.90	5.53	4.92
5.78	5.04	5.93	4.94	5.80	5.36	5.57	5.18
5.93	5.06	5.97	5.33	5.99	5.40	6.26	5.20
5.84	5.05	6.13	5.60	6.18	5.09	6.13	4.98
5.85	5.11	5.58	5.31	5.88	5.33	6.30	5.02
6.38	4.92	5.70	5.16	6.30	4.78	6.52	5.04
6.07	5.22	5.77	5.10	5.90	5.25	6.13	5.26
6.07	5.36	6.21	5.20				

27.2

Trace 8

0.50

6.13	4.98	5.90	5.29	6.30	4.98	6.06	5.07
6.26	5.05	6.01	4.96	5.84	5.18	5.95	5.02
6.14	5.76	6.32	5.04	6.29	5.36	6.03	5.10
5.90	5.08	5.92	5.16	6.21	5.05	5.94	5.40
6.01	5.01	6.04	5.22	5.88	5.28	6.34	5.03
6.22	4.87	6.13	5.23	6.19	5.18	5.68	4.98
6.40	5.21	5.86	4.87	6.22	5.32	5.90	5.13
6.28	4.78	5.76	5.08				

29.5

these quantities were measured from the R.H.S. of the paper. The figures after each block of 60 points are, for this record, the length of chart over which the thirty cycles extend. In this case the frequency is obtained from the chart speed which was always set at 12 mms./sec.. Normally timer marks were used to obtain the frequency directly. The traces shown in Figure 7.1 were in fact obtained with this system and at the same flow rate but they are not the traces digitised by Benson-Lehner and hence there is no exact correspondence between Table 1 and Figure 7.1. Note that Figure 7.1 (like Figure 5.6) shows only the traces and not the whole width of the chart.

The voidage - signal calibration curve for this system is shown in Figure 7.2 and Table 2 gives the bed heights and overall mean voidage for the small voidage calibration bed, together with the average signal S_o obtained with each different bed height (the traces used to find S_o were also digitised by Benson-Lehner and their digital results averaged by computer programme). In addition the superficial fluid velocity is given. The smooth curve drawn through these points was fitted to a quadratic equation by means of an existing least squares fit programme for any chosen degree of polynomial. The relationship between ε and S_o for the voidage range encountered was found to be

$$\varepsilon = 0.18535 + 0.07333\, S_o - 0.00317\, S_o^2 .$$

This calibration was obtained at a datum level of $2\frac{1}{2}$ inches above the distributor.

Table 3 gives the bed heights at which the traces in Table 1 were obtained, the datum level signal correction factor R(x) for these heights and the values of the mean amplitude, mean frequency and mean voidage, obtained from the computer programme, at these heights.

It is obviously quite out of the question to reproduce all the digital records made by Benson-Lehner Ltd. and for all the systems studied only data similar to that given in Tables 2 and 3 below is reported. This data is given in Appendix 3. Note that the mean "amplitude" appearing in these tables is really the average difference in voidage between the maxima and the following minima and is thus, in fact, twice the true mean amplitude. This is unimportant however, as the required quantity is A(x)/A(o).

From the measured amplitudes and frequencies reported in Appendix 3, growth distances and basic frequencies were calculated. These are the subject of the rest of this chapter.

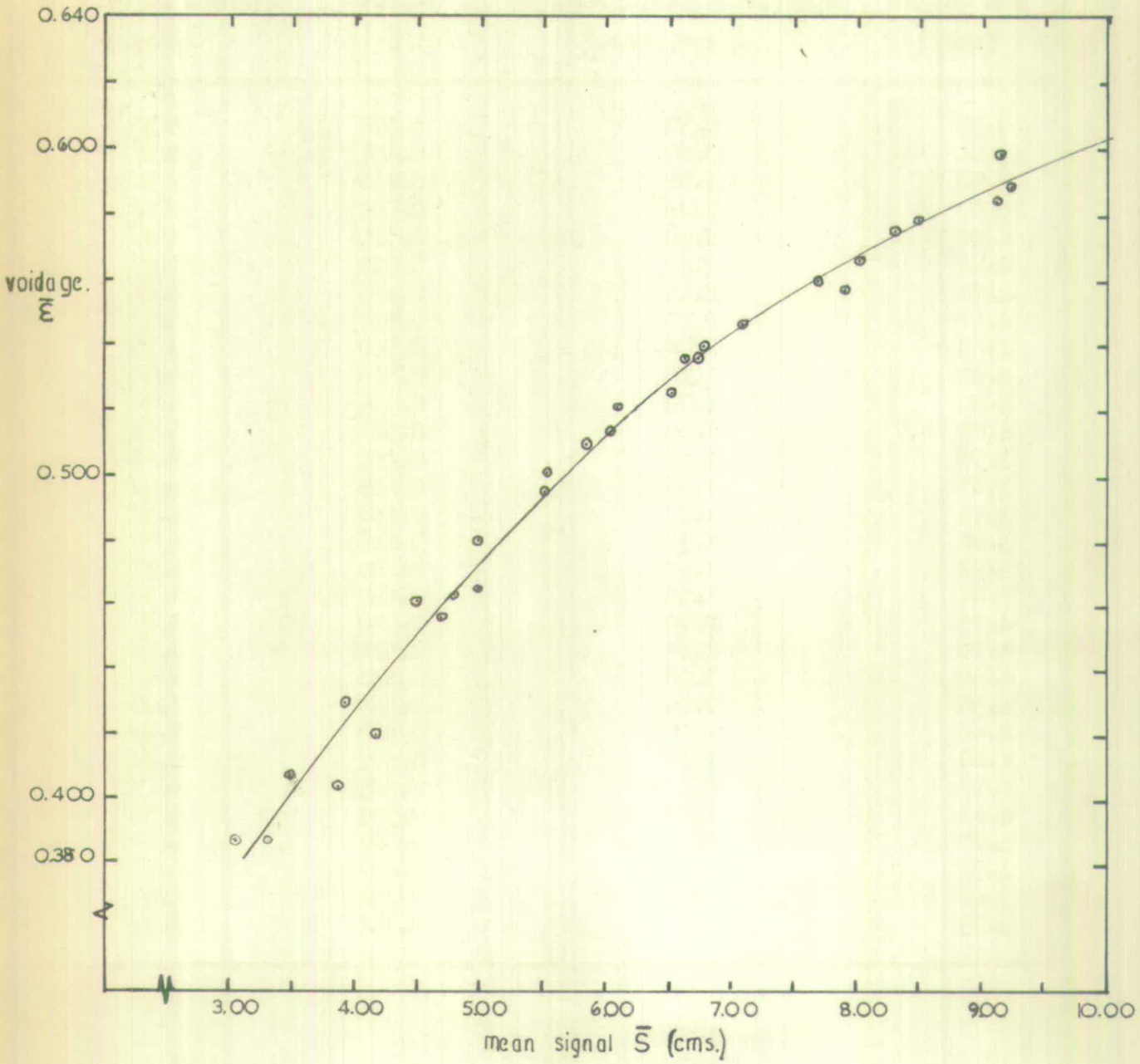


FIGURE 7.2 VOIDAGE – SIGNAL CALIBRATION FOR No.5 B./H_2O. 1" I.D.T.

Table 2:- Voidage - Signal Calibration Data.

No. 5B/H2O. 1" I.D.T. Datum level 2½" above distributor

ρ_s = 2.86 gms./cc. Ballotini Charge = 75 gms.

Bed Height (ins.)	Superficial Fluid Velocity $\bar{u}_s$ (cms./sec.)	Voidage $\bar{\varepsilon}$	Average Deflection $\bar{S}$ (cms.)
3.33	0.77	0.387	3.30
3.44	0.87	0.407	3.50
3.58	1.01	0.430	3.94
5.09	2.66	0.599	9.14
4.96	2.58	0.589	9.22
4.84	2.47	0.579	8.49
4.70	2.35	0.566	8.01
4.61	2.20	0.557	7.90
4.43	2.04	0.540	6.76
4.30	1.88	0.526	6.52
4.20	1.73	0.514	6.01
4.09	1.60	0.501	5.53
3.96	1.48	0.485	5.27
3.81	1.36	0.465	4.98
3.75	1.23	0.456	4.69
3.80	1.30	0.463	4.79
3.92	1.42	0.480	4.97
4.04	1.55	0.495	5.50
4.16	1.70	0.510	5.85
4.26	1.81	0.521	6.09
4.40	1.96	0.536	6.63
4.50	2.09	0.547	7.08
4.64	2.24	0.560	7.69
4.80	2.40	0.575	8.28
4.92	2.55	0.585	9.11
4.41	1.99	0.537	6.74
3.70	1.15	0.449	4.61
3.52	0.96	0.420	4.16
3.42	—	0.404	3.86
3.33	—	0.387	3.30

Table 3:- Results from the digital records.

No. 5 B./H_2O, 1" I.D.T. $\bar{u}_o$ = 1.47 cms./sec.

Trace Number	Height x (ins.)	Correction Factor R(x)	Mean Voidage $\varepsilon(x)$	Mean Amplitude A(x)	Mean Frequency f(x) (c/sec.)
1	2.5	1.000	0.455	0.013	1.28
2	4	0.980	0.459	0.015	1.36
3	6	0.871	0.438	0.019	1.53
4	9	0.834	0.425	0.031	1.28
5	12	0.862	0.441	0.032	1.38
6	15	0.809	0.430	0.029	1.27
7	18	0.802	0.428	0.032	1.32
8	21	0.828	0.435	0.037	1.22
9	24	0.847	0.439	0.033	1.25
10	30	0.830	0.438	0.042	1.06
11	36	0.806	0.430	0.031	1.13

The method used to evaluate growth distance, basic frequency and dominant wave-length from the experimental data was dealt with in Chapter 6. Basically the dominant frequency is obtained by extrapolating the frequency-height relationship back to give the frequency at the distributor. The amplitudes given in Appendix 3 are adjusted to take account of coalescence by multiplying by the ratio f(x)/f(o)

i.e. $$A'(x) = \frac{f(x)}{f(o)} A(x) \quad .$$

The adjusted amplitude $A'(x)$ is plotted on the logarithmic scale of semi-log paper against the height above the distributor (x) in inches. If the initial growth is exponential, a straight line through the first few points allows the equation

$$\frac{A'(x)}{A(o)} = \exp(cx) \quad \text{to be found.}$$

By reading off values of $A'(x)$ at a number of values of x, the ratio $A'(x)/A(o)$ can be formed and the quantity "cx" found from tables of the exponential function. Thus c can be found and the growth distance readily obtained as the reciprocal of this constant c. The dominant wave length is obtained from the measured phase velocity V_p and the basic frequency f(o).

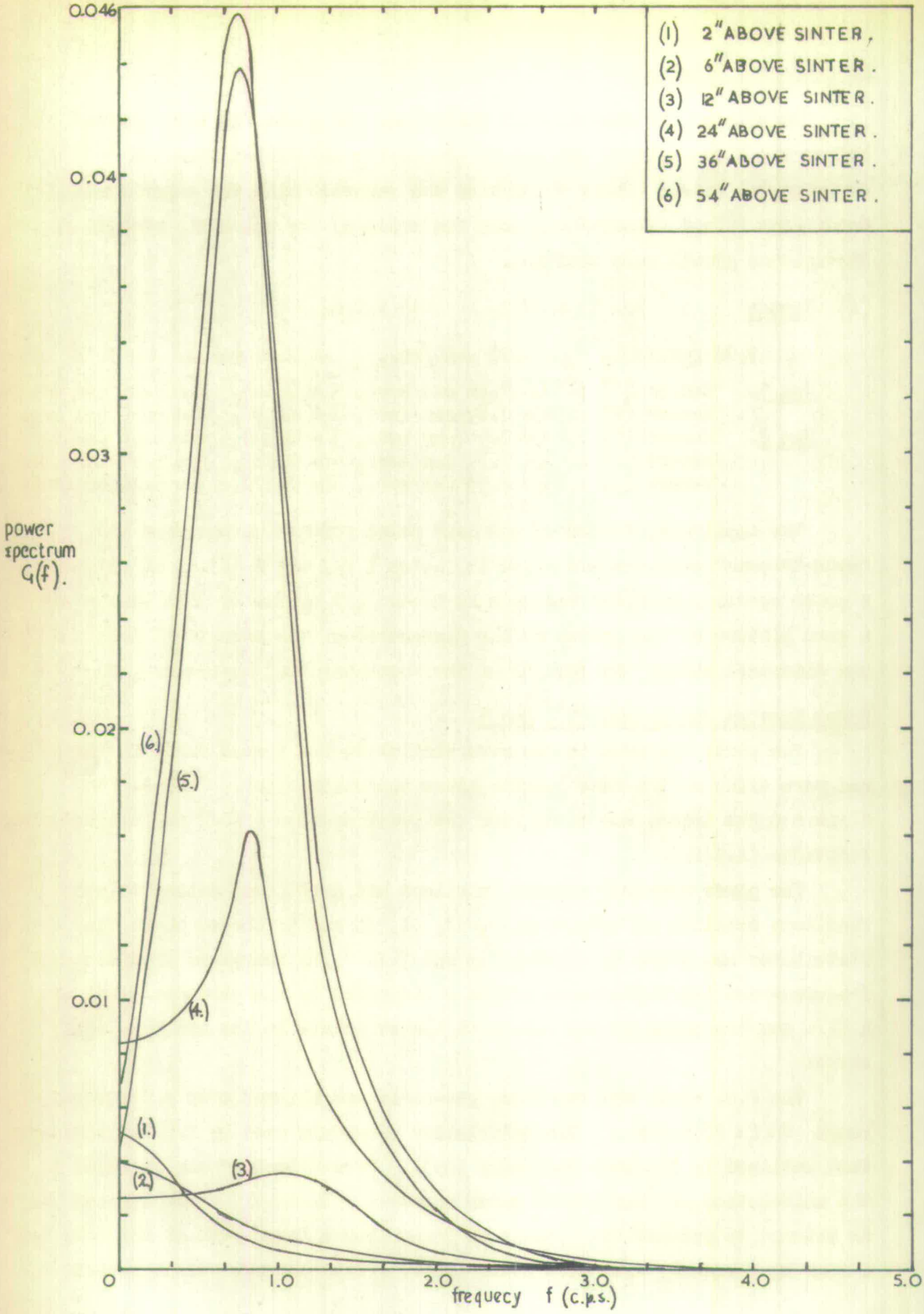


FIGURE 7.3 POWER SPETRAL DENSITY FUNCTIONS FOR THE SYSTEM No. 3 B./H_2O, 1" I.D.T.

Experimental Results

Details of the experimental conditions are given for each system before the discussion of the growth properties calculated from the experimental data. Phase velocities are reported with the experimental conditions (fluid velocity and mean bed voidage) for which the records of disturbance growth were obtained.

(i) System No. 3 B./H_2O, 1" I.D.T.

ρ_s = 2.86 gms./cc., ρ_f = 1.00 gms./cc., μ = 0.01 poise, d_p = 0.127 cms.

Run 1.	Record (1) :	$\bar{u}_o$ = 2.46 cms/sec.,	$\bar{\varepsilon}$ = 0.463,	V_p = 5.25 cms/sec.
	Record (2) :	$\bar{u}_o$ = 2.89 cms/sec.,	$\bar{\varepsilon}$ = 0.496,	V_p = 6.10 cms/sec.
Run 2.	Record (1) :	$\bar{u}_o$ = 2.96 cms/sec.,	$\bar{\varepsilon}$ = 0.500,	V_p = 6.48 cms/sec.
	Record (2) :	$\bar{u}_o$ = 2.72 cms/sec.,	$\bar{\varepsilon}$ = 0.483,	V_p = 5.87 cms/sec.
	Record (3) :	$\bar{u}_o$ = 2.55 cms/sec.,	$\bar{\varepsilon}$ = 0.470,	V_p = 5.36 cms/sec.

The amplitude, frequency and mean point voidage values from the "peak-to-peak" analysis are given in Tables A 2/3 and A 4/3. In addition a power spectrum analysis was made on Record (1) of Run 1. As this gives a good picture of the growth of the disturbances, the results of this analysis are discussed before the results of the "peak-to-peak" analysis.

Power Spectra for Record (1), Run 1.

The power spectrum traces were similar to the traces shown in Figure 5,6 and were taken at the same heights above the distributor. I.C.I. Ltd. digitised the traces and calculated the power spectra (P.S.) and autocorrelation functions (A.C.F.).

The power spectral density functions and normalised autocorrelation functions obtained at heights 2, 6, 12, 24, 36 and 54 inches above the distributor are shown in Figures 7.3 and 7.4. The emergence of a dominant frequency and the disturbance growth - indicated by the periodicity of the A.C.F. and the peaks in the P.S. - at higher points in the bed is clearly shown.

The P.S. shown are smoothed, one-sided and aliased over a frequency range $0 \leq f \leq 10$ c.p.s.. The calculation procedure used by I.C.I. is roughly that outlined by Blackman and Tukey (39). "Prewhitening" was employed in the calculation of this set of power spectra. Basically "prewhitening" is an attempt to prevent the leakage of power from a large peak of the P.S. to a near-by frequency with much lower power. This leakage occurs because of

the numerical methods used in smoothing the true power spectrum of the raw data which presents a very jagged fine structure of no real physical significance.

There is little indication of a dominant frequency appearing until after 6 inches above the distributor and the power is distributed over the frequency range 0 - 2 c.p.s. (the large concentration of power near f = 0 would seem a little suspect, and probably arises from calculation procedures). These very low flat spectra indicate there is little periodicity in the disturbances at 2" and 6 inches above the distributor. At 12 inches above the distributor a dominant frequency is beginning to emerge and this dominant frequency is well established at 24 inches above the distributor. The effect of coalescence in decreasing the dominant frequency is clearly shown.

The signals shown in Figure 5.6 are obviously not strictly periodic but those taken further up the bed do have a strong periodic component. The increase in periodicity of the A.C.F. corresponds very well with the increasingly periodic nature of the traces. The average period of the A.C.F. gives an estimate of the dominant frequency at each height. Note however that the reliability of any estimate of the A.C.F. decreases with increase in the lag time.

Table 4 shows estimates of the frequency obtained from the P.S. and A.C.F. and these are plotted in Figure 7.5. Smoothed frequency values taken from this plot are also tabulated.

Table 4:- Frequencies from the P.S. and A.C.F.

Ht. x (ins.)	P.S. f(x)	A.C.F. f(x)	Smoothed f(x)	f(x)/f(o)
0	—	—	1.43	1.000
2	—	—	1.37	0.958
6	—	1.25	1.26	0.882
12	1.09	1.14	1.10	0.770
24	0.82	0.83	0.86	0.601
36	0.77	0.80	0.78	0.546
54	0.75	0.79	—	—

No.3 B./H_2O POWER SPECTRA RESULTS.

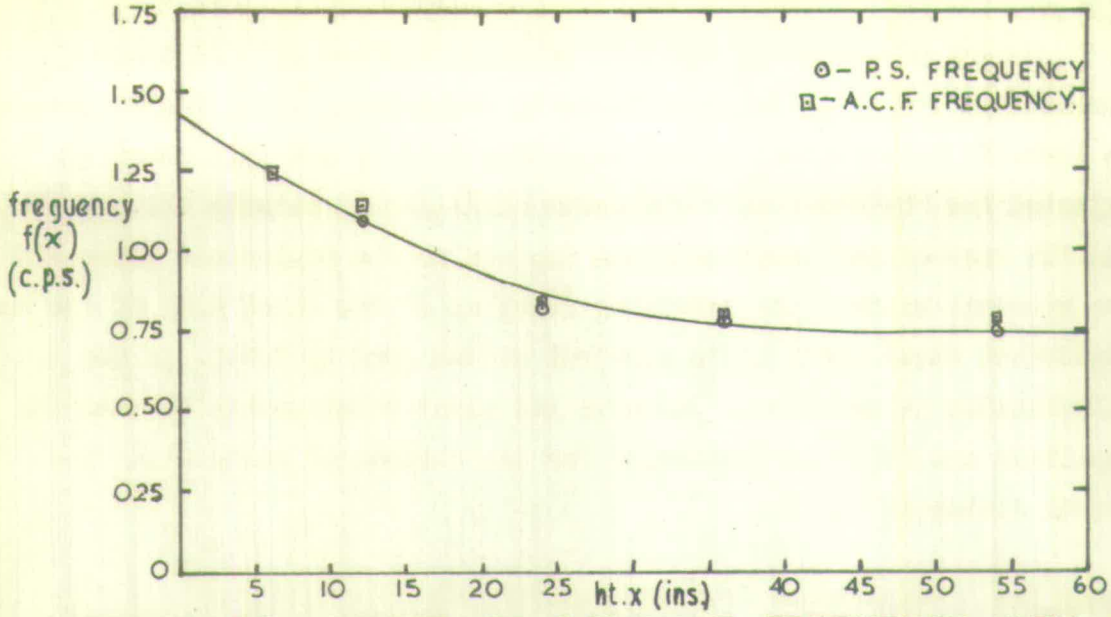


FIGURE 7.5 CHANGE OF DOMINANT FREQUENCY WITH HEIGHT.

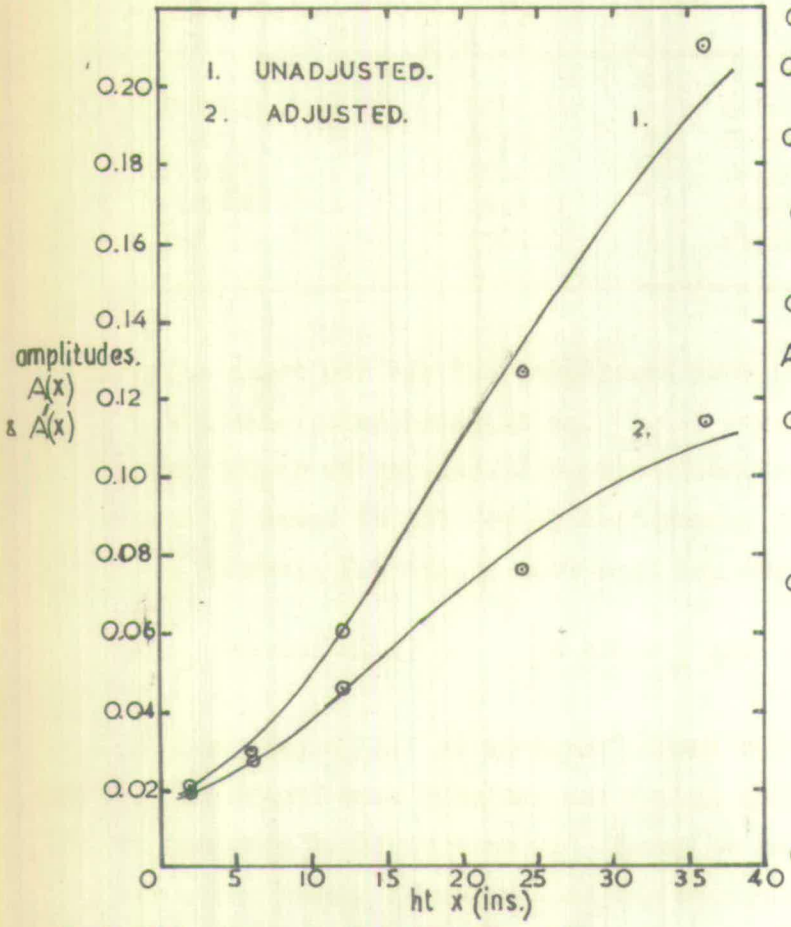


FIGURE 7.6 AMPLITUDE AS A FUNCTION OF HEIGHT.

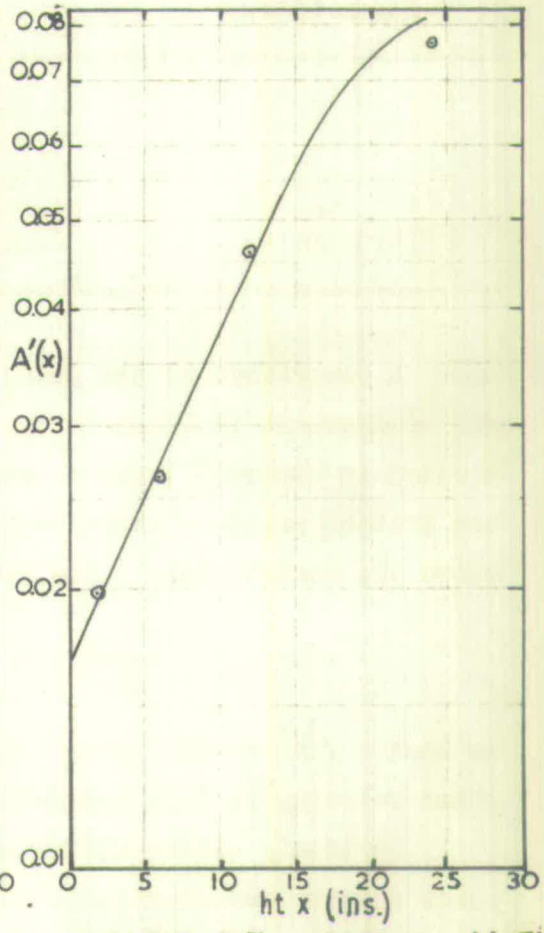


FIGURE 7.7 INITIAL AMPLITUDE GROWTH.

Values of the power spectral density function G(f) at these frequencies are given below in Table 5, along with $\sqrt{G(f)}$, (this quantity is directly proportional to the amplitude A(x)), and this quantity adjusted for coalescence. The exact relationship between the amplitude and the root of the power spectrum depends on the equivalent bandwidth of the spectral window (the smoothing function of the exact P.S. of the raw unsmoothed data) used. The spectral window used by I.C.I. in the calculations is not known. However the exact relationship between the amplitude and $\sqrt{G(f)}$ is immaterial for the purpose of calculating the growth distance.

Table 5:- Amplitudes from the P.S.

Ht. x (ins.)	G(f)	$\sqrt{G}$	$f(x).\sqrt{G}/f(o)$
2	0.00043	0.0208	0.0199
6	0.00090	0.0300	0.0264
12	0.00360	0.0600	0.0462
24	0.01620	0.1270	0.0763
36	0.04380	0.2095	0.1145

A comparison of the unadjusted amplitudes and the amplitude adjusted for coalescence is shown in Figure 7.6. The adjusted amplitudes are plotted in Figure 7.7 and a reasonable straight line can be drawn through the initial points - indicating exponential growth for at least 12 inches above the distributor. The straight line from Figure 7.7 gives

$$\frac{A'(x)}{A(o)} = \exp\left[0.084\ x\right] \qquad (x \text{ in inches})$$

so that $\Delta x = 30.2$ cms. The basic frequency is 1.43 c.p.s. and the phase velocity is 5.25 cms./sec., giving the dominant wave-length as 3.67 cms.

Obviously better estimates of growth distance could be obtained if power spectra were available for more heights under 15 inches above the distributor. However the P.S. for this system were the first obtained and a general picture of the growth of the disturbances was required. Apart

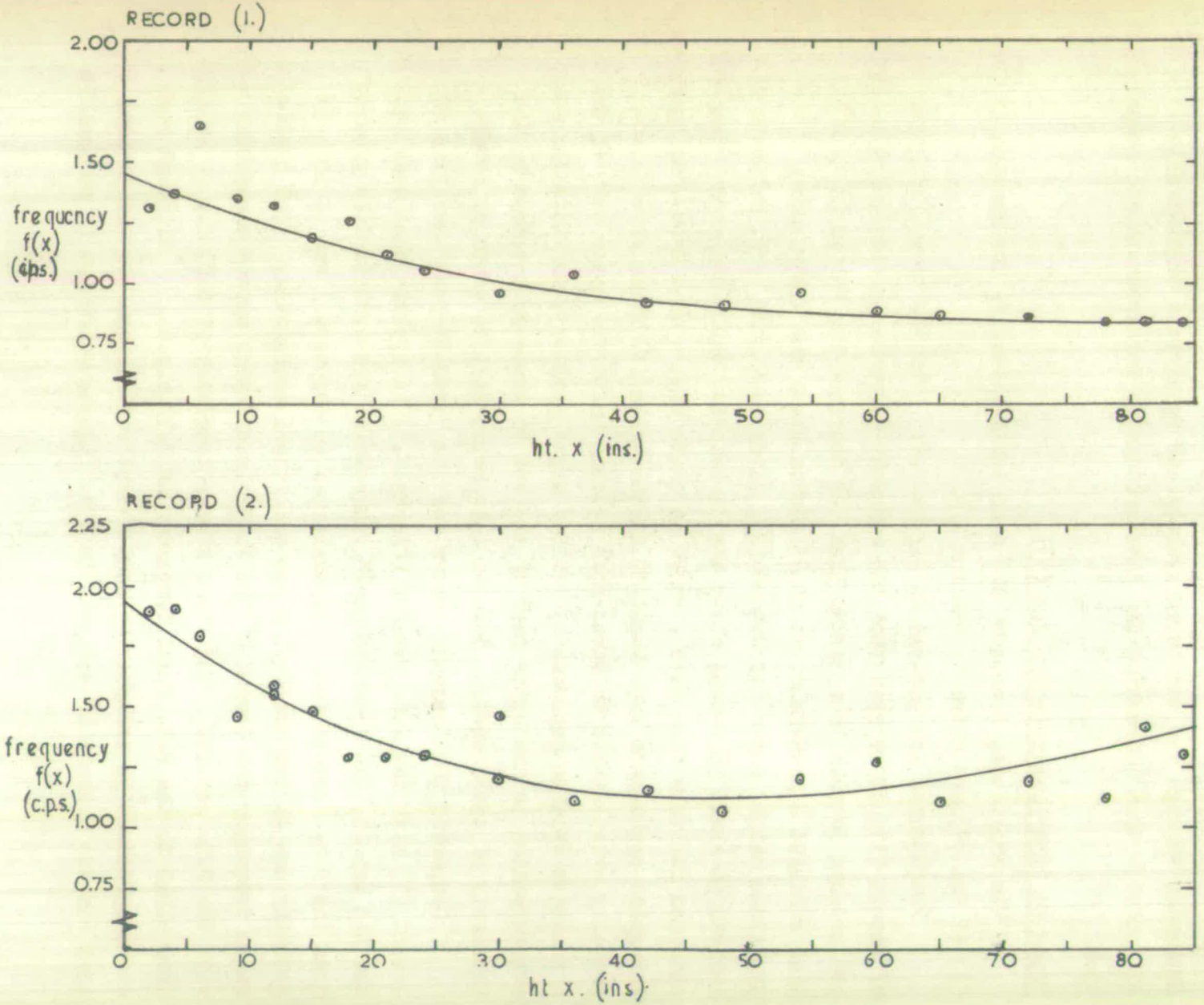


FIGURE 7.8 FREQUENCY AS A FUNCTION OF HEIGHT ABOVE THE DISTRIBUTOR.

No. 3 B./ H2O.

from this lack of information about the initial growth, there is a further source of inaccuracy in the growth distance calculations because of some uncertainty about the exact height of the peaks in the P.S.. Spectral densities were calculated at $\frac{1}{3}$ c.p.s. intervals only. Any attempt to obtain high resolution in the spectra introduces inaccuracy into the actual estimates through the smoothing methods and requires a considerable length of record - thus increasing the data-processing requirements and computation time.

"Peak to Peak" Analysis for Run (1).

The amplitude, frequency and mean voidage results for Records (1) and (2) of Run (1) are given in Table A 2/3.

Frequencies are plotted in Figure 7.8. For the lower flow rate case of Record (1), it is seen that the apparent decrease in frequency due to coalescence is much less marked than the decrease for Record (2) - which also exhibits a minimum at about 45 inches above the distributor. The amplitude height curve for Record (2), given in Figure 7.9, exhibits a maximum at about 35 inches above the distributor while the actual traces obtained for this flow rate - which is quite high - also showed an increasingly irregular appearance from about 40 inches height. These effects are probably attributable to turbulence setting in in the upper part of the bed. A positive voidage gradient in the bed might produce a sufficiently low concentration in the upper part of the bed to cause an increase in the intensity of turbulence. However this point will be taken up later.

Comparing the frequency curve for the "peak-to-peak" analysis of Record (1) with the P.S. results (Figure 7.5) it appears that over most of the bed height, the "peak-to-peak" frequencies are considerably greater than the P.S. frequencies. As explained in Chapters 5 and 6, this is probably due to the crudity of the analytical techniques. The predicted basic frequency for Record (1) is 1.45 c.p.s. which agrees remarkably well with the P.S. result. The final steady frequency of 0.83 c.p.s. is also very close to the P.S. final frequency of 0.78 c.p.s.. Although such close agreement is probably to some extent fortuitous, the indications are that the two methods of analysis do give figures which are in reasonable

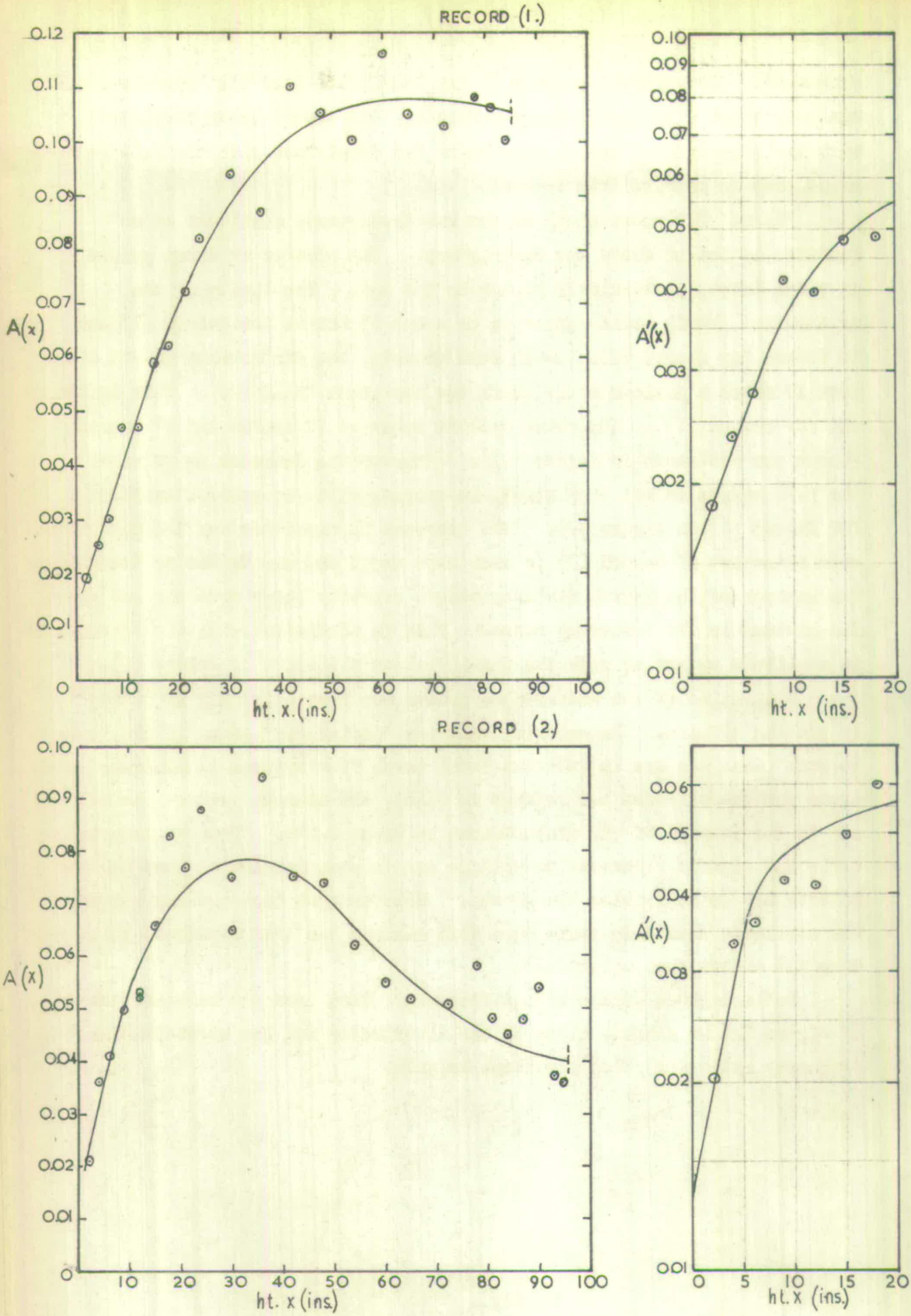


FIGURE 7.9 GROWTH OF DISTURBANCES WITH HEIGHT.

agreement. In general, because of the likelihood that the "peak-to-peak" analysis would give high frequency results, the lowest lines consistent with the experimental points were taken and comparison with the P.S. results would seem to confirm this course.

Figure 7.9 shows plots of the raw disturbance amplitude as a function of height above the distributor. The scatter on these points is quite large, particularly higher up the bed. The limits of the exponential growth would appear to be about 15 inches for Record (1) and 10 inches for Record (2). With both records, the disturbance growth would seem to reach a maximum after which the amplitude falls off. This is borne out for Record (1) by the power spectra taken at 72 inches and 87 inches (these are not shown in Figure 7.3). However the decrease in value of the P.S. maxima is not very great, in keeping with the gradual decrease for Record (1) in Figure 7.9. The decrease in amplitude for the high flow rate situation of Record (2) is much more rapid and may be due to turbulence. The maximum of the growth distance occurs slightly lower down the bed than the minimum in the frequency curve. This is consistent with the decrease in amplitude occurring with the non-turbulent situation of Record (1).

Saturation of the disturbance growth for Record (1) may be caused by packing effects. Remembering that the "amplitudes" given in the "peak-to-peak" analyses are in fact the total swing from maximum to minimum, then since the overall mean bed voidage is 0.463, the minimum voidage reached due to the passage of the disturbances is about 0.410. This voidage is below the minimum fluidisation voidage and is some indication that packing effects may be inhibiting the growth. However this does not explain why the amplitude should decrease once this maximum has been attained (turbulence does not affect this situation).

Table 6 gives values of the frequency taken from the smoothed curves of Figure 7.8 at heights close to the distributor and the corresponding frequency ratio f(x)/f(o) for these heights.

Table 6/

Table 6:- Frequencies from "Peak to Peak" Analysis.

Ht. x (ins.)	RECORD (1)		RECORD (2)	
	f(x)	f(x)/f(o)	f(x)	f(x)/f(o)
0	1.45	1.000	1.94	1.000
2	1.41	0.972	1.86	0.959
4	1.37	0.945	1.78	0.918
6	1.33	0.917	1.72	0.887
9	1.28	0.882	1.63	0.840
12	1.23	0.848	1.54	0.794
15	1.18	0.813	1.46	0.753
18	1.14	0.786	1.40	0.722

Raw amplitudes and amplitudes adjusted for coalescence by the frequency ratios of Table 6 are given in Table 7.

Table 7:- Disturbance Growth.

Ht. x (ins.)	RECORD (1)		RECORD (2)	
	A(x)	A'(x)	A(x)	A'(x)
2	0.019	0.0185	0.021	0.0201
4	0.025	0.0236	0.036	0.0331
6	0.030	0.0275	0.041	0.0360
9	0.047	0.0414	0.050	0.0420
12	0.047	0.0399	0.052	0.0413
15	0.059	0.0481	0.066	0.0497

These adjusted amplitudes are also plotted in Figure 7.9. The initial value of A(x) for Record (1) is 0.0152 and for Record (2) it is 0.0136. For Record (1), the growth equation is

$$\frac{A'(x)}{A(o)} = \exp\left[0.098\ x\right]$$

giving Δx as 25.9 cms. while for Record (2) it is

$$\frac{A'(x)}{A(o)} = \exp.\left[0.206\ x\right]$$

So that Δx is 12.3 cms..

Photographs of the disturbances were taken in an attempt to measure the wave-length. However it was not possible to distinguish sufficiently the disturbances close to the distributor and this method proved fruitless for measurement purposes. Thus the dominant wave-length had to be estimated from the frequency-phase velocity relationship. For Record (1), $f(o)$ = 1.45 c.p.s. and V_p = 5.25 cms./sec. so that λ = 3.62 cms. and k_x = 1.74 cms.$^{-1}$. The wave-length for Record (2) is 3.14 cms. ($f(o)$ = 1.94 c.p.s. and V_p = 6.10 cms./sec.) and k_x = 2.0 cms.$^{-1}$.

Because of the previously mentioned limitations of the "peak-to-peak" analysis and because of the large scatter on the results themselves, the frequency and growth results quoted above must not be regarded as accurate estimates but rather as indications of the magnitudes and the way the quantities change. This large scatter may be due to the crude averaging procedure.

It is obvious that other lines - equally valid without a least-squares analysis - could be drawn through the experimental points and different values of the propagation properties thus obtained. This is part of the subjective character of the "peak-to-peak" results which does not apply to nearly the same extent to the P.S. results (given P.S. at enough points close to the distributor). The growth distance from the power spectra was 30.2 cms. which is reasonably close to the "peak-to-peak" result of 25.9 cms.. The frequency results are likewise very close so that the "peak-to-peak" results, while approximate, would seem to give not unreasonable estimates of the growth properties.

The above general remarks on the reliability of the estimates of the propagation properties do not apply specifically to the system under discussion but are relevant to all the experimental results obtained in this work. They should be borne in mind when all subsequent results are reported.

"Peak-to-Peak" Analysis for Run (2).

Frequencies for these records are plotted in Figure 7.10. As with the results of Run (1), there is a very pronounced minimum in the frequency curve for Record (1) - the high flow rate record - but with the other two records, the frequency decreases monotonically up the bed. Short beds were used for this run as the main interest lay in the initial growth and coalescence of the disturbances for Records (2) and (3) has not ceased even at the top of the bed.

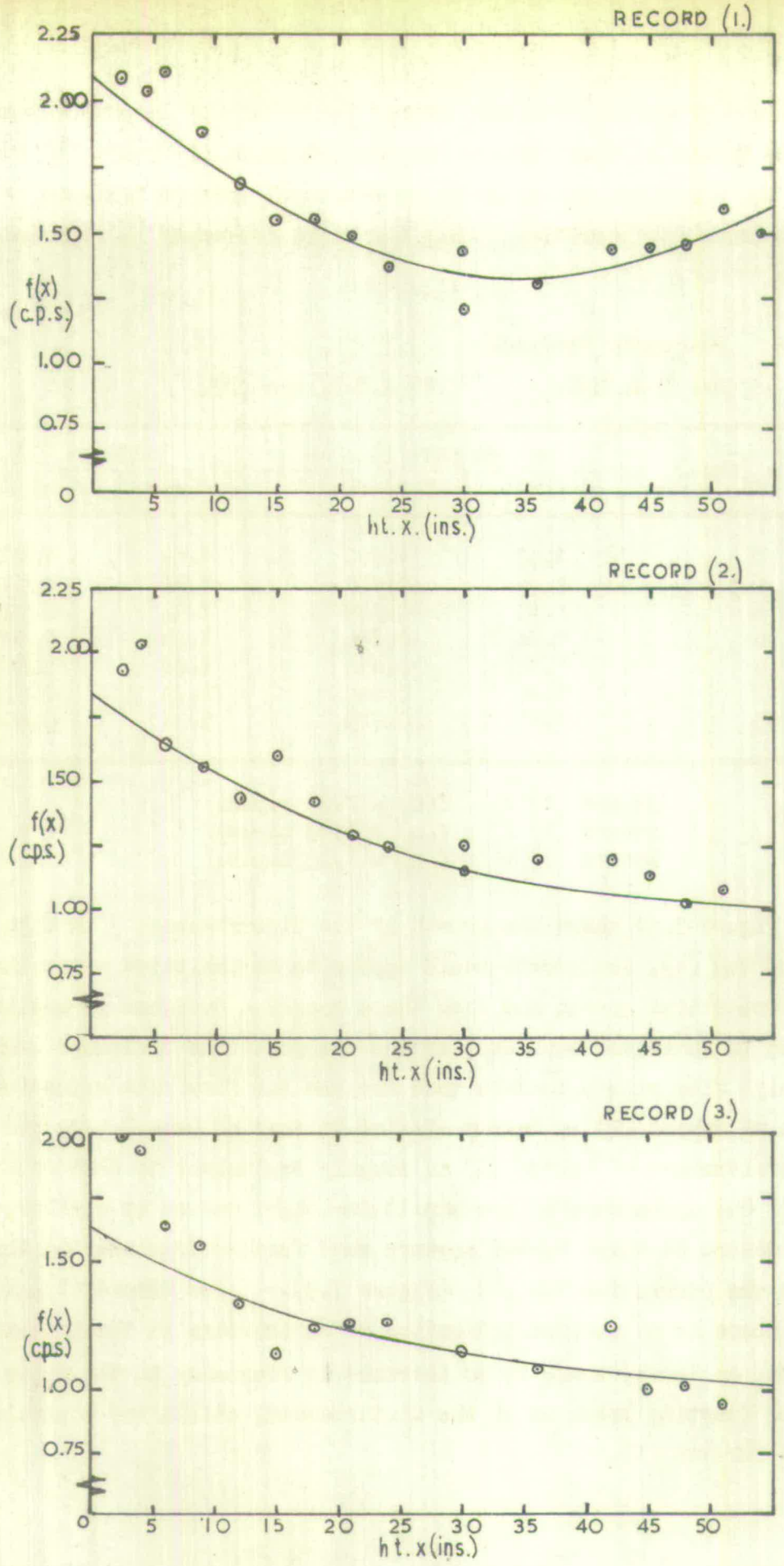


FIGURE 7.10. CHANGE OF DISTURBANCE FREQUENCY WITH HEIGHT.

Table 8 gives the frequency ratios f(x)/f(o) for Records (2) and (3). The growth of disturbances for the situation of Record (1) was so fast and the amplitude measurements so scattered that no estimate of the growth distance was possible. Only the basic frequency is reported for this case.

Table 8:- Frequency Results.

No. 3 B./H_2O. 1" I.D.T. Run (2).

Ht. x (ins.)	RECORD (2)		RECORD (3)	
	f(x)	f(x)/f(o)	f(x)	f(x)/f(o)
0	1.83	1.000	1.63	1.000
2.5	1.74	0.951	1.56	0.957
4	1.70	0.929	1.52	0.933
6	1.64	0.896	1.48	0.909
9	1.56	0.852	1.41	0.865
12	1.48	0.809	1.36	0.834
15	1.41	0.770	1.31	0.804

Record (1) : f(o) = 2.09 c.p.s.
Record (2) : f(o) = 1.83 c.p.s.
Record (3) : f(o) = 1.63 c.p.s.

Figure 7.11 shows the growth of the disturbances. As with the records of Run (1), the growth would appear to be inhibited after the initial exponential growth and then there occurs a decrease in amplitude. The growth is inhibited much earlier and the amplitude decreases much faster for the high flow rate situation than for the low flow rate situation. The situation of Record (2) is fairly similar to that of Record (2), Run (1) while the situation of Record (3) is roughly equivalent to that of Record (1), Run (1). The appearance of the amplitude-height curves is similar, except that the maxima in these curves appears much further down the bed than the maxima in the curves for Run (1) (Figure 7.9). For Record (2), Run (2), however, there is no obvious indication of an increase in the intensity of turbulence, at least, there is no increase in frequency in the upper part of the bed denoting break up of the disturbances, unlike the equivalent situation for Run (1).

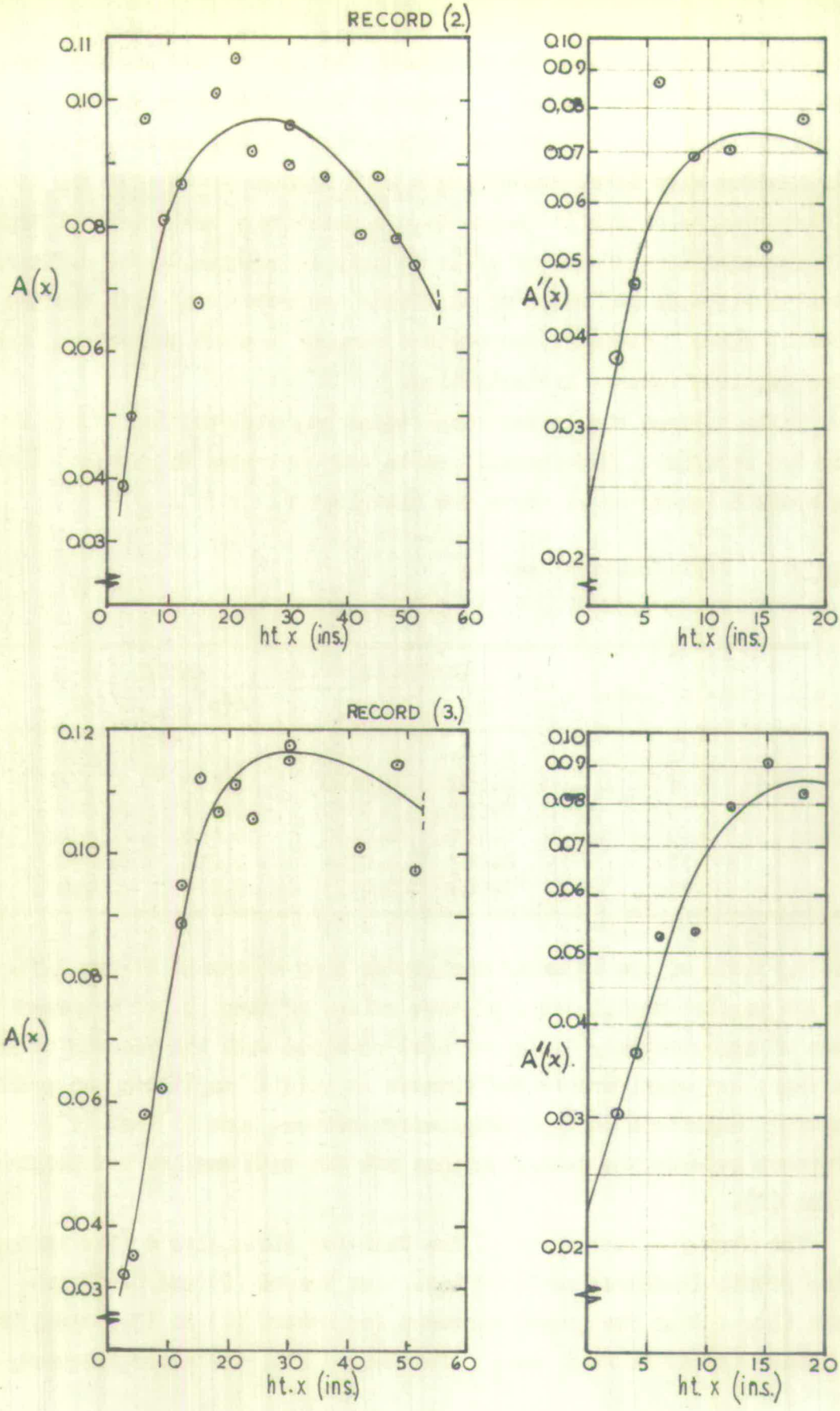


FIGURE 7.11 GROWTH OF DISTURBANCES WITH HEIGHT.

The initial disturbance amplitudes for Run (2) are greater than those for Run (1) (see below). Hence if the growth rate is similar for the two systems, the disturbances with larger initial amplitude will reach their maximum size after travelling a much shorter distance up the bed than the disturbances of Run (1) which have a relatively small initial amplitude.

The equations of motion offer no help in explaining the different initial amplitudes and rates of amplitude decrease found with the two different runs. Certainly no obvious reasons present themselves, and the matter requires further investigation.

Table 9 gives the initial amplitudes and adjusted amplitudes for these two records. Exponential growth does not seem to persist further than about 8 inches or so above the distributor.

Table 9: Amplification Results

No. 3 B./H_2O. 1" I.D.T., Run (2).

Ht. x (ins.)	RECORD (2)		RECORD (3)	
	A(x)	A′(x)	A(x)	A′(x)
2.5	0.039	0.0372	0.032	0.0306
4	0.050	0.0465	0.035	0.0368
6	0.097	0.0869	0.058	0.0528
9	0.081	0.0690	0.062	0.0536
12	0.087	0.0704	0.095	0.0792
15	0.068	0.0523	0.113	0.0908

Semi-log plots of the adjusted amplitudes also appear in Figure 7.11. Note that the initial amplitudes A(o) have values of about 0.022 compared to the values of approximately 0.014 for A(o) obtained with the records of Run (1). Thus there are considerable differences in initial amplitude and position of maximum amplitude of the disturbances between Runs (1) and (2). The only difference between the two situations was the much smaller bed heights used for Run (2).

The straight line parts of the semi-log plots give c (the reciprocal of the growth distance) as 0.182 $ins.^{-1}$ for Record (2) and 0.125 $ins.^{-1}$ for Record (3). Thus the growth distance for Record (2) is 13.9 cms., while for Record (3) it is 20.3 cms.. For Record (1), the basic frequency is

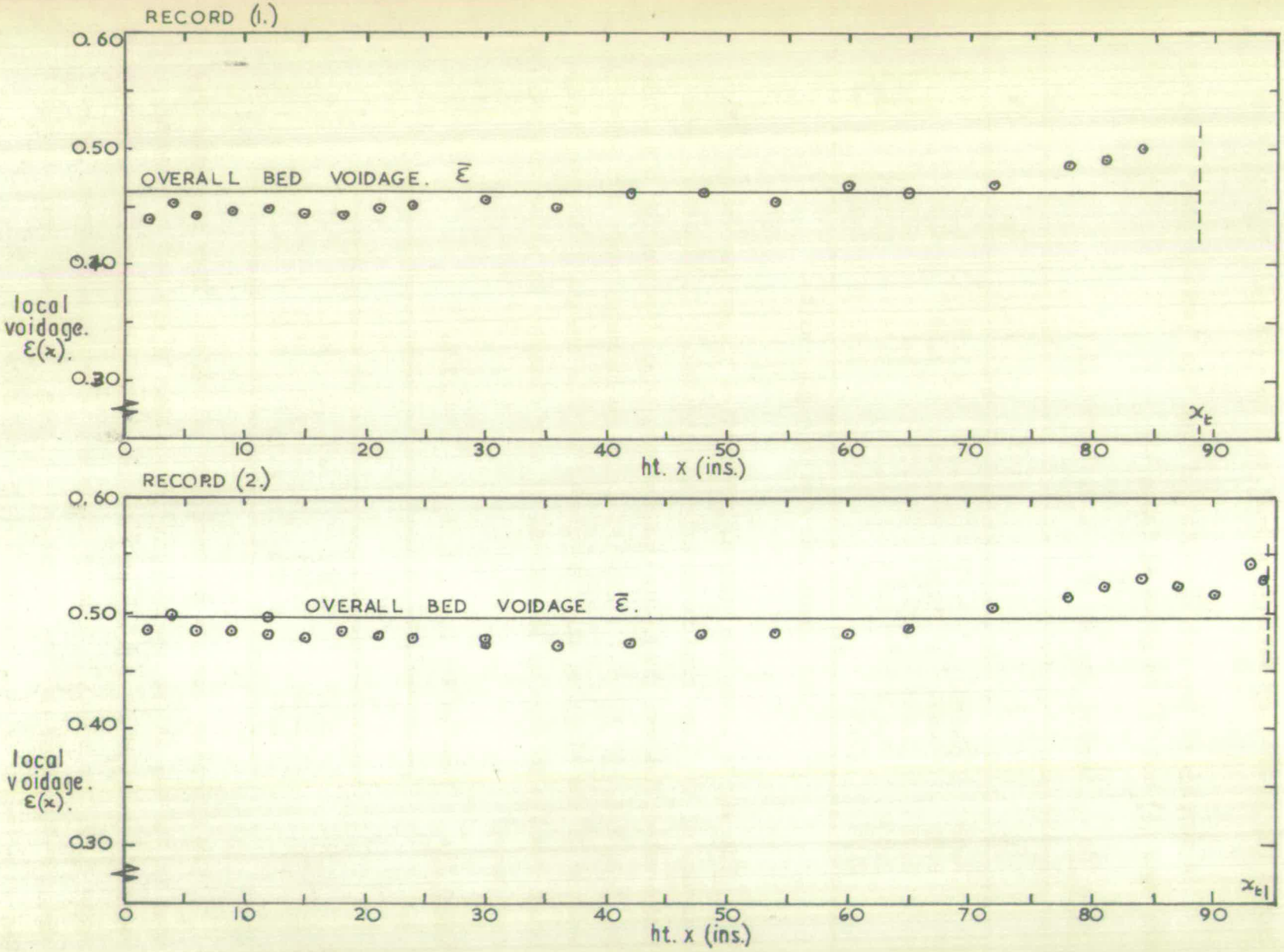


FIGURE 7.12 VOIDAGE PROFILES FOR THE SYSTEM No. 3 B./ H_2O RUN 1.

2.09 c.p.s. and the phase velocity 6.48 cms., giving the dominant wave-length as 3.10 cms. The dominant wave-length for Record (2) is 3.21 cms., (V_p = 5.87 cms./sec. and f(o) = 1.83 c.p.s.) while for Record (3) it is 3.29 cms. (V_p = 5.36 cms./sec. and f(o) = 1.63 c.p.s.).

A summary of the results obtained from the "peak-to-peak" analysis for Runs (1) and (2) is given in Table 10.

Table 10: Results for No. 3 B./H_2O. 1" I.D.T.

$\bar{u}_o$	$\bar{\varepsilon}$	V_p	f(o)	λ	k_x	Δx
2.46	0.463	5.25	1.45	3.62	1.74	25.9
2.55	0.470	5.36	1.63	3.29	1.91	20.3
2.72	0.483	5.87	1.83	3.21	1.96	13.9
2.89	0.496	6.10	1.94	3.14	2.00	12.3
2.96	0.500	6.48	2.09	3.10	2.03	—

All quantities are in c.g.s. units.

The way in which the various propagation properties change with increase of the flow rate is clearly illustrated. In addition, some phase velocities and frequency measurements were obtained for the system No. 3 B./H_2O, ½" I.D.T.. Amplification measurements were not possible because of the slugging which developed in this system. However these rough results do show up the effect of tube diameter on phase velocity and frequency.

Table 11: Results for No. 3 B./H_2O. ½" I.D.T.

$\bar{u}_o$	$\bar{\varepsilon}$	V_p	f	λ
2.53	0.503	3.92	2.3	1.7
2.70	0.515	4.42	2.5	1.8
2.87	0.528	4.75	2.6	1.8

The frequency results are not very reliable. They were measured low down in the bed before the slugging point both by eye and by records. The records contained a large amount of noise (this was generally found when the ratio d_p/d_t was high). However the phase velocities do appear to be considerably lower and the frequencies higher than those found in the 1" tube. The wave-length is thus correspondingly reduced.

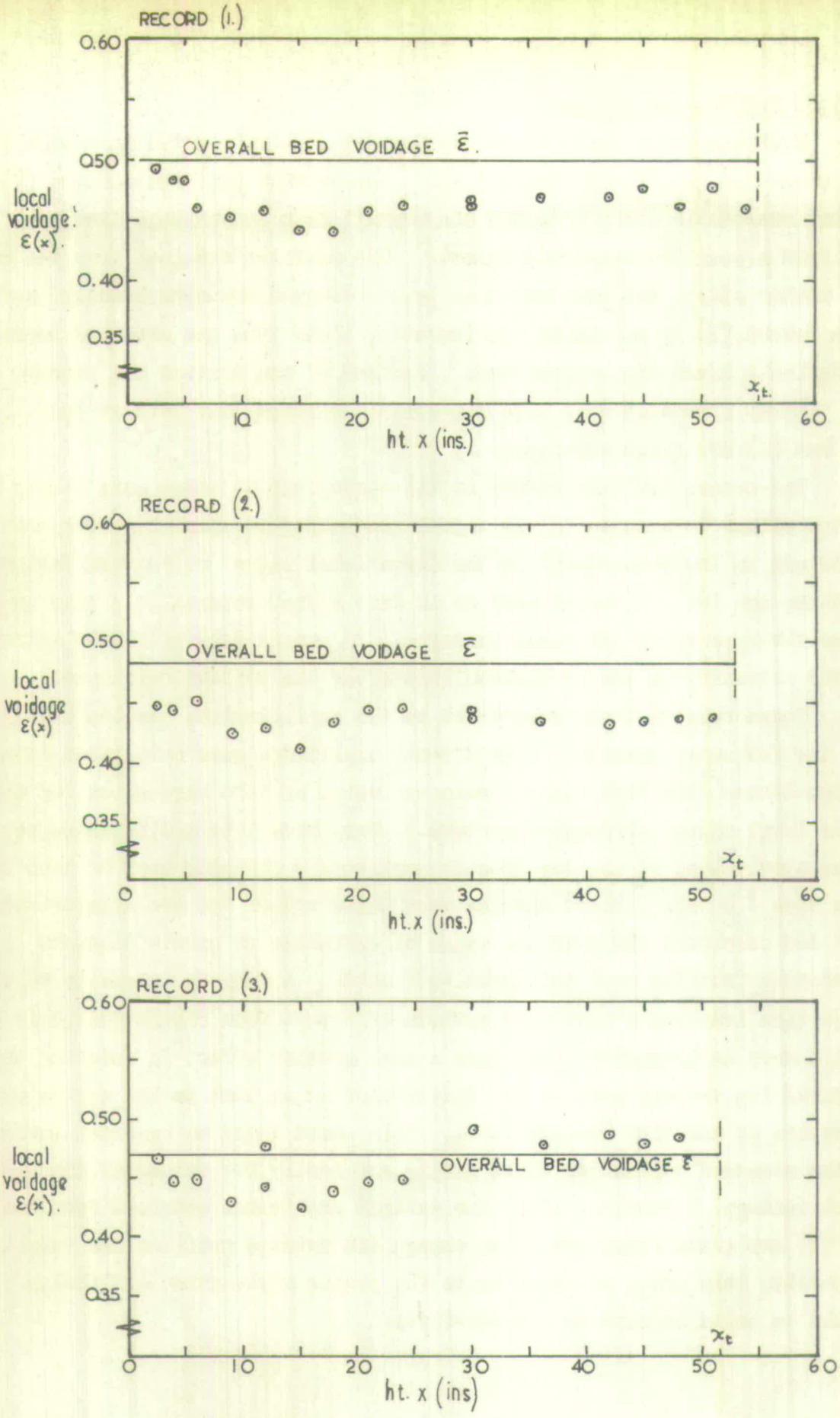


FIGURE 7.13 VOIDAGE PROFILES FOR THE SYSTEM No. 3 B/ H_2O RUN 2.

Voidage Profiles in the Bed.

The mean point voidage results for Run (1) are plotted in Figure 7.12 and those for Run (2) in Figure 7.13. The voidage profiles for Run (1) appear reasonable (they straddle the overall mean bed voidage line) and indicate a positive voidage gradient. The profiles obtained from Run (2) are rather odd. The measured mean point voidages are consistently apart from Record (3) , and quite considerably, lower than the mean bed voidage. No definite trend can be observed. Because of the scatter and because they are totally irreconcilable with the overall voidage, the voidage profiles for Run (2) are quite worthless.

The reason for this is not at all clear, but it seems most likely to be due either to changes in the signal generating or measuring equipment or to errors in the measurement of the datum level signal correction factors. If these are low - although they do in fact appear reasonable - this would cause the apparently low point voidages. A second possibility is a drop in the intensity of the projection lamp after the voidage calibration.

These results throw some doubt on the amplification results (though not the frequency results). As a test, amplitudes were calculated from the Benson-Lehner data tape using a constant value of 1.00 throughout for the datum level signal correction factors. This made little difference to the calculated values of the disturbance amplitude - changing most of them by less than $\pm$ 0.003. These changes were quite random and are unimportant when one considers the possible range of estimates of growth distance obtainable from the amplitude results quoted. A drop in intensity of the projection lamp has a much more serious effect. From Figure 7.2 it is seen that a drop in intensity would have a much greater effect in reducing the measured low voidage part of the disturbance swing than in the equivalent reduction of the high voidage part. This would cause an apparent increase in the measured amplitudes while giving apparently low values of the mean point voidage. However, since the maximum amplitudes obtained from Runs (1) and (2) are quite consistent even though the voidage profiles are totally disparate, this would not seem to be the proper explanation - although it should be borne in mind as a possibility.

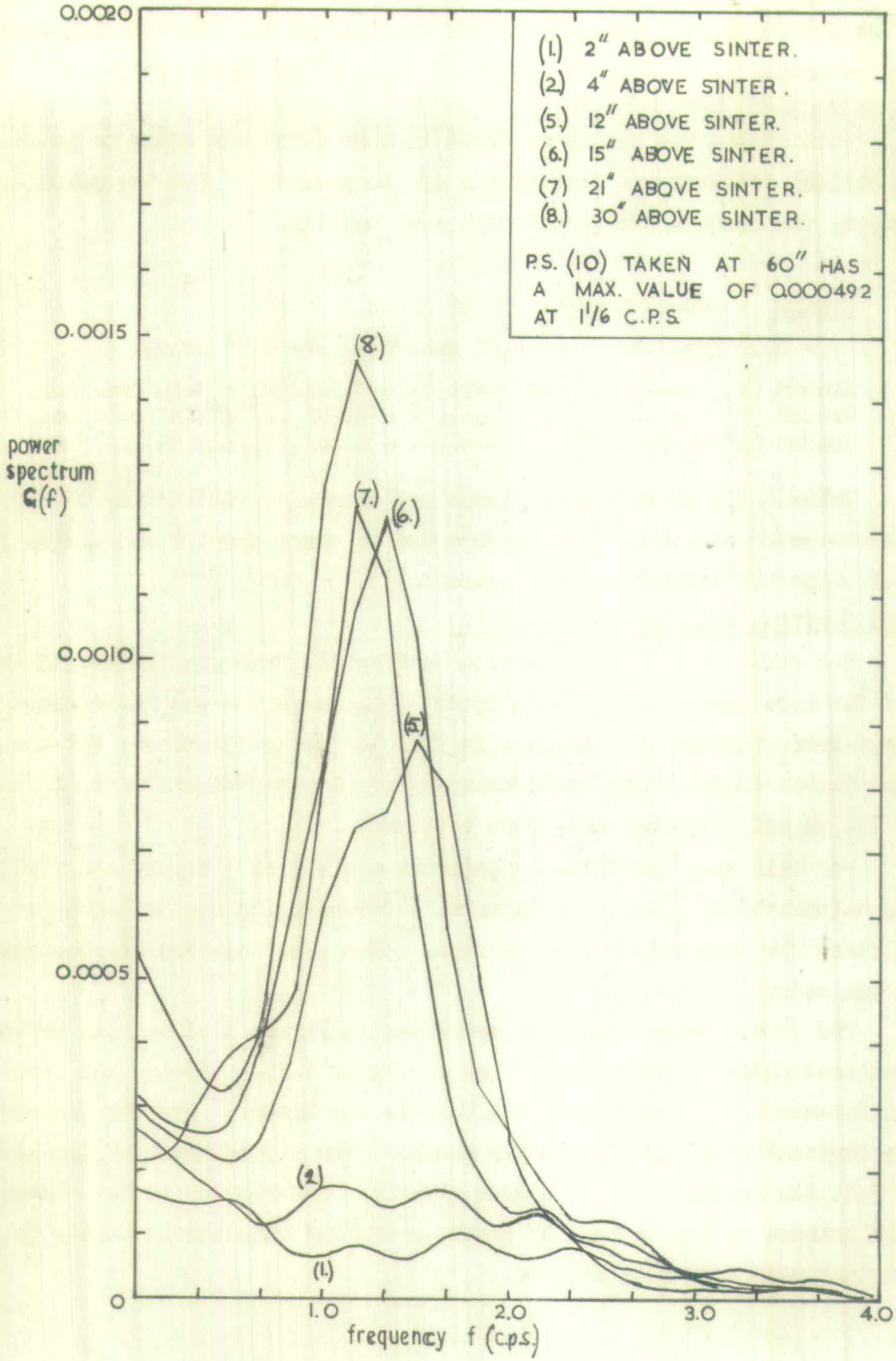


FIGURE 7.14 POWER SPECTRAL DENSITY FUNCTIONS FOR THE SYSTEM No. 5 B./H_2O ½" I. D. T.

Thus, provided any possible change in the optical equipment occurred before the voidage-signal calibration was carried out, the amplification results should be relatively little affected by any such change.

This system has been considered in some detail in order to point out the salient features and limitations of the results. For the other systems studied, the results are quoted much more briefly.

(ii) System No. 5 B./H_2O. $\frac{1}{2}$" I.D.T.

ρ_s = 2.86 gms./cc., ρ_f = 1.00 gms./cc., μ = 0.01 poise, d_p = 0.086 cms.

Record (1) : $\bar{u}_o$ = 1.42 cms./sec., $\bar{\varepsilon}$ = 0.504, V_p = 3.46 cms./sec.
Record (2) : $\bar{u}_o$ = 1.64 cms./sec., $\bar{\varepsilon}$ = 0.529, V_p = 3.91 cms./sec.
Record (3) : $\bar{u}_o$ = 1.77 cms./sec., $\bar{\varepsilon}$ = 0.541, V_p = 4.23 cms./sec.

Table A 5/5 gives the amplitude and frequency results for the "peak-to-peak" analysis. The second set of power spectra calculated by I.C.I. were for the situation of Record (2).

Power Spectrum Results for Record (2).

The first set of power spectra obtained in this work indicated the need for more spectra at heights up to 15 inches above the distributor. Traces were obtained at 6 heights in this bed up to 15 inches, but two of these traces faded during processing and results at heights of 2, 4, 12, 15, 21, 30 and 60 inches only were obtained.

For this set, the folding frequency was set at 5 c.p.s. and the P.S. calculated at $\frac{1}{6}$ c.p.s. intervals. Prewhitening was not thought necessary for this set of calculations. The power spectra are smoothed and one sided ($0 \leq f \leq 5$).

The power spectra obtained are shown in Figure 7.14 and the corresponding normalised autocorrelation functions in Figure 7.15. Again, the level of significance of the peaks in the A.C.F. is not known. However the emergence of a dominant frequency is clearly shown. The significance of the peaks in the P.S. for heights 2 and 4 inches above the distributor is not clear. They could perhaps be due to lack of prewhitening but this should hardly be important with such flat spectra.

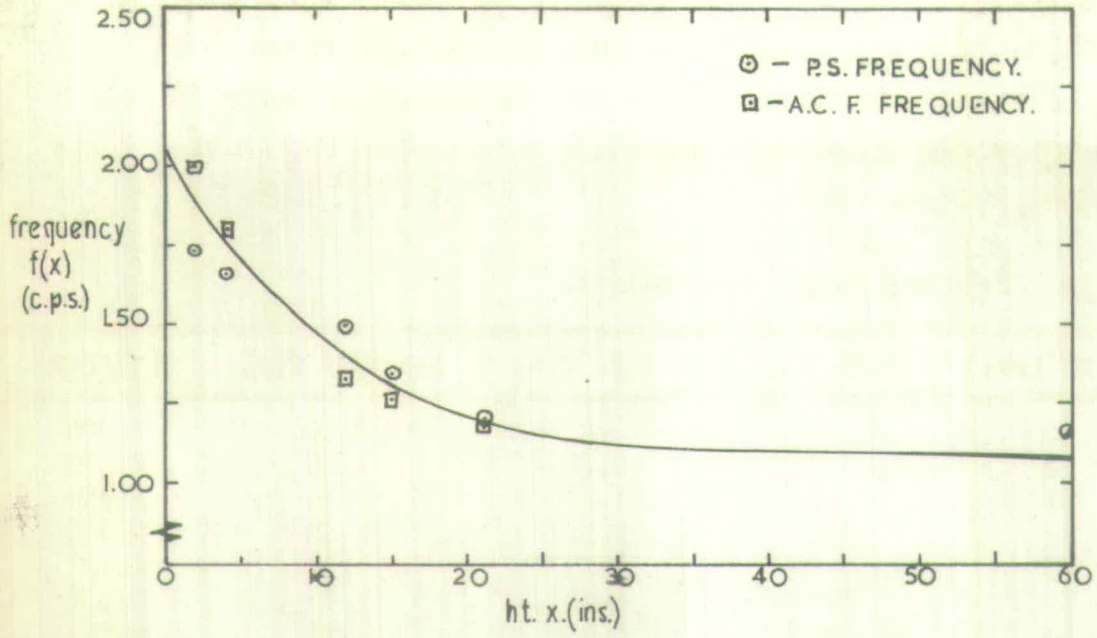


FIGURE 7.16 CHANGE OF DOMINANT FREQUENCY WITH HEIGHT.

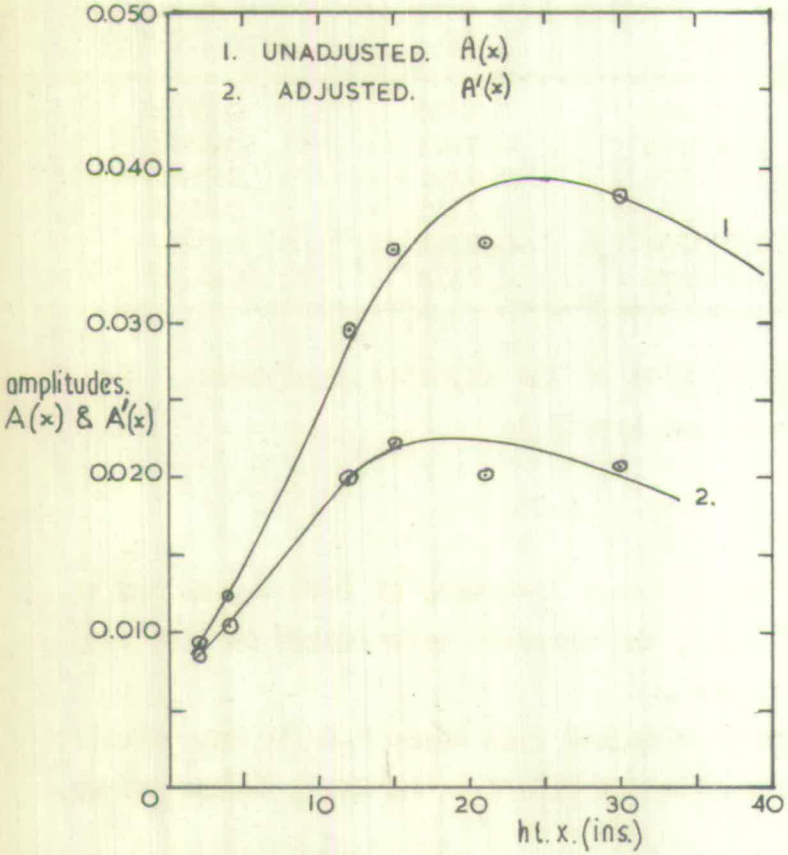


FIGURE 7.17 CHANGE OF AMPLITUDE WITH HEIGHT.

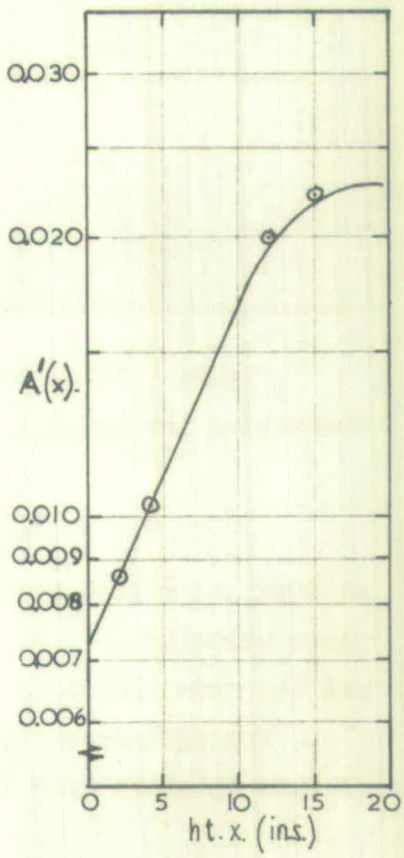


FIGURE 7.18 INITIAL AMPLITUDE GROWTH.

Frequencies from the P.S. and A.C.F. measurements are given in Table 12, together with frequencies from the curve of Figure 7.16. Table 13 gives the values of G(f) at the frequencies of Table 12, also the measure of the disturbance amplitude and adjusted amplitude. These are plotted in Figure 7.17.

Table 12: P.S. and A.C.F. frequencies.

Ht. x (ins.)	P.S. f(x)	A.C.F. f(x)	Smoothed f(x)	f(x)/f(0)
0	—	—	2.07	1.000
2	1.73	2.00	1.89	0.912
4	1.66	1.80	1.76	0.850
12	1.50	1.32	1.40	0.676
15	1.33	1.25	1.31	0.633
21	1.17	1.18	1.19	0.575
30	1.17	1.15	1.12	0.541

Table 13: Amplitudes from the P.S.

Ht. x (ins.)	G(f)	$\sqrt{G}$	$f(x).\sqrt{G}/f(0)$
2	0.000088	0.0094	0.0086
4	0.000150	0.0123	0.0105
12	0.000878	0.0296	0.0200
15	0.001224	0.0350	0.0221
21	0.001238	0.0352	0.0202
30	0.001470	0.0383	0.0207

Figure 7.18 is a semi-log plot of the adjusted amplitudes. The line describing the initial exponential growth is

$$\frac{A'(x)}{A(0)} = \exp.\left[0.082\ x\right]$$

so that $\Delta x = 31.0$ cms. With a basic frequency of 2.07 c.p.s. and a phase velocity of 3.91 cms./sec., the dominant wave-length is 1.89 cms. and the wave number is 3.33 cms.$^{-1}$.

The picture of the growth obtained from these P.S. is very similar to that obtained from the first set of P.S. for the No. 3 B./H_2O system.

No. 5 B./ H_2O, $\frac{1}{2}$ I.D.T.

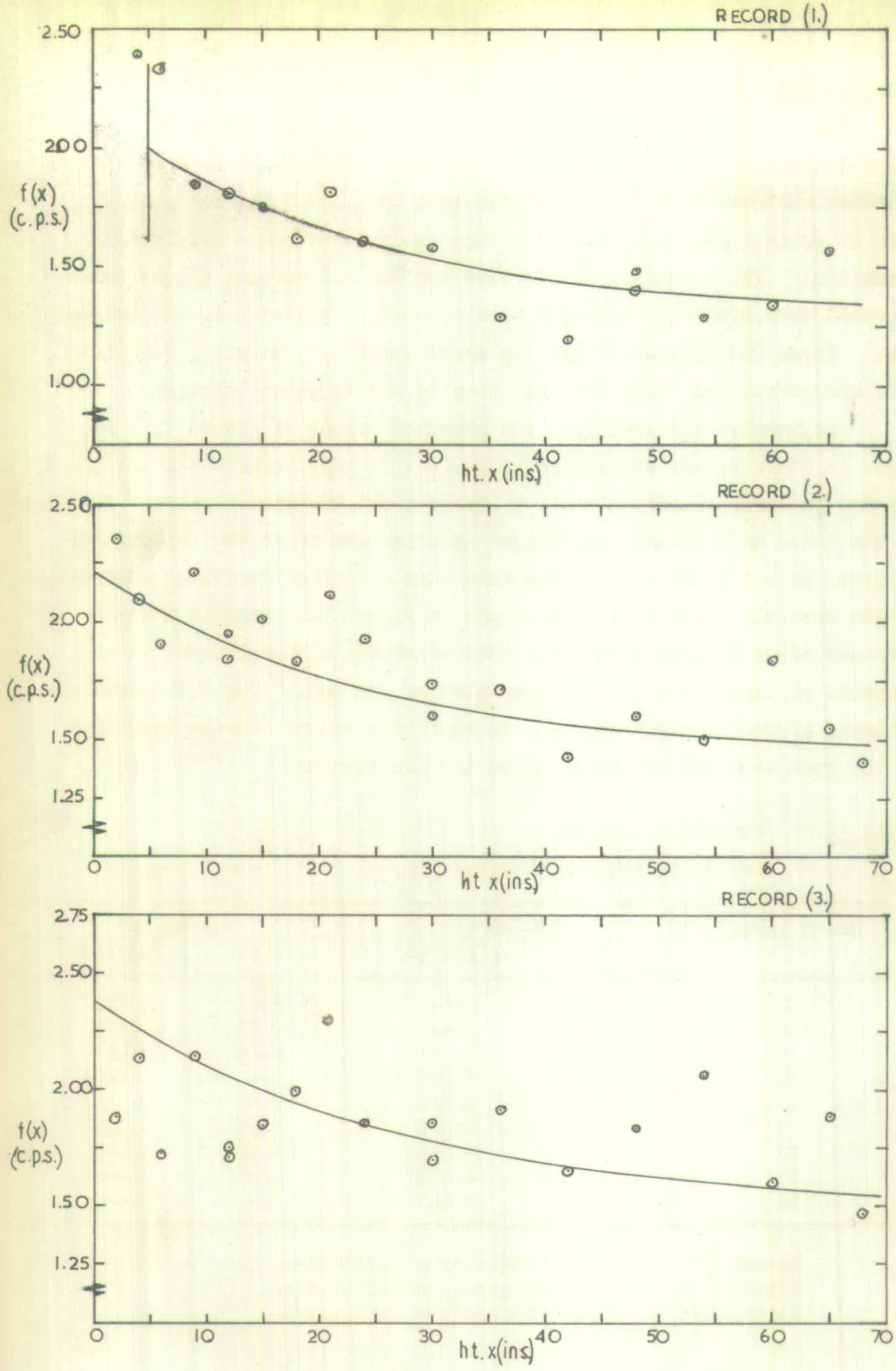


FIGURE 7.19 CHANGE OF DISTURBANCE FREQUENCY WITH HEIGHT.

"Peak-to-Peak" Analysis Results

The results for this are rather unsatisfactory. There is a very large scatter on both amplitude and frequency results, so much so that no estimate whatsoever of the growth distance for Record (3) was possible. From an optical point of view, the tube used was not in a very good condition. The extrusion of the tube was bad and several slight bends remained even after the tube had been clamped in position in the optical box. These faults also affect the power spectra. However, for what they are worth, the "peak-to-peak" results are as given below.

Frequencies obtained from the smoothed curves of Figure 7.19 are given in Table 14 and amplitudes in Table 15. For Record (1), the bed was not properly fluidised until 5 inches above the distributor. Although it was taken as 5 inches, the height at which the onset of fluidisation occurred is not known exactly and this adds a further degree of uncertainty to the results. The amplitudes shown in Figure 7.20 exhibit a rapid decrease after maximum growth has been attained, although there is no evidence of turbulence in the upper part of the bed. The P.S. gives no evidence of such a rapid decrease in amplitude except for the low value of the peak obtained 60 inches above the distributor.

Table 14: Frequency Results

No. 5. B./H_2O, $\frac{1}{2}$" I.D.T.

Ht. x (ins.)	RECORD (1)		RECORD (2)	
	f(x)	f(x)/f(o)	f(x)	f(x)/f(0)
0	—	—	2.21	1.000
2	—	—	2.15	0.973
4	—	—	2.09	0.947
5	2.01	1.000	—	—
6	1.97	0.980	2.04	0.922
9	1.88	0.945	1.97	0.891
12	1.81	0.900	1.90	0.859
15	1.75	0.870	—	—
18	1.69	0.841	—	—

Record (1) : Basic frequency = 2.01 c.p.s.
Record (2) : Basic frequency = 2.21 c.p.s.
Record (3) : Basic frequency = 2.40 c.p.s.

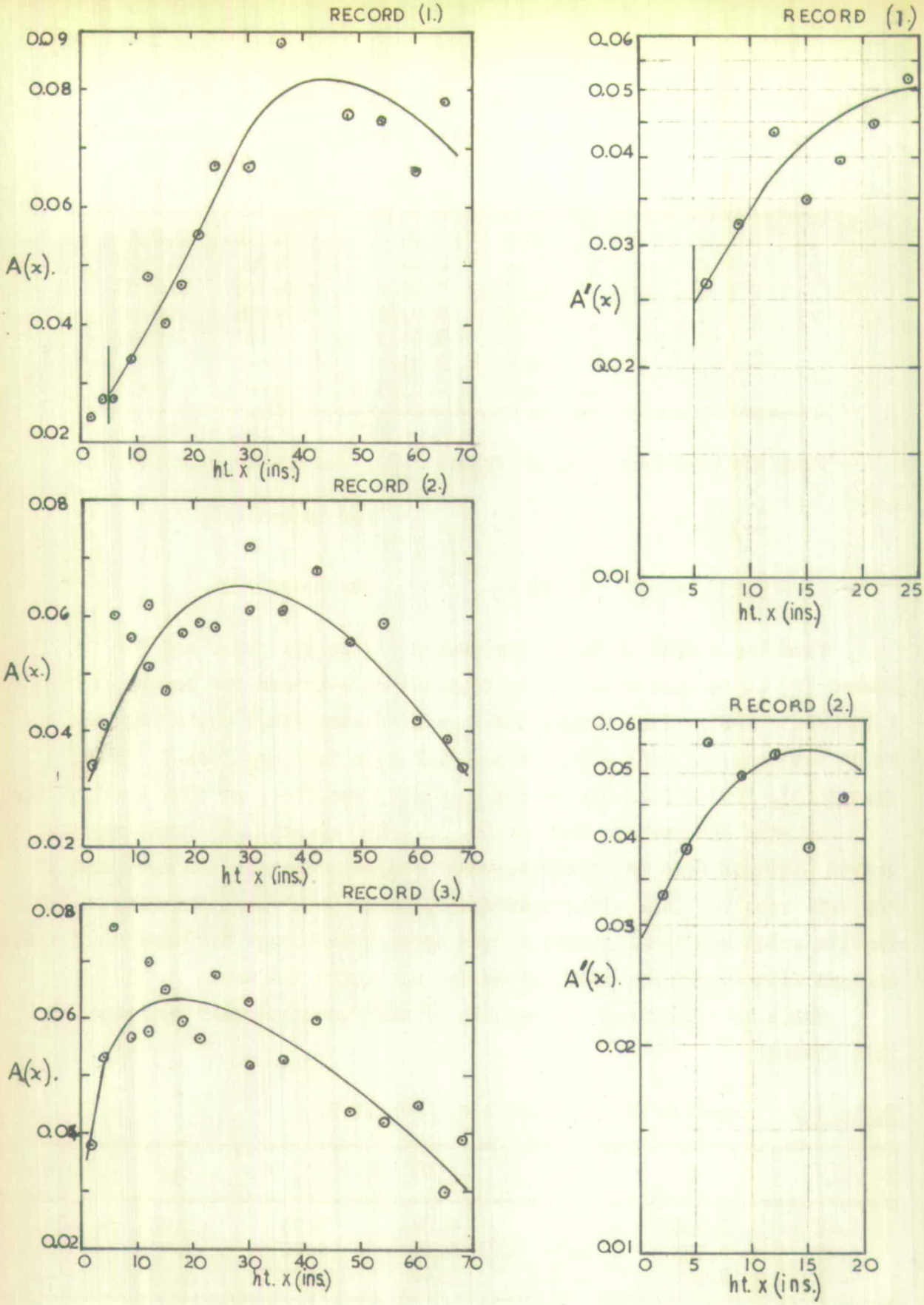


FIGURE 7.20 GROWTH OF DISTURBANCES WITH HEIGHT.

Table 15: Amplification Results. No. 5 B./H_2O, ½" I.D.T.

Ht. x (ins.)	RECORD (1)		RECORD (2)	
	A(x)	A′(x)	A(x)	A′(x)
2	—	—	0.034	0.0331
4	—	—	0.041	0.0388
6	0.027	0.0264	0.060	0.0553
9	0.034	0.0321	0.056	0.0499
12	0.048	0.0433	0.062	0.0532
15	0.040	0.0348	—	—
18	0.047	0.0395	—	—

From the semi-log plots of Figure 7.20, the growth relationships are

$$\frac{A'(x)}{A(0)} = \exp\left[0.065\ x\right] \qquad \text{for Record (1),}$$

and

$$\frac{A'(x)}{A(0)} = \exp\left[0.074\ x\right] \qquad \text{for Record (2).}$$

Thus the growth distance for Record (1) is 39.1 cms. and for Record (2) it is 34.3 cms. The dominant wave-length for Record (1) is 1.73 cms. ($f(0) = 2.01$ c.p.s. and $V_p = 3.46$ cms./sec.) while for Record (2) it is 1.77 cms. ($f(0) = 2.40$ c.p.s. and $V_p = 3.91$ cms./sec.). For Record (3), $f(0) = 2.40$ c.p.s. and $V_p = 4.23$ cms./sec. so that $\lambda = 1.77$ cms.

As with the results for the No. 3 B./H_2O system, the frequency and growth distance from the "peak-to-peak" analysis are not too different from the P.S. results, indicating that the "peak-to-peak" analysis does not give results which are totally wide of the mark, even though the ways the frequency changes with height for each method are not quite the same.

Table 16 summarises the results of the "peak-to-peak" analysis for this system.

Table 16: Results for No. 5 B./H_2O, ½" I.D.T.

$\bar{u}_o$	$\bar{\varepsilon}$	V_p	f(0)	λ	k_x	x
1.42	0.504	3.46	2.01	1.73	3.63	39.1
1.67	0.529	3.91	2.21	1.77	3.55	34.3
1.77	0.541	4.23	2.40	1.77	3.55	—

All quantities are in c.g.s. units.

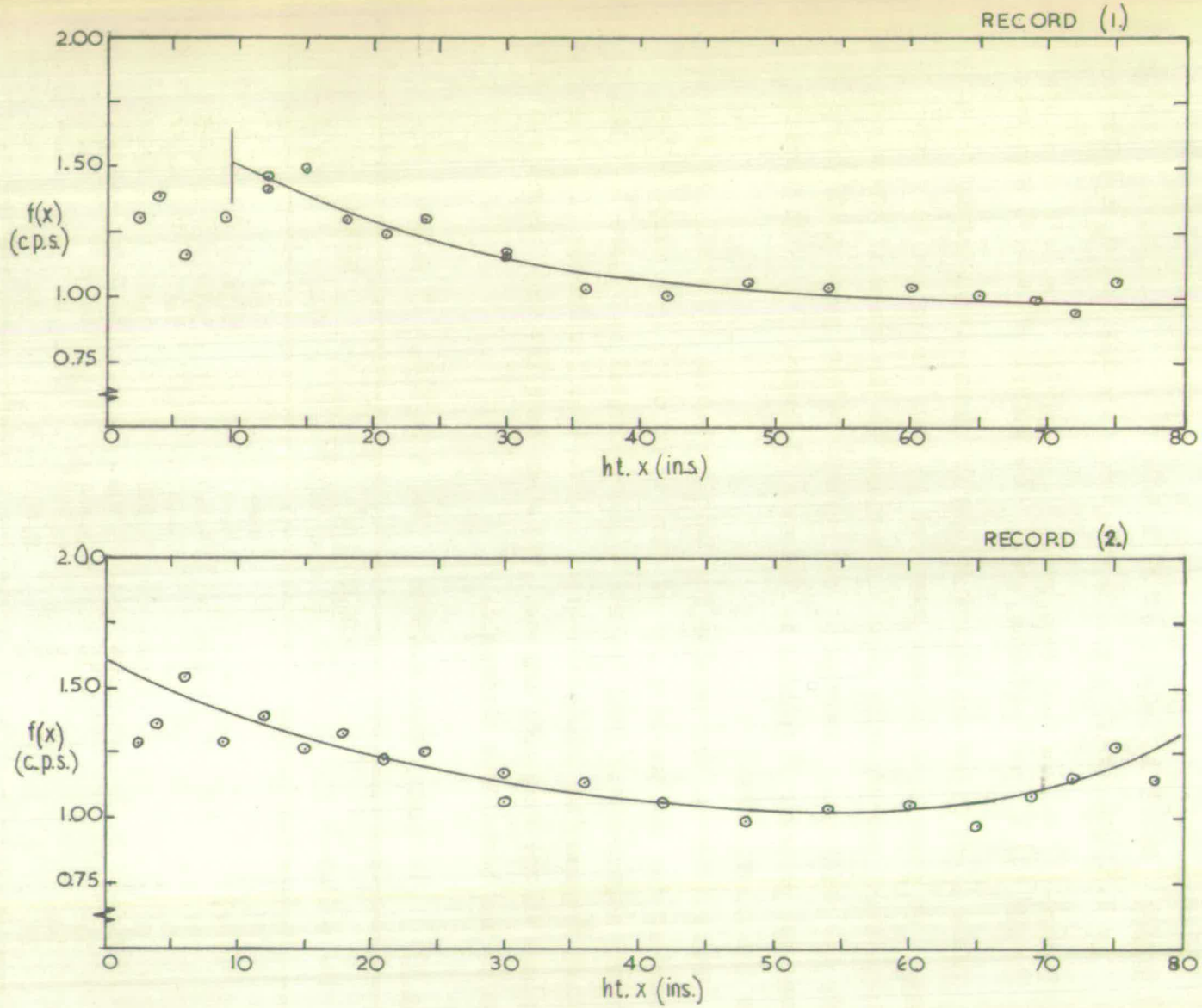


FIGURE 7.21 CHANGE OF DISTURBANCE FREQUENCY WITH HEIGHT.

The mean point voidages from Table A 5/5 are consistently lower than the overall mean bed voidage. Because of this (the measurement of the overall mean bed voidage is quite accurate) and the unsatisfactory optical characteristics of the tube, no useful information on voidage profiles can be obtained from these measurements.

(iii) System No. 5 B./H_2O. 1" I.D.T.

ρ_s = 2.86 gms./cc., ρ_f = 1.00 gms./cc., μ = 0.01 p., d_p = 0.086 cms.

Record (1) : $\bar{u}_o$ = 1.34 cms./sec., $\bar{\varepsilon}$ = 0.469, V_p = 3.70 cms./sec.
Record (2) : $\bar{u}_o$ = 1.47 cms./sec., $\bar{\varepsilon}$ = 0.485, V_p = 4.30 cms./sec.

Table A 8/5 gives the amplitude and frequency measurements for this system. No power spectra were measured in this system and only two "peak-to-peak" records were possible because of the onset of turbulence at fairly low voidages. Because of the narrow voidage range available, the bed was not properly fluidised in the case of Record (1) until 9 inches above the distributor.

The scatter on the results for this system is not nearly so bad as the scatter for the previous set of results in the ½ inch tube. The frequency measurements from Table A 8/5 are plotted in Figure 7.21 and smoothed frequencies tabulated below. Note that for Record (2), there is a minimum in the frequency curve. The flow rate for this record was very close to the turbulence threshold.

Table 17: Frequency Measurements No. 5 B./H_2O, 1" I.D.T.

Ht. x (ins.)	RECORD (1)		RECORD (2)	
	f(x)	f(x)/f(0)	f(x)	f(x)/f(0)
0	—	—	1.61	1.000
2.5	—	—	1.54	0.957
4.	—	—	1.51	0.938
6	—	—	1.46	0.907
9	1.52	1.000	1.40	0.869
12	1.46	0.960	1.35	0.839
15	1.39	0.914	1.31	0.814
18	1.33	0.875	—	—
21	1.27	0.836	—	—

Record (1), Basic frequency = 1.52 c.p.s.
Record (2), Basic frequency = 1.61 c.p.s.

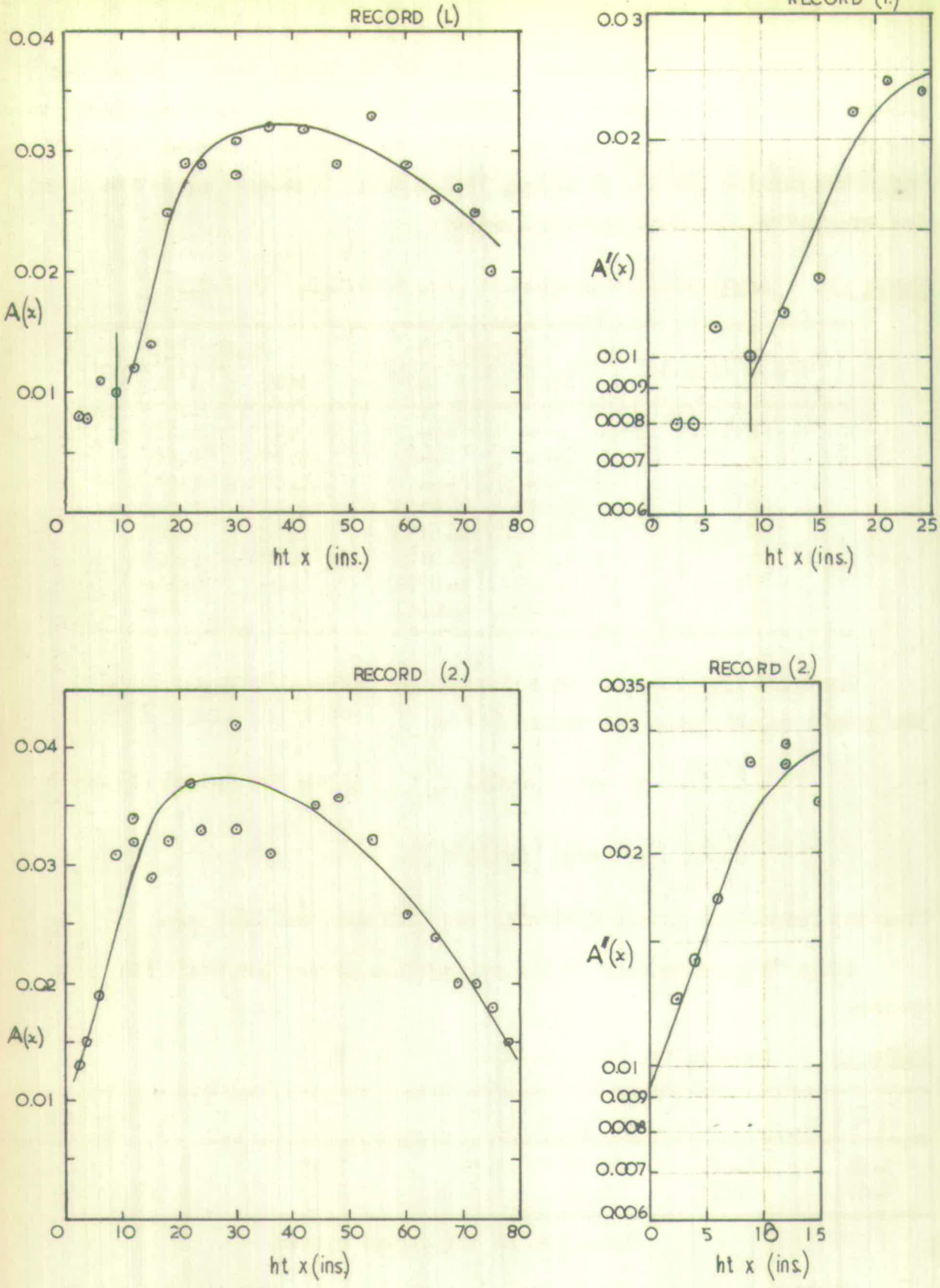


FIGURE 7.22 CHANGE OF DISTURBANCE AMPLITUDE WITH HEIGHT.

The amplitude measurements are plotted in Figure 7.22. After the initial growth, the decrease in amplitude for the high flow rate situation (Record (2)) is very much more rapid than for the low flow rate situation (cf. the results for No. 3 B./H_2O, 1" I.D.T.). Table 18 gives the first few amplitudes and their adjusted values.

Table 18: Amplification Results. No. 5 B./H_2O, 1" I.D.T.

Ht. x (ins.)	RECORD (1)		RECORD (2)	
	A(x)	A′(x)	A(x)	A′(x)
2.5	—	—	0.013	0.0124
4	—	—	0.015	0.0141
6	—	—	0.019	0.0172
9	0.010	0.0100	0.031	0.0269
12	0.012	0.0155	0.032	0.0268
15	0.014	0.0128	0.029	0.0236
18	0.025	0.0218	—	—
21	0.029	0.0242	—	—

The semi-log plots of the adjusted amplitudes in Figure 7.22 give the growth relationship for Record (1) as

$$\frac{A'(x)}{A(0)} = \exp\left[0.090\ x\right]$$, and for Record (2) it is

$$\frac{A'(x)}{A(0)} = \exp\left[0.104\ x\right].$$

Thus the respective growth distances are 28.2 cms. and 24.4 cms.

Table 19 is a summary of the propagation properties found for this system.

Table 19: Results for No. 5 B./H_2O. 1" I.D.T.

$\bar{u}_o$	$\bar{\varepsilon}$	V_p	f(0)	λ	k_x	Δx
1.34	0.469	3.70	1.52	2.45	2.57	28.2
1.47	0.485	4.30	1.61	2.67	2.36	24.4

Units are in the c.g.s. system.

Voidage profiles were plotted from the results given in Table A 8/5. Again all the measured points lay below the overall mean bed voidage so that no information can be gleaned from this set of results.

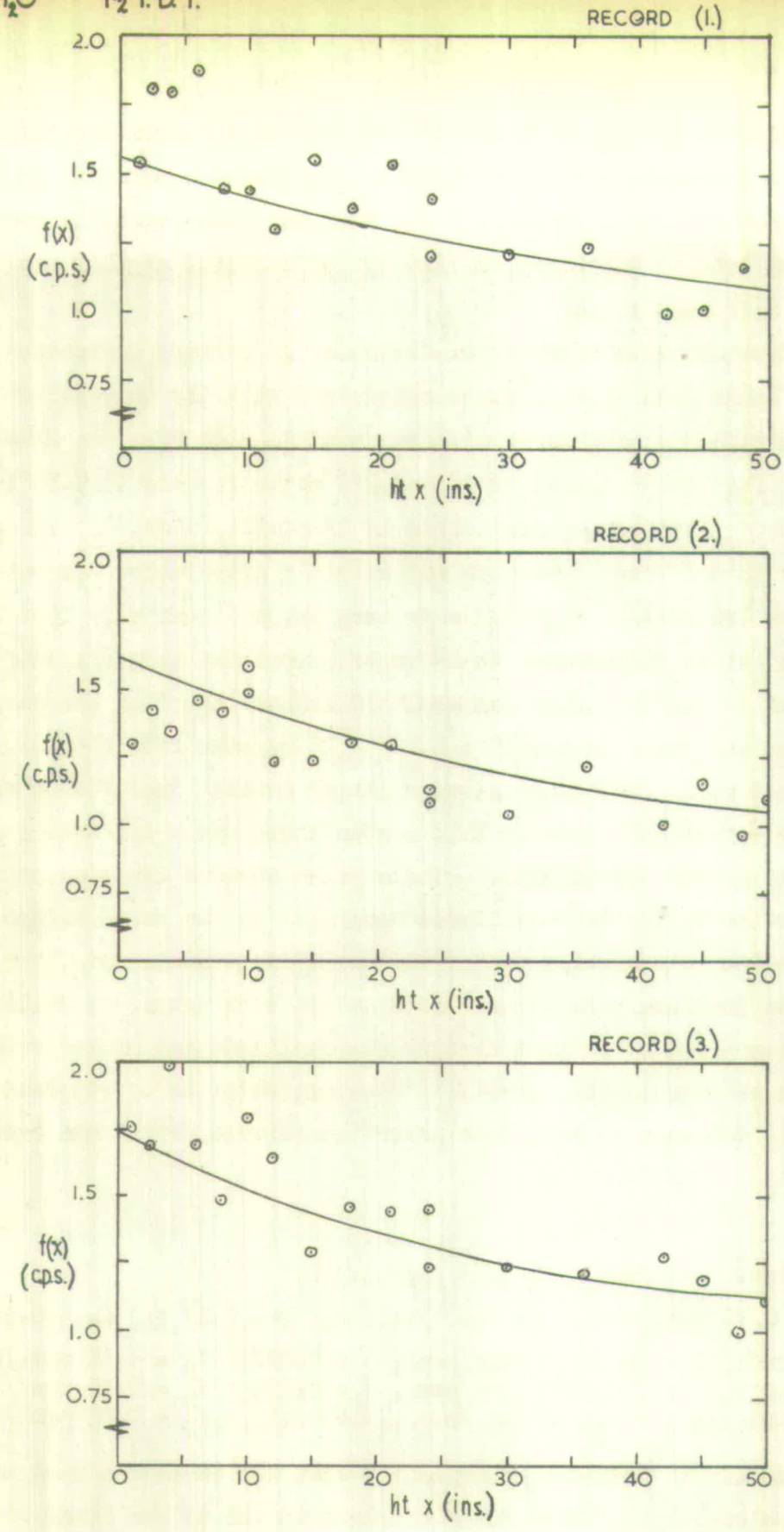


FIGURE 7.23 CHANGE OF DISTURBANCE FREQUENCY WITH HEIGHT.

A comparison of Tables 19 and 16 indicate that increasing the tube diameter increases the phase velocity and causes a decrease in the growth distance and the frequency. The dominant wave-length is greater in the larger tube. The No. 3. B./H_2O system exhibits similar behaviour in tubes of different sizes.

The effect of tube diameter on frequency is perhaps unexpected but it is shown later that this is quite consistent with the theory.

The initial disturbance amplitudes found in each tube are also quite different. For the ½" I.D.T., $A(0) \sim 0.027$ while for the 1" I.D.T. $A(0) \sim 0.010$. Although, as explained in Chapter 6, absolute voidage measurements in different tubes are not strictly comparable, the difference between these two initial amplitudes is very large - much more than could be accounted for by differences in averages across the tube diameter. The packed height in the ½" I.D.T. was about 12 inches less than the packed height of the ballotini in the 1" I.D.T. It appears from the No. 3 B. results that a small bed height gives a larger initial disturbance amplitude than a large bed height, but for this system there was a difference of about 30 inches in packed bed heights. There is no obvious explanation for the large difference in initial amplitudes occurring in the No. 5 B./H_2O system, unless it is due to a combination of the two effects mentioned above.

For the low flow rate records obtained in both tubes, it would seem, from a consideration of maximum disturbance amplitude and packed voidage, that packing effects inhibit growth. However, there is no apparent reason for the rapid decrease in amplitude after the maximum growth has been reached.

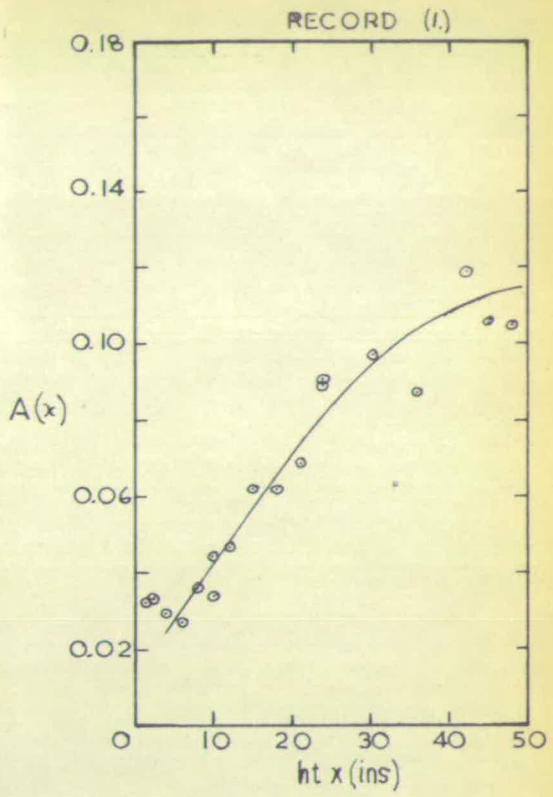
(iv) System. 2mm. B./H_2O. 1½" I.D.T.

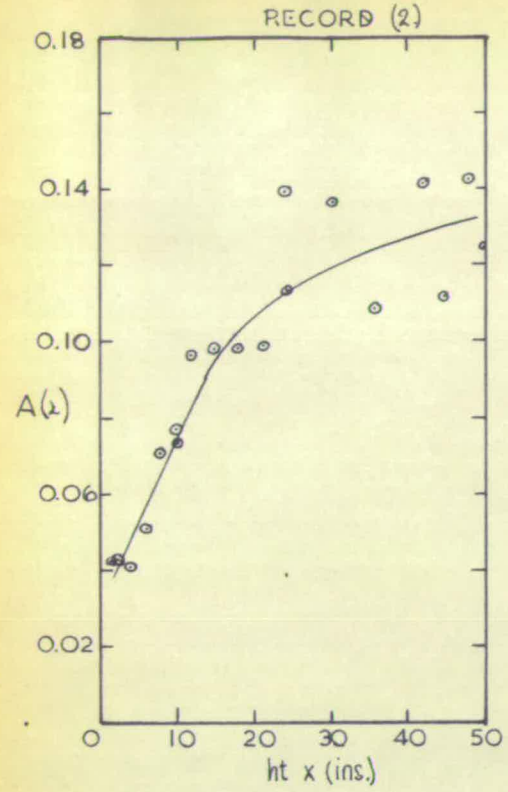
$\rho_s = 2.70$ gms./sec., $\rho_f = 1.00$ gms./cc., $\mu = 0.01$ p., $d_p = 0.207$ cms.

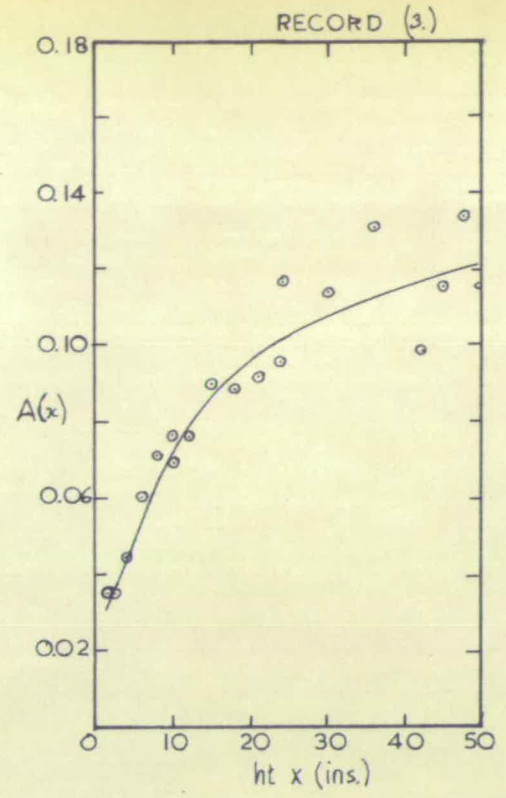
Record (1) : $\bar{u}_o = 3.72$ cms./sec., $\bar{\varepsilon} = 0.418$, $V_p = 6.62$ cms./sec.
Record (2) : $\bar{u}_o = 3.93$ cms./sec., $\bar{\varepsilon} = 0.433$, $V_p = 8.01$ cms./sec.
Record (30 : $\bar{u}_o = 4.28$ cms./sec., $\bar{\varepsilon} = 0.451$, $V_p = 8.95$ cms./sec.

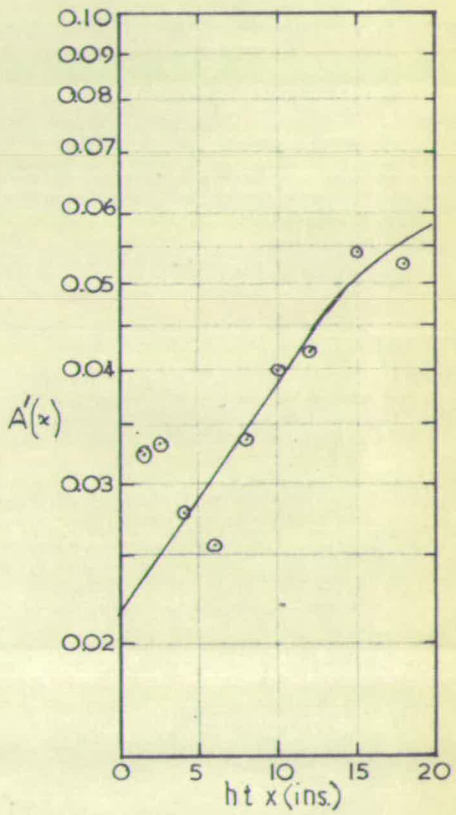
The results of previous experimental work had shown the need to obtain readings as close to the distributor as possible and it was found with this tube that readings as close to the distributor as 1.5 inches were possible.

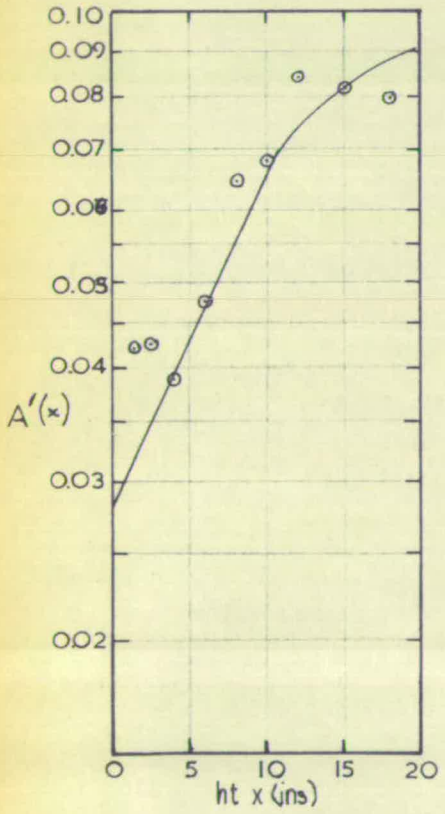
2 mm. B_1/H_2O $1\frac{1}{2}$ I.D.I.











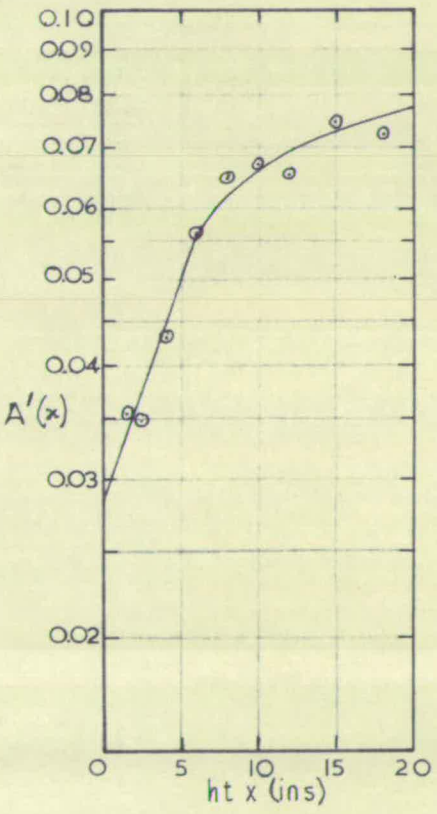


FIGURE 7.24 CHANGE OF DISTURBANCE AMPLITUDE WITH HEIGHT.

Small beds were used for this system because it is only the initial growth which is of real interest for the present work. Typical disturbances found in this system are shown in Plate 5.1.

The frequency measurements from Table A 9/2 are plotted in Figure 7.23 and the frequencies and frequency ratios obtained from the smooth curve are given in Table 20.

Table 20: Frequency Results 2m.m. B./H_2O. 1½" I.D.T.

Ht. x (ins.)	RECORD (1)		RECORD (2)		RECORD (3)	
	f(x)	f(x)/f(0)	f(x)	f(x)/f(0)	f(x)	f(x)/f(0)
0	1.56	1.000	1.62	1.000	1.74	1.000
1.5	1.53	0.981	1.59	0.982	1.71	0.983
2.5	1.52	0.975	1.57	0.969	1.69	0.971
4	1.50	0.961	1.54	0.951	1.66	0.954
6	1.48	0.949	1.51	0.932	1.61	0.925
8	1.45	0.929	1.47	0.907	1.57	0.902
10	1.42	0.910	1.43	0.883	1.53	0.879
12	1.40	0.895	1.41	0.870	1.49	0.856
15	1.36	0.871	1.36	0.839	1.44	0.828
18	1.33	0.852	1.32	0.815	1.40	0.805

Amplitude growth for these three records is shown in Figure 7.24. Note that the saturation point of the growth does not seem to have been reached even 50 inches above the distributor.

The plots indicate clearly that growth rate increases as the flow rate is increased and the frequency plots show no sign of turbulence setting in in the upper part of the bed.

Table 21: Amplification Results. 2 m.m. B./H_2O. 1½" I.D.T.

Ht. x (ins.)	RECORD (1)		RECORD (2)		RECORD (3)	
	A(x)	A′(x)	A(x)	A′(x)	A(x)	A′(x)
1.5	0.033	0.0324	0.043	0.0422	0.036	0.0354
2.5	0.034	0.0332	0.044	0.0426	0.036	0.0349
4	0.029	0.0278	0.041	0.0390	0.045	0.0429
6	0.027	0.0256	0.051	0.0475	0.061	0.0564
8	0.036	0.0334	0.071	0.0644	0.072	0.0649
10	0.044	0.0400	0.077	0.0680	0.077	0.0670
12	0.047	0.0421	0.097	0.0844	0.077	0.0659
15	0.062	0.0540	0.098	0.0822	0.090	0.0746
18	0.062	0.0528	—	—	—	—

Raw amplitudes and adjusted amplitudes are given in Table 21 and these adjusted amplitudes are also plotted in Figure 7.24.

The values of A(0) for Records (1), (2) and (3) are 0.0216, 0.0282 and 0.0283 respectively and the straight line graphs of Figure 7.24 give growth distances of 43.7 cms., 29.5 cms. and 22.5 cms..

The disturbance propagation properties derived from the measurements of phase velocity, frequency and growth distance are summarised in Table 22.

Table 22: Results for 2 m.m. B./H_2O. $1\frac{1}{2}$" I.D.T.

$\bar{u}_o$	$\bar{\varepsilon}$	V_p	f(0)	λ	k_x	Δx
3.72	0.418	6.62	1.56	4.24	1.47	43.7
3.93	0.433	8.01	1.62	4.94	1.27	29.5
4.28	0.451	8.95	1.74	5.14	1.22	22.5

Units are c.g.s. units.

In addition, some frequency and phase velocity measurements were made on this ballotini grade in a 1" tube, despite the onset of slugging at about eight inches above the distributor. These results appear in Table 23.

Table 23: Results for 2 m.m. B./H_2O. 1" I.D.T.

$\bar{u}_o$	$\bar{\varepsilon}$	V_p	f(0)	λ
4.04	0.457	5.84	1.3	4.50
4.76	0.496	7.58	2.2	3.30

The frequency results are probably higher than indicated above. However the general features found with the other results for ballotini in different tube sizes are also found here (higher frequency, lower phase velocity and increased measured voidage).

Plots of the point voidage results from Table A 9/2 show that they consistently lie above the overall mean bed voidage, unlike most of the other systems. No trend is discernible.

No. 7B./H_2O. $\frac{1}{2}$ L.D.T.

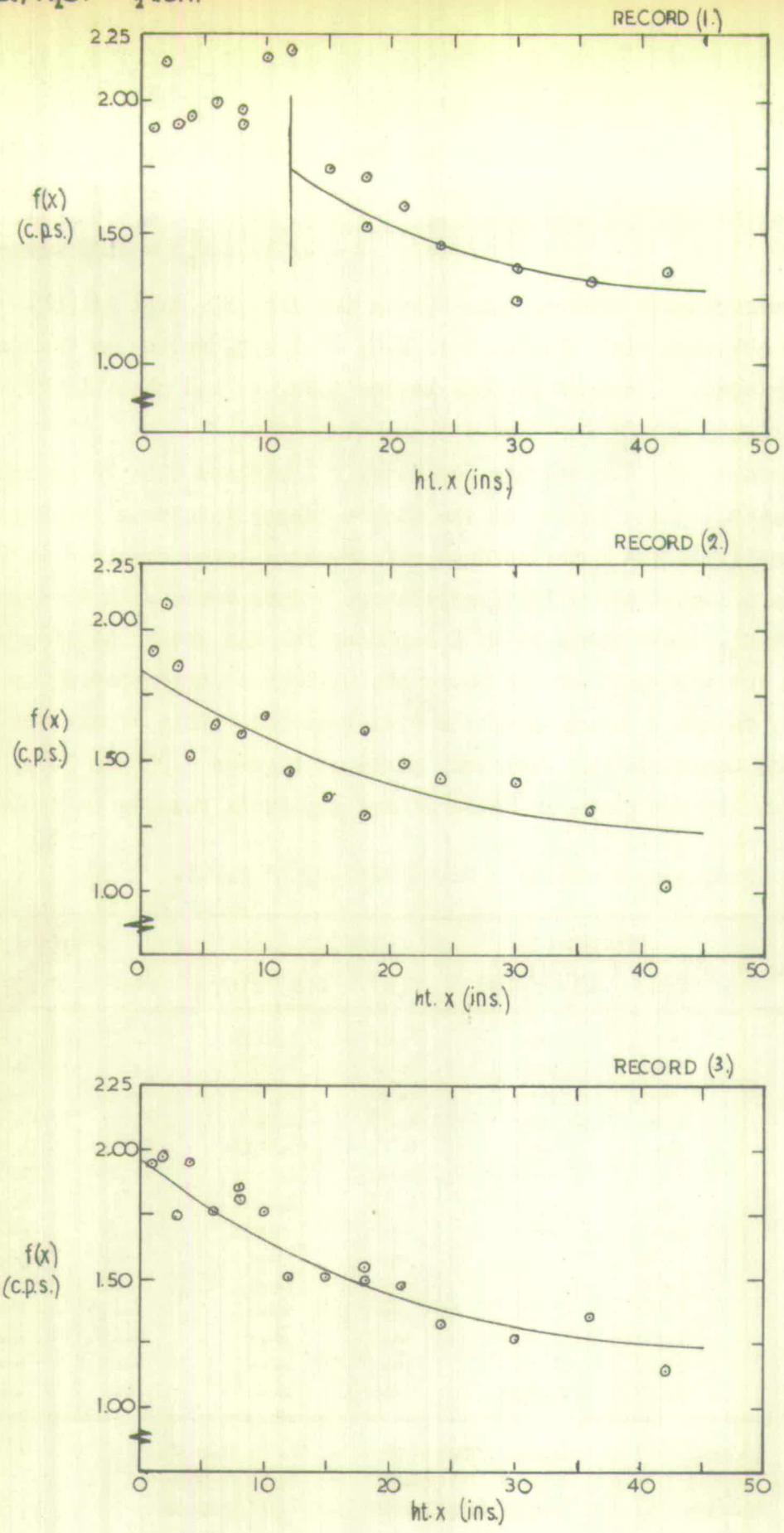


FIGURE 7.25 CHANGE OF DISTURBANCE FREQUENCY WITH HEIGHT.

(v) System No. 7 B./H_2O. ½" I.D.T.

ρ_s = 2.95 gms./cc., ρ_f = 1.00 gms./cc., μ = 0.01 p., d_p = 0.064 cms.

Record (1) : $\bar{u}_o$ = 0.86 cms./sec., $\bar{\varepsilon}$ = 0.495, V_p = 2.54 cms./sec.
Record (2) : $\bar{u}_o$ = 0.98 cms./sec., $\bar{\varepsilon}$ = 0.507, V_p = 2.76 cms./sec.
Record (3) : $\bar{u}_o$ = 1.10 cms./sec., $\bar{\varepsilon}$ = 0.519, V_p = 3.05 cms./sec.

The measurements made on this system are probably more reliable than the results obtained with the No. 5 B./H_2O, ½" I.D.T. system as the faulty tube was replaced. Because of this better tube, it was possible to obtain traces at heights only 1 inch above the distributor.

For Record (1), the bed was not totally fluidised till 12 inches above the distributor. Also faults on the Benson-Lehner data tape for Record (2) prevented amplitude and point voidage measurements being obtained at heights greater than 8 inches above the distributor. Once again with the smaller sized ballotini, there seems to be a tendency for the growth to stop very quickly and for the amplitude to decrease, without a corresponding increase of frequency caused by break-up of the disturbances. This effect can be seen from the amplitude and frequency plots of Figures 7.25 and 7.26. Frequency results are given in Table 24 and amplitude results in Table 25.

Table 24: Frequency REsults. No. 7 B./H_2O, ½" I.D.T.

Ht. x (ins.)	RECORD (1)		RECORD (2)		RECORD (3)	
	f(x)	f(x)/f(0)	f(x)	f(x)/f(0)	f(x)	f(x)/f(0)
0	—	—	1.86	1.000	1.97	1.000
1	—	—	1.82	0.978	1.93	0.980
2	—	—	1.78	0.957	1.89	0.959
3	—	—	1.75	0.941	1.85	0.939
4	—	—	1.73	0.930	1.82	0.924
6	—	—	1.68	0.903	1.76	0.893
8	—	—	1.63	0.876	1.70	0.863
10	—	—	—	—	1.65	0.838
12	1.74	1.000	—	—	1.60	0.812
15	1.65	0.957	—	—	1.54	0.782
18	1.57	0.902	—	—	—	—
21	1.51	0.867	—	—	—	—
24	1.46	0.839	—	—	—	—
30	1.37	0.788	—	—	—	—

Record (1) : Basic frequency = 1.74 c.p.s.
Record (2) : Basic frequency = 1.86 c.p.s.
Record (3) : Basic frequency = 1.97 c.p.s.

No. 7 B./ H_2O. $\frac{1}{2}$" I.D.T.

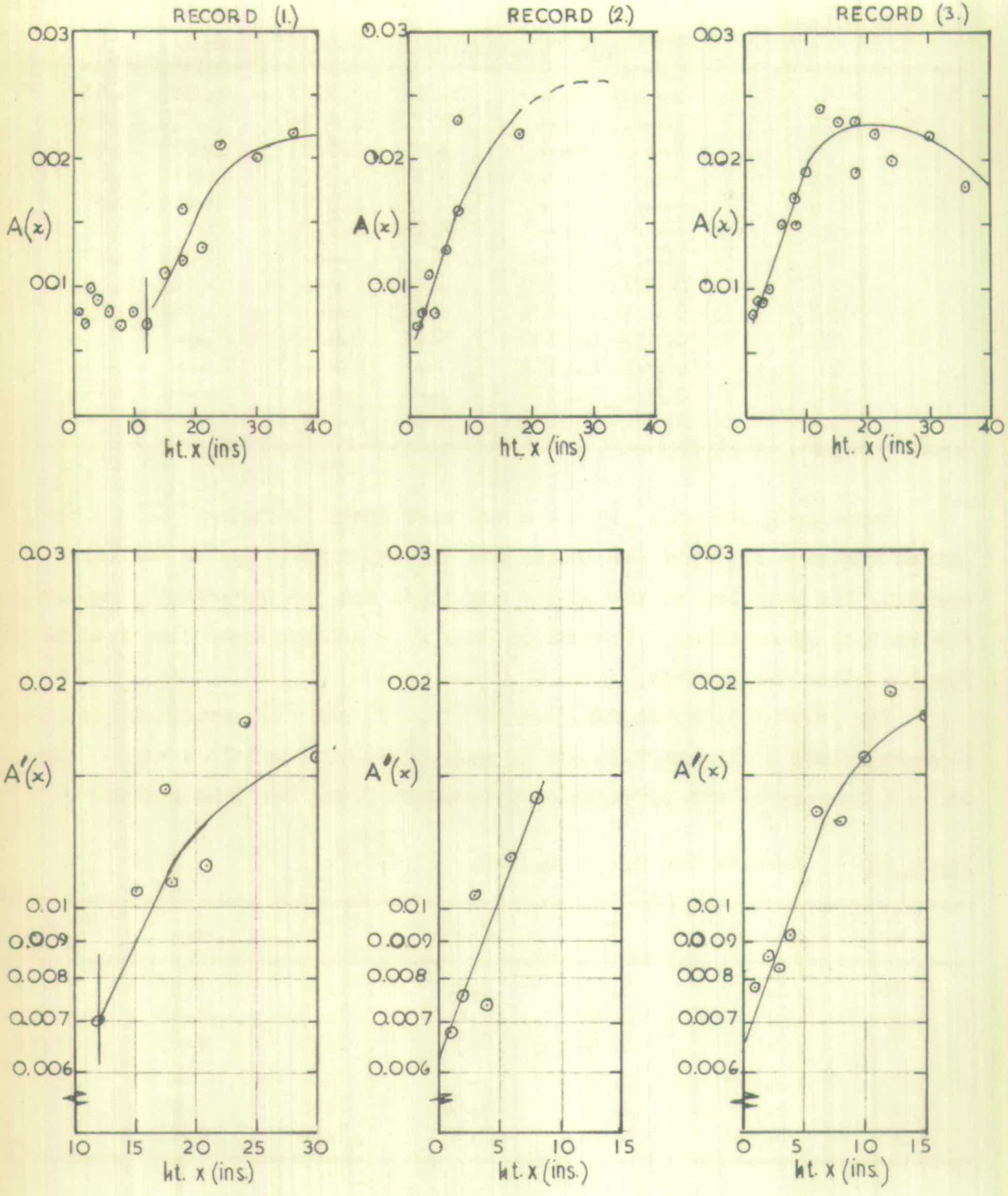


FIGURE 7.26 CHANGE OF DISTURBANCE AMPLITUDE WITH HEIGHT.

Table 25: Amplitude Results. No. 7 B./H_2O, $\frac{1}{2}$" I.D.T.

Ht. x (ins.)	RECORD (1)		RECORD (2)		RECORD (3)	
	A(x)	A′(x)	A(x)	A′(x)	A(x)	A′(x)
1	—	—	0.007	0.0068	0.008	0.0078
2	—	—	0.008	0.0076	0.009	0.0086
3	—	—	0.011	0.0104	0.009	0.0083
4	—	—	0.008	0.0074	0.010	0.0092
6	—	—	0.013	0.0117	0.015	0.0134
8	—	—	0.016	0.0140	0.015	0.0130
10	—	—	—	—	0.019	0.0159
12	0.007	0.0070	—	—	0.024	0.0195
15	0.011	0.0105	—	—	0.023	0.0180
18	0.012	0.0108	—	—	—	—
21	0.013	0.0113	—	—	—	—
24	0.021	0.0176	—	—	—	—
30	0.020	0.0158	—	—	—	—

Semi-log plots of A′(x) vs. x are also shown in Figure 7.26. The growth distance estimate for Record (1) is very rough, due to the large scatter, the very low values of the amplitude and the uncertainty concerning the initial conditions. However it does give a comparison with the results for the other two records.

The growth distances for Records (1), (2) and (3), obtained from the semi-log plots of Figure 7.26 are 50 cms., 26.6 cms. and 23.8 cms. Table 26 is a summary of the propagation properties found for this system.

Table 26: Results for No. 7 B./H_2O, $\frac{1}{8}$" I.D.T.

$\bar{\mu}_o$	$\bar{\varepsilon}$	V_p	f(0)	λ	k_x	Δx
0.86	0.495	2.54	1.74	1.46	4.30	50
0.98	0.507	2.76	1.86	1.48	4.25	26.6
1.10	0.579	3.05	1.97	1.55	4.05	23.8
0.93	0.497	2.67	—	—	—	—
1.02	0.511	2.95	1.86	1.58	3.97	—
1.20	0.530	3.26	2.14	1.52	4.13	—

The second set of three results in the above table were from a set of records for which the amplification results were quite valueless (due to the faulty tube).

The only voidage profile obtainable was that for Record (3). The results are fairly scattered and only the initial few points lie above the mean bed voidage line. A negative voidage gradient would seem to be indicated but the mean value of the voidage from the profile is well below the overall mean bed voidage.

(vi) System. Polystyrene Beads/H_2O, 1" I.D.T.

ρ_s = 1.06 gms./cc., ρ_f = 1.00 gms./cc., μ = 0.01 p., d_p = 0.093 cms.

The fluidising velocity used for this system was very low - of the order of 0.20 cms./sec.. Voidage measurements on this bed were not possible because of the very diffuse upper surface. No disturbances whatsoever were visible in the bed, it having a completely uniform appearance throughout most of its height.

The experimental measurements of the propagation properties of small disturbances are set out in detail in the above pages and the limitations of the experimental method and sources of inaccuracy in the results have been fully dealt with in the foregoing and present chapters. Again it must be emphasised that the results are fairly approximate and give only a fairly rough indication of the magnitudes of the propagation properties. However they do indicate how the properties change with flow rate and from system to system.

It is of interest to classify the growth in the above systems on the basis proposed by Jackson (5), i.e. the ratio of growth distance to disturbance size or wave-length. This basis is here slightly altered as the dominant wave-length is used rather than a wave-length which is the same multiple of the particle size in every system. For consistency, any classification or comparison should properly be carried out for systems at incipient fluidisation. However data for incipient fluidisation is lacking and the next best thing is to compare growth at the lowest fluid velocity used in each system.

The following table gives values of λ/d_p, $\Delta x/\lambda$ and the Froude number for the systems investigated. All quantities are given in the c.g.s. system of units.

Ballotini	d_p	d_t	$\bar{u}_o$	λ	λ/d_p	Δx	$\Delta x/\lambda$	Fr.
2 m.m.	0.207	3.81	3.72	4.24	20.5	43.7	10.3	0.068
No. 3.	0.127	2.54	2.46	3.62	28.5	25.9	7.1	0.048
No. 5.	0.086	2.54	1.34	2.45	28.5	28.2	11.5	0.021
No. 5.	0.086	1.27	1.42	1.73	20.1	39.1	22.6	0.024
No. 7.	0.064	1.27	0.86	1.46	22.8	50	34.2	0.012

Considering the entries in the above table it is seen that $\Delta x/\lambda$ increases as the particle diameter decreases (except for the first two entries), and in general the order above is the order one would place the systems in from visual observations of instability. Visual observation could however be deceptive over the initial disturbance growth as it relies to a large extent on disturbances which have already grown significantly. The Froude number decreases in the expected way (except for the No. 5 B. entries) but this is an effect of tube diameter and the Froude number cannot account for this. One striking feature brought out by the table is that the ratio λ/d_p lies consistently in the range 20 to 30. In general it would seem that the ratio $\Delta x/\lambda$ decreases as the observed aggregative nature of the bed increases.

Obviously more experimental work on a wider variety of systems is still required to fully investigate the effects of fluid density and viscosity on the propagation properties. There are also a number of possible improvements to the apparatus which would lead to more accurate results. The optical properties of perspex are not wholly satisfactory and glass faces and tubes are preferable. The perspex faces of the optical box could be replaced by plate glass set into a metal frame to give it the necessary strength for handling and resistance to fluid pressure. In any future work, this pressure need not be too great as a bed height of only 3 feet at most is required for measurement of the initial exponential growth. Glass tubes could replace the perspex tubes used for the bed without too much trouble. In addition, a constant voltage light source would guard against changes in intensity due to mains fluctuations.

The distributor used in this work was badly designed, having a very low pressure drop compared to the pressure drop across the bed. This is the probable reason why some of the beds were not properly fluidised at low liquid rates. A much thicker sintered plate with a smaller porosity would increase the pressure drop and probably eliminate channeling in the lower portion of these beds. The present work has also shown the need to obtain measurements right down to the distributor. This could not be achieved in the equipment used in this work but if a cylinder of sintered bronze were used as a distributor and this cylinder pushed up inside the fluidising tube so that its upper surface was well clear of any connecting flanges, then both the pressure drop and measurement criteria could be satisfied. Care would have to be taken, of course, to ensure that the walls of the cylinder were properly sealed against the tube walls to prevent bypassing and maldistribution of the fluidising liquid.

The experimental work has brought to light some interesting aspects of the disturbance behaviour which cannot readily be explained by reference to the equations of motion or to the known physics of fluidisation. These rather puzzling phenomena are :

(i) The apparent effect of bed height on the initial disturbance amplitude: From the results for No. 3 B./H_2O, 1" I.D.T. it would seem that an increase in bed height (i.e. amount of material in the bed) causes the initial amplitude of the disturbances to decrease, although the disturbance propagation properties are unaffected.

(ii) The effect of tube size on the initial disturbance amplitude: The results for No. 5 B./H_2O in the 1" and ½" I.D.T.'s indicate that in the larger tube, the disturbance has a smaller initial amplitude than in the smaller tube. This could perhaps be due to the relative extent of wall effects and their effect on the averaging of the signal across the tube diameter. It is also possibly a product of the effect of bed height mentioned above.

(iii) The increase of frequency in the upper part of some beds: This occurred at high flow rates close to the onset of turbulence throughout the bed. The increase of frequency is probably due to an increase in the intensity of turbulence in the upper part of the bed. A possible explanation is

the presence of a positive voidage gradient - the concentration of particles in the upper part of the beds being too low to suppress turbulence.

(iv) The decrease of disturbance amplitude after the disturbances have grown to their maximum size: For high flow rates, this is in part due to break up of the disturbances, shown by the frequency increase discussed above, but even with records for which the fluidising velocity was low, there was a very rapid decrease in amplitude after the growth was saturated. The effect was much more marked with the smaller sizes of ballotini, but this may have been because the bed height for the larger sizes was not large enough for this effect to show.

However the real purpose of the experimental work was to test the equations. The experimental results indicate that the initial amplitude of the disturbances is small compared to the bed voidage and that, initially at least, these disturbances grow exponentially. Thus there is a reasonable basis for a comparison between the experimentally determined propagation properties and those predicted by the solution of the linearised equations of motion.

Apart from predicting the actual values obtained within any one situation, the equations of motion should be capable of explaining the variation in propagation properties of the same particles and fluid in tubes of different size and also the variation of propagation properties with flow rate. This comparison of measured and predicted propagation properties is the subject of the next chapter.

Table 1:- Experimentally Determined Propagation Properties

d_t (cms)	$\bar{u}_o$ (cms/sec.)	$\bar{\varepsilon}$	V_p (cms/sec.)	$f(0)$ (c.p.s.)	λ (cms)	k_x (cms^{-1})	Δx (cms)	ξ ($secs^{-1}$)
System: 2 m.m. B/H_2O								
3.81	3.72	0.418	6.62	1.56	4.24	1.48	43.7	0.151
	3.93	0.433	8.01	1.62	4.94	1.27	29.5	0.273
	4.28	0.451	8.95	1.74	5.14	1.22	22.5	0.398
2.54	4.04	0.457	5.84	1.3	4.50	1.40	-	-
	4.76	0.496	7.58	2.2	3.30	1.90	-	-
System: No.3 B/H_2O								
2.54	2.46	0.463	5.25	1.45	3.62	1.74	25.9	0.203
	2.55	0.470	5.36	1.63	3.29	1.91	20.3	0.264
	2.72	0.483	5.87	1.83	3.21	1.96	13.9	0.422
	2.89	0.496	6.10	1.94	3.14	2.00	12.3	0.496
	2.96	0.500	6.48	2.09	3.10	2.03	-	-
1.27	2.53	0.503	3.92	2.3	1.7	3.7	-	-
	2.70	0.515	4.42	2.5	1.8	3.5	-	-
	2.87	0.528	4.75	2.6	1.8	3.5	-	-
System: No.5 B/H_2O								
2.54	1.34	0.469	3.70	1.52	2.45	2.57	28.2	0.131
	1.47	0.485	4.30	1.61	2.67	2.36	24.4	0.176
1.27	1.42	0.504	3.46	2.01	1.73	3.63	39.1	0.088
	1.64	0.529	3.91	2.21	1.77	3.55	34.3	0.114
	1.77	0.541	4.23	2.40	1.77	3.55	-	-
System: No.7 B/H_2O								
1.27	0.86	0.495	2.54	1.74	1.46	4.31	50	0.051
	0.93	0.497	2.67	-	-	-	-	-
	0.98	0.507	2.76	1.86	1.48	4.25	26.6	1.104
	1.02	0.511	2.95	1.86	1.58	3.98	-	-
	1.10	0.519	3.05	1.97	1.55	4.06	23.8	0.128
	1.20	0.530	3.26	2.14	1.52	4.13	-	-

CHAPTER 8

Comparison of Experimental Measurements with Theoretical Predictions of the Disturbance Growth

The experimental work was undertaken principally to test the predictions of disturbance growth obtainable from the linearised equations and, if possible, to ascertain the existence of voidage gradients in the bed. Unfortunately the voidage profile measurements were quite inconclusive, but propagation property measurements were made for a number of systems. The results of these measurements are summarised in Table 1. The general features of disturbance growth and propagation were dealt with partly in Chapter 6 (coalescence, turbulence and slugging) and partly at the end of Chapter 7. Most of these features concern disturbances which have grown to a fairly large size and the discussion of them is rather qualitative. Because of the large amplitudes, these features cannot be explained by studying the solutions of the linearised equations of motion.

Before the equations of motion can be accepted as giving a reasonable description of the fluidised state, they must be shown to be capable of predicting the propagation properties and explaining the variation in these quantities for different tube sizes and systems. Unfortunately, because of a lack of precision in the measurements and a further lack of precise information on some of the main bed parameters, an exact comparison between experimental and theoretical values is not altogether possible. It is shown in the following pages, however, that a choice of reasonable values for these bed parameters leads to propagation properties which are consistent with the measured values.

From Table 1, it is seen that the variation in propagation properties with flow rate is much as expected from the discussion in Chapter 4. An increase of flow rate causes an increase in the phase velocity and frequency and a decrease in the growth distance. For some systems the dominant wave length appears to increase with flow rate and for others it decreases. One would generally expect that the dominant wave-length would decrease with increasing flow rate but theoretically this depends very much on the relative

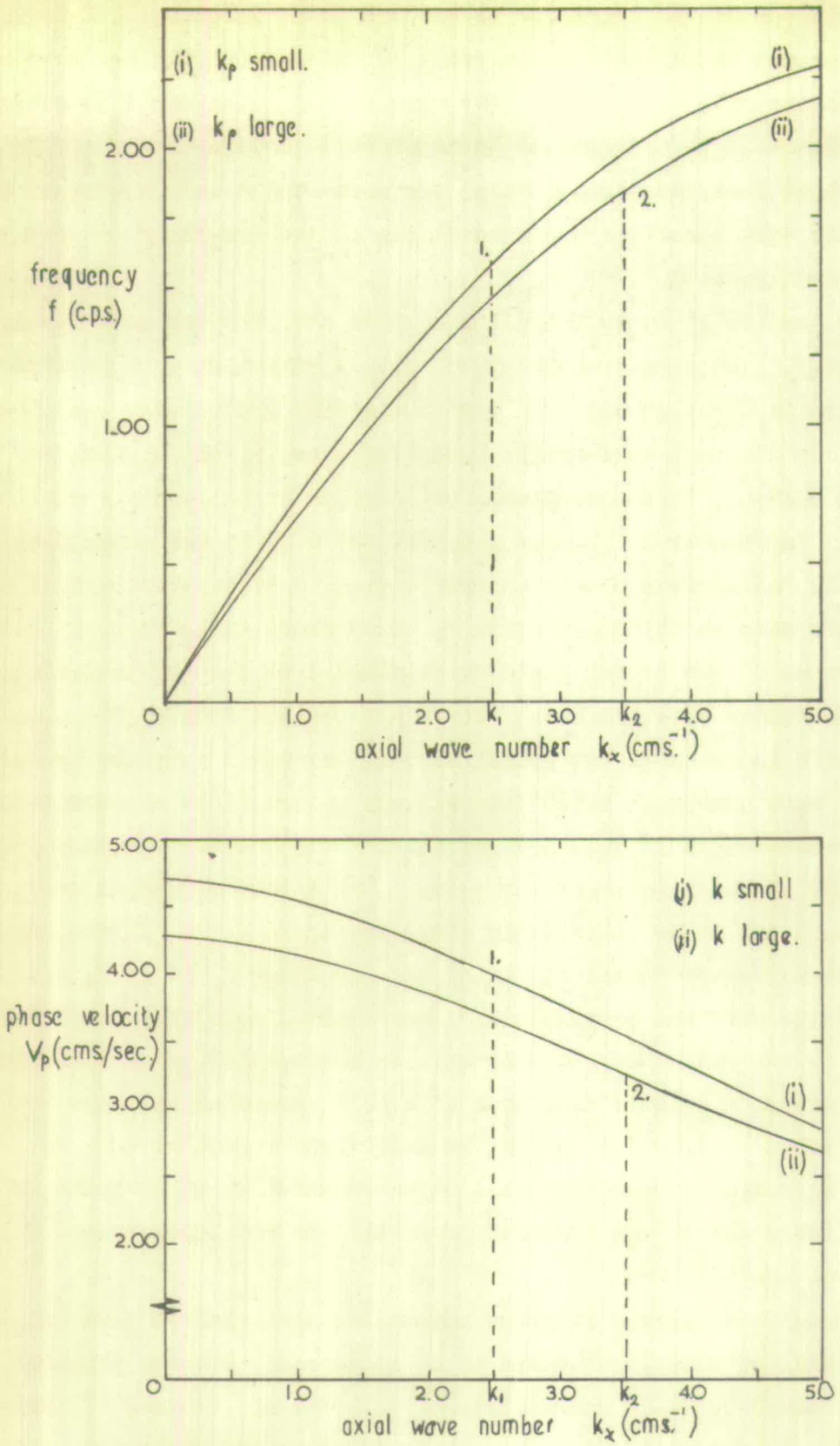


FIGURE 8.1 EFFECT OF RADIAL WAVE NUMBER ON FREQUENCY AND PHASE VELOCITY.

rates of change of amplification factor and phase velocity with axial wave number and it is quite conceivable on this basis that the wave-length might increase with flow rate. For some of the experimental systems, the dominant wave-length appeared to be constant. However it is difficult to tell if these observed variations in the wave-length are genuine as this quantity is very sensitive to inaccuracies in the frequency and phase velocity measurements.

The results given in Table 1 also show that for the same system at approximately the same fluidising velocity a reduction in tube size causes an increase in the frequency and growth distance and reduces the phase velocity and dominant wave-length (see, for example, the systems No. 3 B./H_2O and No. 5 B./H_2O). It also causes an increase in the overall mean bed voidage. In Chapter 4 (Figures 4.6, 4.7 and 4.8) it was shown that an increase in radial wave number (corresponding to a decrease in tube size), keeping the same velocity and voidage, would cause an increase in the minimum value of the growth distance obtained from the growth distance - axial wave number relationship. It is not obvious from Figure 4.8, however, whether this increase in the radial wave number would increase or decrease the axial wave number at which this minimum occurs (this minimum gives the dominant wave-length in the bed) but intuitively one might expect a smaller disturbance to occur in a smaller tube. The effect of radial wave number on frequency and phase velocity is shown in Figure 8.1. If the dominant axial wave number for small k_ρ is k_1 and for large k_ρ it is k_2 with $k_2 > k_1$ in accordance with the experimental observations, then it is seen that an increase in the radial wave number will be accompanied by an increase in the phase velocity. This is also true if $k_2 < k_1$ provided they are sufficiently close in value. Provided that k_2 is sufficiently greater than k_1, the increase in radial wave number will be accompanied by an increase in frequency. Thus the behaviour of the measured properties is not inconsistent with the theoretical predictions.

As mentioned above, it seems reasonable that smaller wave-lengths occur in smaller tubes, but there is no immediately obvious physical reason why this should be so. The analytical expressions, because of their complexity, do not yield very much information on the variation of the growth distance with k_x and k_ρ. The criterion for the dominant wave-length is

$$\frac{d\Delta x}{dk_x} = 0 \quad \text{and since} \quad \Delta x = \frac{V_p}{\xi}$$

this is $\frac{dV_p}{dk_x} = \frac{V_p}{\xi} \frac{d\xi}{dk_x}$. Now $\frac{dV_p}{dk_x}$ is negative so that $\frac{d\xi}{dk_x}$ is negative and the value of k_x corresponding to minimum growth distance is greater than the value of k_x corresponding to maximum amplification factor. In the expressions for the propagation properties, the radial wave number complements the effects of the particulate phase stress tensor terms $(\alpha_o + 2\lambda_o)$ and Ω_o' . Increase of the radial wave number decreases the maximum value of the amplification factor while the value of k_x at which it occurs remains virtually unaltered, so that one might expect from this that the value of k_x for minimum growth distance would also remain constant with increase of k_ρ . Experimentally this is obviously not the case. Thus the variation of the phase velocity with k_x and k_ρ would seem to be the principal factor causing the increase in dominant wave-number with reduction of the tube size.

From the results given in Table 1, systems in different tubes at the same fluidising velocity have markedly different overall mean bed voidages. The voidage determining the initial disturbance growth is obviously the voidage at the foot of the bed. Specifically it is the more or less uniform voidage (neglecting the periodic effects of disturbances, the mean voidage change of which is zero) extending over the area in the centre of the tube where wall effects on voidage have died out. Likewise the fluid velocity of interest is the absolute fluid velocity in this region. The overall mean bed voidage, if there are no voidage gradients up the bed, is given by the expression

$$\bar{\varepsilon} = \frac{4}{d_t^2} \int_0^{d_t/2} \varepsilon(\rho)\, \rho\, d\rho. \qquad (\bar{\varepsilon} \text{ is essentially a volumetric average})$$

Thus $\bar{\varepsilon} \geq \varepsilon_c$.

If the wall effect is large then $\bar{\varepsilon}$ could be considerably greater than the voidage in the unifrom core ε_c*. The fluid velocity in the uniform core (u_c) will, because of flow resistance, be lower in the centre of the tube than at the sides. The superficial fluid velocity is given by

$$\bar{u}_o = \frac{4}{d_t^2}\int_0^{d_t/2} u(\rho)\,\varepsilon(\rho)\,\rho\,.\,d\rho \geq u_c\varepsilon_c$$

The measured quantities $\bar{\varepsilon}$ and $\bar{u}_o$ will be reasonable approximations to the parameters ε_c and u_c which determine disturbance growth only if the extent of wall effects is small.

The situation is probably more complex than this simple uniform core model would indicate and is further complicated by the possible existence of voidage gradients. However without quantitative information on the extent of the wall effects and their magnitude it is impossible to assess the difference between $\bar{\varepsilon}$ and ε_c and $\bar{u}_o$ and ($u_c\varepsilon_c$). If d_p/d_t is small, the differences are not likely to be significant. In the absence of further information, the best estimates available for use in the calculations for growth properties in any situation are the measured values of $\bar{\varepsilon}$ and $\bar{u}_o$.

Bound up with this question of wall effects and their effect on voidage are the boundary conditions for the disturbances. The effect of radial wave number was discussed above and in Chapter 4. In Chapter 3 it was assumed that single disturbances were axisymmetric and that the wall effects in narrow tubes were such that the particle concentration disturbance at the edge of the uniform core was zero, i.e. $n_1(x,\rho) = 0$ at $\rho = d_u/2$, where $d_u = d_t\,(1 - c'd_p/d_t\,)$ and $k_\rho = 4.810/d_u$.
The constant c' is positive and probably less than 10. It was also assumed that disturbances originated at the distributor.

---

* This difference also affects the voidage-signal calibration. The quantities correlated are the signal, dependent on the average voidage taken across a diameter, and the mean voidage based on bed volume. Only if wall effects are negligible will these two averages be equivalent, if there are no voidage gradients present.

The experimental work has shown that the disturbances do in general originate at the distributor and that the assumption of axial symmetry is quite reasonable for the narrow diameter tubes used in the present work. However, it is also obvious that, because of particle slip at the walls, the boundary condition imposed above is much too strong. The obvious inhibitory effect of the walls can still be taken into account by the above conditions, by making the constant c' negative i.e. the equivalent uniform core is made to extend well beyond the bounds of the tube so that $n_1 \neq 0$ at values of ρ close to the tube radius. In the calculations an arbitrary value of $c' = -20$ was used to estimate the radial wave number for any one system or tube size.

The propagation properties for comparison with the experimental results were calculated from the same Sirius programme as was used to give the results of Chapter 4. All the propagation properties were thus calculated as functions of the axial wave number for different values of the parameters $|d\Omega/d\varepsilon|$ and $(\alpha_o + 2\chi_o)$. The other parameters $n_o \beta_o'/\beta_o$ and θ_o were kept constant throughout the calculations for any one situation.

Appendix 2 gives full details of the way in which values of the above parameters were obtained. The "viscosity" term $(\alpha_o + 2\chi_o)$ was obtained from measurements of χ_o made on two of the ballotini systems investigated in this work; these measurements were extrapolated to give values for the other two systems. The range of values of $(\alpha_o + 2\chi_o)$ covered in the calculations was $(\alpha_o + 2\chi_o) = 0$ to $(\alpha_o + 2\chi_o) = 4\chi_o$. The normal stress term was taken equal to the fluid momentum term appearing with it in the coefficient of $d\varepsilon/dx$ in equation (3,19). The value

$$\left|\frac{d\Omega}{d\varepsilon}\right| = \rho_f \bar{u}_o^2 \frac{(1-\varepsilon)}{\varepsilon^3}\left(1 + \frac{\theta(\varepsilon)}{\varepsilon}\right)$$ was generally, but not always, taken as the maximum value for use in the computations. The drag parameter $n_o \beta_o'/\beta_o$ was obtained from the Richardson and Zaki expansion law (Figure A. 3) and the virtual mass coefficient was taken constant at 0.5. The overall mean bed voidages given in Table 1 were used throughout in the calculations and h_o/λ give values of the above parameters; possible voidage gradient effects and the effect of the walls on the voidage and fluid velocity were ignored.

Because of the range of values of $(\alpha_o + 2\chi_o)$ and $|d\Omega/d\varepsilon|$ which had to be covered for any one situation, the calculations necessary for a detailed comparison were rather long and tedious. To completely cover only one situation, the print-out time for the computer output was anything between two and three hours. Thus it was quite out of the question to cover all the situations investigated experimentally. However detailed comparisons for about twelve of these situations are given in the following pages.

The criterion for the selection of the "predicted" propagation properties from the search of values carried out by the computer was the minimum value in the growth distance - axial wave number relationship which gave predicted values of frequency, phase velocity, and dominant wave-length close to the measured values of these quantities and which was itself close to the measured growth distance.

Note that all quantities given in the tables in the following pages are in c.g.s. system units.

(i) System: 2m.m. B./H_2O.

For this system, growth properties were calculated for fluidising velocities of 3.72 cms./sec. and 4.28 cms./sec. for the 1½" I.D.T. and, for the 1" I.D.T., the fluidising velocity of 4.04 cms./sec.

For the first of these situations, $\bar{u}_o$ = 3.72 cms./sec., $\bar{\varepsilon}$ = 0.418, $n_o \beta'_o/\beta_o$ = 2.92, $\chi_o \sim 30$ poise and the maximum value of $|d\Omega/d\varepsilon|$ used in the calculations was 240 dynes/cm^2 unit voidage change. With the constant c' set equal to -20, a radial wave number of 0.61 cms.$^{-1}$ was obtained.

The figures given below are extracted from the computer print-out.

With $(\alpha_o + 2\chi_o) = 90$, $|d\Omega/d\varepsilon| = 100$, $k_\rho = 0.61$,

λ	k_x	ξ	f	V_p	Δx
6.28	1.0	0.230	1.37	8.62	37.4
4.19	1.5	0.187	1.59	6.67	35.6
3.14	2.0	0.121	1.61	5.07	41.8

and with $(\alpha_o + 2\chi_o) = 90$, $|d\Omega/d\varepsilon| = 150$, $k_\rho = 0.61$,

λ	k_x	ξ	f	V_p	Δx
12.57	0.5	0.030	0.83	10.48	345.8
6.28	1.0	0.128	1.37	8.63	67.2
4.19	1.5	0.035	1.59	6.68	189.0
3.14	2.0	-0.072	1.61	5.07	-70.0

The measured values are, in the same order,

4.24	1.48	0.151	1.56	6.62	43.7

In both cases quoted, the minimum in the $\Delta x - k_x$ relationship lies somewhere between $k_x = 1.0$ and $k_x = 1.5$ and the values of the two minima straddle the experimental value, as do the corresponding values of the amplification factor. The agreement between the experimental values of the frequency and phase velocity* and the calculated values of these quantities at $k_x = 1.5$ is very good. Thus a value of $|d\Omega/d\varepsilon|$ somewhere between 100 and 150, retaining the same values of $(\alpha_o + 2\chi_o)$ and k_ρ would give predicted propagation properties which correspond almost exactly to the experimental values.

With $\bar{u}_o = 4.28$ cms./sec. and $\bar{\varepsilon} = 0.451$, the bed parameters obtained from Appendix 2 are $n_o \beta'_o / \rho_\Theta = 2.70$ and $\chi_o \sim 20$ poise. The maximum value of $|d\Omega/d\varepsilon|$ is 230. Computational results are as follows - (over page)

---

*. It is of interest to compute the group velocity, given in Chapter 3 as $2\pi (df/dk_x)$, at the wave-length of maximum amplification. From graphs of frequency vs. axial wave number for the tabulated values above (for $\bar{u}_o = 3.72$ cms./sec.), the group velocity is calculated to be 4.8 cm./s at $k_x = 1.0$ and 1.5 cms./sec. at $k_x = 1.5$ cms.$^{-1}$/sec. The predicted group velocity is very much less than the measured velocity which can thus be identified with the phase velocity. This conclusion is borne out by calculations on the other systems investigated.

With $(\alpha_o + 2\chi_o) = 40$, $|d\Omega/d\varepsilon| = 100$, $k_\rho = 0.61$.

λ	k_x	ξ	f	V_p	Δx
6.28	1.0	0.481	1.57	9.89	20.6
4.19	1.5	0.588	1.99	8.35	14.2
3.14	2.0	0.498	2.18	6.86	13.8
2.51	2.5	0.378	2.22	5.59	14.8

$(\alpha_o + 2\chi_o) = 40$, $|d\Omega/d\varepsilon| = 200$, $k_\rho = 0.61$.

λ	k_x	ξ	f	V_p	Δx
12.57	0.5	-0.003	0.89	11.28	-3401.2
6.28	1.0	0.211	1.58	9.93	47.2
4.19	1.5	0.151	2.00	8.39	55.7

$(\alpha_o + 2\chi_o) = 60$, $|d\Omega/d\varepsilon| = 100$, $k_\rho = 0.61$.

λ	k_x	ξ	f	V_p	Δx
6.28	1.0	0.320	1.43	9.01	28.1
4.19	1.5	0.316	1.72	7.20	22.8
3.14	2.0	0.232	1.79	5.62	24.2

The measured values of the propagation properties were

5.14	1.22	0.398	1.74	8.95	22.5

In this case, a value of $(\alpha_o + 2\chi_o)$ somewhat greater than 40 poise and a value of $|d\Omega/d\varepsilon|$ between 100 and 200 (but probably closer to 100) would predict propagation properties very close to those actually obtained.

For the 1" I.D.T., $\bar{u}_o = 4.04$ cms./sec. and $\bar{\varepsilon} = 0.457$ give bed parameters $n_o \beta_o'/\beta_o = 2.66$, $\chi_o \sim 20$ poise and a maximum value of 195 for the normal stress term. The constant $c' = -20$ gives a radial wave number of 0.72 cms.$^{-1}$.

For this situation the comparison cannot be so exact because the results are much less complete than the others. However computation gives the following results.

$(\alpha_o + 2\chi_o) = 60$, $|d\Omega/d\varepsilon| = 100$, $k_\rho = 0.72$

λ	k_x	ξ	f	V_p	Δx
6.28	1.0	0.187	1.32	8.28	44.2
4.19	1.5	0.182	1.60	6.69	36.7
3.14	2.0	0.107	1.68	5.28	49.5

$(\alpha_o + 2\chi_o) = 80, |d\Omega/d\varepsilon| = 100, \quad k_p = 0.72$

λ	k_x	ξ	f	V_p	Δx
12.57	0.5	0.005	0.73	9.16	1762.7
6.28	1.0	0.108	1.20	7.56	69.8
4.19	1.5	0.081	1.40	5.87	72.5

The actual values are

4.50	1.40	—	1.3	5.84	—

The agreement in this case is not nearly so striking, although the predicted values are still reasonably close to the experimental values. It should be borne in mind, however, that the experimental results for this situation are very much more inaccurate than those for the previous two situations. It is felt, in fact, from the other frequency measurement in this tube and from the way the propagation properties vary from tube to tube for other systems, that the frequency result is probably too low and hence, the wave-length too high. The value of the radial wave number might also be rather low considering the rather large value of d_p/d_t. However reasonable values for $(\alpha_o + 2\chi_o)$ and $|d\Omega/d\varepsilon|$ would appear to be around 60 poise and 100 dynes/cm.^{2} unit voidage change.

Thus for the three cases considered above, it is seen that the equations of motion predict propagation properties in very good agreement with the experimental values, given a suitable choice of bed parameters and it is fairly obvious that an investigation of the remaining two situations would yield the same conclusions. However the high degree of accuracy obtained with the prediction of growth properties for the first situation discussed above is probably rather fortuitous. Because of the uncertainties in the various terms, it would seem unlikely that the equations always give such exact agreement, although they should predict values reasonably close to those measured - assuming, of course, that the equations are in fact correct.

Even making allowance for the somewhat arbitrary values assigned to the particulate phase stress tensor terms, the values necessary to give agreement with experiment are remarkably consistent. For the values of the shear "viscosity" used (extrapolated from the two known systems), it would seem that $(\alpha_o + 2\chi_o) \sim 3\chi_o$. For the normal stress term, the value necessary seems to be $\left|\frac{d\Omega}{d\varepsilon}\right| \sim \frac{1}{2}\rho_f \bar{u}_o^2 \frac{(1-\varepsilon)}{\varepsilon^2}\left(1 + \frac{\theta(\varepsilon)}{\varepsilon}\right)$

(ii) System: No. 3 B./H_2O.

For the 1" I.D.T., the flow rates investigated were $\bar{u}_o$ = 2.72 cms./sec. and $\bar{u}_o$ = 2.89 cms./sec. and for the ½" I.D.T., the flow rate chosen was 2.53 cms./sec.

For a flow rate of 2.72 cms./sec., $\bar{\varepsilon}$ = 0.483, $n_o\beta'_\omega/\beta_o$ = 2.64, χ_o = 8 poise and the maximum value of $|d\Omega/d\varepsilon|$ used in the calculations was 70 dynes/cm.^{2} unit voidage change. With c' = -20, the radial wave number for the 1" I.D.T. was 0.95 cms.$^{-1}$ The following results were obtained -

$(\alpha_o + 2\chi_o)$ = 16, $|d\Omega/d\varepsilon|$ = 70, k_ρ = 0.95.

λ	k_x	ξ	f	V_p	Δx
4.19	1.5	0.188	1.53	6.42	34.2
3.14	2.0	0.266	1.91	6.00	22.6
2.51	2.5	0.274	2.20	5.53	20.2
2.09	3.0	0.214	2.41	5.05	23.7

$(\alpha_o + 2\chi_o)$ = 16, $|d\Omega/d\varepsilon|$ = 35, k_ρ = 0.95.

λ	k_x	ξ	f	V_p	Δx	
4.19	1.5	0.329	1.53	6.42	19.5	
3.14	2.0	0.470	1.91	6.00	12.7	
2.51	2.5	0.549	2.20	5.53	10.0	
2.09	3.0	0.562	2.41	5.05	9.0	
1.80	3.5	0.525	2.55	4.57	8.7	MIN.

$(\alpha_o + 2\chi_o)$ = 24, $|d\Omega/d\varepsilon|$ = 35, k_ρ = 0.95.

λ	k_x	ξ	f	V_p	Δx
4.19	1.5	0.257	1.44	6.04	23.5
3.14	2.0	0.332	1.75	5.49	16.6
2.51	2.5	0.345	1.96	4.92	14.3
2.09	3.0	0.312	2.09	4.37	14.0
1.80	3.5	0.260	2.15	3.86	14.8

The actual values of the propagation properties are

3.21	1.96	0.422	1.83	5.87	13.9

Because the frequency and phase velocity appear to be practically independent of the normal stress term, a value of $(\alpha_o + 2\chi_o)$ somewhere between 16 and 24 poise would give the experimental values of these quantities at a wave number of approximately 2.00 cms. A value of the normal stress term between 35 and 70 should give a growth distance corresponding to the experimental growth distance at the measured axial wave number.

For $\bar{u}_o = 2.89$ cms./sec., $\bar{\varepsilon} = 0.496$, $n_o \beta_o' / \beta_o = 2.57$, $\chi_o \sim 6$ p., and the maximum value of $|d\Omega/d\varepsilon|$ is again approximately 70.

$(\alpha_o + 2\chi_o) = 12$, $|d\Omega/d\varepsilon| = 35$, $k_\rho = 0.95$

λ	k_x	ξ	f	V_p	Δx
4.19	1.5	0.395	1.59	6.66	16.9
3.14	2.0	0.587	2.00	6.28	10.7
2.51	2.5	0.720	2.33	5.86	8.1
2.09	3.0	0.780	2.59	5.42	7.0

$(\alpha_o + 2\chi_o) = 12$, $|d\Omega/d\varepsilon| = 70$, $k_\rho = 0.95$

λ	k_x	ξ	f	V_p	Δx
4.19	1.5	0.241	1.59	6.67	27.6
3.14	2.0	0.364	2.00	6.30	17.3
2.51	2.5	0.416	2.34	5.88	14.1
2.09	3.0	0.391	2.60	5.44	13.9
1.80	3.5	0.297	2.78	5.00	16.8

$(\alpha_o + 2\chi_o) = 18$, $|d\Omega/d\varepsilon| = 35$, $k_\rho = 0.95$

λ	k_x	ξ	f	V_p	Δx
4.19	1.5	0.322	1.51	6.33	19.6
3.14	2.0	0.441	1.86	5.84	13.2
2.51	2.5	0.490	2.11	5.31	10.8

The actual values obtained are

3.14	2.0	0.496	1.94	6.10	12.3

None of the computer results correspond exactly with the experimental results, although they are very similar. It is possible that the radial wave number is too high, as is shown by the results below for $k_\rho = 0$.

$(\alpha_o + 2\chi_o) = 18$, $|d\Omega/d\varepsilon| = 70$, $k_\rho = 0$

λ	k_x	ξ	f	V_p	Δx
4.19	1.5	0.318	1.58	6.62	20.8
3.14	2.0	0.378	1.94	6.08	16.1
2.51	2.5	0.350	2.19	5.52	15.8
2.09	3.0	0.251	2.37	4.95	19.7

The minimum in the growth distance curves occurs at a value of k_x very close to the experimental values and the values of frequency and phase velocity are also in line. The predicted growth distance is rather

large but with lower values of $|d\Omega/d\varepsilon|$ together with a value of k_ρ smaller than 0.95, but still considerably greater than 0, the experimental values could probably be achieved. Thus it would appear that $(\alpha_o + 2\chi_o)$ lies between $2\chi_o$ and $3\chi_o$ and $|d\Omega/d\varepsilon|$ is rather less than $\rho_f \bar{u}_o^2 \frac{(1-\varepsilon)}{\varepsilon^3}\left(1+\frac{\Theta(\varepsilon)}{\varepsilon}\right)$

The experimental results for the ½" I.D.T. are less reliable and much less complete than the 1" I.D.T. results. This is especially true of voidage, since wall effects might be quite significant in the narrow diameter tube. For $\bar{u}_o = 2.53$ cms./sec., $\bar{\varepsilon} = 0.503$, $n_o \beta'_o/\beta_o = 2.53$, $\chi_o \sim 6$ poise. The maximum value of $|d\Omega/d\varepsilon|$ was again taken as 70. The radial wave number in this case was 1.26 cms.$^{-1}$ Calculations give

$(\alpha_o + 2\chi_o) = 12$, $|d\Omega/d\varepsilon| = 35$, $k_\rho = 1.26$

λ	k_x	ξ	f	V_p	Δx
2.51	2.5	0.367	2.00	5.03	13.7
2.09	3.0	0.402	2.24	4.69	11.7
1.80	3.5	0.394	2.42	4.34	11.0
1.57	4.0	0.353	2.55	4.00	11.4

$(\alpha_o + 2\chi_o) = 18$, $|d\Omega/d\varepsilon| = 35$, $k_\rho = 1.26$

λ	k_x	ξ	f	V_p	Δx
2.51	2.5	0.228	1.82	4.56	20.0
2.09	3.0	0.218	1.98	4.15	19.1
1.80	3.5	0.180	2.09	3.75	20.9
1.57	4.0	0.129	2.15	3.38	26.3

Experimental values are

1.7	3.7	—	2.3	3.92	—

Again a value of $(\alpha_o + 2\chi_o)$ between 12 and 18 will produce "correct" frequency and phase velocity, and a value of $|d\Omega/d\varepsilon|$ greater than 35 would probably lengthen the growth distance sufficiently to make it greater, at the measured axial wave number, than the growth distances obtained in the 1" I.D.T..

On the whole, theoretical predictions correspond quite well with the experimental values. The picture which emerges is similar to that from the first system studied (2 m.m. B./H_2O) in that reasonable estimates of the

particulate phase stress tensor terms are

$$(\alpha_o + 2\chi_o) \sim 3\chi_o.$$

$$\left|\frac{d\Omega}{d\varepsilon}\right| \sim \frac{1}{2}\rho_f \bar{u}_o^2 \frac{(1-\varepsilon)}{\varepsilon^3}\left(1+\frac{\theta(\varepsilon)}{\varepsilon}\right)$$

Note that $|d\Omega/d\varepsilon|$ is not much greater than the above quantity.

(iii) System: No. 5 B./H_2O.

For this system, one situation in the 1" I.D.T. and two situations in the ½" I.D.T. were investigated on the computer.

For the 1" I.D.T., $\bar{u}_o$ = 1.34 cms./sec. and $\bar{\varepsilon}$ = 0.469. The values of the bed parameters used were as follows – $n_o \beta'_o/\beta_o$ = 3.38, $\chi_o \sim 5$ poise. The value of the quantity $\rho_f \bar{u}_o^2 (1-\varepsilon)(1+\theta(\varepsilon)/\varepsilon)/\varepsilon^3$ for this situation is 19 dynes/cm.^{2} unit voidage change but calculations were carried out with $|d\Omega/d\varepsilon|$ = 15 and 30. Unlike all other calculations, the value of c' used to obtain the radial wave number was taken as –5 instead of –20 and this explains the relatively high value of k_ρ. However the wave numbers used are somewhat arbitrary and recalculation of this case with a more consistent wave number is hardly justified.

Predicted values of the propagation properties were as follows.

$(\alpha_o + 2\chi_o)$ = 15, $|d\Omega/d\varepsilon|$ = 30, k_ρ = 1.62

λ	k_x	ξ	f	V_p	Δx
3.14	2.0	0.055	1.32	4.14	75.3
2.51	2.5	0.086	1.58	3.97	46.1
2.09	3.0	0.104	1.81	3.79	36.3
1.80	3.5	0.107	2.00	3.59	33.7
1.57	4.0	0.092	2.16	3.39	36.7

$(\alpha_o + 2\chi_o)$ = 20, $|d\Omega/d\varepsilon|$ = 15, k_ρ = 1.62

λ	k_x	ξ	f	V_p	Δx
3.14	2.0	0.099	1.27	3.97	40.0
2.51	2.5	0.135	1.50	3.78	28.0
2.09	3.0	0.157	1.70	3.56	22.6

$(\alpha_o + 2\chi_o)$ = 20, $|d\Omega/d\varepsilon|$ = 30, k_ρ = 1.62

λ	k_x	ξ	f	V_p	Δx
3.14	2.0	0.038	1.27	3.98	104.6
2.51	2.5	0.057	1.50	3.78	66.7
2.09	3.0	0.061	1.70	3.56	58.7
1.80	3.5	0.049	1.86	3.33	67.8

The measured values of the growth properties are

2.45	2.57	0.131	1.52	3.70	28.2

It is seen that a value for $(\alpha_o + 2\chi_o)$ of 20 poise and $|d\Omega/d\varepsilon|$ with a value around 20 would give predicted values for the growth properties very close to those actually obtained.

For the $\frac{1}{2}$" I.D.T., the first situation investigated was $\bar{u}_o = 1.42$ cms./sec $\bar{\varepsilon} = 0.504$. The parameter values used were $n_o \beta'_o/\beta_o = 3.45$, $|d\Omega/d\varepsilon|$ equal to 18 and 36. The shear viscosity from Appendix 2 is given as 3 poise but was taken as 4 poise in the calculations. The value of c' was this time taken as -20, giving a value of 1.61 for the radial wave number.

The computational results are -

$(\alpha_o + 2\chi_o) = 16$, $|d\Omega/d\varepsilon| = 18$, $k_\rho = 1.61$

λ	k_x	ξ	f	V_p	Δx
2.09	3.0	0.183	1.80	3.78	20.7
1.80	3.5	0.194	1.98	3.56	18.3
1.57	4.0	0.189	2.12	3.33	17.6
1.40	4.5	0.170	2.22	3.10	18.3

$(\alpha_o + 2\chi_o) = 16$, $|d\Omega/d\varepsilon| = 36$, $k_\rho = 1.61$.

λ	k_x	ξ	f	V_p	Δx
2.51	2.5	0.053	1.59	4.00	75.2
2.09	3.0	0.058	1.81	3.78	65.7
1.80	3.5	0.043	1.98	3.56	81.9
1.57	4.0	0.012	2.12	3.33	272.3

The actual values obtained were

1.73	3.63	0.088	2.01	3.46	39.1

The correspondence in this case is very good. A value of the particulate phase normal stress term not much greater than 18 would probably increase the minimum growth distance sufficiently and reduce the corresponding value of the axial wave number far enough to give an almost exact correspondence.

The conditions for the second case investigated in the 1" I.D.T. were $\bar{u}_o = 1.77$ cms./sec., $\bar{\varepsilon} = 0.541$. For this situation, $n_o \beta'_o/\beta_o = 3.10$, χ_o was again taken as 4 poise, although the value given in Appendix 2 for this situation is actually 2 poise. As before, $|d\Omega/d\varepsilon|$ was given the values 18 and 36 (the value of the quantity $\rho_f \bar{u}_o^2 (1-\varepsilon)(1+\Theta(\varepsilon))/\varepsilon^3$) used as

a starting point for $|d\Omega/d\varepsilon|$ in the calculations is 17.5). The experimental data were such that the growth distance could not be evaluated but a value of 30 cms. would seem reasonable from the other results obtained with this system and tube size.

Computed values for the growth properties are -

$(\alpha_o + 2\chi_o) = 12$, $|d\Omega/d\varepsilon| = 18$, $k_\rho = 1.61$.

λ	k_x	ξ	f	V_p	Δx
2.09	3.0	0.264	1.92	4.03	15.3
1.80	3.5	0.283	2.11	3.79	13.4
1.57	4.0	0.281	2.25	3.54	12.6
1.40	4.5	0.260	2.36	3.30	12.7

$(\alpha_o + 2\chi_o) = 8$, $|d\Omega/d\varepsilon| = 36$, $k_\rho = 1.61$.

λ	k_x	ξ	f	V_p	Δx
2.09	3.0	0.200	2.08	4.36	21.8
1.80	3.5	0.222	2.32	4.17	18.8
1.57	4.0	0.218	2.52	3.97	18.2
1.40	4.5	0.189	2.69	3.76	19.9

The experimental values are -

1.77	3.55	—	2.40	4.23	30

The correspondence in this case is not very exact, especially with regard to the frequency and phase velocity. However a value of $(\alpha_o + 2\chi_o)$ between 8 and 12 and a value of $|d\Omega/d\varepsilon|$ between 18 and 36 might bring the dominant wave-length into line. However all quantities are of the correct order and the disagreement is not terribly great.

In general, for the above three cases, the predictions of the equations of motion are more or less consistent with the experimental growth properties. Unlike the previous two systems discussed, however, agreement between theory and experiment seem to be reached when $(\alpha_o + 2\chi_o)$ is of the order of $4\chi_o$ and when $|d\Omega/d\varepsilon|$ lies between $\rho_f \bar{u}_o^2 (1-\varepsilon)(1+\theta(\varepsilon)/\varepsilon)/\varepsilon^3$ and twice this quantity.

(iv) System: No. 7 B./H_2O.

All measurements on this system were carried out in the $\frac{1}{2}$" I.D.T. and computations were done for two of the experimental situations.

The first situation was $\bar{u}_o = 0.98$ cms./sec., $\bar{\varepsilon} = 0.507$. Values of the bed parameters are $n_o \beta'_o/\beta_o = 3.42$, and $\chi_o = 3$ poise, even though the assumed value in Appendix 2 was listed as 2 poise. The value of

$$\rho_f \bar{u}_o^2 \frac{(1-\varepsilon)}{\varepsilon}\left(1+\frac{\Theta(\varepsilon)}{\varepsilon}\right)$$

for this situation is 8, and the calculations covered the range 4 to 16. A radial wave number of 1.89 cms.$^{-1}$ is obtained with $c' = -20$.

The computed values of the propagation properties are -

$(\alpha_o + 2\chi_o) = 9$, $|d\Omega/d\varepsilon| = 12$, $k_\rho = 1.89$.

λ	k_x	ξ	f	V_p	Δx
1.80	3.5	0.105	1.61	2.90	27.5
1.57	4.0	0.124	1.79	2.81	22.7
1.40	4.5	0.137	1.95	2.72	19.8
1.26	5.0	0.144	2.09	2.62	18.2

$(\alpha_o + 2\chi_o) = 9$, $|d\Omega/d\varepsilon| = 16$, $k_\rho = 1.89$.

λ	k_x	ξ	f	V_p	Δx
1.57	4.0	0.090	1.79	2.81	31.2
1.40	4.5	0.097	1.95	2.72	28.0
1.26	5.0	0.098	2.09	2.62	26.7
1.14	5.5	0.093	2.21	2.53	27.2

The measured values are

1.48	4.25	0.104	1.86	2.76	26.6

Thus a value of 9 for $(\alpha_o + 2\chi_o)$ gives the experimental frequency and phase velocity but the minimum value of the growth distance does not occur at the measured dominant wave-length. This could be effected by increasing the value of $|d\Omega/d\varepsilon|$ but the growth distance would probably be increased beyond the measured value. However the agreement is not unreasonable.

For the second set of calculations, $\bar{u}_o = 1.10$, $\bar{\varepsilon} = 0.519$, $n_o \beta'_o/\beta_o = 32.9$, χ_o was again taken as 3 poise and the range of values for $|d\Omega/d\varepsilon|$ was, as before, 4 to 16.

$(\alpha_o + 2\chi_o) = 6$, $|d\Omega/d\varepsilon| = 12$, $k_\rho = 1.89$.

λ	k_x	ξ	f	V_p	Δx
1.80	3.5	0.164	1.77	3.18	19.3
1.57	4.0	0.199	1.97	3.10	15.6
1.40	4.5	0.229	2.16	3.02	13.2

$(\alpha_o + 2\chi_o) = 6$, $|d\Omega/d\varepsilon| = 16$, $k_\rho = 1.89$.

λ	k_x	ξ	f	V_p	Δx
1.80	3.5	0.132	1.77	3.18	24.1
1.57	4.0	0.160	1.97	3.10	19.4
1.40	4.5	0.182	2.16	3.02	16.6

$(\alpha_o + 2\chi_o) = 9$, $|d\Omega/d\varepsilon| = 16$, $k_\rho = 1.89$.

λ	k_x	ξ	f	V_p	Δx
1.80	3.5	0.100	1.68	3.02	30.3
1.57	4.0	0.114	1.86	2.92	25.6
1.40	4.5	0.121	2.02	2.82	23.2
1.26	5.0	0.121	2.15	2.71	22.4
1.14	5.5	0.113	2.27	2.59	23.0

Actual values are

1.55	4.06	0.128	1.97	3.05	23.8

The frequency and phase velocity agree at the experimental dominant wave-length, when $(\alpha_o + 2\chi_o) = 6$, but the predicted dominant wave-length and growth distance are rather low. With $(\alpha_o + 2\chi_o) = 9$ and $|d\Omega/d\varepsilon| = 16$, the predicted dominant wave-length is approximately 1.25, but the frequency is increased and the phase velocity decreased.

In the above two cases agreement between predicted and measured values, while not being completely exact, is sufficiently good for the present purpose. Similar to the other relatively small ballotini grade, a reasonable value for $(\alpha_o + 2\chi_o)$ would seem to be $4\chi_o$, and for the normal stress term, a value

$$\left|\frac{d\Omega}{d\varepsilon}\right| \sim 2\rho_f \bar{u}_o^2 \frac{(1-\varepsilon)}{\varepsilon^3}\left(1 + \frac{\theta(\varepsilon)}{\varepsilon}\right)$$ is in keeping with the results.

(v) System: Polystyrene Beads / H_2O.

For this system, the fluid velocity and voidage were quite unknown. However the Richardson and Zaki equations (21) were used to calculate the fluidising velocity for an assumed voidage of 0.450 from the known physical properties and an estimated terminal velocity. For this voidage, the estimated velocity was $\bar{u}_o = 0.20$ cms./sec.; this is in keeping with a rough estimate obtained from the rotameter (for which no exact calibration was available) used to monitor the water flow.

Calculations were carried out with the following assumed values of the parameters - $n_o \beta'_o/\beta_o = 3$, $(\alpha_o + 2\chi_o) = 20$ p. (probably very high) and $|d\Omega/d\varepsilon| = 20$. The physical properties of the beads were $\rho_s = 1.06$ gms./cc. and $d_p = 0.092$ cms.

As stated in Chapter 7, no disturbances were visible at all in this system and the results of calculations for the growth properties are quite consistent with this observation. For $(\alpha_o + 2\chi_o) = 0$, $|d\Omega/d\varepsilon| = 0$, the frequency increased linearly to 0.66 c/sec. at $k_x = 6.5$ cms.$^{-1}$ and the phase velocity was constant at 0.64 cms./sec. With $(\alpha_o + 2\chi_o) = 10$ p., the frequency was reduced to a maximum value of 0.20 c.p.s. at $k_x = 4.0$ cms.$^{-1}$, corresponding to a phase velocity of 0.35 cms./sec. and a growth distance of about 40 cms. Inclusion of the normal stress term immediately made the amplification factor go negative.

Thus it is hardly surprising, from the results quoted above, that disturbances were not visible in the bed.

The above comparisons demonstrate quite adequately that the equations of motion can give predictions of the growth properties of small disturbances which are consistent with experiment. Although exact agreement was not obtained in all cases, this is not wholly unexpected because of the insufficiently exact experimental results and an almost total lack of information on several of the parameters appearing in the theoretical equations. Variation of these unknown quantities within reasonable limits was found to almost always produce a set of predicted propagation properties close to the experimental

results. (In the comparisons above where agreement is not exact, sets of predicted properties are quoted which generally straddle the experimental values and inspection of the bed parameters used shows roughly the values necessary to give better agreement). Manipulation of these several unknown quantities to give agreement with the experimental work in no way invalidates the comparison as it was found that the required values of these unknowns varied in a consistent and well defined manner from system to system. Thus in addition to being fairly convincing evidence for the form of the equations of motion, the comparisons also give useful information about hitherto largely unknown bed parameters.

There is some doubt about the experimental values of $\bar{u}_o$ and $\bar{\varepsilon}$ being truly representative of the conditions determining disturbance propagation at the foot of the bed. It was shown earlier in this chapter that, for situations where the ratio d_p/d_t is high, the superficial fluid velocity and the overall mean voidage may be overestimates of the actual growth determining conditions. However it is readily shown by computation of a few cases that an increase in (with a corresponding increase in $n_o\beta'_o/\beta_o$) causes a decrease in frequency, phase velocity and amplification factor if $\bar{u}_o$ and all other parameters are kept constant. On the other hand, an increase of $\bar{u}_o$ with all other quantities constant causes an increase in the growth quantities mentioned above. Hence if they are overestimates, the use of $\bar{u}_o$ and $\bar{\varepsilon}$ will give rise to effects which to some extent cancel each other out.

However the real unknowns in this situation are the radial wave number, the virtual mass term and the two terms arising from the particulate phase stress tensor.

In retrospect, the method used to evaluate the radial wave number is rather inconsistent; for example, keeping $c' = -20$ in all the calculations gives a radial wave number of 0.72 for the system 2 m.m. B./H_2O in a 1" I.D.T. ($d_p/d_t = 0.082$) compared to a value of 0.92 for the radial wave number of the system No. 3 B./H_2O in the same tube ($d_p/d_t = 0.050$). If, as postulated, the boundary conditions for an axisymmetric disturbance are strongly dependent on the ratio of particle diameter to tube diameter, then it would be expected that the radial wave number for the smaller ballotini would be less than that for the large ballotini in the same tube. A rather more consistent method

of evaluating boundary conditions for an axisymmetric disturbance in a small tube is to assume that the extent of the uniform core is given, as before, by

$$d_u = d_t \left(1 - c' \, d_p/d_t \right)$$

with c' some positive constant, say, in the range $c' < 10$. A piston source of disturbances is then assumed to act over the flow area and the walls are assumed to inhibit all disturbances to the same extent, no matter the tube size provided only one mode appears in the tube. Thus $n_1 \left(x, \frac{d_u}{2} \right) = a \, n_1 (x,0)$ where a is constant in the range $0 < a < 1.0$. It is obvious from experimental observations (see Plate 5.1) that the walls do not inhibit the disturbances to a very marked extent and a value of the constant "a" somewhere between 0.5 and 0.75 would be a reasonable guess.

Thus if the disturbance at the edge of the uniform core is assumed to be 0.75 times the disturbance at the tube centre,

$$J_o (k_\rho \cdot \rho) = 1.00 \text{ at } \rho = 0$$

$$\text{and } J_o (k_\rho \cdot \rho) = 0.75 \text{ at } \rho = d_u/2$$

$$\text{so that } k_\rho = 2/d_u.$$

If the constant c' is given the value 4, the system 2 m.m. B./H_2O, 1" I.D.T. has $k_\rho = 1.17$ cms.$^{-1}$ and the system No. 3 B./H_2O, 1" I.D.T. has $k_\rho = 0.98$ cms.$^{-1}$

Time did not permit recalculation of the cases discussed above with more consistent wave numbers. The effects the above method would have are listed below. The radial wave numbers given are for $a = 0.75$ and $c' = 4$. The radial wave numbers actually used in the calculations are given in brackets.

2 m.m. B./H_2O.	1½" I.D.T. :	d_u = 2.99,	k_ρ = 0.67	(0.61)	
2m.m. B./H_2O.	1" I.D.T. :	d_u = 1.71,	k_ρ = 1.17	(0.72)	
No. 3 B./H_2O.	1" I.D.T. :	d_u = 2.03,	k_ρ = 0.98	(0.95)	
No. 3 B./H_2O.	½" I.D.T. :	d_u = 1.06,	k_ρ = 1.88	(1.26)	
No. 5 B./H_2O.	1" I.D.T. :	d_u = 2.20,	k_ρ = 0.91	(1.62)*	
No. 5 B./H_2O.	½" I.D.T. :	d_u = 0.93,	k_ρ = 2.16	(1.61)	
No. 7 B./H_2O.	½" I.D.T. :	d_u = 1.02,	k_ρ = 1.97	(1.89)	

* for this situation c' was taken as -5 unlike the others for which $c' = -20$.

These figures, if used, might change the picture slightly for the systems 2 m.m. B./H_2O, 1" I.D.T., No. 3 B./H_2O, $\frac{1}{2}$" I.D.T., No. 5 B./H_2O, 1" I.D.T. and No. 5 B./H_2O, $\frac{1}{2}$" I.D.T. In each case, except for No. 5 B./H_2O, 1" I.D.T., it would probably necessitate slight reductions in the particulate phase stress tensor terms, but probably to not much lower a value than the lowest value quoted in the appropriate sections above. However there is no guarantee that these values are any more correct than the values used in the calculations - they are only a little more consistent.

The above method of estimating boundary effects is based on an assumed axial symmetry for one disturbance in a narrow tube. When the bed becomes wider this condition is not likely to be met because of unevenness in the porosity of the distributor. When the bed becomes very wide and several disturbances appear at any one time at different points in the flow area, then each disturbance must be treated as a separate entity by the equations. It is obvious that in this case the tube walls are unimportant and that the specific variation of voidage in the horizontal plane of each disturbance is governed by some other mechanism - probably again unevenness in the distributor causing unevenness in the flow through it.

From the detailed comparisons given above it was seen that agreement between theory and experiment was generally reached when the particulate phase stress tensor terms were of the following orders of size -

$$(\alpha_o + 2\lambda_o) \sim 3\lambda_o \text{ to } 4\lambda_o$$

$$\left|\frac{d\Omega}{d\varepsilon}\right| \sim \frac{1}{2}\rho_f \bar{u}_o^2 (1-\varepsilon)(1+\Theta(\varepsilon)/\varepsilon)/\varepsilon^3 \text{ to } 2\rho_f \bar{u}_o^2 (1-\varepsilon)(1+\Theta(\varepsilon)/\varepsilon)/\varepsilon^3$$

Obviously the exact size of these terms required depends on the values of the radial wave number used. However approximate agreement between theory and experiment can be reached with radial wave numbers taken as zero if the above stress parameters are increased sufficiently. For example, for the first situation discussed in the No. 3 B./H_2O system, approximate agreement with experiment requires that $(\alpha_o + 2\lambda_o)$ be of the order of 24 and that $35 < \left|\frac{d\Omega}{d\varepsilon}\right| < 70$ if the radial wave number is taken as zero. It is clear from this that, regardless of radial wave number, the quantity $(\alpha_o + 2\lambda_o)$ must be several times the value of the particulate phase shear "viscosity" and that

$\left|d\Omega/d\varepsilon\right|$ must be of the same order as the fluid momentum quantity $\rho_f \bar{u}_o^2 \frac{(1-\varepsilon)}{\varepsilon^3}\left(1+\frac{\Theta(\varepsilon)}{\varepsilon}\right)$

The second almost totally unknown quantity in the equations is the virtual mass coefficient $\Theta(\varepsilon)$. This quantity can have a profound effect on the amplification factor and the growth distance - as can be readily seen from Figure 4.9 - but it apparently has little or no effect on the frequency and phase velocity, although this is not at all obvious from the analytical expression for the angular frequency (equation (3,12)). Using values obtained from Figure 4.9, it can be shown that the value of the amplification factor λ at any axial wave number increases almost linearly with the virtual mass coefficient. Thus a decrease in the virtual mass coefficient from the value of 0.5 used throughout these calculations would reduce the amplification factor and hence increase the growth distance. This would then necessitate a decrease in either or both of the particulate phase stress tensor terms to obtain agreement with the measured growth distances; although it should be noted that changing the "viscosity" alters the frequency and phase velocity. Increasing the virtual mass coefficient has the opposite effect.

However not only is the actual value of the coefficient unknown, there is some doubt about the form of the term itself. The form

$$\frac{d}{dt}(\underline{u}-\underline{v}) = \left\{\frac{\partial \underline{u}}{\partial t} + (\underline{u}.\,\mathrm{grad})\underline{u}\right\} - \left\{\frac{\partial \underline{v}}{\partial t} + (\underline{v}.\,\mathrm{grad})\underline{v}\right\}$$

was used almost exclusively throughout this work. This leads to the coefficient of $d\varepsilon/dx$ in the voidage gradient equation (3,19) having the form

$$\left[\left|\frac{d\Omega}{d\varepsilon}\right| - \rho_f \bar{u}_o^2 \frac{(1-\varepsilon)}{\varepsilon^3}\left(1+\frac{\Theta(\varepsilon)}{\varepsilon}\right)\right]$$

A stable solution to equation (3,19) requires that this quantity be positive. If the alternative form of the virtual mass term is used, i.e.

$$\frac{d}{dt}(\underline{u}-\underline{v}) = \frac{\partial}{\partial t}(\underline{u}-\underline{v}) + (\underline{v}.\,\mathrm{grad})(\underline{u}-\underline{v})$$

then the coefficient of $d\varepsilon/dx$ in (3,19) is simply

$$\left[\left|\frac{d\Omega}{d\varepsilon}\right| - \rho_f \bar{u}_o^2 \frac{(1-\varepsilon)}{\varepsilon^3}\right]$$

and the condition for a stable solution is

$$\left|\frac{d\Omega}{d\varepsilon}\right| > \rho_f \bar{u}_o^2 \frac{(1-\varepsilon)}{\varepsilon^3}$$

For many of the situations discussed above, it was found that a value of $\left|\frac{d\Omega}{d\varepsilon}\right| \sim \frac{1}{2}\rho_f \bar{u}_o^2 \frac{(1-\varepsilon)}{\varepsilon^3}\left(1+\frac{\theta(\varepsilon)}{\varepsilon}\right)$ was necessary to give agreement between theory and experiment. For the voidage ranges encountered in this work, the quantity $(1 + \theta(\varepsilon)/\varepsilon)$ has a value of approximately 2 if $\theta(\varepsilon)$ is taken as 0.5. Thus the second form of the virtual mass term leads to values of $|d\Omega/d\varepsilon|$ which give agreement with experimental growth results and which are also consistent with the, admittedly assumed, stable solution of the voidage gradient equation. However, this form for the virtual mass term changes the equations for the growth properties. The roots of the auxiliary equation equivalent to (3,6) now have the form

$$s_{1,2} = \frac{B}{2A}\left[-\left(1+\frac{cD}{B}+j\frac{Fb}{B}\right) \pm \sqrt{}\right.$$

$$\left. \pm \sqrt{\left(1+\frac{Dc}{B}\right)^2 + 4\left(\frac{b}{B}\right)^2\left\{A-\frac{F}{4}-\frac{ADe}{b^2}\right\} - j4\left(\frac{b}{B}\right)\left\{AE-\frac{F}{2}-\frac{F}{2}\frac{Dc}{B}\right\}}\right]$$

where the quantity F is redefined as $F = 2 + \theta_o/\varepsilon_o$. With a virtual mass coefficient of 0.5, the amplification factor obtained from this revised equation will be intermediate in value between the amplification factor obtained with $\theta = 0.5$ and that obtained with $\theta = 0$. (The virtual mass term following the particle motion only is weaker in its effect than the virtual mass term following both particle and fluid motions; this result was discussed in Chapter 3.) This will in turn lengthen the predicted growth distance and the normal stress term might even have to be reduced below the least value quoted above, i.e. it is possible that $|d\Omega/d\varepsilon|$ may still have to be lower than $\rho_f \bar{u}_o^2(1-\varepsilon)/\varepsilon^3$. However this cannot be tested without extensive computer calculations on the actual systems.

All in all, the balance of evidence, and it is a very slight balance indeed, would seem to suggest that the virtual mass term should have the form

$$\frac{d}{dt}(\underline{u}-\underline{v}) = \frac{\partial}{\partial t}(\underline{u}-\underline{v}) + (\underline{v}.\text{grad})(\underline{u}-\underline{v})$$

Although the virtual mass term may be quite important in determining the behaviour of the bed, the calculations described above have highlighted yet again the essential part played by the particulate phase stress tensor terms in producing a dominant wave-length within any one situation. Very roughly the expected values of these terms would be

$$\alpha_o + 2\chi_o \sim 3\chi_o$$

and $\left|\frac{d\Omega}{d\varepsilon}\right| \sim \rho_f \bar{u}_o^2 \frac{(1-\varepsilon)}{\varepsilon^3}$

although the actual values might be greater or less than those quoted. This large value of the "viscosity" term implies a considerable value of the particulate phase bulk "viscosity" - about twice the value of the shear "viscosity" ($K = \alpha + \frac{2}{3}\lambda$ for the Newtonian character of the flow assumed in the present work). It must be emphasised that the use of the quantity $\rho_f \bar{u}_o^2(1-\varepsilon)/\varepsilon^3$ to evaluate $|d\Omega/d\varepsilon|$ does not mean that these two quantities are in any way physically related. Indeed they are quite distinct. Nor does it imply that, since these quantities were found to be of the same order of magnitude, voidage gradients are absent from the bed. The two quantities were found to be only of the same order of magnitude and not equal.

It is appropriate at this stage to mention the possible effects of voidage gradients on the predicted initial growth of disturbances. For this situation, the uniform force balance used to eliminate $\beta(\varepsilon_o)$ from the linearised equations must be replaced by the expression for $\beta(\varepsilon_o)$ obtained from equation (3,19). viz.

$$u_o \beta(\varepsilon_f) = (1-\varepsilon_f)(\rho_s - \rho_f) g - K$$

where ε_f is the voidage at the foot of the bed and K is some quantity dependent on $d\varepsilon/dx$ etc. For the initial disturbance growth covered by the linearised equations, K could be considered a constant, and moreover its value in comparison to $(1-\varepsilon_f)(\rho_s - \rho_f)g$ is likely to be small. Thus the effect of voidage gradients on the actual expressions for the growth quantities would not be too great. However a further degree of uncertainty is added to the actual estimate of the voidage at the foot of the bed and to the estimate of the drag parameter $n_o \beta_o'/\beta_o$.

Chapter 9

Discussion of the Present Work and Recommendations for Future Work

In the first few chapters of this work, general equations of motion and continuity were developed, based on the concept of continuum flow of both phases, for a dispersed two phase flow situation. These equations were further developed in detail for a fluidised bed. Because of their non-linear nature, it is possible to obtain a solution for these equations in only a limited number of cases and of these, only one - the stability of the state of uniform fluidisation - has been dealt with in any detail in this work. The investigation of this case, because of the linear form assumed by the equations, readily lends itself to theoretical and experimental treatment and was undertaken to test the proposed equations and to determine the relative importance of the various forces acting in the bed.

The main forces acting in the bed are body forces, the interaction force arising from the stress in the fluid acting on the particles (this gives rise to a fluid stress term due to bulk motion of the fluid and a viscous drag and virtual mass force arising from the rapid local variations in flow in the immediate vicinity of the particles) and particle-particle interaction forces due to collisions and interference. Previous investigations by Jackson (5) and Pigford (6) have shown that, if the effect of particle-particle interaction is neglected, the state of uniform fluidisation is unstable, i.e. a small perturbation in the flow fields which define this state will amplify as it propagates upwards through the bed. Solution of the equations showed that a disturbance component took the form of a monochromatic plane wave whose amplitude increased with time. The amplification factor and frequency are functions of the disturbance wave-length and the bed parameters. In the present work, a formal solution of the equations leads to the conclusion that small disturbances may either amplify or attenuate on propagation upwards through the bed. The difference lies in the inclusion of a term representing normal stresses caused by particle collisions, although other terms also cause some reduction in the amplification. However numerical work using reasonable values of the bed parameters indicate that most fluidised systems should in practice be unstable.

The conclusion that the state of uniform fluidisation is unstable is verified by experiment. Bubbles or voids are found to occur in most gas fluidised systems and in non-turbulent liquid fluidised systems, regular bands of reduced particle concentration are seen to rise upwards through the bed.

From the equations of motion and their solution, the principal cause of this instability is the inertia of the particles and the fluid. If these inertial terms are not included in the equations, stability is predicted. Inclusion of either one of these terms leads however to instability. The basic bed parameters arising from the drag and interaction forces are functions, in some cases quite unknown functions, of the physical properties of the system and the fluid flow rate, and these parameters determine the propagation properties of the growing disturbance. For particles of similar size, the solid to fluid density ratio determines to a major extent the speed and extent of disturbance growth - systems with a large value of this ratio amplify faster than systems with a small value of the ratio. However within any one situation, it is principally the parameters arising from the particle-particle interaction force which determine the dominant wave-length of any disturbances appearing in that situation, although the other bed parameters (e.g. drag coefficient, virtual mass coefficient) play their not inconsiderable part.

The "viscosity" coefficients of the particulate phase stress tensor, when this term is included in the equations, are responsible for the appearance of a disturbance wave-length which amplifies faster in time than any other wave-length. (This effect was first noted by Pigford (6)). However because a fluidised system is dispersive (i.e. phase velocity is a function of wave number) this maximum in the amplification factor-wave-length relationship does not necessarily produce a corresponding minimum growth distance. As it is the growth distance which determines the amplification of a disturbance with distance travelled, a maximum amplification factor does not necessarily mean that a dominant wave-length would appear from a spectrum of disturbances travelling up through the bed. The appearance of a minimum in the growth distance-wave number relationship is determined mainly by the particulate phase static normal stress term (equivalent to the hydrostatic pressure of a fluid) i.e. it is this quantity which is responsible for a disturbance component which amplifies fastest with distance, although an

extremely large "viscous" term alone might also have the same effect. The drag coefficient, which is much less of an unknown, fixes, together with the system properties and flow rate, the general order of the propagation properties as functions of axial wave number, but within this general situation, it is the particulate phase stress tensor terms which fix the dominant wave-length. The other unknown quantities modify the propagation properties of the dominant wave-length but their general effect is not nearly so spectacular.

Boundary conditions determine the horizontal components of the wave number vector and these components appear only in terms containing the parameters from the particulate phase stress tensor. Thus if these components are of much the same order as the axial wave number, their effect is merely to reinforce the effects of the "viscosity" term and the normal stress term. It would appear that, in general for the narrow tubes used in the present work, the horizontal wave number components are of the same order as, or lower than, the dominant vertical component of the wave number. The virtual mass coefficient appears to effect only the amplification factor and growth distance. Increase of the virtual mass coefficient increases the amplification factor presumably because this is also an effective increase of the particle inertia. However the above effects, although important from a quantitative viewpoint, are relatively minor compared to the predicted occurrence of a specific wave-length of maximum amplification with distance travelled. Out of a disturbance composed of components with a spectrum of wave-lengths, this component will emerge and dominate the other components.

The power spectra and autocorrelation functions obtained in the experimental work indicate clearly the emergence of a dominant frequency (the wave-length determines the frequency) from a spectrum of disturbance components close to the distributor. Propagation properties were measured for a number of systems and, in general, within the limitations of experimental accuracy and considering the lack of precise information about some of the bed parameters, the agreement between theory and experiment is good enough to justify the use of the proposed equations (2,17) and (2,18) to describe the phenomenon of fluidisation.

However information about the bed parameters - especially the particulate phase stress terms and the virtual mass coefficient - is still very inadequate. It was assumed in this work that the particulate phase "continuum" behaved as a quasi-Newtonian fluid and shear measurements in fluidised beds indicate that this is reasonable - at least for the linearised equations. Based on this assumption, a rough value for the bulk "viscosity" would seem to be about twice the shear "viscosity". The effect of the bulk "viscosity" in attenuating sound waves in a gas is well known and the effect in the present case is similar, but the very large value required is perhaps a little surprising. The normal stress term was found to be of the same order, or larger than the quantity $\rho_f \bar{u}_0^2(1-\varepsilon)/\varepsilon^3$, and an upper bound is set on $|d\sigma/d\varepsilon|$ by the requirement of instability of the bed. It is rather disappointing that the measured voidage profiles were not good enough to give any information about this term or about the validity of the arguments and speculations set out in the second section of Chapter 3. For the virtual mass term, the general indications are that the differential operator has the form

$$\frac{d}{dt}(\underline{u}-\underline{v}) = \frac{\partial}{\partial t}(\underline{u}-\underline{v}) + (\underline{v}.\text{grad})(\underline{u}-\underline{v})$$

but this conclusion presupposes a virtual mass coefficient of 0.5 as in the single particle case.

The experimental work shows that disturbances (or concentration waves) originate at the distributor and propagate upwards with a frequency and phase velocity characteristic of the system. The theoretical work shows also that the propagation properties are an inherent characteristic of the bed and are determined by its properties and not by external factors. All of these features tie in with Tamarin's qualitative explanation (29) of "the origin of self-excited oscillations in a fluidised bed". Briefly he maintains that as the flow rate is increased and the bed expands from its initial packed state, the voidage increases until the flow rate reaches a steady level. Because of the inertia of the particles they continue to move apart for a short period and hence this causes a reduction in drag force so that it drops below the equilibrium (i.e. uniform) value (this is due to voidage increase and simultaneous drop in the local fluid velocity). However this

"overshoot" must halt because there is not sufficient energy available in the fluid to keep the particles moving apart (the drag on the particles has dropped) and they move closer together again. Again their inertia causes them to overshoot the equilibrium spacing until the consequent increase in drag causes them to move apart. Thus according to Tamarin, a self-sustained train of oscillations in local voidage are set up. According to the linearised equations of motion, these small oscillations in the voidage at the foot of the bed amplify on propagation and cause complete instability of the uniformly fluidised state.

This explanation emphasises the importance of inertia in producing instability and shows that this instability is an inherent feature of the bed's behaviour caused by the initial expansion from the packed to the fluidised state. This is in accord with experience - disturbances are observed to appear immediately the bed becomes fluidised. These oscillations propagate through the bed because of the fluid motion and in accordance with continuity. If, as seems likely from the explanation quoted above, the amplitude of these oscillations at the distributor is small in magnitude, their initial growth from their point of origin should be well described by the linearised equations of motion.

One of the important results of the stability theory is that it distinguishes correctly between typically aggregative and typically particulate systems (see ref. (5) and Appendix 1). The results given in Appendix 1 were obtained from equations in which the solids stress terms and the virtual mass effect had been omitted. However there is no reason to suppose that including these terms would alter the general picture in any way - witness the results in Chapter 4 for the systems No. 5 B./H_2O and No. 5 B./AIR. Disturbances in typically aggregative systems amplify very rapidly while in typically particulate systems the growth is relatively slow. There is no direct evidence that the rapid amplification of disturbances causes them to develop into the complete voids which are the typical feature of aggregative beds, but the circumstantial evidence is strong indeed. Once the disturbances have developed to an appreciable size, the non-linearity of the equations become important and mathematically the growth cannot be followed further.

Because of the inhibition of the disturbance growth in particulate systems, the non-linear mechanism must act quite differently in the two cases. With aggregative systems, it might be thought that after the initial fast growth packing effects would limit the growth, but since with these systems, the disturbances can amplify to about three times their original amplitude in less than a wave-length, the development into a complete void could take place on almost the first high voidage swing, aided perhaps by the non-linear mechanism, even though packing effects limit the low voidage swing. A large part in this non-linear mechanism is probably played by the large density ratio, since the particle inertia will be comparatively great. Thus while packing effects limit the low voidage swing, the high voidage swing may continue its very rapid growth into a complete void; the rest of the bed being, as it were, "pushed" into a fairly close packed state. Pigford (6) has shown that the low voidage part of a sinusoidal disturbance propagates faster than the high voidage part so that distortion of the wave-form sets in. Thus a sort of shock-wave structure develops. Because the low voidage part of the disturbance ahead of the growing void is travelling faster, this shock-wave structure would complement and make easier the growth of the void. This tentative explanation is in keeping with the experimental observation that the dense phase in an aggregative bed is very close to the voidage at incipient fluidisation - this voidage being almost a packing limit - and with the apparent fairly sudden appearance of bubbles very close to the distributor. Once the bubble has formed, some important features of its behaviour can be deduced from the equations of motion (see Jackson (5)).

The significance of regular concentration waves in particulate systems was not generally appreciated before Jackson's work. Liquid fluidised systems used in any practical situation were generally turbulent. In general, two types of fluidised system were found to occur - bubbling beds (with streamline flow) and the homogenous particulate beds with turbulent flow. It is not at all clear why gas - fluidised beds should not also be turbulent unless the high concentrations of particles in the dense phase caused by the bubbles (and hence, by the initial fast growth of disturbances) prevent this. Regular disturbances do not appear in turbulent systems and it is highly unlikely that amplification of disturbances causes this turbulence. (see Chapter 6). The main theoretical difference between the two types of

system resides in the growth rate and it is probable that fast growth prevents the appearance of turbulence while slow growth allows the competing turbulence mechanism to set in. (This statement refers, of course, to beds which are normally turbulent and not to the systems studied in the present work). However the existence of quite large concentration waves in typical particulate systems to some extent renders superfluous the idea that there are two totally different types of fluidisation and that these are quite distinct.

A turbulent liquid fluidised system is similar in many respects to the ideal state of uniform fluidisation - and in fact is often identified with it - but differs from it in that the particle velocity $\underline{y}$ is not everywhere zero because of the large turbulent fluid eddies. The distinction between turbulent and non-turbulent beds has caused some confusion in the past. In a recent paper on turbulent heat and mass transfer, Ruckenstein (44) remarks that "the instability theory seems able to complete, in some cases, the information on the dependence of the diffusion coefficient given by the renewal models". This was illustrated by calculations of disturbance frequency in fluidised beds based on Pigford's results (6). The example is totally inappropriate within the context of this paper (a) because disturbances are not a turbulent phenomenon and (b) because they are not caused by external factors to any great extent but are an inherent characteristic of the system.

In general, although the non-linearity of the general equations makes it impossible to follow mathematically the complete disturbance growth, the linearised equations do give a ready means of predicting the type of fluidisation to be expected in any system, given a sufficient knowledge of the bed parameters. They highlight the crucial part played by inertia in causing the disturbances to appear and explain the factors determining the disturbance growth - thus filling-out our knowledge of the basic mechanics of fluidisation and of bubble formation in fluidised systems and giving an insight into the nature, size and significance of the forces acting in a fluidised bed.

Nevertheless a considerable amount of work remains to be done on the subject of disturbance growth - both to check the conclusions of the present work and to increase our knowledge of the bed parameters.

With the improvements in equipment suggested at the end of Chapter 7, measurements of disturbance growth and propagation should be extended to cover a wider range of fluid densities and viscosities in tubes of varying size. It is unlikely that much variation in particle density could be obtained because transparent particles (e.g. glass) are required by the light transmission technique. This limitation could be avoided if X-ray photographs of the bed were used to measure voidage changes, but careful development and calibration of the plates would be required. This method would be time-consuming, complex and costly.

If possible, power spectrum analysis should be used in any future work to measure growth and frequency. In addition, measurement of the frequency response function of sections of the bed (this would involve finding the cross power spectral density function for pairs of points in the bed) would provide a further check on theory as this quantity can be calculated for a sinusoidal disturbance component with a small amplitude. However coalescence and frequency change would complicate the problem enormously here.

In aggregative systems, measurement of bubble frequencies at their point of appearance just above the distributor would provide a worthwhile check on the assumption that disturbances develop into complete voids in this type of system. In narrow tubes with only one disturbance filling the whole flow area, frequencies are readily predicted from the equations of motion. It is envisaged that in an experiment of this type, tube diameters would be increased to the point where more than one bubble appeared and this would provide information on the boundary conditions and radial limits of a disturbance or bubble. This investigation would be relatively simple to carry out with either the light beam technique or with the capacitance ring technique as no calibration of the signal in terms of voidage is required. It might be, in fact, that the capacitance ring technique is all that can be used because of the possibility that the light beam would be completely obscured in the larger tubes.

The measurement of voidage gradients in the present work was quite unsatisfactory and this could best be done by either of two methods. One of these is to measure the pressure at a number of small intervals up the bed.

It is an observed fact of the present work that the pressure drop across the bed (excluding hydrostatic head) is equal to the buoyant weight of the particles and that the other quantities in equation (3,21) are small in comparison to these terms. If the steps are small enough so that each can be considered as having a uniform voidage, this step voidage can be obtained from the pressure drop measurements. The other method is the use of X-ray transmission. Since only a time-average point voidage is required, a small count-rate (and, hence, a small source) would suffice. The transmission equipment could perhaps be calibrated against packed beds of known voidage. For any of this work, it is essential that finely graded particles are used to eliminate segregation effects. Either of these methods should provide some basis on which to evaluate the unknown quantities in equations (3,21) and (3,19).

Two phenomena observed in this work and needing clarification are turbulence and slugging. Slugging occurs in both gas and liquid fluidised beds but the mechanism appears to be quite different in each case. In aggregative beds, the slugs are the result of normal bubble growth and coalescence until one bubble fills the whole flow area. This appears to be a fairly gradual happening. In liquid fluidised beds, there is an apparently abrupt transition from a normal disturbance filling the whole flow area to a complete void or slug. This may be partly the result of coalescence, but it is obvious, from the high values of the particle diameter to tube diameter ratio involved, that wall effects play a very important part in the process. The parameters governing the transition from streamline to turbulent flow in liquid fluidised beds are not known, and a programme of work to discover these and arrive at some transition criterion is necessary.

Finally more information is required on the bed parameters, especially the particulate phase stress terms and the virtual mass term. It must be ascertained just how reasonable is the assumption of the quasi-Newtonian character of the solids phase "continuum" and this will entail a study of the degree of anisotropy in the bed. (It seems likely that the bed is to some extent anisotropic because the bulk of the fluid flow is in the x-direction and thus particle random velocity components in the y and z directions are likely to be smaller than the x-direction component). This could perhaps

be done by measurement of particle velocity fluctuations. Further measurements of the shear "viscosity" of fluidised systems are also required. At present, however, the bulk "viscosity" is quite intractable. Unfortunately it is also one of the most important parameters. The form of the virtual mass term and evaluation of the coefficient may have to be inferred from the size of the normal stress term and from voidage gradient measurements coupled with the requirements of disturbance growth.

The present work has shown the important parameters for disturbance growth and has provided fairly rough estimates of these quantities. However it has also demonstrated just how scanty is our knowledge of the fine structure of these parameters and functions and how much work is yet to be done.

APPENDICES

APPENDIX 1

The following discussion appeared as a short note under the authorship of R. Jackson and the present writer in the journal Chemical Engineering Science (ref. (8), Chem. Eng. Sci., 19 (1964), P. 509):-

"The Nature of Aggregative and Particulate Fluidisation"

"In the past year or so accounts have been published of two different approaches to a theoretical explanation of the hitherto puzzling difference between the smooth or particulate fluidisation of most liquid fluidised systems and the bubbling or aggregative fluidisation of most gas fluidised systems.

In 1961, Harrison, Davidson and de Kock (45) published a theory of stability of bubbles in fluidised beds, postulating that a bubble can survive only if the maximum upward velocity of fluid in its interior does not exceed the free falling velocity of the particles fluidised in the bed. From this they were able to show that there would be a maximum stable bubble size for each system, characteristic of the particles and the fluidising fluid, and calculations showed this to be very large compared with the particle size in most gas fluidised systems and relatively small in most liquid fluidised systems. They therefore concluded that fluidisation is visibly aggregative when the maximum stable bubble size is large and particulate when it is small compared with the particle size.

More recently one of the present writers (5) investigated the hydrodynamic stability of the state of uniform fluidisation, and found that it is always unstable in the sense that small disturbances in the distribution of the particles will rise through the bed and will become more pronounced as they rise. The rate of growth is found to be very slow in most liquid fluidised systems, which will therefore fluidise quite smoothly. In most gas fluidised systems, on the other hand, the rate of growth is very rapid and a smoothly fluidised state cannot survive.

The purpose of the present note is to point out that these two

theories are not to be regarded as rival explanations of the phenomenon of aggregative and particulate fluidisation, but rather as complementary to each other.

The theory of Harrison et al. accounts for the possibility of large bubbles in certain fluidised systems, but says nothing whatever about the state of uniform fluidisation. Thus it shows that a large bubble, once formed, can survive in a gas fluidised bed, but it gives no reason for supposing that such bubbles would form, unless artificially injected. In particular, the theory gives no reason to suppose that the uniformly fluidised state could not exist perfectly stably in the absence of external disturbance, even in those systems which it shows to be capable of supporting large bubbles.

The stability theory proposed by one of the present writers, on the other hand, shows that uniform fluidisation is necessarily confined to certain systems, mostly fluidised by liquids, and that this state cannot survive in the majority of gas fluidised systems. However it gives no indication of what sort of behaviour will result from the breakdown of the uniformly fluidised state, and certainly does not show that the very characteristic bubbling pattern will develop.

The complementary nature of the two theories is revealed when one compares the growth distances of disturbances in the uniformly fluidised state, calculated from the stability theory (5), with the maximum stable bubble size, calculated from the theory of Harrison et al., for a number of different systems. Such a comparison is presented here in Table 1 for those systems investigated in the early work of Wilhelm and Kwauk (4), and it is seen that those systems for which the growth distance is long (i.e. the uniformly fluidised state is relatively stable) also have small values of the maximum stable bubble size, while those for which the growth distance is short (i.e. the uniformly fluidised state is highly unstable) also have large values of the maximum stable bubble size.

Table 1: Comparison of stability criteria for the systems investigated by Wilhelm and Kwauk

Particles	Fluid	d_p(cms)	Fr	x/D_d	D_{em}/d_p
Glass Beads	Water	0.029	0.00052	332	1.7
Sea Sand	Water	0.040	0.00062	320	2.7
Glass Beads	Water	0.051	0.00067	254	4.0
Sea Sand	Water	0.055	0.0013	155	4.9
Sea Sand	Water	0.101	0.0080	25.2	9.0
Socony Beads	Water	0.336	0.0088	10.6	12
Socony Beads	Water	0.458	0.0099	10.3	13
Glass Beads	Water	0.518	0.036	4.73	21
Lead Shot	Water	0.128	0.13	2.38	57
Glass Beads	Air	0.029	1.10	0.662	2800
Sea Sand	Air	0.040	2.16	0.543	3500
Glass Beads	Air	0.051	2.03	0.541	5000
Sea Sand	Air	0.055	6.05	0.437	5700
Socony Beads	Air	0.336	11.0	0.399	7500
Socony Beads	Air	0.458	13.0	0.388	7700
Glass Beads	Air	0.518	40.0	0.357	12000
Lead Shot	Air	0.128	85.0	0.344	52000

Indeed, this correspondence is so close that an arrangement in decreasing order of growth distance is identical with an arrangement in increasing order of the maximum stable bubble size. Table 2 shows a similar comparison for the transitional systems investigated by Harrison et al. (45). The correspondence is not quite so striking as in Table 1, but it is still true in general that the systems in which large bubbles are stable are just those which have very unstable states of uniform fluidisation. At first sight this may not seem very surprising until one recalls that there is no physical similarity between the two theories, which deal in quite different ways with phenomena between which there is no close mechanical relation. It appears, in a sense, to be a freak of nature that systems with highly unstable states of uniform fluidisation are just those in which large bubbles may survive, so that the

inhomogeneities necessarily present may take the highly ordered form of bubbles in the bed rather than a random form, as in the case of turbulence developing as a result of the instability of laminar flow in a single fluid

Short of a detailed treatment of the development of a disturbance from an infinitesimal fluctuation to a fully developed bubble, the two theories taken together give the best possible justification for thinking that we understand the difference between aggregative and particulate fluidisation.

Table 2: Comparison of stability criteria for systems investigated by Harrison and Davidson

Particles	Fluid	d_p(cms)	Fr	x/D_d	D_{em}/d_p
Lead Shot	75% Glycerol/Water	0.077	0.00030	927	1.7
Rosin	Paraffin	0.060	0.00016	830	1.5
Lead Shot	66% Glycerol/Water	0.077	0.0010	301	4.7
P.M.B.	CO at 600 p.s.i.g.	0.013	0.00064	265	4.3
P.M.B.	CO at 400 p.s.i.g.	0.013	0.0012	202	4.4
P.M.B.	CO at 200 p.s.i.g.	0.013	0.0021	149	8.1
P.M.B.	CO at 100 p.s.i.g.	0.013	0.0028	121	10.4
Glass Beads	Paraffin	0.078	0.0024	98.6	6.2
P.M.B.	CO at 0 p.s.i.g.	0.013	0.0060	60.6	26.6
Lead Shot	39% Glycerol/Water	0.077	0.016	20.1	20.2
Steel	Paraffin	0.077	0.020	15.4	21.8
Lead Shot	Paraffin	0.077	0.049	6.87	38.0
Lead Shot	Water	0.077	0.094	3.53	47.1

For these calculations D_d is taken as twenty particle diameters. The calculations are carried out for minimum fluidisation conditions. For the systems given by Harrison and Davidson, values of the minimum fluidisation voidage and fluid velocity are not known, so the voidage is assumed to be 0.400 and the superficial fluid velocity calculated from a correlation given by Leva (2). Thus, the entries in this table are subject to some uncertainty, as calculated values of growth distance are quite sensitive to this variable."

APPENDIX 2

Discussion of the Functions of Voidage Appearing in the Equations of Motion

(i) Terms from the Fluid - Particle Interaction Force

Virtual Mass Coefficient

For a single sphere moving in a fluid with no separation of the boundary layer, the virtual mass coefficient $\theta(n)$ is constant and equal to 0.50. However for the present situation, this will probably not apply, as seems likely from the results of Lamb (13) for the motion of two particles or a particle close to a wall. The virtual mass coefficient for a representative particle of an assembly is not easy to evaluate. Zuber (20) has attempted this, but his analysis fails for the reasons given in Chapter 1. It is probable that the virtual mass coefficient is some function of voidage and it could possibly be tensorial in character, although this would not seem likely if the bed is isotropic. All that can be said with certainty is that as the voidage tends to unity, the virtual mass coefficient tends to the single particle value. For the calculations reported in the present work, except in specific cases where the virtual mass coefficient was varied, it was assumed constant at 0.50.

The Drag Coefficient

This was defined at the end of Chapter 2 as

$$\beta(n) = \frac{n\phi(n, |\underline{u}-\underline{v}|)}{1-nv}$$

where $\phi(n, |\underline{u} - \underline{v}|)(\underline{u} - \underline{v})$ is the viscous drag exerted on one particle of the assembly. The term $\phi(n, |\underline{u} - \underline{v}|)$ is similar to the quantity $3\pi\mu d_p$ appearing in Stokes law for the force on a single particle, and for a small particle it reduces to this quantity as the particle concentration tends to zero.

Jackson (5) has shown the function $\beta(n)$ to be a monotonic increasing function of n, rising sharply from an almost linear relationship at low concentrations (where the particles are more or less independent and the total drag depends solely on the number present and not on their interaction) to a fairly high value of $\beta(n)$ at a value of n corresponding to close packing, after which the usual packed bed equations hold.

In studying the motion of one single particle or an assembly of particles in an accelerating fluid, Houghton (24) used a form of the drag term such that $\phi(n, |\underline{u} - \underline{v}|) = \alpha |\underline{u} - \underline{v}|^{a-1}$ where $1 \leq a \leq 2$ and α is a coefficient depending on the system properties. For a = 1, the drag force has the same linear dependence on the fluid and particle relative velocity as Stokes' drag. For a > 1, (Stokes' law does not hold for the single particle), the term $\phi(n, |\underline{u} - \underline{v}|)$ and hence $\beta(n)$ will exhibit some dependence on the magnitude of the relative velocity. However for uniform fluidisation, the voidage is related to the fluid velocity and so it is quite in order to treat $\beta(n)$ as a function only of voidage, although this is not strictly correct for other situations.

The Stokes' drag law form has been used by Zuber (20) for his equation of motion for a single particle in a fluidised assembly. Instead of $\phi(n, |\underline{u} - \underline{v}|)(\underline{u} - \underline{v})$ he used a form $3\pi\mu_m d_p(\underline{u} - \underline{v})$ where μ_m is the effective viscosity of the two phase mixture. Zuber used the Brinkman - Roscoe equation (46) to obtain μ_m i.e. $\mu_m = \mu \varepsilon^{-2.5}$ — an extension of the Einstein equation to higher concentrations of particles. Using this relationship and equation (2,20) of the present work, Zuber showed that for the state of uniform fluidisation

$$\bar{u}_o = u_t \varepsilon_o^{4.5}$$

where u_t, the terminal falling velocity of the particles is given by $u_t = d_p(\rho_s - \rho_f)g/18\mu$. This compares well with the Richardson and Zaki equation (21) for liquid fluidised beds of small particles for which Stokes' law holds; this empirical equation of Richardson and Zaki relates the superficial fluid velocity to the overall mean bed voidage. If the effect of voidage gradients in the bed are negligible, the overall mean bed voidage can be identified with the uniform fluidisation voidage.

The Richardson and Zaki equations (21) can be used to give some indication of the possible form of $\beta(n)$ and an estimate of the value of the term $n_o\beta_o'/\beta_o$. The general form of their relationship is, neglecting wall effects, $\bar{u}_o = u_t \varepsilon^N$ where the exponent N depends on the

Reynolds number $u_t d_p \rho_f / \mu$ and is thus constant for any one system. N generally lies in the range $2.4 \leq N \leq 4.7$. For uniform fluidisation, from equation (2,20)

$$\frac{\bar{u}_0 \beta(\varepsilon_0)}{\varepsilon_0} = (1-\varepsilon_0)(\rho_s - \rho_f) g$$

so that

$$\beta(\varepsilon_0) = \frac{(\rho_s - \rho_f) g (1-\varepsilon_0) \varepsilon_0^{1-N}}{u_t} \qquad \text{(A,1)}$$

If Stokes' equation for the terminal velocity of the particles obtains, then

$$\beta(\varepsilon_0) = \frac{18\mu}{d_p^2} (1-\varepsilon_0) \varepsilon_0^{1-N} \qquad \text{(A,2)}$$

An expression for $\beta(\varepsilon_0)$ similar to this may be obtained from the Carman - Kozeny equation (see Coulson and Richardson (25)) for flow through packed beds - assuming that this expression can be extrapolated to fluidised beds at voidages above that of incipient fluidisation. Neglecting the change in hydrostatic head, the pressure drop across a bed of packed spheres is given by

$$\left|\frac{\Delta p}{\Delta x}\right| = \frac{36\mu}{d_p^2} K \bar{u}_0 \frac{(1-\varepsilon)^2}{\varepsilon^3}$$

where K is Kozeny's constant and has a value of approximately 5. For uniform fluidisation $\left|\frac{\Delta p}{\Delta x}\right| = \frac{\bar{u}_0 \beta(\varepsilon_0)}{\varepsilon_0}$

so that

$$\beta(\varepsilon_0) = \frac{18\mu}{d_p^2} \cdot \frac{2K(1-\varepsilon_0)^2}{\varepsilon_0^2} \qquad \text{(A,3)}$$

Rowe (18) has measured the total drag force (due to both viscous drag and fluid motion) on a single sphere in an assembly of other spheres and he found that the drag on a single particle of the assembly in a uniform stream could be represented by

$$g v (\rho_s - \rho_f) = \psi(\varepsilon_0) C_D \frac{\Pi}{4} d_p^2 \frac{\rho_f}{2} \bar{u}_0^2 \quad \left(= \frac{\bar{u}_0}{\varepsilon_0} \frac{\beta(\varepsilon_0)}{m}\right)$$

where $\psi(\varepsilon_0)$ is some function of the voidage, C_D is a drag coefficient defined for an isolated sphere in a fluid stream at the same velocity as the superficial fluid velocity in the assembly and is a function of the Reynold's number $\bar{u}_0 d_p \rho_f / \mu$. The function $\psi(\varepsilon_0)$ is given in terms of the separation ratio of the particles (ratio of distance from circumference to circumference to particle diameter) as

$$\psi(\varepsilon_0) = \frac{0.68}{\delta} + 1$$

For the rhombohedral assembly used by Rowe, δ is related to the voidage

by $\varepsilon_o = 1 - \frac{0.74}{(1+\delta)^3}$ (reference (47))

thus giving $$\psi(\varepsilon_o) = \frac{0.905 - 0.320(1-\varepsilon_o)^{1/3}}{0.905 - (1-\varepsilon_o)^{1/3}} \qquad (A,4)$$

Again using equation (2,20), $\beta(\varepsilon_o)$ is given, for Rowe's drag equation, as

$$\beta(\varepsilon_o) = (1-\varepsilon_o)\varepsilon_o \psi(\varepsilon_o) \frac{3}{4} \rho_f \frac{\overline{u}_o}{d_p} C_D$$

In the range of interest for most fluidised beds, Rowe states that

$$C_D = \frac{24}{Re}\left(1 + 0.15\, Re^{0.687}\right)$$

so that

$$\beta(\varepsilon_o) = \frac{18\mu}{d_p^2} \varepsilon_o(1-\varepsilon_o)\psi(\varepsilon_o)\left(1 + 0.15\, Re^{0.687}\right) \qquad (A,5)$$

Murray (14) also used Rowe's drag equation to evaluate the drag function $\alpha(\varepsilon)$ in his equations (see Chapter 1, equations (1,1) to (1,8)). It is a debatable point whether Murray's equations should be considered equivalent to Pigford's equations or to Jackson's, but either way, his expression for $\alpha(\varepsilon)$ is wrong. After some manipulation of Murray's terms, the expression he uses for $\alpha(\varepsilon)$ reduces to

$$\alpha(\varepsilon) = \frac{18\mu}{d_p^2}(1-\varepsilon_o)\psi(\varepsilon_o)\left(1 + 0.15\, Re^{0.687}\right)$$

If $\alpha(\varepsilon)$ is equivalent to Pigford's μ/K, then $\alpha(\varepsilon)$ must thus be equivalent to $\varepsilon\beta(\varepsilon)$ and it is readily seen that the factor ε^2 has been omitted. If, however, $\alpha(\varepsilon)$ is equivalent to $\beta(\varepsilon)$ (Murray's equations are thus considered equivalent to Jackson's), a factor ε is still missing. This discrepancy arises in part from the fact that Rowe's drag equation is written in terms of the superficial fluid velocity and not, as Murray has assumed, the interstitial fluid velocity. If Murray's equations are equivalent to Pigford's, the second ε factor missing in this case is because Murray has interpreted Rowe's equation as giving only the viscous drag on the particles and not the total drag including pressure drop (see the discussion of uniform fluidisation at the end of Chapter 2).

It is of interest to note that each of the equations (A,2), (A,3) and (A,5) contains the same term $18\mu/d_p^2$. However these equations are not strictly comparable because of the different flow regimes for which they apply, and a comparison of the three methods for obtaining $\beta(\varepsilon_o)$ is better made between equations (A,1), (A,3) and (A,5).

The following comparison is for the system No.5 ballotini fluidised by water and assumes uniform fluidisation. Experimentally determined

expansion data were available for this system and this affords a further comparison with values of the term $\beta(\varepsilon_o)$ calculated using equation (2,20), assuming the mean bed voidage can be identified with the uniform fluidisation voidage.

For the system No.5 B/H 0, the following are the relevant physical properties -

$\rho_s = 2.86$ gms/c.c., $\rho_f = 1.00$ gms/c.c., $\mu = 0.01p$, $d_p = 0.086$ cms. The terminal falling velocity was calculated by the method of Haywood, given in reference (25) and was found to be 17 cms/sec. Experimental expansion data were obtained in a 1" diameter bed and the following table gives the bed voidage, obtained from a smooth curve drawn through the experimental points, and the corresponding superficial fluid velocity.

$\bar{u}_o$(cms/sec.)	0.83	1.17	1.60	2.13	2.72	3.38
$\bar{\varepsilon}$	0.400	0.450	0.500	0.550	0.600	0.650

Using the Richardson and Zaki relationship, this experimental data gave $u_t = 13$ cms/sec. and $N = 3.16$. The calculated value of N (using the calculated value of u_t) for this situation is $N = 3.08$. (Richardson and Zaki give the equation for the exponent as $N = (4.45 + 18\, d_p/d_t)\, Re^{-0.1}$ where $Re = \frac{u_t d_p \rho_f}{\mu}$)

The relationships for $\beta(\varepsilon_o)$ to be compared are

$$\beta(\varepsilon_o) = \frac{(\rho_s - \rho_f) g}{u_t} (1-\varepsilon_o)\varepsilon_o^{1-N}$$ - from the Richardson and Zaki relationship (A,1)

$$\beta(\varepsilon_o) = \frac{18\mu}{d_p^2} \frac{2K(1-\varepsilon_o)^2}{\varepsilon_o^2}$$ - from the Carman - Kozeny equation (A,3)

$$\beta(\varepsilon_o) = \frac{18\mu}{d_p^2} \varepsilon_o (1-\varepsilon_o) \psi(\varepsilon_o) (1 + 0.15 Re^{0.687})$$ - from Rowe's drag equation

In addition, these expressions are to be compared with the values of $\beta(\varepsilon_o)$ obtained from equation (2,20),

$$\beta(\varepsilon_o) = \frac{\varepsilon_o (1-\varepsilon_o)(\rho_s - \rho_f) g}{\bar{u}_o}$$

using the above experimental values for $\bar{u}_o$ and $\bar{\varepsilon}$.

For ease of calculation, the exponent N in equation (A,1) was taken as 3 and the Kozeny constant K was taken as 5. If u_t is taken as 17 cms/sec., the Richardson and Zaki equation gives $\beta(\varepsilon_o) = 107.3(1-\varepsilon_o)/\varepsilon_o^2$ and the Carman - Kozeny equation gives $\beta(\varepsilon_o) = 243(1-\varepsilon_o)^2/\varepsilon_o^2$. The table below gives values of $\beta(\varepsilon_o)$ calculated from these two equations using the measured values of ε_o and $\bar{u}_o$.

ε_o	$\beta(\varepsilon_o)$ - R and Z	$\beta(\varepsilon_o)$ - C - K	$\beta(\varepsilon_o)$ - Exp.
0.400	403	547	521
0.450	291	362	387
0.500	215	243	283
0.550	159	163	211
0.600	119	107	161
0.650	89	70	122
0.700	65	44	-

The equation for $\beta(\varepsilon_o)$ obtained from Rowe's drag equation for the system No.5 B/H O is

$$\beta(\varepsilon_o) = 24 \cdot 3\varepsilon_o(1-\varepsilon_o)\,\psi(\varepsilon_o)\left[1 + 0.15(\bar{u}_o d_p \rho_f/\mu)^{0.687}\right].$$

and this is tabulated below. The function $\psi(\varepsilon_o)$ was calculated using equation (A,4).

ε_o	$\bar{u}_o$	$\psi(\varepsilon_o)$	$(1 + 0.15\,Re^{0.687})$	$\beta(\varepsilon_o)$
0.400	0.83	10.02	1.579	92
0.450	1.17	7.67	1.733	80
0.500	1.60	5.86	1.905	66
0.550	2.13	4.75	2.108	60
0.600	2.72	3.98	2.307	54
0.650	3.38	3.39	2.511	47

The four relationships for $\beta(\varepsilon_o)$ are plotted in Figure A.1.

From this figure it is seen that Rowe's drag law gives values of $\beta(\varepsilon_o)$ much lower than the other three relationships. The reason for this lies in the term $\psi(\varepsilon_o)$ - given by equation (A,4) for the rhombohedral assumbly used by Rowe. This term is very sensitive to the geometry assumed for the bed, and it only becomes large when $(1-\varepsilon_o)^{1/3}$ is slightly

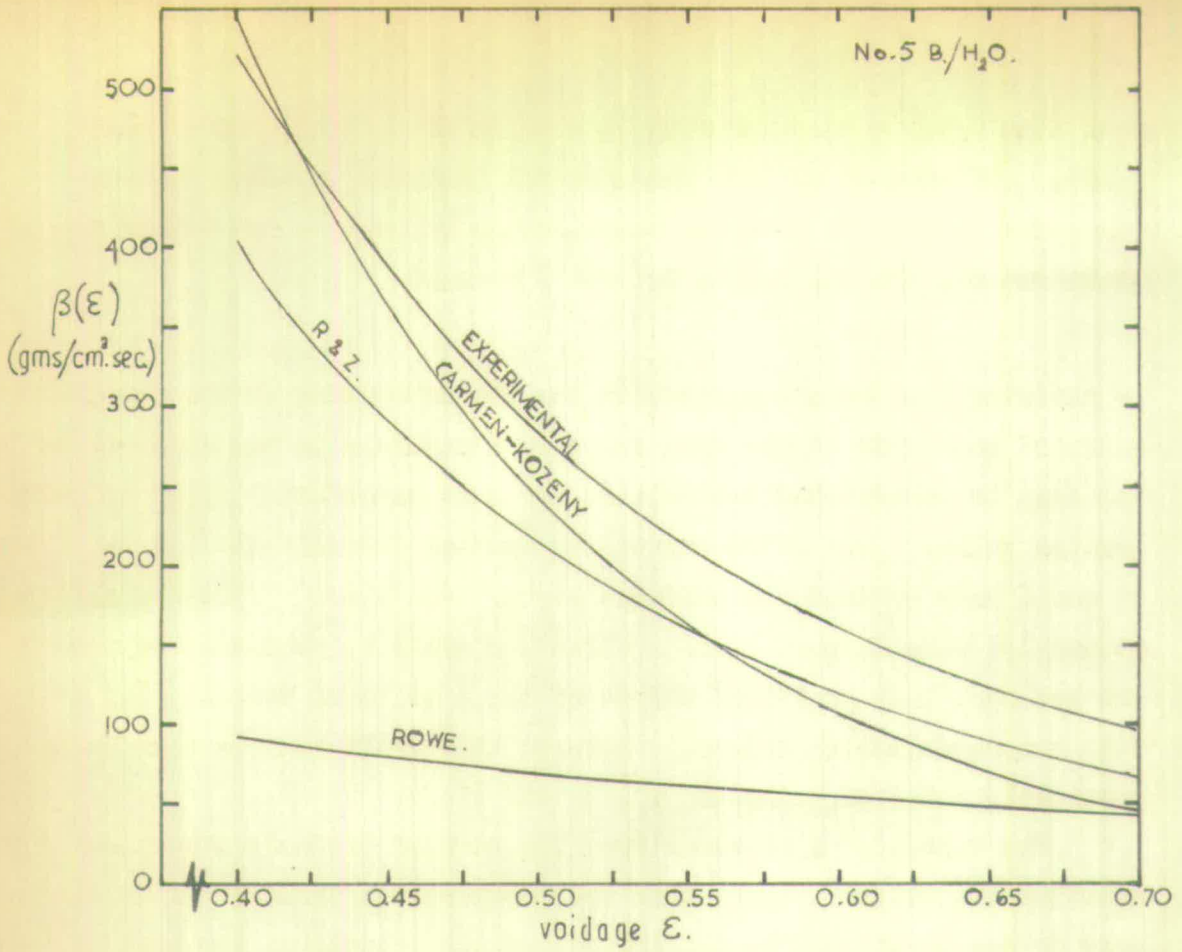


FIGURE A.1 COMPARISON OF METHODS FOR ESTIMATION OF DRAG COEFFICIENT $\beta(\varepsilon)$.

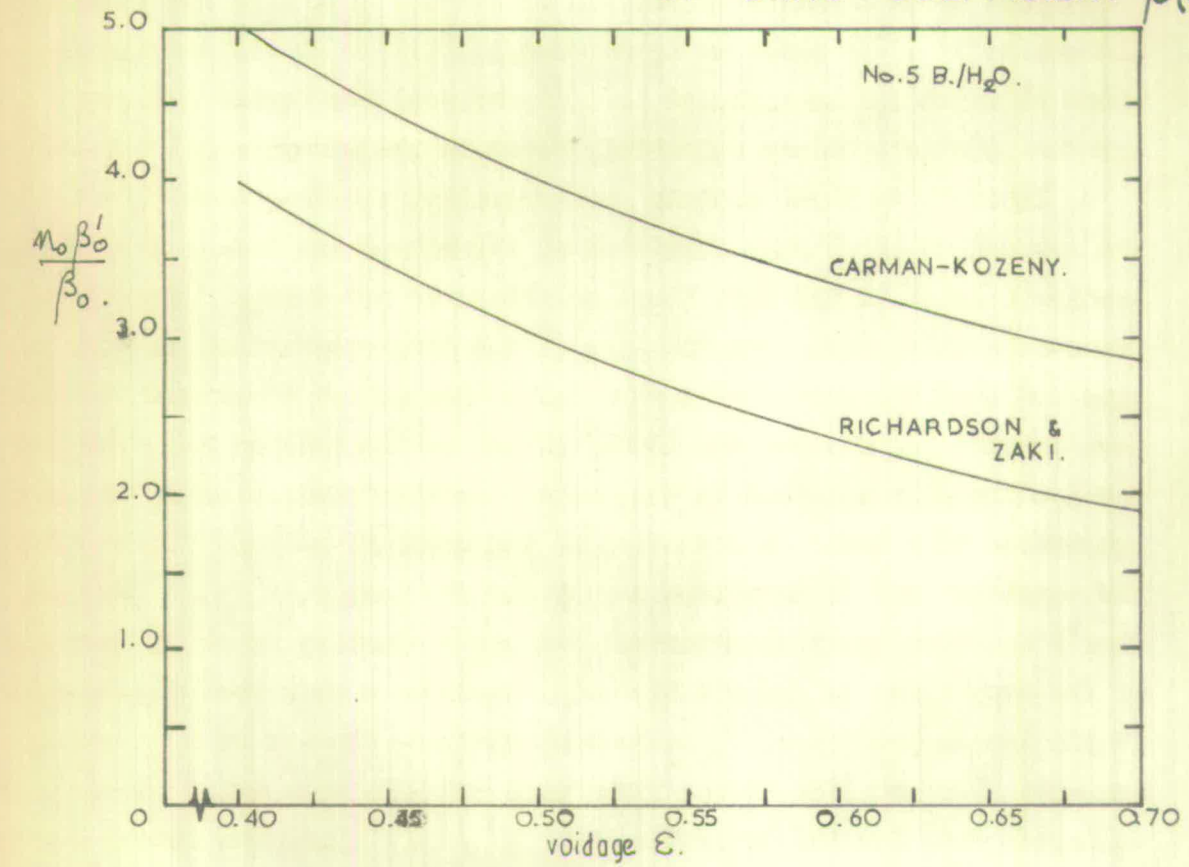


FIGURE A.2 COMPARISON OF METHODS FOR ESTIMATION OF $m_0\beta_0'/\beta_0$.

less than 0.905 - corresponding to a value of ε_o just greater than 0.260. If instead of this rhombohedral geometry, a cubic lattice structure is used to give the relationship between ε_o and δ (the separation ratio), the expression for $\psi(\varepsilon_o)$ becomes

$$\psi(\varepsilon_o) = \frac{0.805 - 0.320\,(1-\varepsilon_o)^{1/3}}{0.805 - (1-\varepsilon_o)^{1/3}}$$

- assuming that Rowe's expression for the dependence on the separation ratio of the ratio of the drag force on a particle in the assembly to the drag on an isolated particle at the same superficial fluid velocity remains valid. The above expression becomes infinite at $\varepsilon_o = 0.478$ and it could only be used for voidages higher than this. Thus, fairly obviously, some form of lattice structure could be chosen to represent the bed such that predicted values of $\beta(\varepsilon_o)$ would be brought into line with the experimental values. However this could only be done using previously obtained values of $\bar{u}_o$, ε_o and $\beta(\varepsilon_o)$.

The values of β obtained from the assumed Richardson and Zaki equation are slightly lower than the experimental values. This discrepancy is due mainly to the difference between calculated terminal velocity and the terminal velocity obtained when the bed expansion data are correlated by an equation of the Richardson and Zaki type and it largely disappears if u_t is taken as 13 cms/sec.. Except at higher voidages where it would not be expected to apply anyway, the Carman - Kozeny equation predicts values remarkably close to the experimental values.

Implicit in these methods for predicting the drag coefficient is the assumption of uniform fluidisation throughout the bed. If voidage gradients exist in the bed, these equations do not apply. However it is reasonable to suppose that the form of the drag coefficient is much the same and that the curves give some indication of the dependence of this term on voidage, whether the local voidage or the uniform bed voidage. Because the main interest in the present work is prediction of the growth properties of a small perturbation of the state of uniform fluidisation, the quantity $\beta(\varepsilon)$ is important mainly for the term $n_o \beta_o' / \beta_o$. Because Rowe's equation requires empirical data as a starting point and because of the complexity of the relationship, there is a very real disadvantage in its use to predict $n_o \beta_o' / \beta_o$ in comparison to the use of a relatively uncomplicated equation of the Richardson and Zaki type which requires no expansion data for the evaluation of $n_o \beta_o' / \beta_o$. Therefore Rowe's equation

will not be used further in the present work.

The main interest is in prediction of the quantity $n_o \beta_o' / \beta_o$.

Since $\varepsilon_o = 1 - n_o v$, $\quad \beta_o' = \left(\frac{d\beta}{dn}\right)_{n_o} = -v\left(\frac{d\beta}{d\varepsilon}\right)_{\varepsilon_o}$

so that $$\frac{n_o \beta_o'}{\beta_o} = -\frac{(1-\varepsilon_o)}{\beta(\varepsilon_o)}\left(\frac{d\beta}{d\varepsilon}\right)_{\varepsilon_o}$$

If equation (A,3), from the Carman - Kozeny equation, is used

$$n_o \beta_o' / \beta_o = 2/\varepsilon_o$$

and if equation (A,1), from the Richardson and Zaki equation, is chosen,

$$n_o \beta_o' / \beta_o = \frac{1}{\varepsilon_o}\left[(N-1)(1-\varepsilon_o) + \varepsilon_o\right] \qquad \text{(A,6)}$$

For the system No.5 B/H O, these two expressions are plotted in Figure A.2. Note that as $\varepsilon_o \to 1$, $n_o \beta_o' / \beta_o \to 2$ for the former expression and $n_o \beta_o' / \beta_o \to 1$ for the latter expression. It is hardly likely that the Carman - Kozeny equation will apply at such high voidages so that equation (A,6) is used to predict $n_o \beta_o' / \beta_o$ in the present work. Experimentally determined expansion data could also be used to predict $n_o \beta_o' / \beta_o$, but there seems little advantage in this because of the uncertainties in other terms determining the growth properties. Expansion data seem to be well correlated by an expression of the Richardson and Zaki type and so the use of experimental data could only really give a more accurate value for the exponent N to be used with fairly unreliable data. Thus for all the calculations of propagation properties, equation (A,6) was used to predict the term $n_o \beta_o' / \beta_o$. Richardson and Zaki give the following equations for the exponent N for the various ranges of the Reynolds number

$$\begin{aligned}
Re &< 0.2, && N = 4.65 + 19.5(d_p/d_t)\\
0.2 < Re &< 1, && N = (4.35 + 17.5(d_p/d_t))Re^{-0.03}\\
1 < Re &< 200, && N = (4.45 + 18(d_p/d_t))Re^{-0.01}\\
200 < Re &< 500, && N = 4.45\, Re^{-0.01}\\
500 < Re & && N = 2.39
\end{aligned}$$

For the experimental work, No.7, No.5 and No.3 grades, and 2 m.m. diameter ballotini was used. Water was used as the fluidising medium. The No.7 B was fluidised in a $\frac{1}{2}$" diameter tube, the No.5 B and No.3 B in $\frac{1}{2}$" and 1" tubes and the 2 m.m. B in 1" and 1$\frac{1}{2}$" diameter tubes. The following table summarises the physical properties of the ballotini and

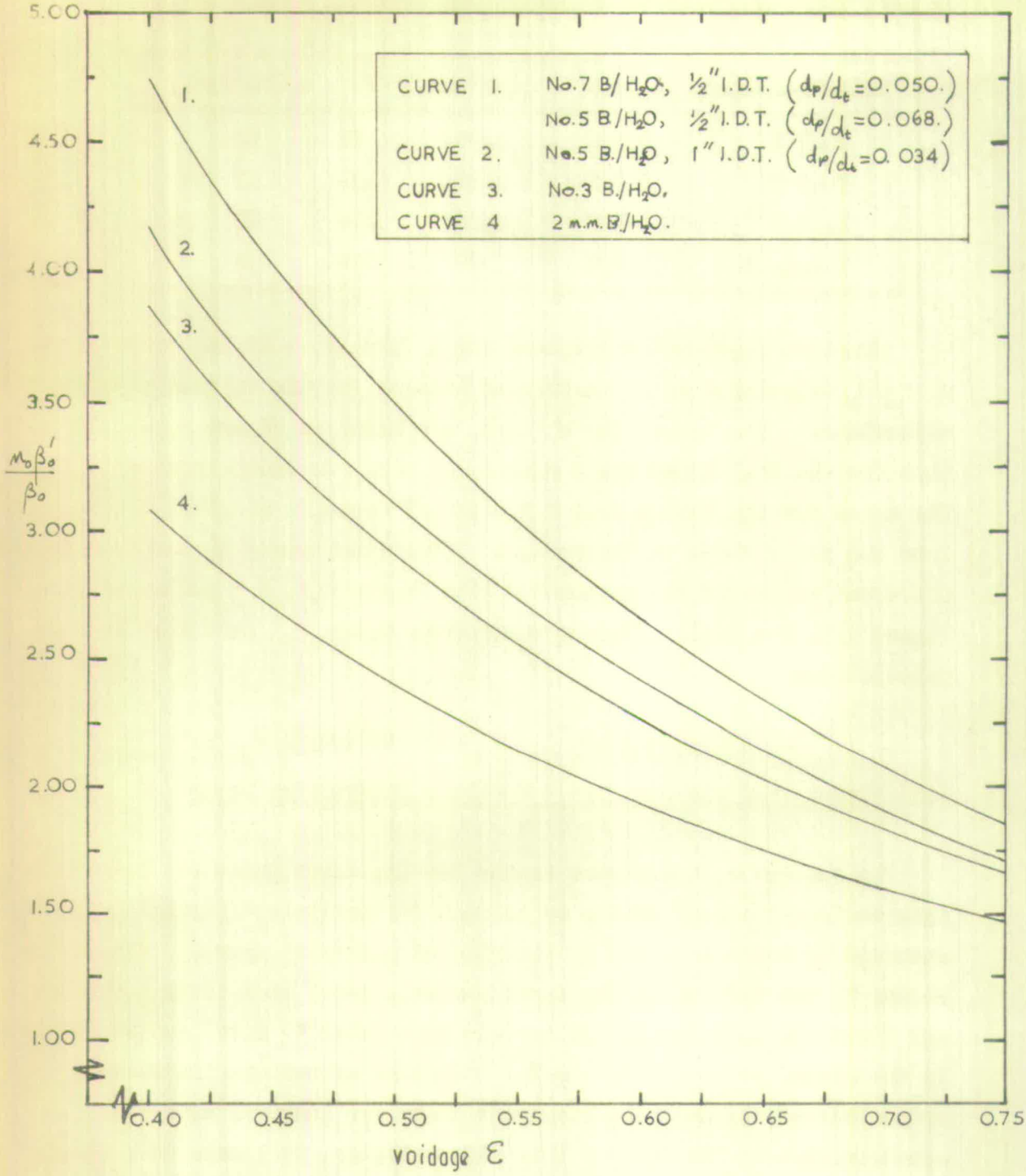


FIGURE A.3 PREDICTED DRAG TERMS FOR SYSTEMS USED IN THE EXPERIMENTAL WORK.

their calculated terminal falling velocities (the method of Haywood, given in ref. (25), was used to calculate the terminal velocities).

Ballotini Grade	d_p(cms)	ρ_s(gm/c.c.)	Re	u_t(cm/sec.)
No.7 B	0.064	2.95	72	12
No.5 B	0.086	2.86	130	17
No.3 B	0.127	2.86	270	22
2 m.m. B	0.207	2.70	620	31

Equation (A,6) was programmed for a Ferranti - Sirius computer and $n_o \beta_o' / \beta_o$ calculated as a function of voidage for the various experimental situations. The curves for $n_o \beta_o' / \beta_o$ are shown in Figure A,3. Note that for the No.3 B and the 2 m.m. B, $n_o \beta_o' / \beta_o$ is independent of d_p/d_t. The curve for the system No.5 B/H_2O in a 1" tube is slightly different from the curve shown in Figure A,2. This discrepancy is due to slightly different values of the exponent N (for Figure A,2, N = 3.0 and for Figure A,3, N = 3.1). Values taken from Figure A,3 were used in the calculations.

(ii) Terms From the Particle - Particle Interaction Force

In Chapter 2, the stress tensor for the solid phase was introduced into the equations of motion to account for particle - particle momentum exchange by collisions and by shearing of particle layers. The stress vector $\underline{t_s}$ was defined as the force per unit total area (both particles and fluid are included in the surface over which $\underline{t_s}$ acts) and is related to the stress tensor by $\underline{t_s} = \underline{n}.\underline{T_s}$. Because of certain fluid-like properties of the bed, the dispersed phase was assumed, as a first approximation to the form of this stress tensor, to behave as a quasi-Newtonian fluid and thus the stress tensor is given by

$$T_{s_{ij}} = \left(-\Omega(n) + \alpha(n)\frac{\partial v_k}{\partial x_k}\right)\delta_{ij} + \chi(n)\left(\frac{\partial v_i}{\partial x_j} + \frac{\partial v_j}{\partial x_i}\right)$$

in accordance with the continuum model used in the derivation of the equations of motion. This is probably an extremely simplified approach but it should serve to give some indication of the relative importance of

the particle - particle interaction force.

In a fluidised bed the particles are seen to move about in a more or less random fashion over very short path lengths and when the bed is not very turbulent these random velocities do not appear to be very large. This rapid random movement indicates a possible method of estimating the terms $\Pi(n)$, $\alpha(n)$ and $\chi(n)$.

The Particulate Phase Normal Stress Term $\Omega(n)$

The particle - particle normal stress in a fluidised bed probably arises from direct collisional forces and is akin to the hydrostatic pressure of a gas or liquid. This term will depend on the number of collisions per second per unit area and the momentum change involved in each collision. This, in turn, will depend on the mean random speed of the particles, in turn dependent on the fluid velocity, and on the particle concentration. Thus for a volume of the bed similar to the volume of the averaging sphere used in Chapter 2,

$$\Omega = \Omega(\underline{u}, n)$$

For any one physical situation, $\underline{u}$ will be determined by the superficial fluid velocity and the local concentration so that

$$\Omega = \Omega(\bar{u}_o, n)$$

Thus for the stability calculations, it is quite in order to treat the particle normal stress as a function of the concentration only (apart from its dependence on the system properties).

For constant u , the closer the particles are together, the greater the fluid velocity and the number of collisions and hence Ω should be an increasing function of n. As n increases and the particles approach close packing, the number of collisions increases until at close packing (effectively an infinite number of collisions per second) the normal stress should become infinite. Close packing puts an upper limit on the possible particle concentration encountered in a fluidised bed. As the particle concentration tends to zero, so also does the normal stress.

When the particles are free to move, an estimate of the particle "pressure" can be obtained by direct analogy with the kinetic theory of dense gases developed by Enskog (see reference (23)) and applied to rigid spherical molecules. If V is the random speed of the particles such that $V_x^2 = V_y^2 = V_z^2 = \overline{V^2}/3$ (the bed is assumed isotropic) then $\Omega(n)$ is given, after all the kinetic theory terms have been translated into their

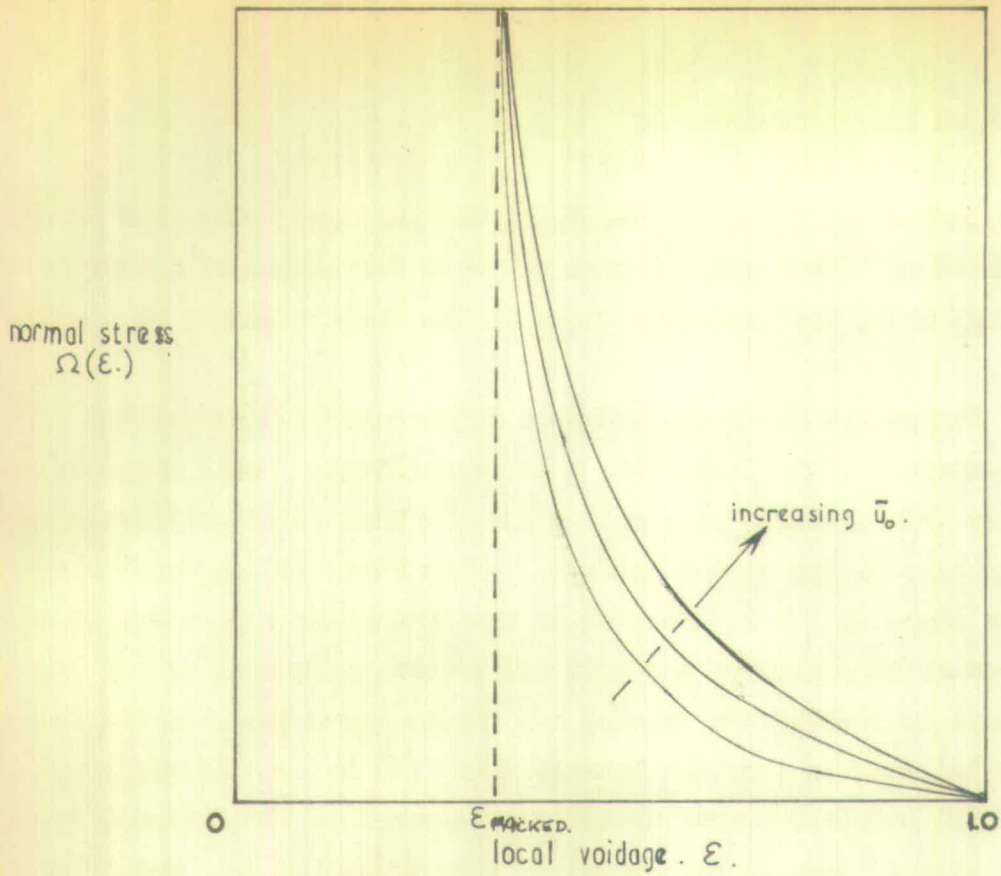


FIGURE A.4 DEPENDENCE OF PARTICULATE PHASE STATIC NORMAL STRESS ON LOCAL VOIDAGE.

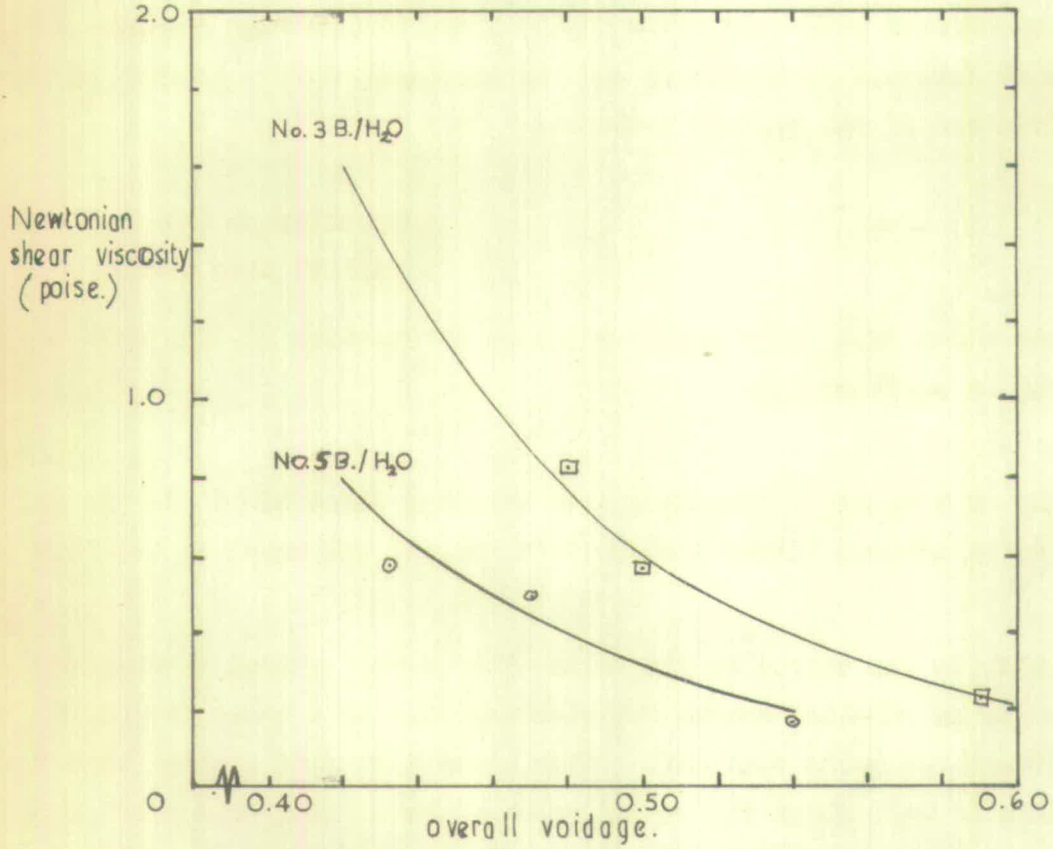


FIGURE A.5 ANDERSON'S AND BRYDEN'S RESULTS FOR THE SHEAR VISCOSITY OF LIQUID FLUIDISED BEDS.

fluidised bed equivalent, by

$$\Omega(n) = \tfrac{1}{3}\rho_s \overline{V^2}\left(nv + 0.500(nv)^2 + 0.156(nv)^3 + \text{----}\right)$$

This equation will only be valid, if the analogy holds, for fairly low values of n. Obviously it does not hold for values of n near to close packing, where the analogous state in the kinetic theory is a condensed gas.

Figure A.4 shows the probable dependence of Ω on voidage ($\varepsilon = 1 - nv$) at a constant fluid flow rate. It seems likely Ω will decrease fairly rapidly from infinity at close packing to some relatively small value fairly near to the packed voidage. Note that $\Omega(n)$ approaches zero with finite slope as $\varepsilon \to 1.0$ because of the particular dependence of $\Omega(n)$ on the number of particles per unit bed volume. In view of the limited evidence available, the form of $\Omega(n)$ shown seems the most likely, but is is quite possible that the behaviour of $\Omega(n)$ is totally different.

The particle normal stress term appears in the dispersion relationships as $n_o\Omega_o'$ i.e. as the quantity $(1 - \varepsilon_o)\left|\frac{d\Omega}{d\varepsilon}\right|_{\varepsilon=\varepsilon_o}$ and it is necessary to assign some value to this quantity before any stability calculations can be carried out. Equation (3,19) gives the voidage gradient in a bed with no internal disturbances and the quantity $|d\Omega/d\varepsilon|$ appears in the coefficient of the voidage gradient. This coefficient is

$$\left|\frac{d\Omega}{d\varepsilon}\right| \doteq \rho_f \bar{u}_o^2 \frac{(1-\varepsilon)}{\varepsilon^3}\left(1 + \frac{\Theta(\varepsilon)}{\varepsilon}\right)$$

(depending on the form of the virtual mass term)

It was shown that for a stable solution of equation (3,19), this coefficient should be positive i.e.

$$\left|\frac{d\Omega}{d\varepsilon}\right| > \rho_f \bar{u}_o^2 \frac{(1-\varepsilon)}{\varepsilon^3}\left(1 + \frac{\Theta(\varepsilon)}{\varepsilon}\right)$$

Purely as a means of obtaining some starting value of $|d\Omega/d\varepsilon|$ to use in the calculations, it was assumed that $|d\Omega/d\varepsilon|$ was equal to the term

$$\rho_f \bar{u}_o^2 \frac{(1-\varepsilon)}{\varepsilon^3}\left(1 + \frac{\Theta(\varepsilon)}{\varepsilon}\right)$$

and this is the source of the values for $|d\Omega/d\varepsilon|$ quoted in Chapter 4. There is no physical reason for choosing this as a value for $|d\Omega/d\varepsilon|$ - the two terms are quite distinct. This assumption also implies that the voidage is well above the packed voidage where large values of $|d\Omega/d\varepsilon|$ are expected to occur.

It was found in most stability calculations that if $|d\Omega/d\varepsilon|$ was made

much greater than twice, and sometimes less, this quantity, the bed would become stable to small internal disturbances. Most fluidised beds appear to be unstable so that this limit of instability sets some upper bound on the possible values of $|d\Omega/d\varepsilon|$.

The "Viscosity" Terms $\alpha(n)$ and $\chi(n)$

For the assumed behaviour of the dispersed phase, the quantity $\alpha(n)$ is related to the shear "viscosity" $\chi(n)$ and the bulk "viscosity" $\kappa(n)$ by

$$\alpha(n) = \kappa(n) - \tfrac{2}{3}\chi(n).$$

As for the normal stress term, α and χ will be functions of the local fluid velocity and the particle concentration, i.e.

$$\alpha = \alpha(\underline{u}, n) \text{ and } \chi = \chi(\underline{u}, n)$$

and both terms will tend to zero as the particle concentration tends to zero. Both terms could be estimated from the analogy with the kinetic theory of dense gases. If the mean free path of the particles can be obtained from an assumed cubic lattice structure of the bed, then the shear "viscosity" would be given by

$$\chi(n) = 0.246\,\rho_s d_p \sqrt{\overline{V^2}}\,(n\nu)^{2/3} f(n\nu)$$

where $f(n\nu)$ is a complex function of particle concentration which has a value of about 1.3 for $n\nu = 0.40$. The work of Anderson and Bryden (31) indicates that, at this concentration, a reasonable value for the shear "viscosity" of the system No.5 B/H 0 is about 2 poise. This would give a root mean square particle velocity of about 45 cms/sec., and thus a normal stress term, $\Omega(n)$, of the order of 1000 dynes/cm^2. Now if

$$\left|\frac{d\Omega}{d\varepsilon}\right| \sim \rho_f \overline{u_o^2}\,\frac{(1-\varepsilon)}{\varepsilon^3}\left(1 + \frac{\Theta(\varepsilon)}{\varepsilon}\right)$$

then at this voidage $|d\Omega/d\varepsilon|$ has a value around 25 dynes/cm^2 unit voidage change. The value of $\Omega(n)$ is quite incompatible with the likely form of $\Omega(n)$ and the value of $|d\Omega/d\varepsilon|$; further, the value of $\sqrt{\overline{V^2}}$ is about 10 times the value of the fluid velocity. The value of $\Omega(n)$ is probably much smaller than the value predicted above. A root mean square velocity of 3 cms/sec. would give a normal stress of about 50 dynes/cm^2 - a much more reasonable value - but would produce a very low shear "viscosity". There is little doubt that the shear "viscosity" is large (of the order of one poise), and so it does not seem likely that the kinetic theory analogy is valid for the "viscosity" terms. Reasonable values of the mean square particle velocity do however give reasonable values of Ω (at voidages well above the packed voidage) and this implies that some additional mechanism

is involved in governing the dispersion's behaviour under shear and that this mechanism dominates the mechanism of momentum transport by collisions and particle transfer across shearing layers implicit in the kinetic theory analogy.

This additional mechanism is perhaps more akin to the mechanism envisaged acting in the Eyring rate theory of viscosity of dense gases and liquids, where the particle has to climb a high potential barrier to move relative to its neighbouring particles during shearing of adjacent layers. It may be that at fairly high voidages, where the particles are more widely spaced, the direct kinetic theory analogy is valid for both normal and shear stress terms.

Numerous attempts have been made to measure the viscosity of fluidised beds. Most of the work has been carried out for gas fluidised systems (e.g. Matheson, Herbst and Holt (48), Diekman and Forsythe (49) and Schugerl, Mertz and Fetting (50)) in a variety of measuring devices. It has been generally found that the viscosity increases with the size of particles forming the bed and that the viscosity drops very rapidly as the bed becomes fluidised, thereafter decreasing more slowly. Schugerl, Mertz and Fetting carried out a comprehensive series of measurements in a concentric cylinder apparatus with a number of different materials (e.g. sand, glass ballotini) and generally found the viscosity to lie in the range 1 - 20 poise in common with a number of other workers.

However little work has been done on liquid fluidised beds, and it was the need for some fairly reliable estimate of the "viscosity" of the systems used in the present work which occasioned the work of Anderson and Bryden (31). They studied the systems No.5 B/H_2O and No.3 B/H_2O in a rotating cylinder viscometer. In common with Schugerl et al. they found that for small shearing stresses, the bed behaved as a Newtonian fluid, that this Newtonian "viscosity" decreased with increasing fluid flow and that the viscosity increased with increase in particle size. The values of the "viscosity" they found are remarkably close to the values found by Schugerl et al. for similar particles fluidised by air, indicating that the bulk of the bed's resistance to shearing stresses is due to the particles and that the fluid plays very little part. Thus measurement of bed viscosity gives a reasonable estimate of particulate phase shear "viscosity". This experimental work also shows that the assumption of quasi-Newtonian behaviour for the dispersed phase should be quite

reasonable, at least in the stability calculations, where the rate of strain is small.

The measurements of the overall "viscosity" of the bed made by Anderson and Bryden are used in the present work to give an estimate of $\chi(n)$ or, strictly speaking, χ_0. Disturbances may have been present in the bed, but it is felt that these would have a relatively minor effect on the measured "viscosity", unlike the presence of bubbles in a gas fluidised bed. Figure A.5 shows the variation of Newtonian "viscosity", obtained for small shearing stresses, with overall voidage found for the systems No.5 B/H_2O and No.3 B/H_2O.

Extrapolated and interpolated values for the shear "viscosity" from Anderson's and Bryden's results were used for estimates of χ_0. The values chosen are shown in the table below.

ε_0	No.5 B/H_2O χ_0(poise)	No.3 B/H_2O χ_0(poise)
0.420	8	16
0.460	5	10
0.500	3	6
0.540	2	4

From these figures, reasonable values for χ_0 for the systems No.7 B/H_2O and 2 m.m. B/H_2O would seem to be as follows:

ε_0	No.7 B/H_2O χ_0(poise)	2 m.m. B/H_2O χ_0(poise)
0.420	5	28
0.460	3	17
0.500	2	11
0.540	1	8

It must be emphasised that the values in this table are no more than inspired guesswork. Having no alternative, however, these values were used in the stability calculations.

To obtain values of the quantity $(\alpha_0 + 2\chi_0)$ appearing in the dispersion relationship (equation (3,5)), some estimate of the bulk "viscosity" term $\kappa(n)$ is necessary. If $\bar{P}$ is the mean of the normal

stresses due to particle - particle interaction, then it is easily shown, assuming Newtonian behaviour, that

$$\bar{P} - \Omega(n) = K(n)\frac{1}{n}\frac{dn}{dt}$$ (considering only the principal stresses T_{sii} - see reference (22))

where $\frac{dn}{dt} = \frac{\partial n}{\partial t} + (\underline{v}.\text{grad})n$

Murray (14) has attempted to derive an expression for the bulk "viscosity" and shear "viscosity" and found that this bulk "viscosity" should be about three times the value of the shear"viscosity". However, as explained in Chapters 1 and 2, there is some confusion about the actual meaning of Murray's particulate phase stress tensor and little reliance can be placed on the expressions he derives. For water fluidised systems, the particulate phase shear "viscosity" predicted by Murray's expression would be about 3 cp. at a voidage of 0.50, in contrast to the experimental values of about 5 poise.

The evaluation of the bulk "viscosity" is a matter of some difficulty. For ideal dilute gases with no internal degrees of freedom, the bulk viscosity is zero. For dense gases and gases with polyatomic molecules it is not zero and is related to a molecular relaxation time - this characterises the time necessary for energy transfer from the translational to other degrees of freedom. Murray (14) has shown that the particulate phase bulk "viscosity" is necessary to predict the observed attenuation of surface waves. However for particles in a fluidised bed, there is no really analogous situation to the transfer of energy between translational and other degrees of freedom on a molecular level, other than for rotational energy if the particles are rough or not strictly spherical. Transfer of translational energy to rotational energy in particle collisions will however be enormously complicated by the presence of the fluid and it seems highly unlikely that any analogy with the kinetic theory of gases would give anything like a reasonable estimate.

For the stability calculations, a range of $0 \leq K_o \leq 3\chi_o$ has been chosen. The values of α_o and $(\alpha_o + 2\chi_o)$ are given below.

K_o	α_o	$(\alpha_o + 2\chi_o)$
0	$-2\chi_o/3$	$4/3\,\chi_o$
χ_o	$\chi_o/3$	$7/3\,\chi_o$
$2\chi_o$	$4\chi_o/3$	$10/3\,\chi_o$
$3\chi_o$	$7\chi_o/3$	$13/3\,\chi_o$

The values of the quantity $(\alpha_o + 2\chi_o)$ covered in the stability calculations are 0, χ_o, $2\chi_o$, $3\chi_o$ and $4\chi_o$.

APPENDIX 3

Expansion Data and Experimentally Determined Amplitudes and Frequencies

The amplitude and frequency data given here were all obtained from the records digitised by Benson - Lehner Ltd.. Propagation properties estimated from this data are discussed in Chapter 7. When calibrating the voidage against signal in the small calibration bed, flow rates were also measured. The expansion equation for each bed - an equation of the Richardson and Zaki type viz. $\bar{u}_o = u_t \varepsilon^N$ - could thus be calculated and these equations are reported in Chapter 6.

For each system, the fluid velocity and overall mean voidage at which each set of amplification measurements were made is given. The overall bed voidages reported were taken from bed height measurements and from the expansion equations for the system where it was available. In all cases the two methods agreed to within 0.003 in their estimates.

In the following tables, x is the height above the distributor in inches at which the record was taken, A(x) is twice the mean amplitude (see Chapter 7), f(x) is the mean frequency and $\varepsilon(x)$ is the mean voidage. The overall mean bed voidage is $\bar{\varepsilon}$ and $\bar{S}_o$ is the datum level signal at height x . The height of the top of the bed is x_t . The entries marked F in the calibration tables denote the point of incipient fluidisation for the small beds. The first and last voidages given in these tables generally are the closest random packed beds which could be obtained.

(i) SYSTEM: No.3 B/H_2O. 1" I.D.T.

Run 1:- Record 1. $\bar{u}_o$ = 2.46 cms/sec.
$\bar{\varepsilon}$ = 0.463

Record 2. $\bar{u}_o$ = 2.89 cms/sec.
$\bar{\varepsilon}$ = 0.496

Table A1/3:- Voidage - signal calibration

x_o = 2", ρ_s = 2.86 gms/c.c., W = 75 gms.

x_t (ins)	$\bar{u}_o$ (cms/sec.)	$\bar{\varepsilon}$	$\bar{S}_o$ (cms)
3.32	1.48	0.386	2.07
3.40	1.77	0.400	2.32
3.50	1.90	0.417	2.57
3.59	2.05	0.432	2.73
3.66	2.22	0.443	2.80
3.75	2.36	0.456	3.03
3.85	2.54	0.470	3.34
3.98	2.72	0.487	3.39
4.08	2.92	0.500	3.74
4.22	3.15	0.517	4.10
4.29	3.28	0.524	4.33
4.35	3.44	0.531	4.63
4.47	3.70	0.544	5.13
4.60	3.94	0.552	5.45
4.74	4.10	0.570	5.94
4.90	4.26	0.584	6.52
5.07	4.59	0.598	7.14
5.10	4.75	0.602	7.50
4.96	4.43	0.589	6.79
4.69	4.03	0.565	5.63
4.54	3.77	0.551	5.44
4.25	3.20	0.520	4.44
4.19	3.08	0.513	4.23
4.04	2.82	0.495	3.92
3.95	2.66	0.484	3.64
3.81	2.46	0.465	3.50
3.71	2.33	0.450	3.24
3.33	-	0.387	2.12

F

The quadratic voidage signal calibration curve is

$\varepsilon = 0.23870 + 0.08240\ S - 0.00442\ S^2$.

Table A2/3:- Growth Measurements

x	R(x)	Record 1			Record 2		
		ε(x)	A(x)	f(x)	ε(x)	A(x)	f(x)
2	1.00	0.440	0.019	1.32	0.485	0.021	1.89
4	1.02	0.454	0.025	1.37	0.498	0.036	1.90
6	0.883	0.443	0.030	1.65	0.485	0.041	1.79
9	0.848	0.446	0.047	1.35	0.485	0.050	1.46
12	0.868	0.447	0.047	1.32	0.482	0.052	1.59
15	0.848	0.445	0.059	1.19	0.478	0.066	1.48
18	0.795	0.444	0.062	1.26	0.484	0.083	1.29
21	0.791	0.449	0.072	1.12	0.480	0.077	1.29
24	0.779	0.451	0.082	1.04	0.478	0.088	1.30
30	0.755	0.456	0.094	0.96	0.471	0.075	1.20
36	0.736	0.450	0.087	1.03	0.472	0.094	1.11
42	0.763	0.462	0.110	0.91	0.473	0.075	1.15
48	0.783	0.462	0.105	0.90	0.482	0.074	1.07
54	0.759	0.455	0.100	0.96	0.483	0.062	1.20
60	0.786	0.468	0.116	0.88	0.482	0.055	1.27
65	0.821	0.461	0.105	0.86	0.487	0.052	1.10
72	0.799	0.469	0.103	0.86	0.504	0.051	1.19
78	0.811	0.485	0.108	0.84	0.514	0.058	1.12
81	0.839	0.491	0.106	0.84	0.522	0.048	1.42
84	0.872	0.500	0.100	0.83	0.529	0.045	1.30
87	0.879				0.522	0.048	1.30
90	0.821				0.516	0.054	1.22
93	0.899				0.542	0.037	1.43
94.5	0.839				0.529	0.036	1.34
30	0.755				0.476	0.065	1.46
12	0.868				0.496	0.053	1.55

The traces shown in Figure 5.6 were obtained under the same experimental conditions as the Record 1 for this system.

Run 2:- Record 1. $\bar{u}_o$ = 2.96 cms/sec.
$\bar{\varepsilon}$ = 0.500

Record 2. $\bar{u}_o$ = 2.72 cms/sec.
$\bar{\varepsilon}$ = 0.483

Record 3. $\bar{u}_o$ = 2.55 cms/sec.
$\bar{\varepsilon}$ = 0.470

Table A3/3:- Voidage - signal calibration

$x_o = 2\frac{1}{2}$", ρ_s = 2.86 gms/c.c., W = 75 gms.

x_t (ins)	$\bar{u}_o$ (cms/sec.)	$\bar{\varepsilon}$	$\bar{S}_o$ (cms)
3.32	1.48	0.386	2.82
3.40	1.57	0.400	2.91
3.47	1.86	0.412	2.85
5.21	4.73	0.609	8.12
5.05	4.37	0.596	7.67
4.87	4.24	0.581	6.73
4.70	4.01	0.566	6.43
4.55	3.81	0.552	5.70
4.39	3.61	0.535	5.42
4.30	3.28	0.526	4.97
4.24	3.23	0.519	4.96
4.17	3.05	0.511	4.80
3.94	2.71	0.482	4.23
3.87	2.63	0.473	4.02
3.78	2.43	0.460	3.74
3.69	2.25	0.447	3.39
3.57	2.02	0.429	2.97
3.60	2.14	0.433	3.14
3.75	2.36	0.456	3.46
3.83	2.53	0.467	3.80
4.05	2.86	0.496	4.29
4.20	3.15	0.514	4.26
4.32	3.38	0.528	4.95
4.50	-	0.547	5.53
5.31	-	0.616	8.18
4.27	3.24	0.522	4.87
4.13	3.01	0.506	4.52
3.95	2.69	0.484	4.18
3.69	2.30	0.447	3.49
3.32	-	0.386	3.10

The calibration curve is

$\varepsilon = 0.18990 + 0.08809\ S - 0.00437\ S^2$.

Table A4/3:- Growth Measurements

x	R(x)	Record 1			Record 2			Record 3		
		ε(x)	A(x)	f(x)	ε(x)	A(x)	f(x)	ε(x)	A(x)	f(x)
2.5	1.000	0.492	0.042	2.09	0.448	0.039	1.93	0.466	0.032	2.04
4	0.976	0.484	0.067	2.03	0.445	0.050	2.03	0.446	0.035	1.94
6	0.898	0.460	0.061	2.11	0.453	0.097	1.64	0.449	0.058	1.64
9	0.838	0.454	0.056	1.88	0.425	0.081	1.55	0.429	0.062	1.57
12	0.893	0.458	0.071	1.68	0.429	0.087	1.43	0.441	0.095	1.34
15	0.808	0.442	0.071	1.55	0.412	0.068	1.60	0.423	0.113	1.14
18	0.826	0.440	0.064	1.55	0.433	0.101	1.42	0.438	0.107	1.24
21	0.854	0.457	0.058	1.49	0.444	0.107	1.29	0.445	0.111	1.26
24	0.845	0.462	0.070	1.37	0.444	0.092	1.25	0.448	0.106	1.27
30	0.845	0.462	0.054	1.21	0.438	0.096	1.15	0.489	0.115	1.15
36	0.819	0.469	0.050	1.30	0.434	0.088	1.20	0.478	0.131	1.09
42	0.812	0.470	0.063	1.44	0.434	0.079	1.20	0.486	0.101	1.25
45	0.808	0.477	0.054	1.45	0.435	0.088	1.13	0.479	0.131	1.01
48	0.805	0.461	0.057	1.45	0.436	0.078	1.02	0.483	0.114	1.02
51	0.830	0.476	0.054	1.50	0.437	0.074	1.08	0.469	0.097	0.95
54	0.802	0.460	0.055	1.50	-	-	-	-	-	-
30	0.845	0.465	0.069	1.43	0.442	0.090	1.25	0.490	0.117	1.16
12	0.893	0.459	0.079	1.68	-	-	-	-	-	-

(ii) SYSTEM:- No.5 B/H_2O, 1" I.D.T.

Run 1:- Record 1. $\bar{u}_o$ = 1.34 cms/sec.

$\bar{\varepsilon}$ = 0.469

Record 2. $\bar{u}_o$ = 1.47 cms/sec.

$\bar{\varepsilon}$ = 0.485

The voidage signal calibration data are given in Table 2 of Chapter 7.

Table A5/5:- Growth Measurements

x	R(x)	Record 1			Record 2		
		$\varepsilon(x)$	A(x)	f(x)	$\varepsilon(x)$	A(x)	f(x)
2.5	1.000	0.461	0.008	1.31	0.455	0.013	1.28
4	0.980	0.463	0.008	1.38	0.459	0.015	1.36
6	0.871	0.417	0.011	1.16	0.438	0.019	1.53
9	0.834	0.410	0.010	1.31	0.425	0.031	1.28
12	0.862	0.419	0.012	1.46	0.441	0.032	1.38
15	0.809	0.402	0.014	1.49	0.430	0.029	1.27
18	0.802	0.407	0.025	1.30	0.428	0.032	1.32
21	0.828	0.416	0.029	1.24	0.435	0.037	1.22
24	0.847	0.411	0.029	1.30	0.439	0.033	1.25
30	0.830	0.408	0.031	1.15	0.438	0.042	1.06
36	0.806	0.399	0.032	1.03	0.430	0.031	1.13
42	0.756	0.398	0.032	1.01	0.423	0.035	1.06
48	0.774	0.397	0.029	1.06	0.424	0.036	0.98
54	0.779	0.401	0.033	1.04	0.423	0.032	1.03
60	0.786	0.404	0.029	1.04	0.430	0.026	1.05
65	0.847	0.416	0.026	1.01	0.436	0.024	0.97
69	0.834	0.417	0.027	0.98	0.439	0.020	1.09
72	0.874	0.422	0.025	0.95	0.437	0.020	1.16
75	0.947	0.427	0.020	1.06	0.450	0.018	1.27
78	0.842	-	-	-	0.439	0.015	1.15
30	0.830	0.416	0.028	1.17	0.438	0.033	1.17
12	0.862	0.421	0.012	1.41	0.441	0.034	1.37

Some of the entries for Record 2 have already appeared in Table 3 of Chapter 7. For Record 1 the bed was not properly fluidised until nine inches above the distributor.

(iii) SYSTEM: No.5 B/H_2O, ½" I.D.T.

Run 1:- Record 1. $\bar{u}_o$ = 1.42 cms/sec.
$\bar{\varepsilon}$ = 0.503

Record 2. $\bar{u}_o$ = 1.64 cms/sec.
$\bar{\varepsilon}$ = 0.528

Record 3. $\bar{u}_o$ = 1.77 cms/sec.
$\bar{\varepsilon}$ = 0.541

Table A6/5:- Voidage - signal calibration
x_o = 2", ρ_s = 2.86 gms/c.c., W = 20 gms.

x_t(ins)	$\bar{u}_o$(cms/sec.)	$\bar{\varepsilon}$	$\bar{S}_o$(cms)
3.68	-	0.410	4.04
4.33	1.32	0.499	4.97
4.40	1.42	0.507	4.75
5.95	2.85	0.635	7.92
6.14	3.03	0.647	8.73
5.81	2.74	0.627	7.92
5.65	2.55	0.616	-
5.45	2.42	0.602	7.11
5.27	2.24	0.588	6.59
5.11	2.12	0.575	6.27
5.02	2.04	0.568	6.13
4.85	1.87	0.553	5.71
4.70	1.76	0.538	5.70
4.55	1.54	0.523	5.38
4.47	1.47	0.515	4.95
4.61	1.64	0.529	5.69
4.82	1.79	0.550	5.64
4.95	1.97	0.562	6.27
5.10	2.11	0.575	6.32
5.21	2.20	0.583	6.86
5.39	2.37	0.597	6.92
5.56	2.47	0.610	7.36
5.74	2.66	0.622	7.97
6.00	2.91	0.638	8.73
6.22	3.08	0.651	8.90
5.36	2.37	0.595	7.11
4.67	1.71	0.535	5.42
4.32	1.32	0.498	5.02
4.14	-	0.476	4.38
3.68	-	0.410	3.34

F

The voidage signal correlation is

$\varepsilon = 0.11719 + 0.10088\ S - 0.00461\ S^2$.

Table A7/5:- Growth Measurements

x	R(x)	Record 1			Record 2			Record 3		
		ε(x)	A(x)	f(x)	ε(x)	A(x)	f(x)	ε(x)	A(x)	f(x)
2	1.000	0.498	0.024	2.86	0.525	0.034	2.35	0.542	0.038	1.88
4	0.908	0.494	0.027	2.38	0.522	0.041	2.10	0.528	0.053	2.13
6	0.926	0.491	0.027	2.33	0.531	0.060	1.90	0.534	0.076	1.72
9	0.834	0.453	0.034	1.85	0.507	0.056	2.21	0.491	0.057	2.14
12	0.846	0.472	0.048	1.81	0.492	0.051	1.95	0.498	0.058	1.75
15	0.757	0.428	0.040	1.75	0.470	0.047	2.01	0.468	0.065	1.85
18	0.773	0.443	0.047	1.67	0.446	0.057	1.83	0.472	0.060	1.99
21	0.808	0.462	0.055	1.82	0.475	0.059	2.11	0.493	0.047	2.29
24	0.782	0.450	0.067	1.61	0.454	0.058	1.92	0.485	0.058	1.86
30	0.806	0.453	0.067	1.58	0.465	0.061	1.73	0.491	0.052	1.86
36	0.653	0.436	0.088	1.29	0.443	0.061	1.72	0.461	0.053	1.92
42	0.852	0.464	0.095	1.19	0.479	0.068	1.42	0.493	0.060	1.65
48	0.806	0.442	0.076	1.40	0.454	0.056	1.60	0.473	0.044	1.83
54	0.849	0.452	0.075	1.28	0.460	0.059	1.49	0.482	0.042	2.07
60	0.864	0.446	0.066	1.34	0.463	0.042	1.84	0.483	0.045	1.60
65	0.950	0.493	0.078	1.57	0.448	0.039	1.55	0.472	1.930	1.88
68	0.875	-	-	-	0.406	0.034	1.40	0.451	0.039	1.46
30	0.806	-	-	-	0.476	0.072	1.60	0.492	0.063	1.69
12	0.846	-	-	-	0.491	0.062	1.83	0.512	0.070	1.71

For Record (1) the bed was not properly fluidised until about 5 inches above the distributor.

Note the relatively high values of voidage which occur in Table 7/5. The first and last voidages in the calibration tables are the close packed voidage of the bed.

(iv) SYSTEM:- 2 m.m. B/H_2O, $1\frac{1}{2}$" I.D.T.

Run 1:- Record 1. $\bar{u}_o$ = 3.72 cms/sec.
$\bar{\varepsilon}$ = 0.418

Record 2. $\bar{u}_o$ = 3.93 cms/sec.
$\bar{\varepsilon}$ = 0.433

Record 3. $\bar{u}_o$ = 4.28 cms/sec.
$\bar{\varepsilon}$ = 0.451

Table A8/2:- Voidage - signal calibration

x_o = 2.5", ρ_s = 2.70 gms/c.c., W = 150 gms

x_t (ins)	$\bar{u}_o$ (cms/sec.)	$\bar{\varepsilon}$	$\bar{S}_o$ (cms)
2.93	2.69	0.342	-
3.11	3.22	0.379	-
3.20	3.46	0.396	2.44
3.30	3.73	0.415	2.81
3.39	3.92	0.430	2.82
4.50	6.78	0.571	8.11
4.35	6.41	0.556	6.89
4.19	6.05	0.539	5.93
4.02	5.66	0.519	5.58
3.93	5.36	0.509	5.02
3.80	4.95	0.492	4.34
3.67	4.61	0.474	3.80
3.52	4.31	0.452	3.45
3.42	4.08	0.436	3.19
3.30	3.77	0.415	2.79
3.40	3.98	0.432	3.24
3.48	4.23	0.445	3.34
3.58	4.49	0.461	3.84
3.70	4.85	0.478	4.43
3.86	5.18	0.500	4.93
3.97	5.45	0.514	5.69
4.10	5.81	0.529	6.18
4.24	6.17	0.545	6.47
4.43	6.64	0.564	7.99
4.50	6.78	0.571	8.35
4.13	5.99	0.532	6.35
3.80	5.03	0.492	4.79
3.39	3.88	0.430	3.25
3.21	3.48	0.399	2.62
2.93	-	0.342	-

F

The calibration quadratic is
$\bar{\varepsilon} = 0.24416 + 0.070595\,S - 0.00367\,S^2$.

Table A9/2:- Growth Measurements

x	R(x)	Record 1			Record 2			Record 3		
		ε(x)	A(x)	f(x)	ε(x)	A(x)	f(x)	ε(x)	A(x)	f(x)
1.5	1.090	0.442	0.033	1.55	0.468	0.043	1.30	0.491	0.036	1.76
2.5	1.000	0.421	0.034	1.81	0.448	0.044	1.42	0.476	0.036	1.69
4	1.000	0.435	0.029	1.80	0.447	0.041	1.35	0.484	0.045	1.99
6	0.995	0.428	0.027	1.88	0.443	0.051	1.46	0.477	0.061	1.69
8	1.037	0.424	0.036	1.45	0.456	0.071	1.42	0.477	0.071	1.49
10	0.959	0.414	0.044	1.44	0.442	0.077	1.48	0.468	0.077	2.00
12	0.877	0.405	0.047	1.30	0.448	0.097	1.23	0.466	0.077	1.64
15	0.870	0.427	0.062	1.55	0.440	0.098	1.24	0.461	0.090	1.29
18	0.896	0.419	0.062	1.38	0.444	0.098	1.30	0.477	0.089	1.47
21	0.928	0.443	0.069	1.53	0.452	0.099	1.29	0.480	0.092	1.45
24	0.896	0.437	0.089	1.20	0.446	0.114	1.13	0.473	0.117	1.24
30	0.908	0.431	0.097	1.21	0.454	0.137	1.04	0.470	0.114	1.24
36	0.896	0.424	0.087	1.24	0.449	0.109	1.22	0.474	0.132	1.22
42	0.934	0.441	0.119	0.99	0.456	0.142	1.00	0.466	0.099	1.28
45	0.946	0.436	0.106	1.01	0.443	0.111	1.16	0.473	0.116	1.19
48	1.051	0.437	0.105	1.17	0.451	0.143	0.96	0.478	0.134	1.00
51	0.968	-	-	-	0.453	0.125	1.10	0.466	0.116	1.11
24	0.896	0.443	0.090	1.42	0.467	0.140	1.08	0.468	0.096	1.46
10	0.959	0.423	0.034	2.00	0.444	0.073	1.58	0.458	0.060	1.79

(v) SYSTEM: No.7 B/H_2O, $\frac{1}{2}$" I.D.T.

Run 1:- Record 1. $\bar{u}_o$ = 0.86 cms/sec.

$\bar{\varepsilon}$ = 0.495

Record 2. $\bar{u}_o$ = 0.98 cms/sec.

$\bar{\varepsilon}$ = 0.510

Record 3. $\bar{u}_o$ = 1.10 cms/sec.

$\bar{\varepsilon}$ = 0.521

Table A10/7:- Growth Measurements

x	R(x)	Record 1			Record 2			Record 3		
		ε(x)	A(x)	f(x)	ε(x)	A(x)	f(x)	ε(x)	A(x)	f(x)
1	1.090	0.530	0.008	1.90	0.548	0.007	1.92	0.585	0.008	1.94
2	1.000	0.517	0.007	2.14	0.528	0.008	2.10	0.571	0.009	1.97
3	1.016	0.501	0.010	1.91	0.528	0.011	1.86	0.562	0.009	1.74
4	1.021	0.504	0.009	1.94	0.540	0.008	1.52	0.581	0.009	1.95
6	0.959	0.483	0.008	1.99	0.528	0.013	1.63	0.559	0.015	1.76
8	0.918	0.476	0.007	1.91	0.516	0.023	1.60	0.554	0.015	1.81
10	0.926	0.487	0.008	2.16	-	-	1.67	0.554	0.019	1.76
12	0.914	0.487	0.007	2.19	-	-	1.46	0.552	0.024	1.51
15	0.901	0.481	0.011	1.74	-	-	1.36	0.550	0.023	1.51
18	0.884	0.469	0.012	1.72	-	-	1.62	0.536	0.019	1.55
21	0.880	0.469	0.013	1.60	-	-	1.49	0.539	0.022	1.47
24	0.923	0.484	0.021	1.45	-	-	1.43	0.552	0.020	1.32
30	0.901	0.476	0.020	1.24	-	-	1.42	0.555	0.022	1.27
36	0.901	0.463	0.022	1.31	-	-	1.32	0.509	0.018	1.36
42	0.940	0.461	0.017	1.34	-	-	1.02	0.512	0.014	1.15
18	0.884	0.463	0.016	1.52	0.505	0.022	1.29	0.548	0.023	1.49
8	0.918	0.487	0.008	1.97	0.526	0.016	1.60	0.570	0.017	1.85

The rotameter used for the small flow rates needed for this system was not calibrated and hence flow-rates were obtained by measuring the quantity of water collected in a certain time. There is thus no estimate of the relationship between $\bar{u}_o$ and $\bar{\varepsilon}$. The voidage signal calibration was obtained in the usual way and was found to be

$$\varepsilon = 0.04327 + 0.10469S - 0.00462\ S^2.$$

Mistakes were found in the digital record for Record 2 and only amplification and frequency measurements close to the distributor could be obtained. For Record 1, the bed was not properly fluidised until 12" above the distributor.

REFERENCES

References

(1) Zeny, F.A. and Othmer, D.F., "Fluidisation and Fluid-Particle Systems". Reinhold, New York, 1960.

(2) Leva, M., "Fluidisation". McGraw-Hill, New York, 1959.

(3) Davidson, J.F. and Harrison, D. "Fluidised Particles". Cambridge, 1963.

(4) Wilhelm, R.H. and Kwauk, M., Chem. Eng. Prog., 44 (1948) p.201.

(5) Jackson, R., Trans. Inst. Chem. Eng., 41 (1963) p.13.

(6) Pigford, R.L. and Baron, T., I &EC fund., 4 (1965) p.81.

(7) Kramers, H., Westerman, M.D., de Groot, J.M. and Dupont, F.A.A. in "Symposium on Interaction between Fluids and Particles". The Institution of Chemical Engineers, London, 1963.

(8) Anderson, T.B. and Jackson, R., Chem. Eng. Sci., 19 (1964) p.509.

(9) Van Deemter, J.J. and Van der Laan, E.T., App. Sci. Res. A 10, (1961) p.102.

(10) Soo, S.L. in "Symposium on Interaction between Fluids and Particles". The Institution of Chemical Engineers, London, 1963.

(11) Hinze, J.O., App. Sci. Res., A 11 (1962) p.33.

(12) Basset, A.B., "Treatise on Hydrodynamics" Vol.2., Deighton Bell, Cambridge, 1888.

(13) Lamb, J., "Hydrodynamics". Cambridge, 1932.

(14) Murray, J.D., J. Fluid. Mech., 21 (1965) p. 465.

(15) Wallis, G.B., Private Communication, 1964.

(16) Corrsin, S. and Lumley, J., App. Sci. Res., A 6 (1956) p.114.

(17) Hinze, J.O., "Turbulence". McGraw-Hill, New York, 1959.

(18) Rowe, P.N., Trans. Inst. Chem. Eng., 39 (1961) p.175.

(19) Ruckenstein, E., Rev. de Phys., 7 (1962) p.137.

(20) Zuber, N., Chem. Eng. Sci., 19 (1964) p.897.

(21) Richardson, J.F. and Zaki, W.N., Trans. Inst. Chem. Eng., 32 (1954) p.35.

(22) Aris, R., "Vectors, Tensors and the Basic Equations of Fluid Mechanics" Prentice-Hall International, London, 1962. p.85.

(23) Hirschfelder, J.O., Curtiss, C.F. and Bird, R.B., "Molecular Theory of Gases and Liquids". Wiley and Son. New York, 1954.

(24) Houghton, G.L., Proc. Roy. Soc., A 272 (1963) p.33.

(25) Coulson, J.M., and Richardson, J.F., "Chemical Engineering". Vol.2., Pergamon Press, Oxford, 1960.

(26) Milne-Thomson, L.M., "Theoretical Hydrodynamics". McMillan, London, 1960.

(27) Tchen, C.M., "Mean Value and Correlation Problems connected with the Motion of Small Particles Suspended in a Turbulent Fluid". Ph.D. Thesis, Delft, 1947.

(28) Schlichting, H. "Boundary Layer Theory". Pergamon Press, London, 1955.

(29) Tamarin, A.I., Int. Chem. Eng., 4 (Jan. 1964) p.50.

(30) Redwood, M.R., "Mechanical Waveguides". Pergamon Press, Oxford, 1960.

(31) Anderson, A.B. and Bryden, J.O., "Viscosity of Liquid Fluidised Beds", Research Report, Chem. Eng. Dept., University of Edinburgh, 1965.

(32) Wace, P.F. and Burnett, S.J., Trans. Inst. Chem. Eng., 39 (1961) P. 168.

(33) Rowe, P.N. and Partridge, B.A., U.K.A.E.A. Research Group Report. AERE - R 4660 (1964).

(34) Lancaster, F.H., "The Kinetics of Solid Catalysed Reactions in Fluidised Beds". Ph.D. Thesis, Edinburgh, 1965.

(35) Barer, J. and Underwood, S.B., Journ. Roy. Micro. Soc., LXXVI Series 3. (1956) p. 149.

(36) Bendat, J.S., "Principles and Applications of Random Noise Theory". J. Wiley and Son, New York, 1958.

(37) Lanning, J.H. and Battin, R.H., "Random Processes in Automatic Control". McGraw-Hill, New York, 1956.

(38) Woodward, P.M., "Probability and Information Theory, with Applications to Radar". Pergamon Press, London, 1957.

(39) Blackman, P.B. and Tukey, J.W., "Measurement of Power Spectra from the Point of View of Communications Engineering". Dover, New York, 1960.

(40) Swinnerton-Dyer, H.P.F., Computer Journ., 5 (1962) p.16.

(41) Rowe, P.N. and Partridge, B.A. in "Symposium on Interaction between Fluids and Particles". The Institution of Chemical Engineers, London, 1963.

(42) Bagnold, R.A., Phil. Trans. Roy. Soc., 249 A (1956) p.235.
(43) Wallis, R.P., Engineering, 148 (1934) p. 423.
(44) Ruckenstein, E., Chem. Eng. Sci., 21 (1966) p.113.
(45) Harrison, D., Davidson, J.F. and de Kock, J.W., Trans. Inst. Chem. Eng., 39 (1961), p.202.
(46) Brinkman, H.C., J. Chem. Phys., 20 (1952) p.571.
(47) Rowe, P.N., Private Communication, 1965.
(48) Matheson, G.L., Herbst, W.A. and Holt, P.H., I. & E.C., 41 (1949) p.1099.
(49) Dickman, R. and Forsythe, W.L., I. & E.C., 45 (1953) p.1174.
(50) Schugerl, K., Merz. M. and Fetting, F., Chem. Eng. Sci., 15 (1961) p.1.